NASA Conference Publication 2289

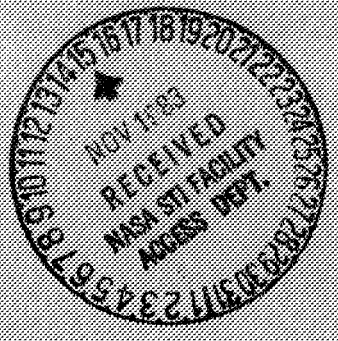

Turbine Engine Hot Section Technology 1983

FOR EARLY DOMESTIC DISSEMINATION

Date for general release October 1985

Proceedings of a conference held at NASA Lewis Research Center Cleveland, Ohio October 25 and 26, 1983

NASA

NASA Conference Publication 2289

Turbine Engine Hot Section Technology 1983

Proceedings of a conference
held at NASA Lewis Research Center
Cleveland, Ohio
October 25 and 26, 1983

NASA
National Aeronautics and
Space Administration

Scientific and Technical
Information Branch

1983

FOREWORD

Competition has pushed aircraft gas turbine engine designs to ever higher levels of performance. The resulting higher pressures and temperatures have led to a decrease in engine durability. In hot section components - the combustor and turbine - the more hostile environments have accelerated the damage and wear out of parts, thus, dramatically increasing maintenance costs. While recent technology advancs have been aimed primarily at improving performance, minimal efforts have been made to assure required durability.

The activities of the NASA Turbine Engine Hot Section Technology (HOST) Project are directed toward durability needs, as defined by industry, and toward a more balanced approach to engine design. The HOST efforts will improve the understanding of aerothermal environments and material structural responses by focused analytical and experimental research activities. The Project supports both contract/grant and Lewis in-house research activities. The overall approach is to assess existing analysis methods for strengths and deficiencies, conduct supporting analytical and experimental research to rectify the deficiencies, incorporate state-of-the-art improvements into the analysis methods, and finally verify the improvements by systematic test programs.

To provide representatives from government, industry, and universities with the latest findings and progress toward improved aircraft turbine engine durability, a two-day workshop was held in October 1983. This publication contains the papers presented at the workshop.

Daniel E. Sokolowski
Manager, HOST Project

Page intentionally left blank

CONTENTS

Page

Turbine Engine Hot Section Technology (Host) Project
Daniel E. Sokolowski and C. Robert Ensign, Lewis Research Center 1

INSTRUMENTATION

Host Instrumentation R&D Program - Overview
D. R. Englund, Lewis Research Center 7

Hot Section Viewing System
William W. Morey, United Technologies Research Center 11

Dynamic Gas Temperature Measurement System
Denny L. Elmore, Woodrow W. Robinson, and William B. Watkins, Pratt and Whitney Aircraft Engineering Division 17

High Temperature Static Strain Sensor Development Program
Charles Hulse and Richard Bailey, United Technologies Research Center, and Howard Grunt, Pratt and Whitney Aircraft 37

Demonstration Test of Burner Liner Strain Measurement Systems: Interim Results
Karl A. Stetson, United Technologies Research Center, and Howard P. Grant, Pratt and Whitney Aircraft 41

Development of Heat Flux Sensors for Turbine Airfoils and Combustor Liners
William H. Atkinson, Pratt and Whitney Aircraft 45

Laser Anemometry for Hot Section Applications
Richard G. Seasholtz, Lawrence G. Oberle, and Donald H. Weikle, Lewis Research Center 57

Time-of-Flight Anemometer for Hot Section Applications
Robert V. Edwards, Case Western Reserve University 69

TURBINE HEAT TRANSFER

Turbine Heat Transfer
John E. Rohde, Lewis Research Center 73

Gas Flow Environmental and Heat Transfer Nonrotating 3D Program
T. Geil and J. Steinhoff, University of Tennessee Space Institute 79

Gas Side Heat Transfer
Larry D. Hylton, General Motors Corp. 87

Assessment of a 3-D Boundary Layer Code to Predict Heat Transfer and Flow Losses in a Turbine
Veer N. Vatsa, United Technologies Research Center 101

Gas-Side Heat Transfer with Rotation
Robert P. Dring, United Technologies Research Center 107

Coolant Passage Heat Transfer with Rotation
L. D. Aceto and G. J. Sturgess, Pratt and Whitney 111

Jet Array Impingement Heat Transfer Characteristics
L. W. Florschuetz and D. E. Metzger, Arizona State University 117

COMBUSTION

Combustion Hot Section Technology
David B. Ercegovic, Lewis Research Center 129

Aerothermal Modeling Program - Phase I
R. Srinivasan, R. Reynolds, K. Johnson, and H. Mongia, Garrett Turbine Engine Co. 131

Aerothermal Modeling - Phase I
G. J. Sturgess, Pratt and Whitney Engineering 135

Aerothermal Modeling - Phase I
M. J. Kenworthy, General Electric Co. 139

Dilution Jet Mixing Program - Phase II
R. Srinivasan, E. Coleman, K. Johnson, and H. Mongia, Garrett Turbine Engine Co. 145

Mass and Momentum Turbulent Transport Experiments
B. V. Johnson, United Technologies Research Center 149

STRUCTURES

Host Structural Analysis Program - Overview
R. H. Johns, Lewis Research Center 153

Burner Liner Thermal/Structural Load Modelling
R. J. Maffeo, General Electric Co. 159

Component-Specific Modeling
M. L. Roberts, General Electric Co. 165

3D Inelastic Analysis Methods for Hot Section Components
L. T. Dame and R. L. McKnight, General Electric Co. 175

3-D Inelastic Analysis Methods for Hot Section Components (Base Program)
E. S. Todd, Pratt and Whitney Engineering 179

Validation of Structural Analysis Methods Using Burner Liner Cyclic Rig Test Data
R. Thompson, Lewis Research Center 181

Host Liner Cyclic Facilities
Donald Schultz, Lewis Research Center 195

FATIGUE

Life Prediction and Constitutive Behavior
G. R. Halford, Lewis Research Center 205

Creep Fatigue Life Prediction for Engine Hot Section Materials (Isotropic)
Vito Moreno, Pratt and Whitney, United Technologies Corp. . . . 209

Constitutive Modeling for Isotropic Materials
A. Kaufman, Lewis Research Center 211

Constitutive Modeling for Isotropic Materials
R. H. Van Stone, L. T. Dame, R. L. McKnight, and J. H. Laflen, General Electric Co. 215

Constitutive Modeling for Isotropic Materials
Ulric S. Lindholm, Southwest Research Institute 217

Life Prediction and Constitutive Models for Anisotropic Materials
Robert C. Bill, Lewis Research Center 221

SURFACE PROTECTION

Surface Protection Overview
Stanley R. Levine, Lewis Research Center 227

Turbine Airfoil Deposition Models
Daniel E. Rosner, Yale University 233

Depostion Model Verification
Suleyman A. Gokoglu, Analex Corp. 241

Effects of Surface Chemistry on Hot Corrosion Life
R. E. Fryxell, General Electric Co. 251

Coating Life Prediction
Michael A. Gedwill, Lewis Research Center 255

Concluding Remarks: Host Second Annual Workshop
Daniel E. Sokolowski, Lewis Research Center 265

D

TURBINE ENGINE HOT SECTION TECHNOLOGY (HOST) PROJECT

Daniel E. Sokolowski
and
C. Robert Ensign

National Aeronautics and Space Administration
Lewis Research Center
Cleveland, OH 44135

The Hot Section Technology (HOST) Project is a NASA-sponsored endeavor to improve the durability of advanced gas turbine engines for commercial and military aircraft. Through improvements in the analytical models and life prediction systems, designs for future hot section components -- the combustor and turbine -- will be more accurately analyzed and will incorporate features required for longer life in the more hostile operating environment of high performance engines.

Started in 1981, the project has activities presently planned through 1989 with an estimated total cost of $50-million. While the focused research activities are necessarily analytical in nature, significant experimental testing is required for benchmark quality assessments as well as model verifications. The efforts are being conducted in-house at the NASA Lewis Research Center, under contracts at major domestic turbine engine manufacturers, and under grants to qualified universities. Currently, the contract and grant funding equals about 60-percent of the total.

At NASA Lewis Research Center, the HOST project is the major element in a project management and coordination office and serves as the focal point for advocacy, funding, technical coordination, and information exchange. This workshop serves as the primary vehicle for this last function; that is, to disseminate information and elicit the exchange of ideas among participants.

The activities of the HOST project are accomplished within six disciplines as shown in Figure 1. Management of the project's efforts is delegated to six Subproject Managers (Figure 2) in the following areas: Structural Analysis, Fatigue & Fracture, Surface Protection, Combustion, Turbine Heat Transfer, and High Temperature Instrumentation. Structural Analysis includes research into thermal mechanical load models, component geometry specific models, and 3-D inelastic analysis methods development. Fatigue and Fracture includes constitutive model development for both isotropic and anisotropic materials, including single crystal and directionally solidified forms. It also includes research in life prediction methods for creep-fatigue interactions, and elastoplastic crack propagation. The Surface Protection research includes studies of corrosion and oxidation phenomena, environmental mechanics models, and metallic and thermal barrier coating analysis method developments. The

Combustion work includes aerothermal model assessment and development, dilution jet modeling, high pressure flame radiation/heat flux testing, and development of a thermal structural cyclic test facility. The Turbine Heat Transfer area is studying 2-D and 3-D flow and heat transfer on airfoil external boundaries, emphasizing boundary layer transition and viscous modeling. It also investigates coolant passage heat transfer, including midchord jet impingement cooling and rotational passage effects. Instrumentation is being developed to obtain high temperature, benchmark quality data to develop and verify the analysis methods. These include flow sensors (LDV), heat flux sensors (thin film), strain sensors (1800^{o}F static thin film), gas temperature sensors (frequency compensated), and hot section optical viewing systems.

Schedules for activities under each discipline are shown in Figures 3-8. Because of the nature of the problem of durability, interdisciplinary cooperation is often required and the synergistic effects have proven to be beneficial. For example, researchers in combustors, high temperature instrumentation, and structural analysis are jointly investigating combustor liner behavior, modeling, and life prediction.

Workshop publications and most contractor final reports carry the label "For Early Domestic Dissemination" (FEDD) to protect national interests and, thus, are available only to qualified U.S. citizens. While several contractor final reports have been published recently, they represent initial phases of multi-phased work. Thus, aside from this annual workshop report, only a few reports are available at this time.

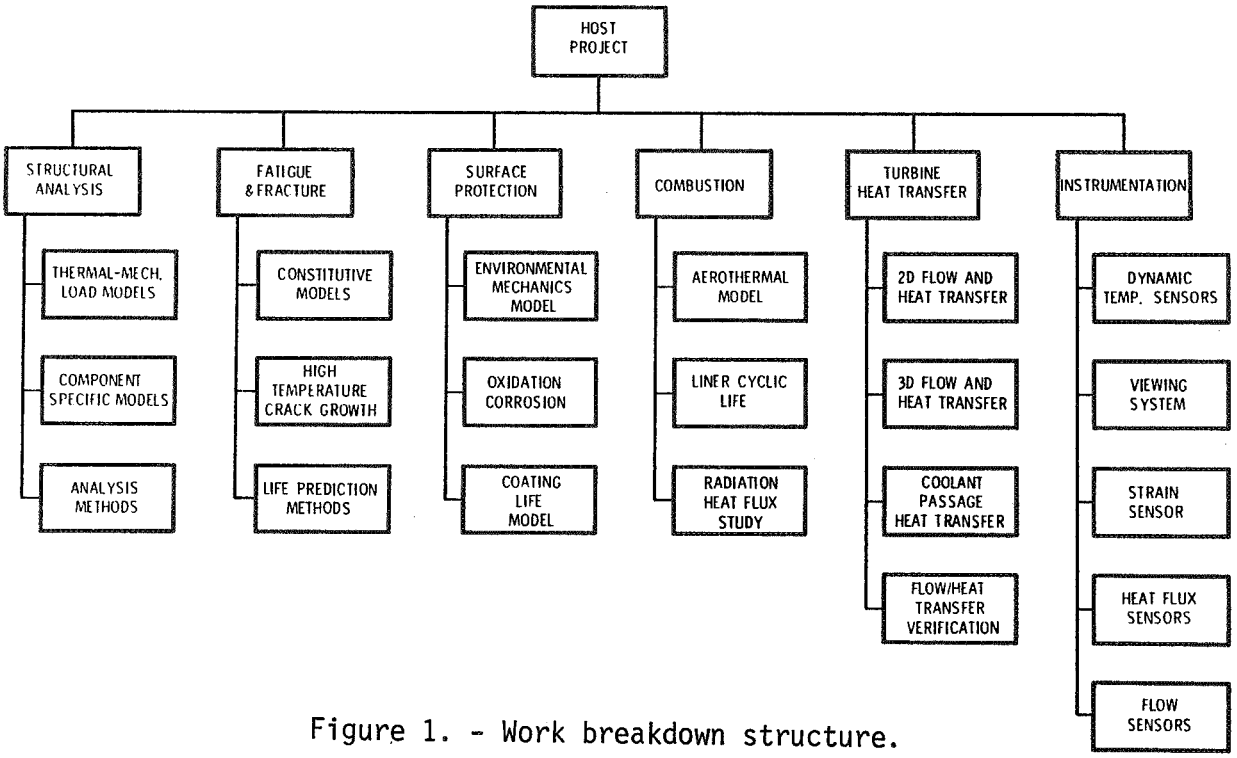

Figure 1. - Work breakdown structure.

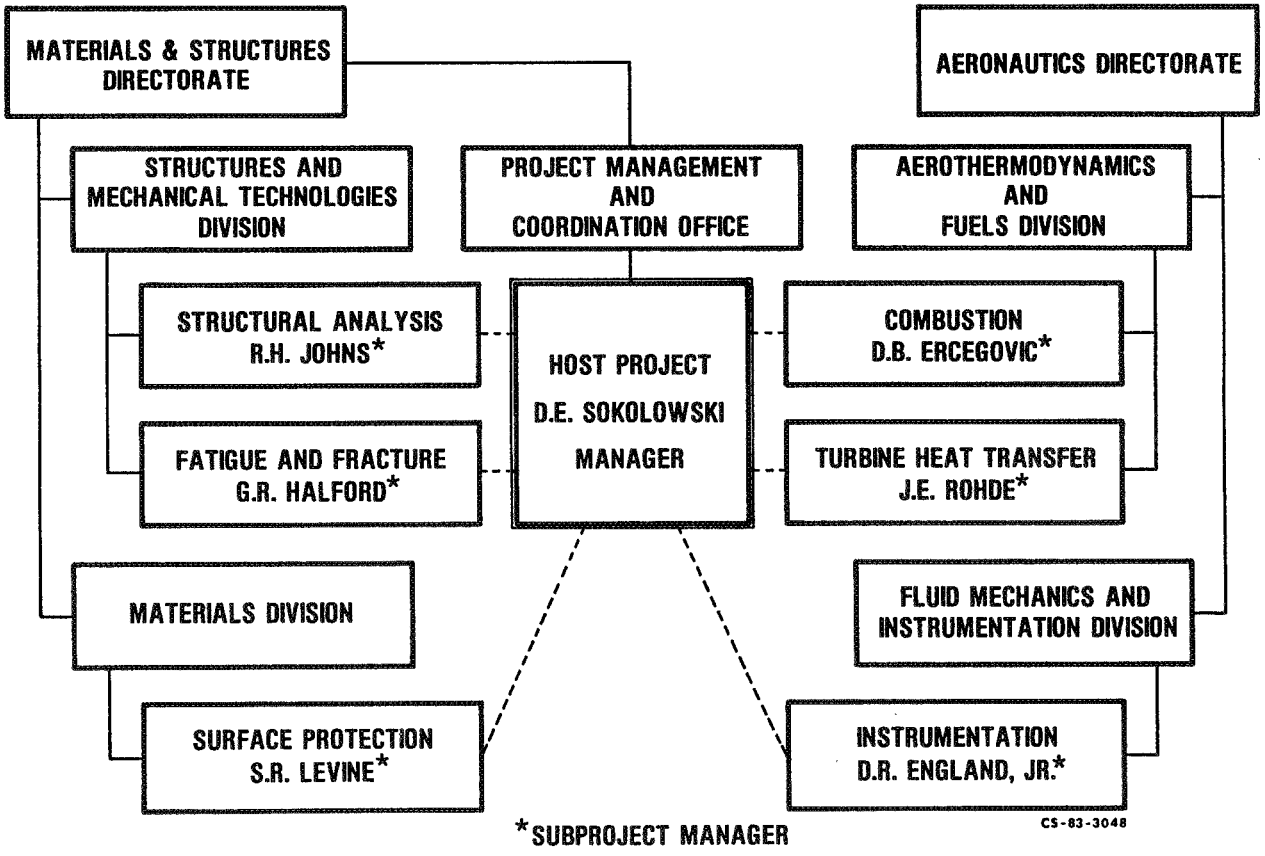

Figure 2. - Project office organization.

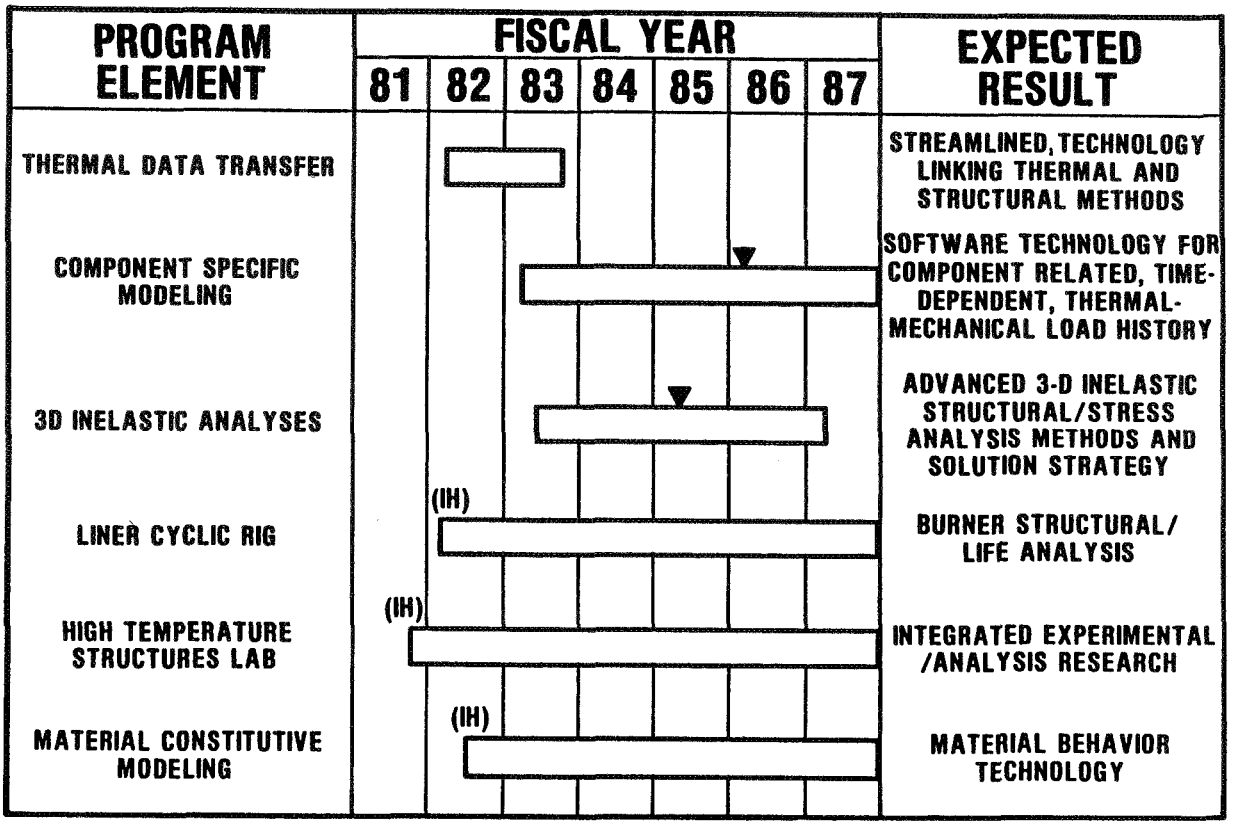

Figure 3. - Structural analysis.

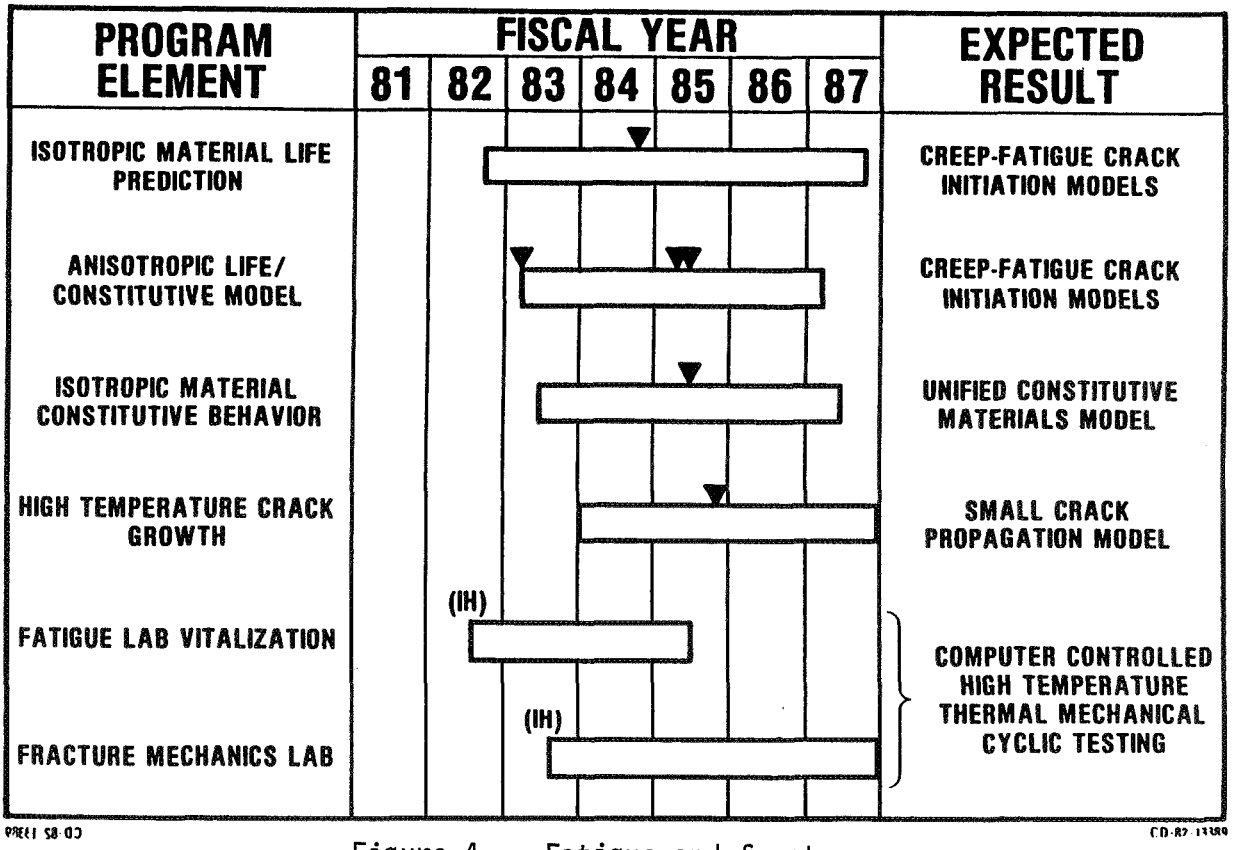

Figure 4. - Fatigue and fracture.

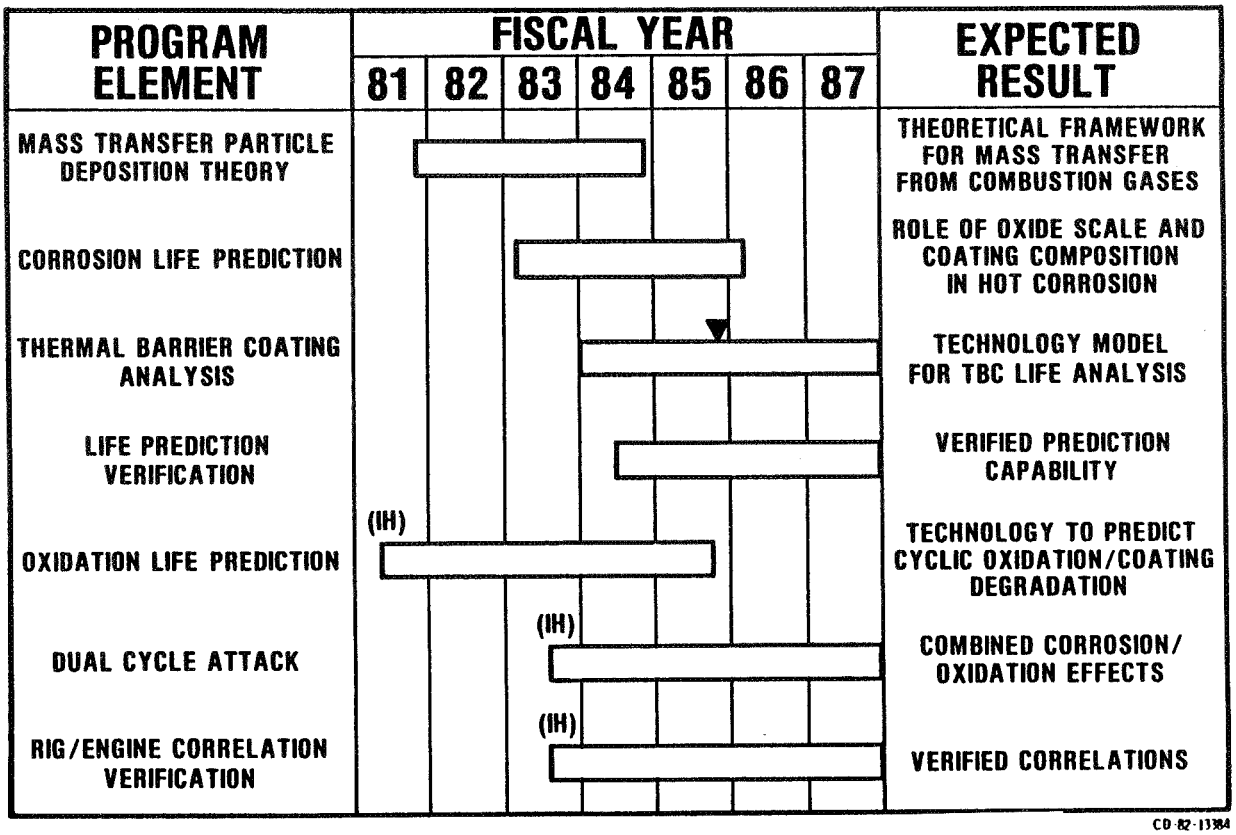

Figure 5. - Surface protection.

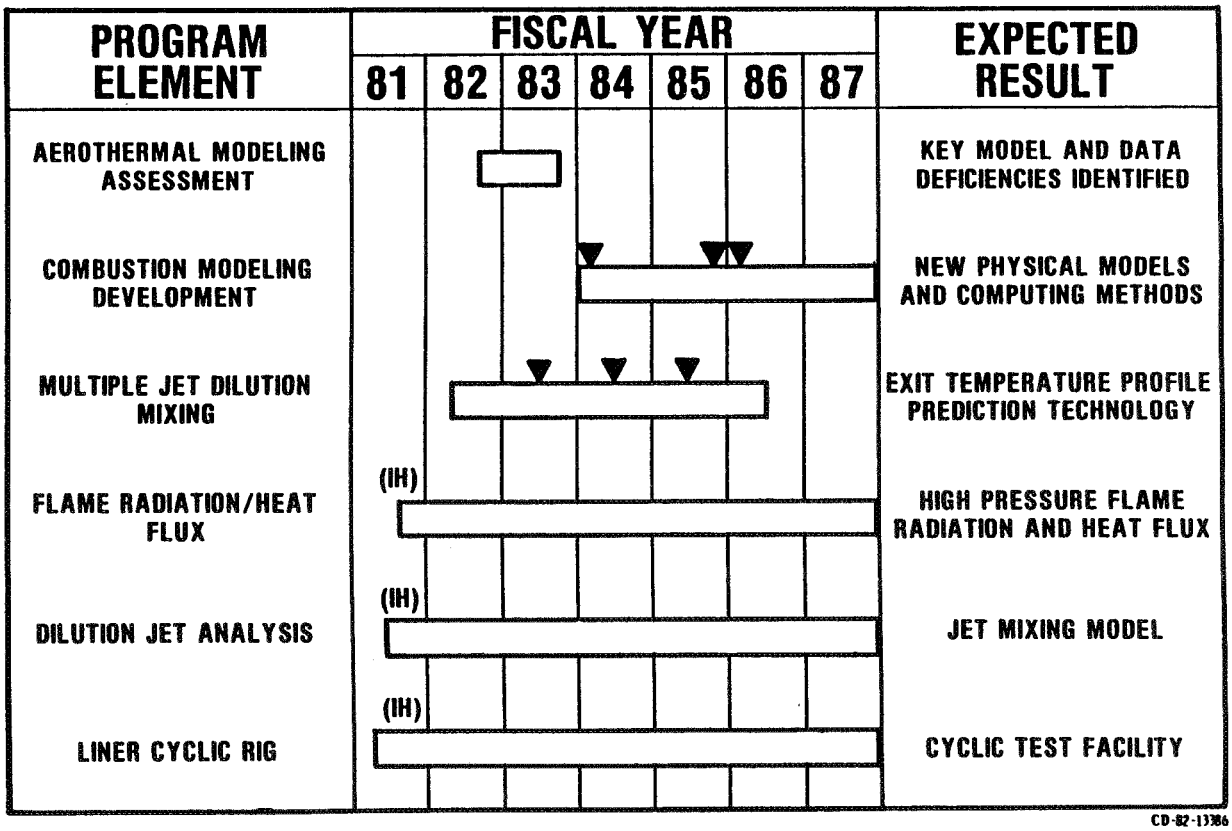

Figure 6. - Combustion.

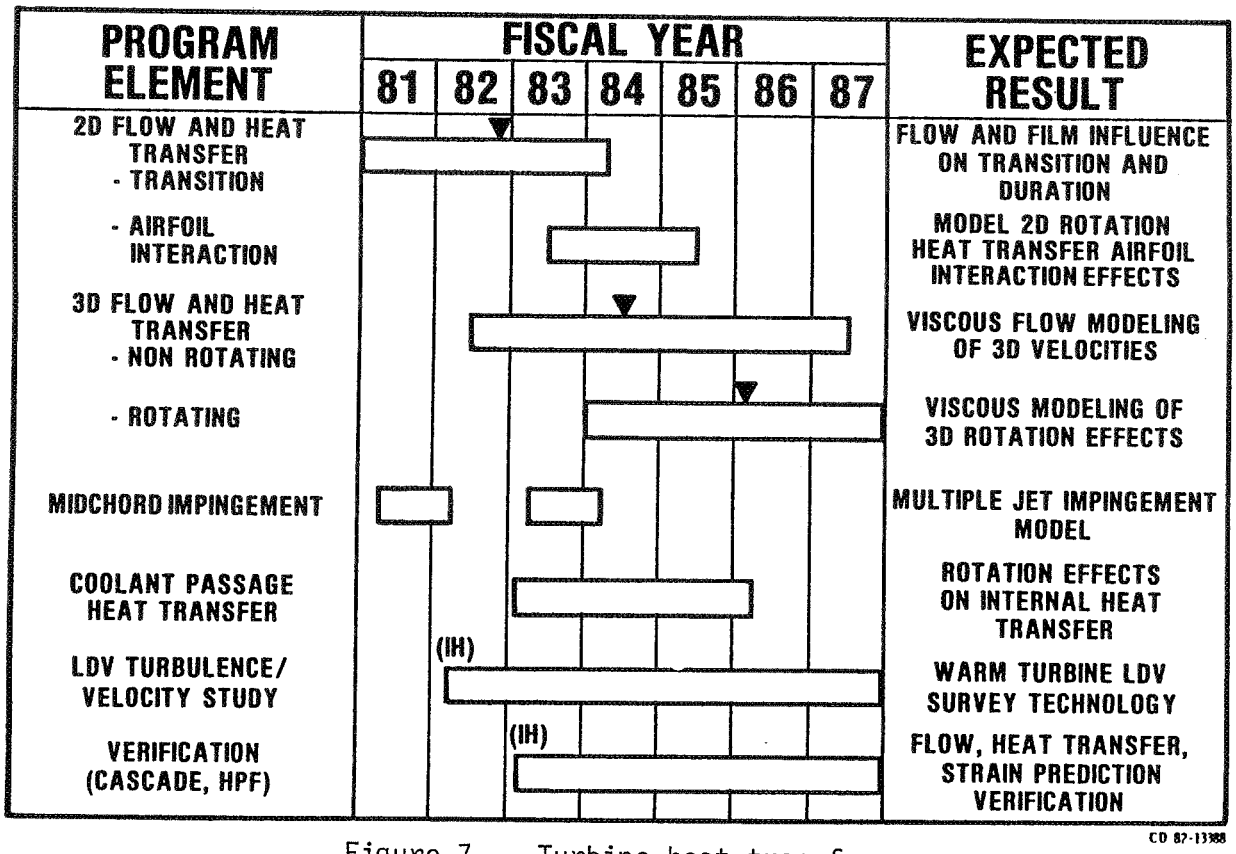

Figure 7. - Turbine heat transfer.

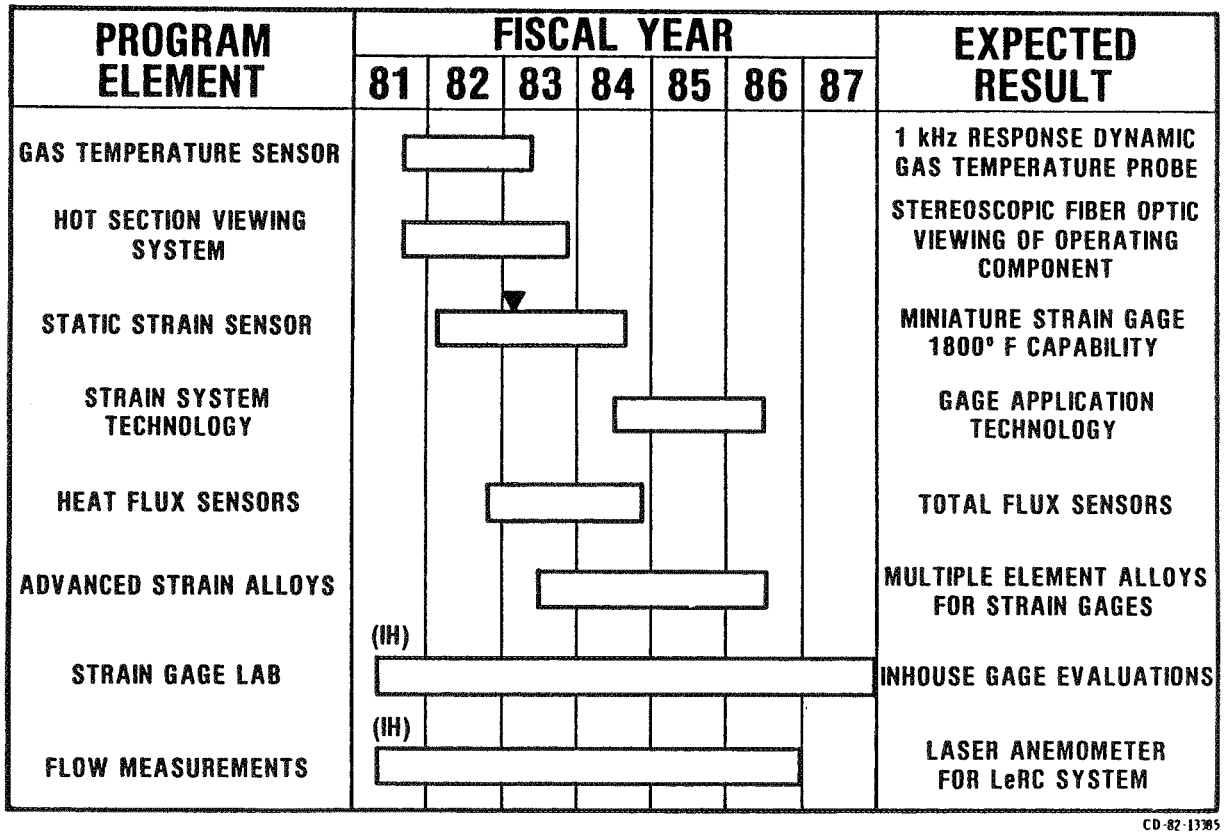

Figure 8. - Instrumentation.

D2

HOST INSTRUMENTATION R&D PROGRAM

OVERVIEW

D. R. Englund
National Aeronautics and Space Administration
Lewis Research Center
Cleveland, Ohio 44135

The HOST Instrumentation R&D program is focused on two categories of instrumentation. One category is that required to characterize the environment imposed on the hot section components of turbine engines. This category includes instruments for measuring gas flow, gas temperature, and heat flux. The second category is that for measuring the effect of the environment on the hot section components. This category includes strain measuring instruments and an optical system for viewing the interior of an operating combustor to detect cracks, buckling, carbon buildup, etc.

The HOST Instrumentation R&D program was formulated to concentrate on the critical measurements that could not be made with commercially available instruments or with instruments already under development via NASA- or DOD-funded efforts, or in IR&D programs. Over the past year we have not added any new measurements to the program.

The HOST Instrumentation R&D program schedule is included in the accompanying figures. The program schedule shows all HOST-funded efforts plus non-HOST-funded efforts that were initiated prior to HOST and which have HOST-related goals. Each line represents a separate effort, either contract, grant, or in-house. In two of these efforts, the turbine blade/vane static strain gage and the dynamic gas temperature measurement system, follow-on work is shown beyond the original contract.

The heaviest resources are concentrated on the measurements of strain and gas flow because these measurements are critical to the success of the HOST program and because the HOST requirements differ from the current state of the art by a considerable margin. Follow-up and complementary efforts not shown in the schedule are being planned for the strain measurement area.

HOST INSTRUMENTATION R&D PROGRAM

GENERAL GOALS:

- DEVELOP INSTRUMENTATION FOR CHARACTERIZING THE ENVIRONMENT AROUND TURBINE ENGINE COMPONENTS
- DEVELOP INSTRUMENTATION FOR CHARACTERIZING THE EFFECT OF THE ENVIRONMENT ON THE TURBINE ENGINE COMPONENTS

CS-83-2793

HOST INSTRUMENTATION R&D PROGRAM

SHOWING ACTIVE EFFORTS AS OF 10/83

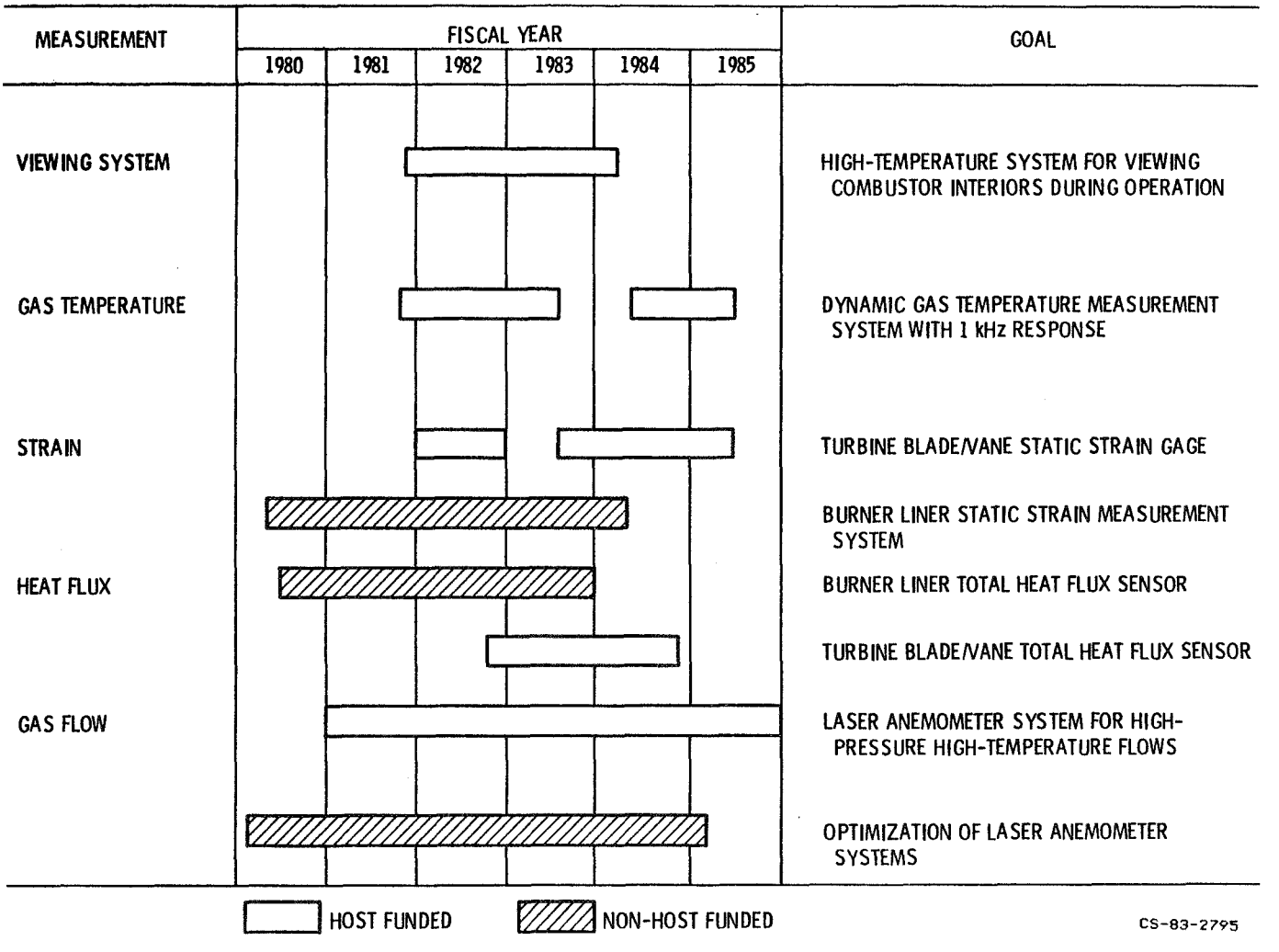

CS-83-2795

TURBINE ENGINE HOT SECTION TECHNOLOGY

INSTRUMENTATION SESSION AGENDA

OVERVIEW	D. ENGLUND, LeRC
COMBUSTOR VIEWING SYSTEM	W. MOREY, UTRC
DYNAMIC GAS TEMPERATURE PROBE	W. WATKINS, P&W GPD
TURBINE BLADE/VANE STATIC STRAIN GAGE	C. HULSE, UTRC
BURNER LINER STRAIN MEASUREMENTS	K. STETSON, UTRC
HEAT FLUX SENSORS FOR BURNER LINERS AND TURBINE BLADES AND VANES	W. ATKINSON, P&W CE
HOT SECTION LASER ANEMOMETRY	R. SEASHOLTZ, LeRC R. EDWARDS, CWRU

CS-83-2794

Page intentionally left blank

D3

HOT SECTION VIEWING SYSTEM

William W. Morey
United Technologies Research Center
East Hartford, Connecticut 06108

The objective of the hot section viewing program is to develop a prototype optical system for viewing the interior of a gas turbine combustor during high temperature, high pressure operation in order to produce a visual record of some causes of premature hot section failures. The program began by identifying and analyzing system designs that would provide clearest images while being able to survive the hostile environment inside the combustion chamber. Different illumination methods and computer techniques for image enhancement and analysis were examined during a preliminary test phase. In the final phase of the program, which will be discussed in this presentation, the prototype system was designed and fabricated and is currently being tested on a high pressure combustor rig.

The combustor viewing system consists of a 12.7 mm diameter viewing probe with an actuator unit that mounts onto a rig or engine, an optical interface unit to transfer images to video and film cameras and provide illumination light, and two control chassis for remote operation of the probe and the optics interface unit. Probe actuation consists of a $\pm 180^{\circ}$ rotation from a downstream view and insertion radially along the combustor axis with a depth range of 7.6 cm. In order to cover a wide range of views, two viewing probes were constructed. One probe has a wide view, the other a narrow view. Both probes have their direction of view angled off the probe axis so that the view can be scanned on rotation. In addition, each probe has a choice of two lenses. The wide field probe has 90° and 60° field-of-view lenses, and the narrow field probe has 35° and 13° field-of-view lenses. For the wide field probe the view is oriented at 45° to the probe axis by bending the fiber optic image bundle. A cross section view of this probe is shown in figure 1. Since the lens focal lengths are much longer for a narrow field-of-view, the narrow field probe had to use a mirror to turn the view from the probe axis. Figure 2 shows a cross section of the narrow field probe.

Both probes are made of copper and have water-cooled walls. Four baffles in the probe walls guide cooling water to the distal end of the probe. Hot, soot-ladened combustor gas is kept from the probe interior and from the fiber and lens exposed surfaces with a flow of purge gas. The gas flows down the center of the probes and exits around the illuminating fibers and out of the lens aperture or across the mirror in the case of the narrow field probe and into the combustor. The probes were designed to handle the high heat fluxes expected in a primary combustion zone. A finite element analysis indicated that the probe tip temperatures were well within material limits and that cooling water at the probe tip should be below the boiling point. Measured temperatures were about 50°C higher than calculated.

The image carrying fiber element is 3 mm in diameter and consists of a fused bundle of about 75,000, 10 μm diameter fibers. Each fiber corresponds to a picture element. The fused fiber bundle is 33 cm long and transfers the image from the viewing lens at the distal end of the probe to the opposite end of the probe where it is butt-coupled to a 3 m long flexible fiber bundle. The flexible bundle transfers the image to the optics interface unit for recording by video or film cameras. One millimeter diameter plastic clad fused quartz fibers, shown in the

figures, were used for transferring the illumination light source. Two fibers were used in each probe. There are also two thermocouples mounted in each probe tip.

The viewing probe mounted in its actuator along with the remote control chassis is shown in figure 3. The purge gas line connects to the upright fitting on the left-hand side of the probe and the four bent tubes with connectors are for the probe water cooling. A separate line is used for cooling the actuator case and mounting plate. The remote control unit has a probe tip temperature indicator along with water, gas, and temperature interlocks. Probe depth is indicated with an LED bargraph meter. Rotation is indicated in degrees with a digital panel meter. The rotational speed can be varied. Another view of the probe and actuator with covers removed is shown in figure 4. The flexible fiber bundle can be seen leaving in the upper left-hand corner of the figure, and the actuator motors for depth and rotation can be easily identified along with their position indicating potentiometers.

The optics interface unit is shown in figure 5. The 3 m long fiber optic image bundle from the probe comes into a filter wheel in the upper left-hand corner of the figure. A series of eight different optical filters can be used such as neutral density, color, and interference filters to vary exposure and spectral range. A pneumatically-controlled slide positions a mirror that directs the image from the filter wheel to a video camera. When the mirror is positioned away from the line-of-view, the image can be seen with a film camera. A mercury arc lamp, its power supply, and the two illuminating fibers are on the right-hand side of the board. A second pneumatically-operated mirror directs the collimated and focused arc lamp light to the fiber ends. With the mirror out of position, a laser light beam can be focused into the fibers. There is also a control chassis that permits remote operation of the filter wheel, mirrors, and cameras with position indicators.

Tests are currently underway with the viewing system in a high pressure combustor rig. A modified JT-12 combustor liner is used in the rig as illustrated in figure 6. Three viewing ports on the side of the rig are available for mounting the probe. Two of the ports are shown in the figure with the probe attached to port 1. The depth range of the probe (7.6 cm) in relation to the combustor is also shown in the figure. Both film and video data of the combustor liner surfaces will be recorded along with probe temperature and operational conditions.

WIDE FIELD PROBE

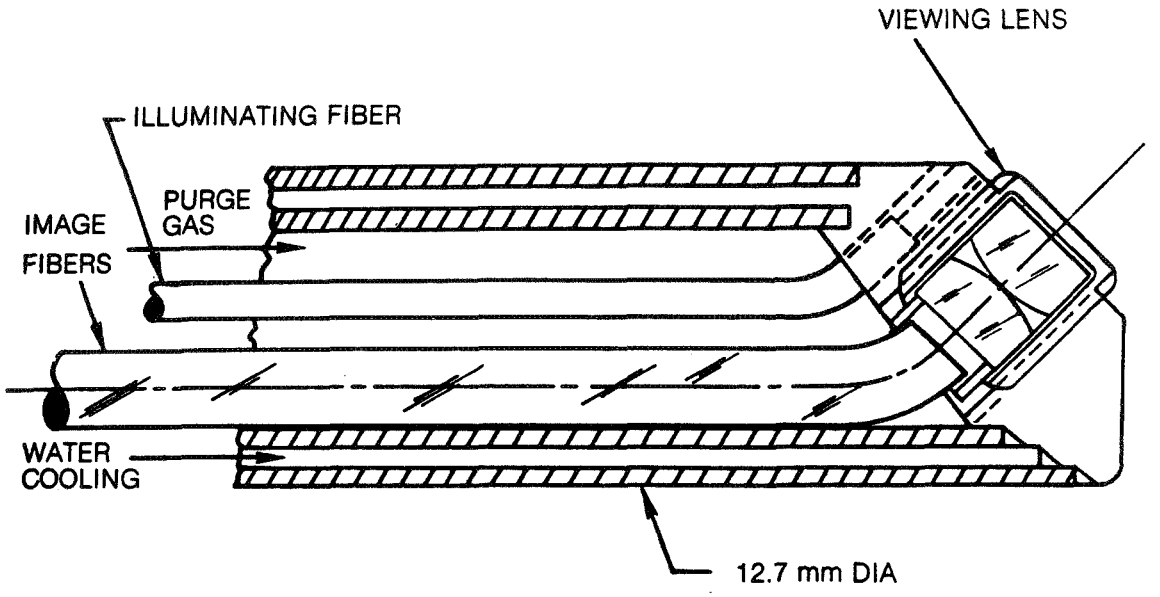

Figure 1

NARROW FIELD PROBE

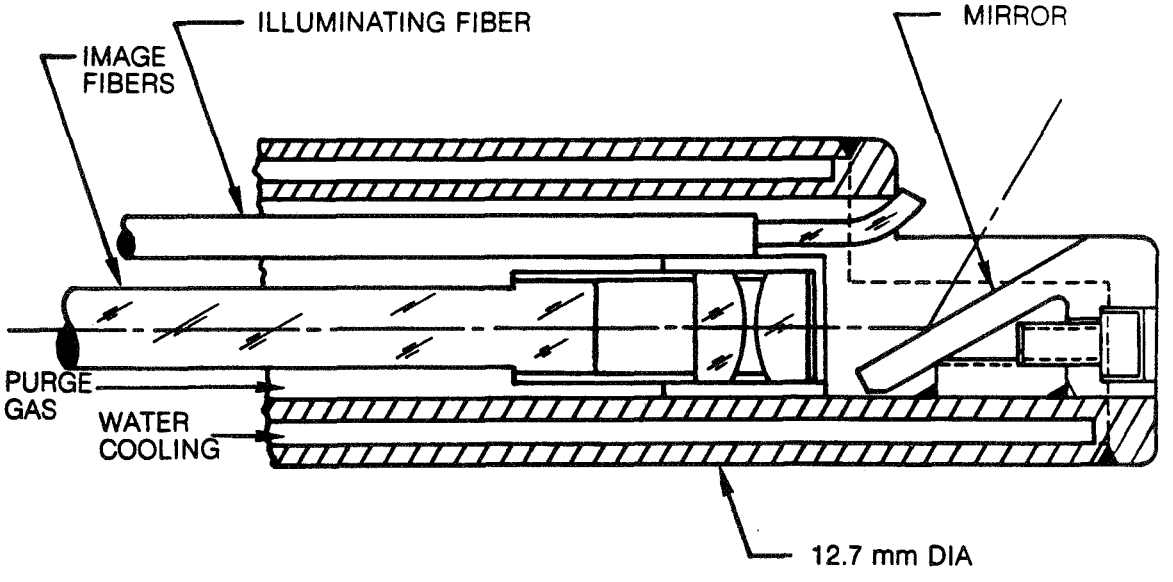

Figure 2

COMBUSTOR VIEWING PROBE AND CONTROL UNIT

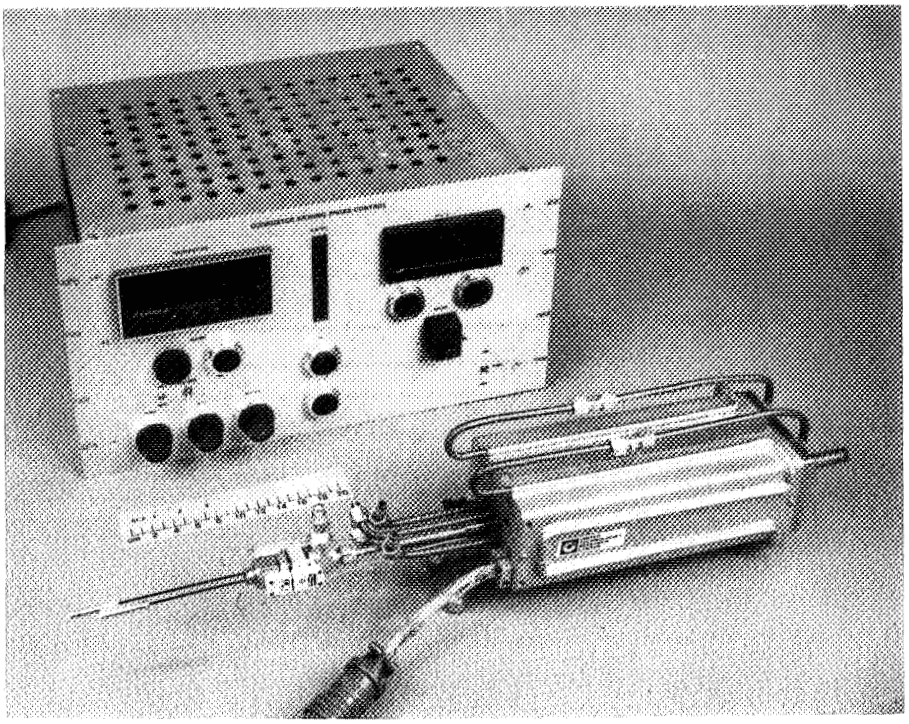

Figure 3

VIEWING PROBE AND ACTUATOR

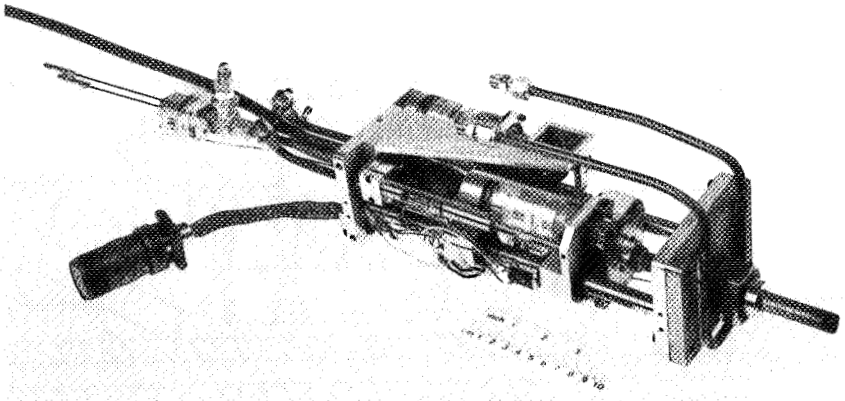

Figure 4

OPTICS INTERFACE BOARD

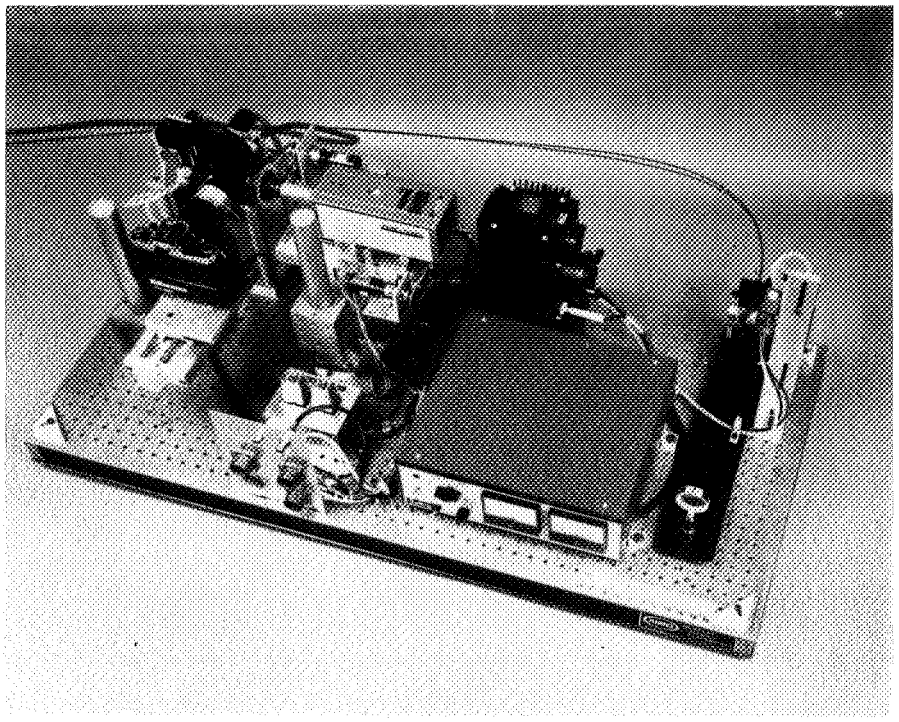

Figure 5

HIGH PRESSURE COMBUSTOR

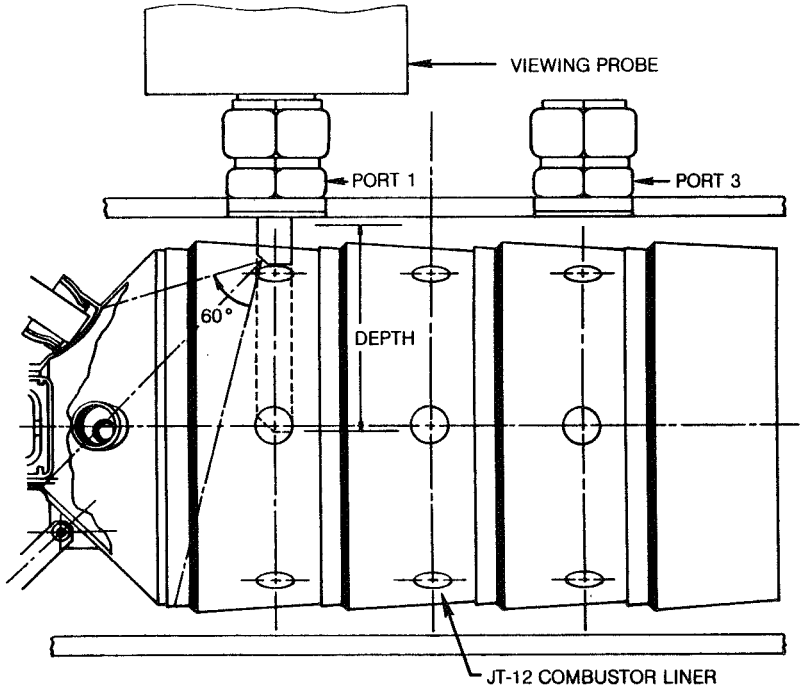

Figure 6

Page intentionally left blank

Dynamic Gas Temperature Measurement System*

Denny L. Elmore, Woodrow W. Robinson and William B. Watkins
Pratt and Whitney Aircraft Engineering Division

SUMMARY

The objective of this effort was to develop a gas temperature measurement system with compensated frequency response of 1 KHz and capability to operate in the exhaust of a gas turbine combustor (Figure 1). Results of the initial portions of this effort were reported in the first Hot Section Technology Conference (Reference 1). Further progress in this development effort is summarized in this presentation. Environmental guidelines for this measurement are presented, followed by a preliminary design of the selected measurement method. Transient thermal conduction effects were identified as important; a preliminary finite-element conduction model quantified the errors expected by neglecting conduction. A compensation method was developed to account for effects of conduction and convection. This method was verified in analog electrical simulations, and used to compensate dynamic temperature data from a laboratory combustor and a gas turbine engine. Detailed data compensations are presented. Analysis of error sources in the method were done to derive confidence levels for the compensated data.

Environmental Guidelines and Sensor Selection

The sensor design and environmental guidelines for this effort are listed in Figure 2. Environmental parameters are representive of a modern gas turbine engine combustor exhaust, and sensor life, accuracy, spatial resolution and vibration capability are nominal goals for experimentation.

The sensor approach chosen for development is shown in Figure 3. The thermocouple employs two wires of different sizes to obtain data necessary for evaluation of the time constant for each wire. If two thermocouples are positioned in close proximity such that both are exposed to the same instantaneous temperature and velocity, the difference in their thermal responses will be governed by their relative diameters. These responses can then be used to obtain time constants for compensating the thermocouples. The unique feature of these wire thermocouples is a beadless laser butt-welded element, which allows the geometry to be modelled as a cylinder in crossflow.

A detailed review of the platinum/rhodium alloys tensile strengths, melting temperatures, emf outputs, thermal conductivities, stresses to rupture, and specific heats was made. Tensile and stress-rupture values are higher for increasing rhodium content, indicating the best thermocouple should have a high rhodium content. The Type B (platinum - 6% rhodium/platinum - 30% rhodium) was selected over the other commercially available thermocouple materials based on its higher emf output, availability, and known fabrication characteristics. Detailed structural analysis revealed that allowable yield stresses contrained design length-to-diameter ratios to less than 6.5 for the support wires and less than 15.5 for the thermocouple elements.

* Work performed under contract NAS3-23154

Probe Thermal Analysis and Compensation Method

A preliminary thermal model of the thermocouple probe wires was generated to evaluate the effects of radiation losses and end conduction losses. Governing equations and the model nodal breakup are shown in Figures 4 and 5 respectively. The physical thermocouple junction, the small wire, and the larger support wires were simulated by a finite difference model. The gas temperatures were assumed to be periodic fluctuations. The worst case gas temperature was assumed to be a mean gas temperature of 1400K ($2520^{o}R$) with fluctuations of $\pm$ 500K ($\pm$ $900^{o}R$). The more realistic case defined in the data acquisition analysis, $\pm$ 65K ($\pm$ $117^{o}R$) was also evaluated. These cases were evaluated at frequencies of 20, 100, and 1000 Hz.

Results of the transient simulations (shown in Figure 6) indicate that radiation heat losses are not significant (less than 10K), but the conduction losses are too large (maximum of 67K) to be ignored and because of structural requirements previously discussed, cannot be reduced by making the wires longer. This discovery required that analysis of the measured temperature data be performed with a second order equation containing both conduction and convection terms, rather than the simplified first order equation containing only convection terms. The second order energy equation is a linear equation in time and space, whereas the first order equation is only time dependent.

A compensation method which accounts for both conduction and convection effects was developed. A second finite difference model using nine nodes (Figure 10) was used for the remainder of the calculations in this effort. The method is outlined in Figure 7 and explained below.

1. The theoretical transfer functions between the 76μm (3 mil) t/c signal θ_1 and the gas stream signal a_n and the 254μm (10 mil) t/c signal θ_2 and the gas stream are computed from the finite difference solution of the differential equations for various values of an aerodynamic parameter Γ, at a number of discrete frequencies falling between the corner frequencies of the two t/c's. These data are then used to compute the theoretical transfer function $H_t(f)$ between the 254μm (10 mil) t/c and the 76μm (3 mil) t/c (θ_2/θ_1) for the corresponding values of Γ and frequency. These curves (θ_2/θ_1) will be used to determine the insitu value of Γ from the measured transfer function of θ_2/θ_1. The process is as follows:

   a. The following parameters are input or already stored in the computer. For the thermocouple wire - L, l, D, d, ρ_w, Kw, Cp_w, and αw. For the gas stream - ρ_g, K_g, Cp_g, γ_g, μ_g and Pr_g.

   b. The average or mean conditions for the test data for the following variables are entered into the computer:

      T = mean gas temperature
      P = mean gas pressure
      F/A = fuel air ratio
      f_1-f_x = frequencies of f_n at which transfer functions will be evaluated
      Mn = Mach No.

   c. The program computes an estimated value of Γ based on the test conditions.

d. The program then computes ζ_9, the transfer function between the wire thermocouples and the gas stream, for the 76 μm (0.003 in.) and the 254 μm (0.010 in.) thermocouple from 0.5 Γ to 1.5 Γ in steps of 0.1 Γ at frequencies f_1 ....., f_x which are user selected to fall in between estimated values of the corner frequencies of the two t/c's. The equations are evaluated until steady state conditions are reached. The computer code determines the sampling interval for each frequency evaluated to ensure mathematical stability of the finite element model and minimize computation time. The normalized ratio of the magnitude of the temperature fluctuation in the wire to the temperature fluctuation of the gas stream ($\zeta_9 = \theta_n/a_n$) at frequency f_n is determined by locating the maximum peak amplitude after the model has iterated to steady-state conditions. The phase shift (η_x) of the temperature fluctuation in the wire is determined by locating the time at which the ζ_9 crossed zero going positive at the beginning of the period in which the model reached steady-state conditions.

e. The data from (d) are then used to compute the theoretical transfer function θ_{2n}/θ_{1n} from 0.5 Γ to 1.5 Γ at frequencies of f_1 through f_x.

2. Thermocouple test data are digitized into the Fourier system computer, typically 32 to 120 records each of the 76 μm t/c dynamic signal and the 254 μm t/c dynamic and dc signals. Each record contains 2048 samples of data. These data are then converted from millivolts to temperature utilizing NBS calibration curve coefficients for type B thermocouples. The 254 μm dc channel is utilized as the mean for both dynamic data channels in converting the nonlinear t/c mv singals to linearized temperature. These data records are then saved for recall for additional processing or plotting.

3. An ensemble averaged FFT (Fast Fourier Transform) transfer function analysis is then performed on x number of records of the dynamic records to yield the measured value of θ_{2n}/θ_{1n} as a function of frequency. The transfer function is computed as the FFT crosspower divided by the FFT autopower of the 76 μm signal:

$$H_e(f) = \frac{\theta_{1n}\,\theta^*_{2n}}{\theta_{1n}\,\theta^*_{1n}} \rightarrow \frac{\theta_{2n}}{\theta_{1n}}$$

where * = complex conjugate multiplication.

In conjunction with the computation of the measured transfer function, the coherence function is computed and utilized to assess the quality of the measurement. For the 2048 time sample data record lengths utilized 1024 line FFT's are produced. For the typical sampling rate of 4096 Hz, the FFT analyses yield spectral information dc to 2048 Hz in 2 Hz intervals. A standard Hewlett Packard windowing function (P301) is utilized prior to computation of the FFT's. This window is characterized by excellent spectral amplitude accuracy ($\pm$ 0.1%). Side lobe suppression is $>$ - 70 db at $\pm$ spectral lines and the effective noise bandwidth is 3.4 spectral lines.

4. Each measured value of θ_{2n}/θ_{1n} at frequencies $f_n = f_1 - f_x$ are used in

conjunction with the theoretical curves of θ_{2n}/θ_{1n} vs Γ to determine a measured value of Γ (the program interpolates between the 0.1 Γ increments computed in (1) above). The arithmetic average obtained for each frequency is taken as the insitu measured value.

5. Using the measured insitu average value of Γ obtained in (4), ζ_9, the normalized transfer function (gain θ_{1n}/a_n and phase η_{1n}) of the 76 μm thermocouple with respect to the gas stream temperature is then computed at all frequencies from the 1st spectral line of the FFT spectrum to the Nyquist frequency of the FFT for each discrete frequency contained in the FFT. This is typically from 2 Hz to 2048 Hz in 2 Hz increments. This spectrum is then used to compensate the 76 μm t/c data as follows.

6. To compute the compensated ensemble averaged power spectral density function, the ensemble averaged auto power spectrum of the 76 μm (3 mil) t/c obtained in (3) above is divided by the auto power of its compensation spectrum:

$$\frac{\theta_{1n}\ \theta_{1n}^*}{\left(\left[\frac{\theta_{1n}}{a_n}\right]\left[\frac{\theta_{1n}}{a_n}\right]^*\right)} \rightarrow a_n^2$$

where * = complex conjugate multiplication.

Scaling factors for effective noise bandwidth and FFT Fourier symmetry are applied.

7. To compute the compensated instantaneous time waveform, an FFT spectrum is made on a specific data record. This spectrum is then divided by the compensation spectrum. The compensated spectrum is then inverse Fourier transformed to yield the compensated instantaneous time waveform. The software contains information on specific techniques employed to prevent time waveform distortions associated with the inverse Fourier transform. A threshold, in relative db, is applied to the frequency spectrum of the data signal prior to division by the compensation spectrum to prevent errors where the signal to noise ratio is too low.

$$\frac{\theta_{1n}\angle\eta_{1n} + \phi_n}{\left(\frac{\theta_{1n}}{a_n}\right)\angle\eta_{1n}} \rightarrow a_n \angle\phi_n$$

Sensor Test Program

The test program summarized in the following section was based on three test series consisting of (1) System Shakedown and Compensation Verification Lab Tests, (2) Laboratory Burner Tests, and (3) Full Scale F100 Engine Tests (Figure 8). These tests allowed for a step by step checkout and optimization of the various components of the system while allowing for the experimental evaluation and substantiation of sensor guidelines and development effort goals.

Equations were derived for the electrical analog equivalent, passive RC network of the nine node finite difference thermocouple model for use in lab evaluations of the dual t/c approach. Two breadboard nine node RC element network models, one for the 76 μm (3 mil) and one for the 254 μm (10 mil) thermocouple were fabricated. The circuits were modeled for the F100 probe geometry operating at the following conditions:

T_T = 1200^oK (1700^oF)
P_T = 19.7 atm (290 psia)
M_n = 0.233
F/A = 0.02.

Design values of resistance and capacitance for these simulators are shown in Figure 11 . Potentiometers were used for the resistive components and values were set by measurement with a digital ohmmeter ($\pm$ 1%). Values of capacitive components were combinations of standard value capacitors ($\pm$ 10%) and were not measured. Schedule constraints precluded obtaining more precise capacitance values.

The purpose of this test was to determine the compensation spectrum (gain and phase as a function of frequency) of the 76 μm (3 mil) analog circuit (and the 254 μm analog circuit) from the measured transfer function taken between the outputs of the analog circuits of the 76 μm (3 mil) t/c and the 254 μm (10 mil) circuit (Figure 9) utilizing the HOST software and compare it with the known frequency response spectrum (measured single input - single output using conventional FFT techniques). Wideband (1250 Hz BW) random noise was input in these measurements. Because of the lack of precision in the analog circuit components, thermocouple length and diameter values input to the HOST program compensation software were varied until best agreement between the HOST program results and the known compensation spectra were obtained. The conventionally measured spectra were generated by measuring the transfer function between the input and output of the analog circuit using the 256 ensemble averaged FFT transfer function:

$$H(f) = \text{Gain} \angle \text{ phase } (f) = \frac{G_{in}(f) G^*_{out}(f)}{G_{in}(f) G^*_{in}(f)}$$

where * = complex conjugate multiplication

The best match for the 76 μm (3 mil) t/c was obtained when it was modeled with an element diameter of 74.9 μm (2.95 mils) and an element length of 711.2 μm (28.00 mils). The analog circuits were designed to model the t/c as 76.2 μm (3.00 mils) diameter with a length of 609.6 μm (24.00 mils). Gain match was within $\pm$ 15% and phase match within + 4.2 to - 0.8 deg. over the frequency range of 4Hz to 1000Hz.

Similarly, for the 254 μm (0.010 in.) thermocouple case, the following parameters produced the best match of compensation spectra: the diameter was 260.4 μm (10.25 mils) and the length was 1587.5 μm (62.5 mils) as opposed to design values of diameter equal to 254 μm (10 mils) and length equal to 1587.5 μm (62.5 mils). Gain disagreement for this case was less than $\pm$ 5% out to 100Hz. The compensation program developed under this contract uses the 254 μm (10 mil) data only out to about 40Hz. The agreement between the two methods is satisfactory despite lack of precision in the capacitance values in the analog model. Experiments performed

with the analog circuits verified that the finite difference models of the thermocouples work as required. Minor discrepancies, due to lack of precision in electrical component values, could easily be corrected, given adequate time and resources.

Subscale combustor probes were fabricated based on the detailed designs shown in Figure 14, which also shows the completed probe. The subscale combustor probe element junctions were inspected to determine the junction's actual dimensions and weld uniformity. Each thermocouple junction was inspected under a Nikon Metaphot microscope at 100X or 200X magnification, Figure 15. Photomicrographs of each junction and a graduated scale were made to measure the junction diameter and uniformity of the wire cross section. Two angular orientations of each wire were photographed 90 degrees apart. A number of different readings of each photograph were obtained to define the mean value and precision of each sample. Measurement uncertainty of the technique is $\pm$ 2 μm (9×10^{-5} in.) for the 76 μm elements and 9 μm (4×10^{-4}) for the 254 μm elements. Effects of these uncertainties on temperature uncertainty were later determined in sensitivity analyses using the completed data reduction method.

The probe was installed and tested in the subscale combustor rig (Figure 16). The probe and a platinum tube used for measuring gas stream total pressure were mounted downstream of the combustor exit plane. The mounting system was retractable so the probe was not in the gas stream except when data were recorded.

Dynamic temperature data and ambient temperature data were recorded on FM tape. The output of each Preston amplifier was double recorded on the FM tape recorder (0.5V rms and 1.0V rms full-scale record level channels). The signal levels were monitored on an oscilloscope and the fixed gain setting(s) of the Preston amplifier(s) were set as necessary to maintain optimum signal levels on the 0.5V rms record channel. Gain settings were correlated with test points to maintain calibration. Data were recorded at ten steady-state combustor test conditions ranging from the minimum conditions obtainable with the combustor facility. Average gas temperatures varied from 1048K (1887°R) to 1797K (3235°R). The gas stream Mach number and total pressure was relatively constant at 0.23 and 1.0 atms, respectively.

Figure 17 are uncompensated and compensated dynamic temperature waveforms for the 3 mil thermocouple and test point 10. The uncompensated waveform has maximum fluctuations of approximately 400°F peak to peak with an rms value of 64°F. The compensated waveform has peak to peak fluctuations of approximately 1200°F and an rms value of 281°F. Figure 18 are uncompensated and compensated power spectral density plots for 120 record averages. Signal to noise ratios for compensated signal to compensated ambient noise are $>$18db up to 500Hz, $>$13db up to 1000Hz and $>$10db out to 2000Hz. A noticeable break in the compensated PSD can be seen at 1200Hz; this results from use of an anti-aliasing low-pass filter, and for this reason, signal to noise ratio from 1200 to 2000Hz is actually greater than 10db. Note that a combustor resonance is indicated by the peak at 145Hz.

The full scale test were conducted as planned in an F100 jet engine which was undergoing testing at P&WA's Government Products Division (GPD) test facility. Test conditions for the data which follows were: P = 158 psia, T = 1790°F, M = 0.355. Figure 19 shows the uncompensated and compensated dynamic temperature waveforms. The uncompensated waveform has peak to peak characteristics of about 400°F and rms value of 73°F. The compensated waveform has peak to peak charac-

teristics of greater than 2000°F, and rms value of 393°F. Figure 20 are power spectral density plots of compensated and uncompensated 120 record average data. Signal to noise ratio is >26db to 500Hz,>20db to 1000Hz and >14db to 2000Hz. The signal is basically wide band random, with no evidence of resonance.

Measurement Uncertainty

The overall compensation uncertainty was obtained by room-sum-squaring errors associated with finite-windowing effects in the Fast Fourier Transform, thermocouple element diameter measurement, temperature waveform ratios, and data acquisition/reproduce noise. These errors are shown in Figure 21 for two input waveforms. The 27°F peak to peak/$\sqrt{Hz}$ wideband random waveform and corresponding errors are representative of the signals observed experimentally.

LIST OF SYMBOLS

$\alpha = \dfrac{K_w}{\rho_w C_{pw}}$ = thermal diffusivity of the wire

L = length of thermocouple support wire

ℓ = one half of length of smaller thermocouple wire

D = diameter of thermocouple support wire

d = diameter of smaller thermocouple wire

ρ_w = density of thermocouple wire

K_w = thermal conductivity of thermocouple wire

C_{pw} = specific heat of ther thermocouple wire

ρ_g = density of the gas stream

C_{pg} = specific heat of the gas stream

P_{rg} = Prandtl number of gas stream

U_g = velocity of the gas stream

μ_g = viscosity of the gas stream

γ_g = ratio of specific heats of gas stream

θ_{1n} = amplitude of the 75 μm (0.003 in.) thermocouple at frequency f_n

θ_{2n} = amplitude of the 254 μm (0.010 in.) thermocouple at frequency f_n

a_n = amplitude of the gas temperature at frequency f_n

ϕ_n = phase shift of the gas temperature with respect to arbitrary time t_o at frequency f_n

η_{1n} = phase shift of 76 μm (0.003 in.) thermocouple with respect to gas temperature at frequency f_n

η_{2n} = phase shift of 254 μm(0.010 in.) thermocouple with respect to gas temperature at frequency f_n

λ_{1n} = phase shift of 76 μm (0.003 in.) thermocouple at frequency f_n with respect to arbitrary time t_o

λ_{2n} = phase shift of 254 μm (0.010 in.) thermocouple at frequency f_n with respect to arbitrary time t_o

$$\Gamma = \frac{0.48 k_g P_{rg}^{1/3} U_g^{1/2}}{\left(\frac{\mu_g}{\rho_g}\right)^{1/2} \rho_w C_{pw}} = \text{Aerodynamic parameter}$$

ζ = Theoretical transfer function (gain and phase) of the wire thermocouple x with respect to the gas temperature at frequency f_n

$H_f(f)$ = Theoretical transfer function between large and small thermocouples

$H_e(f)$ = Experimental transfer function between large and small thermocouple signals

K_g = thermal conductivity of the gas stream

REFERENCES

1. Elmore, D.; "Dynamic Gas Temperature Measurement System", Turbine Engine Hot Section Technology, NASA TM 83022, 1982.

DYNAMIC GAS TEMPERATURE MEASUREMENT SYSTEM

Objective - Develop a temperature measurement system with:

- Compensated frequency response of 1 KHz
- Operation at jet engine combustor exit

Talk Outline -
- Environmental guidelines and sensor selection
- Transient conduction effects and compensation method
- Test program
  - Compensation checkout
  - Lab burner
  - Engine
- Error analysis
- Summary

FIGURE 1

AV238751

SENSOR DESIGN AND ENVIRONMENT GUIDELINES

Geometry: Annular combustor, 2 cm $<$ H $<$ 8 cm

Temperature: T $\sim$ 1400°K (2060°F); T′ $\sim$ 500°K (900°F) -

Frequency response: 1 kHz

Pressure: 10 $<$ P $<$ 20 ATM

Flow: v $\sim$ 150 m/s; v′ $\sim$ 50 m/s -

Gas composition: Fuel (nominal jet A) and air

Sensor life: 5 hr minimum

Accuracy: Temperature uncertainty $\leq$ 5% for f $\leq$ 200 Hz

Temperature uncertainty 10% for 200 Hz $<$ f $<$ 1 kHz

Spatial resolution: D $\leq$ 0.5 cm

Vibration: 10g

FIGURE 2

AV252681

PRELIMINARY DESIGN CONCEPT: DUAL PASSIVE THERMOCOUPLE

- Ratio of T/C responses determines h_g

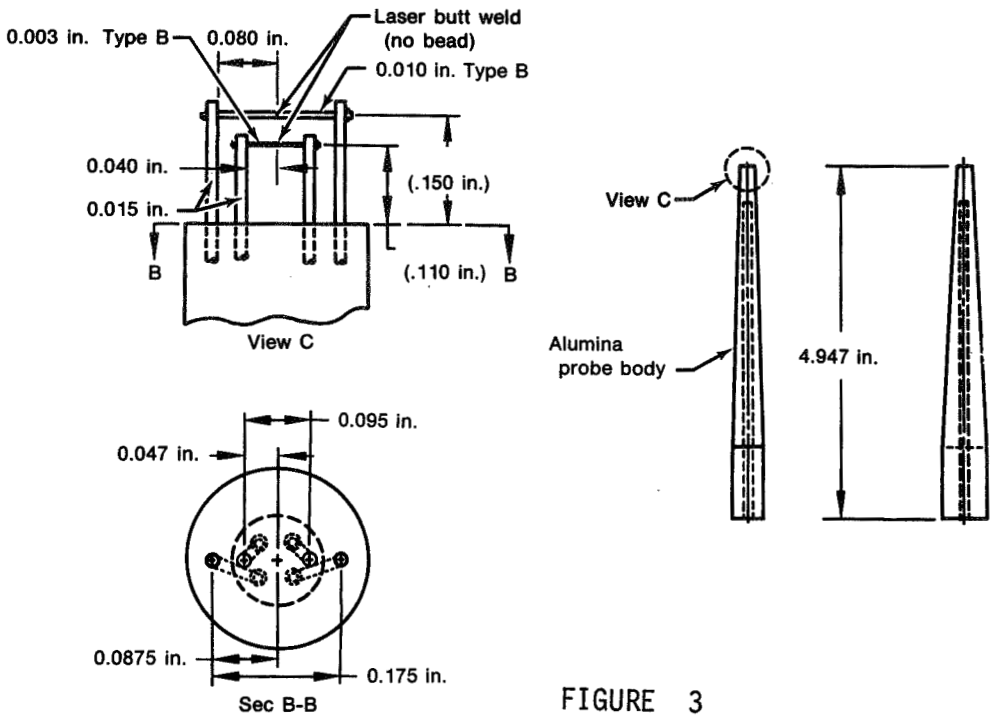

FIGURE 3

AV238759

FIRST-ORDER AND SECOND-ORDER MODELS COMPARED

First-order model

Rate of energy change = $Q_{convection} + Q_{radiation}$

$$\frac{dT}{dt} = \frac{4h}{\rho_w c_{pw} D}(Tg - T) + \frac{4\sigma\epsilon}{\rho_w C_{pw} D}(T_e^4 - T^4)$$

Second-order model

Rate of energy = $Q_{convection} + Q_{conduction} + Q_{radiation}$

$$\frac{dT}{dt} = \frac{4h}{\rho_w c_{pw} D}(Tg - T) + \alpha \frac{\delta^2 T}{\delta x^2} + \frac{4\sigma\epsilon}{\rho_w c_{pw} D}(T_e^4 - T^4)$$

FIGURE 4

AV238777

PHYSICAL MODEL REPRESENTED BY FINITE DIFFERENCE ANALYTICAL MODEL

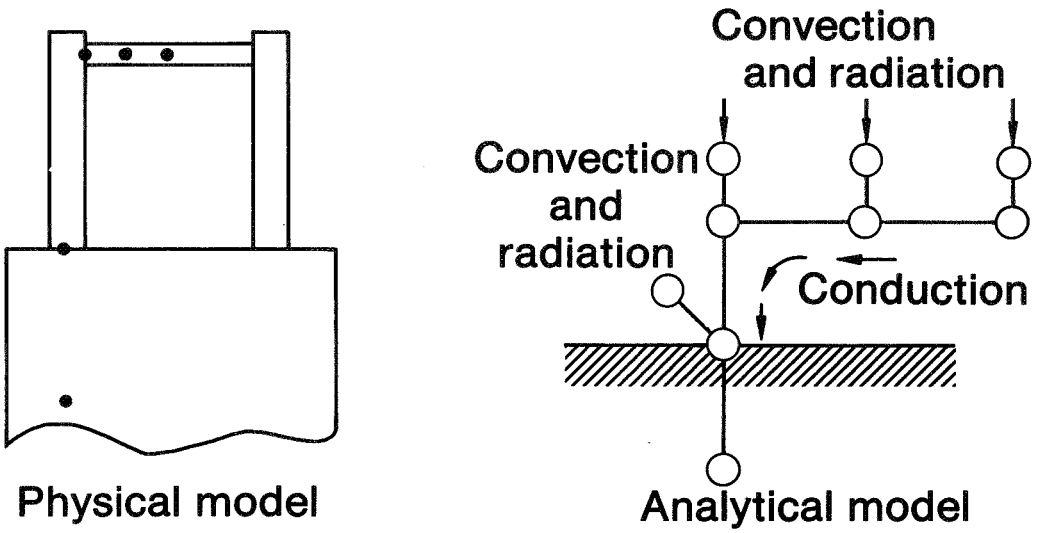

FIGURE 5

AV238776

MAXIMUM DEVIATION IN PREDICTED JUNCTION TEMPERATURE FROM A 1ST ORDER SYSTEM

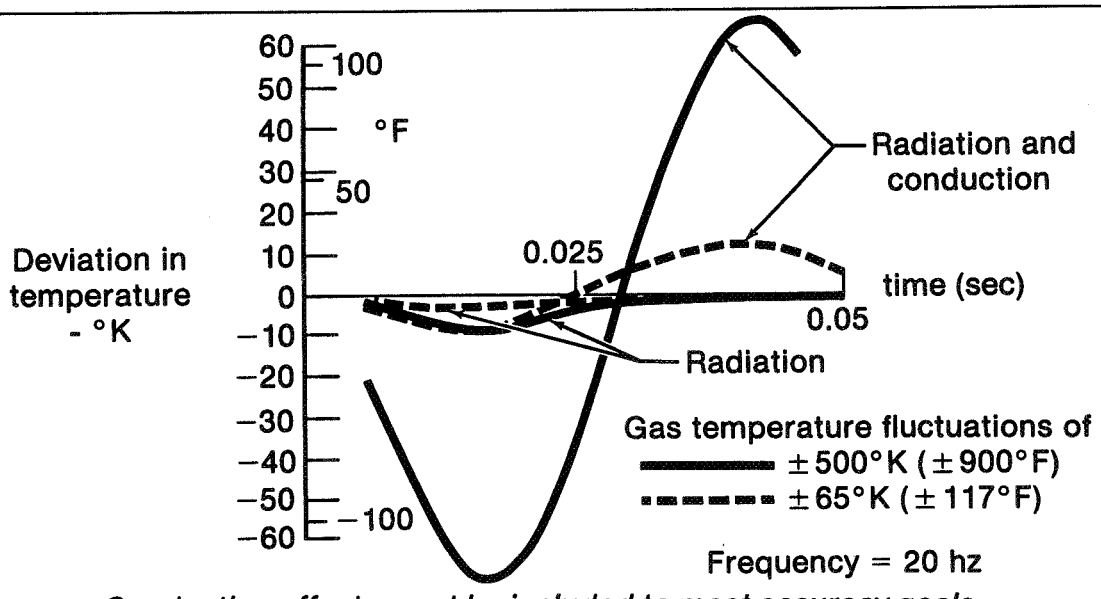

Conduction effects must be included to meet accuracy goals

FIGURE 6

AV238785

COMPENSATION METHOD

- Compute theoretical response (76μm and 254μm T/C's) vs heat transfer coefficient (finite element conduction effects included) over frequency range
- Measure (data) response of 76μm and 254μm T/C's over frequency range (using FFT techniques)
- Determine actual heat transfer coefficient from computed and measured response
- Generate theoretical response of 76μm T/C for actual heat transfer coefficient for frequency range
- Compensate 76μm T/C data in frequency domain
- Inverse Fourier transform to time domain

AV250399

FIGURE 7

DYNAMIC GAS TEMPERATURE MEASUREMENT SYSTEM

Test program

- Compensation method checkout
- Lab burner
- Engine

FIGURE 8

AV260427

SIMULATION OF DUAL WIRE T/C'S

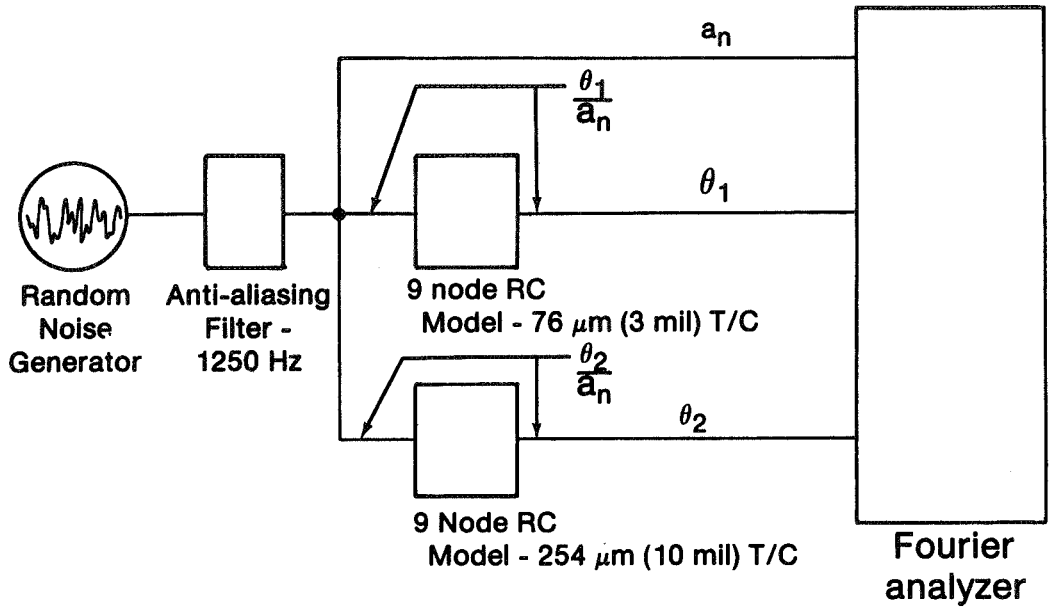

- RC networks modeled as F100 probe
  1200°K (1700°F)
  19.7 ATMS (290 psia)
  Mn = 0.2231
  F/A= 0.02

FIGURE 9

AV257667

FINITE DIFFERENCE THERMAL MODEL

Used in computer compensation program

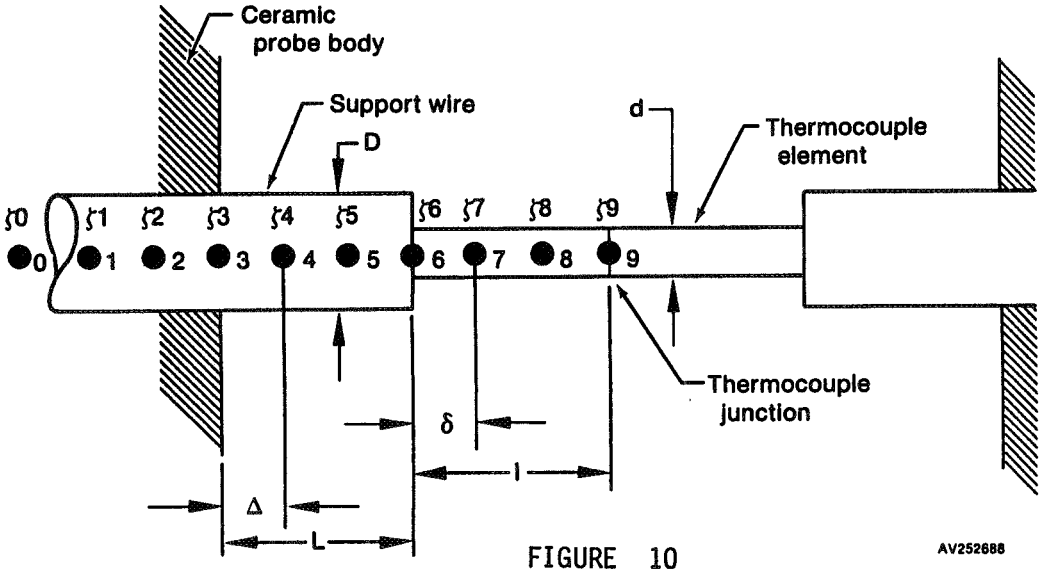

FIGURE 10

AV252688

RC ANALOG NETWORK SIMULATION

Full scale test conditions

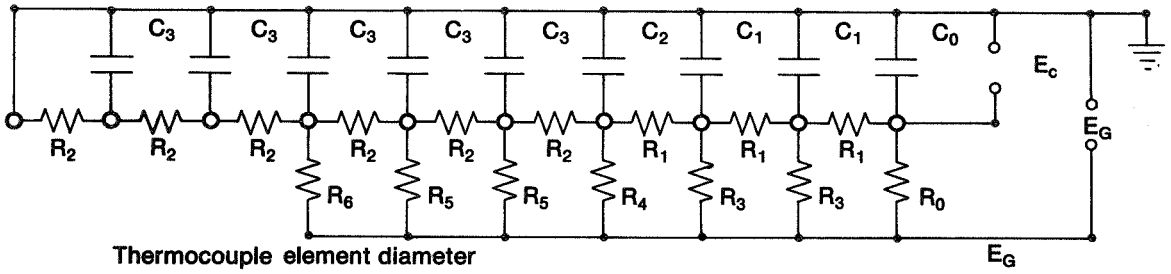

Thermocouple element diameter

Where:	76μm	254μm
R_0	7592 Ω	46.2 KΩ
R_1	1739 Ω	11.8 KΩ
R_2	217.4 Ω	5.66 KΩ
R_3	3796 Ω	23.11 KΩ
R_4	1049 Ω	12.447 KΩ
R_5	543.5 Ω	8.515 KΩ
R_6	1087 Ω	17.031 KΩ
C_0	0.5 μfd	0.5 μfd
C_1	1.0 μfd	1.0 μfd
C_2	2.45 μfd	4.34 μfd
C_3	78 μfd	7.67 μfd

Note: Values listed correspond to F100 probe operating at:
T_T = 1200°K (1700°F)
P_T = 19.7 atm (290 psia)
M_N = 0.2331
F/A = 0.02

AV257666 830902 2493B

FIGURE 11

SIMULATION OF DUAL WIRE TC'S

76 μm (3 mil) compensation spectrum - measured single input/single output

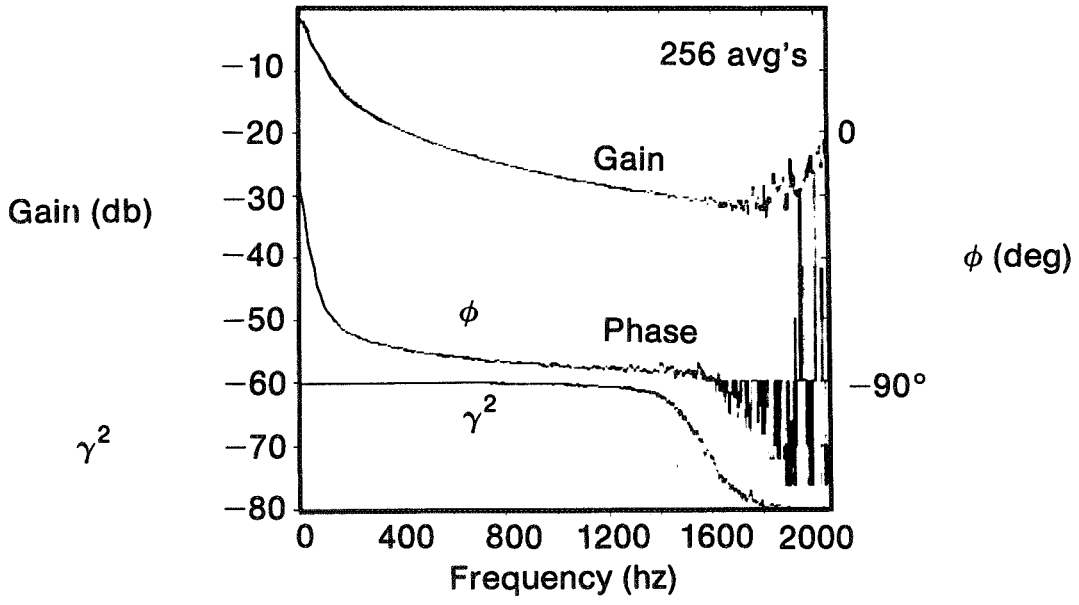

AV260429

FIGURE 12

SIMULATION OF DUAL WIRE TC'S

76 μm (3 mil) compensation spectrum - measured dual wire

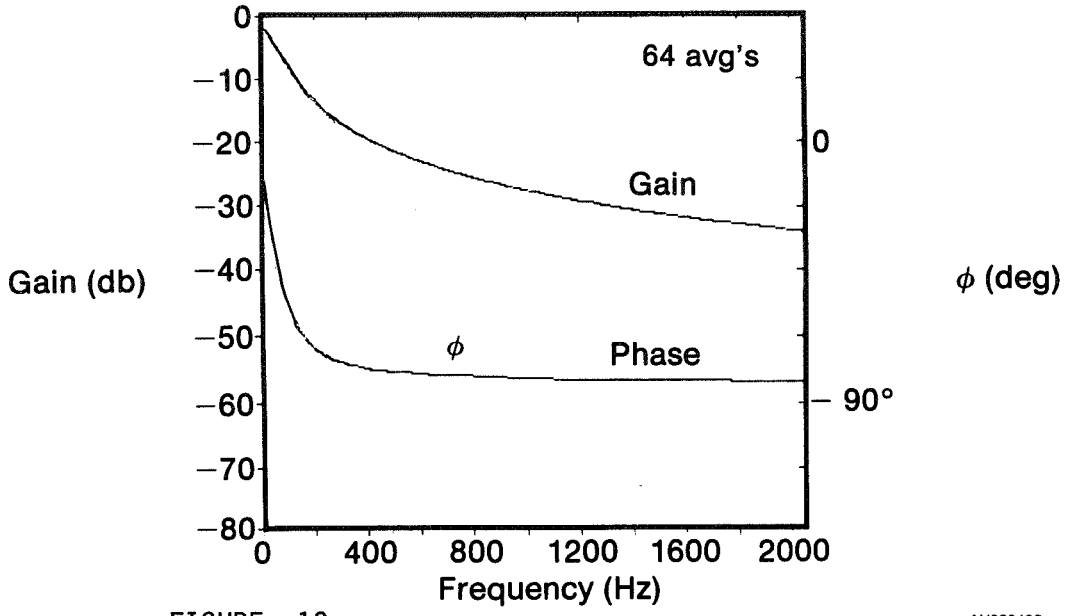

FIGURE 13

AV260428

SENSOR GEOMETRY

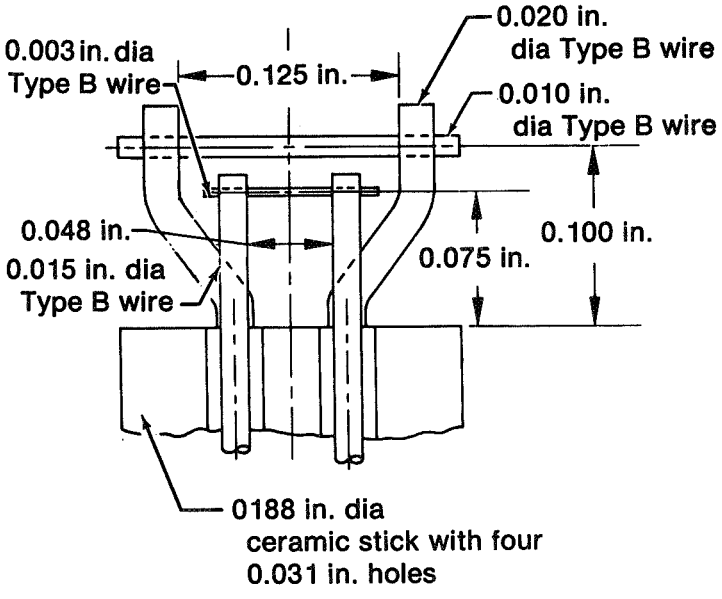

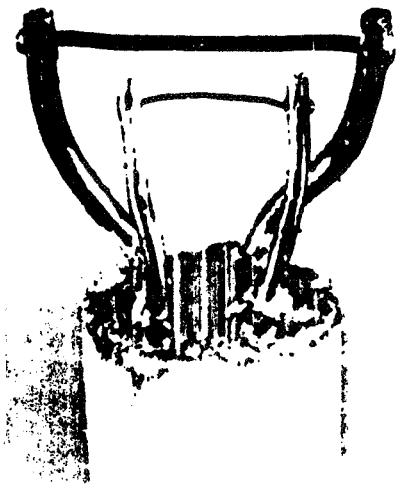

AV260430

FIGURE 14

MICROSCOPIC INSPECTION OF JUNCTIONS

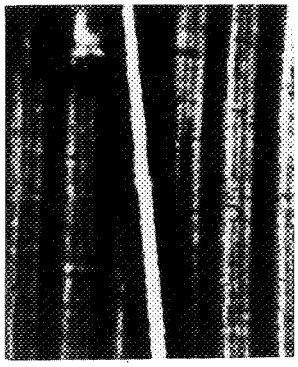

Photomicrograph of 0.003 in. element (200×)

Measured diameter = 0.0029

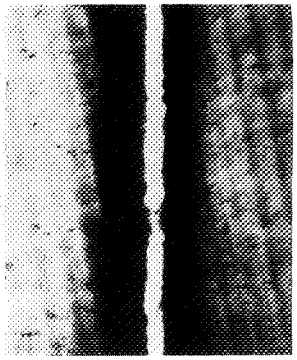

Photomicrograph of 0.010 in. element (100 ×)

Measured diameter = 0.0099

FIGURE 15

AV252691

SUBSCALE COMBUSTOR RIG TEST DATA

- Test pt. No. 10

  Press = 1.04 atms (15.215 psia)

  Probe M_n = 0.227

  Mean temp = 1837°K (2775°F)

  F/A = 0.025 (est'd)

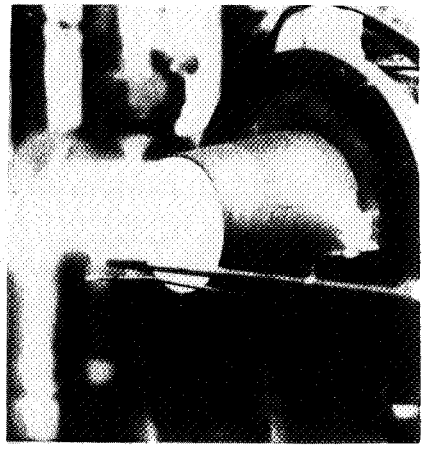

- Ambient - probe retracted/rig running

FIGURE 16

AV260431

SUBSCALE COMBUSTOR RIG TEST DATA

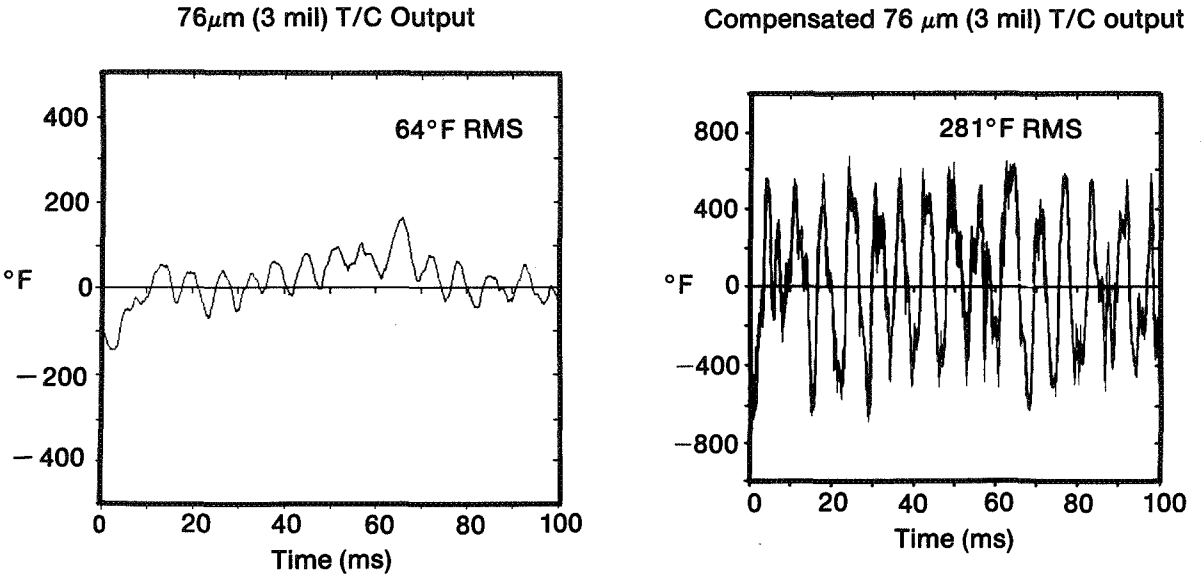

FIGURE 17

AV260432

SUBSCALE COMBUSTOR RIG TEST DATA

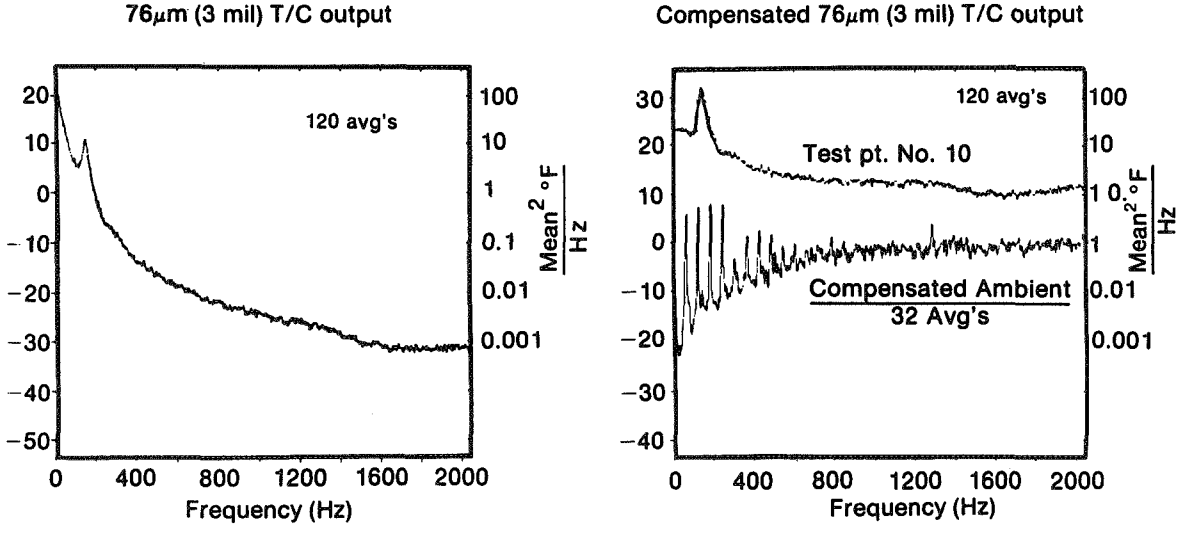

AV260433

FIGURE 18

F100 TEST DATA

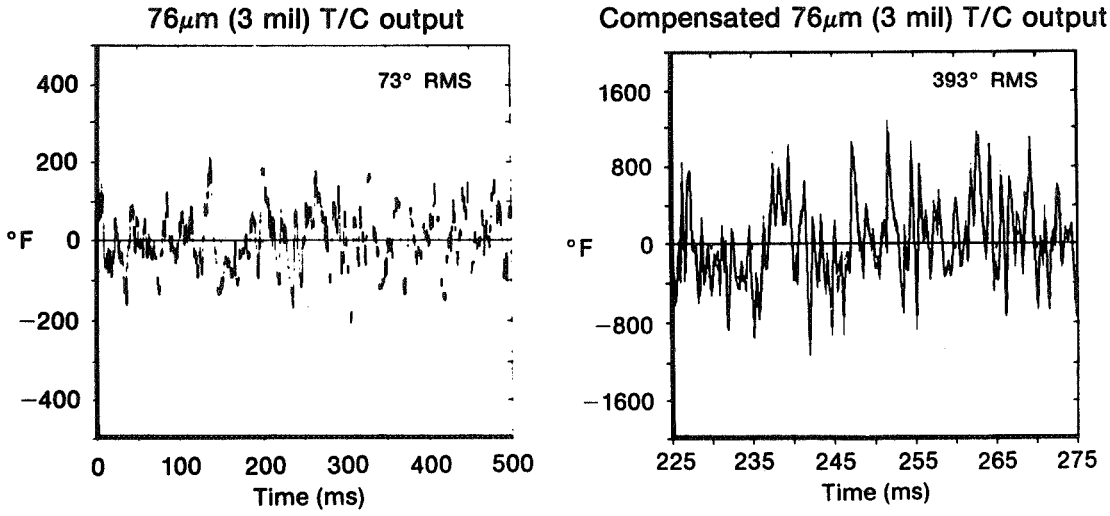

FIGURE 19

AV260434

F100 TEST DATA

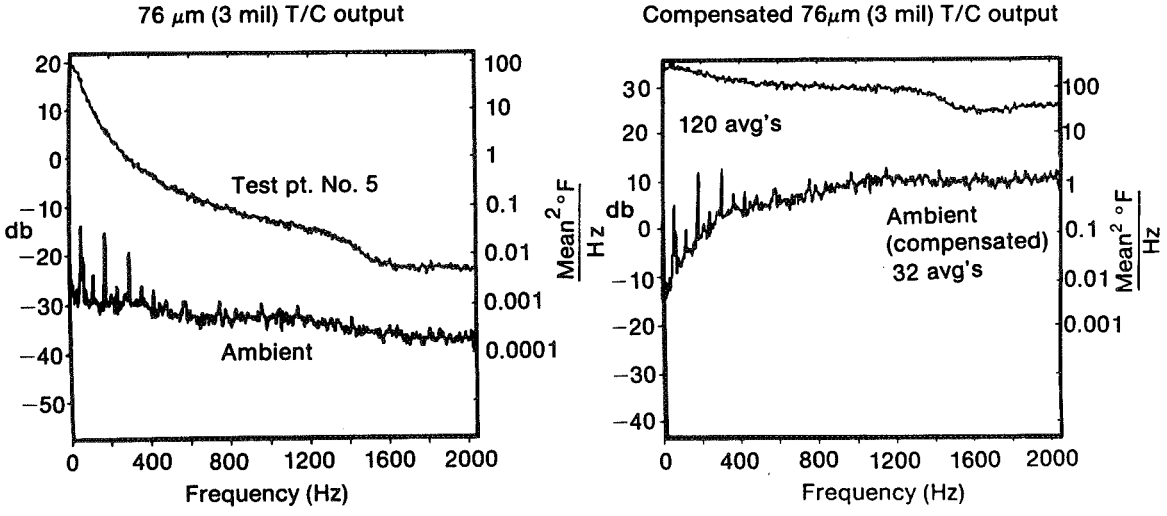

FIGURE 20

AV260435

DYNAMIC GAS TEMPERATURE MEASUREMENT SYSTEM

Overall accuracy - instantaneous time waveform

	Error due to data system SNR	Compensation technique Error	Error (dia's)	Error (θ_2/θ_1)	Total error (RSS)
1000°K (1800°F) p-p at 200 Hz	<0.1%	1.6%	4.9	3.3	6.1%
1000°K (1800°F) p-p at 1000 Hz	<0.1%	2.5%	5.2%	3.5%	6.7%
≃ 15°K (27°F) p-p/$\sqrt{}$Hz 4 Hz-200 Hz	0.7%	4.4%	4.9	3.3	7.4%
≃ 15°K (27°F) p-p/$\sqrt{}$Hz 200 Hz-1000 Hz	3.8%	10.6%	5.2	3.5	12.9%

Overall accuracy - averaged frequency spectrum

	Error due to data system SNR	Compensation Error	Error (dia's)	Error (θ_2/θ_1	Total error (RSS)
1000°K (1800°F) p-p at 200 Hz	<0.1%	1.1%	4.9	3.3	6.0%
1000°K (1800°F) p-p at 1000 Hz	<0.1%	2.0%	5.2	3.5	6.6%
≃ 15°K (27°F) p-p/$\sqrt{}$Hz 4 Hz-200 Hz	0.7%	1.2%	4.9	3.3	6.1%
≃ 15°K (27°F) p-p/$\sqrt{}$Hz 200 Hz-1000 Hz	3.8%	1.9%	5.2	3.5	7.6%

AV260438

FIGURE 21

Page intentionally left blank

D5

HIGH TEMPERATURE STATIC STRAIN SENSOR DEVELOPMENT PROGRAM

Charles Hulse and Richard Bailey
United Technologies Research Center
and
Howard Grant
Pratt & Whitney Aircraft Group

The purpose of this program is to develop electrical resistance strain gages useful for static strain measurements on nickel or cobalt superalloy parts inside a gas turbine engine on a test stand. Measurements of this type are of great importance in meeting the goals of the Host Program because, without reliable knowledge of the stresses and strains which exist in specific components, it will be difficult to fully appreciate where improvements in design and materials can be implemented. The first part of the effort has consisted of a strain gage alloy development program which is to be followed by an investigation of complete strain gage systems which will use the best of the alloys developed together with other system improvements.

The specific goal for the complete system is to make measurements to 2,000με with error of only $\pm$ 10% over a 50 hour period. In addition to simple survival and stability, attaining a low thermal coefficient to resistivity, of order 100 ppm/K or less, is also a major goal. This need results from the presently unavoidable uncertainty in measurements of the exact temperatures in the turbine. The size and thickness requirements to avoid aerodynamic effects suggests the use of the sputtering technique as the best system fabrication approach. The results from the first year of this effort resulted in the identification of an FeCrAl alloy and the Pd-Cr alloy systems as the basis for further alloy modifications and development. Alloy candidates are evaluated and compared using a grading system consisting of the product of the following factors with their total weight potential given in parenthesis: Repeatability (20), Oxidation (18), Resistivity (16), Thermal Coefficient of Resistivity (14), Elastic Range (12), Differential Thermal Expansion (10) and Miscellaneous Judgements (10).

Although the final strain gage system fabrication procedure will probably use the sputtering technique, this is too expensive and too slow a process for alloy development work. A drop-casting technique using repeatedly arc-melted buttons was therefore developed. The cast rods produced are ground and polished using slotted plates to finally produce long, thin strips of material about 17cm long suitable for subsequent testing. Other techniques for producing the strain gage elements, such as wire drawing and melt spinning, are also to be examined in this program.

Work done under NASA contract NAS3-23722.

The specially constructed thermal cycling apparatus developed earlier in this work to make resistivity measurements has been further developed to make more accurate measurements. This system employs a split tube metal heater which can be cycled or held at constant temperature under program control. The test sample is positioned axially in the center of this tube with Platinum leads for voltage measurements and thermocouple wires attached by spot welding. Special provisions have been added to better accomplish the faster (250K/min) heating and cooling rate testing. Additional computer program development has also been accomplished to improve both the data measurement and the data reduction process.

The FeCrAl alloy system studies have defined a ternary area whose edges define compositions whose average thermal coefficients of resistance are zero between room temperature and 1250K. Compositions along these edges provide significant improvements over the previously known best alloy (Kanthal A-1). Measurements of the resistances to oxidation of these alloys with different amounts of Hf, Y, Sc, Co and additional amounts of Al and Cr have shown that, although all show protective behavior, none are significantly better than the base FeCrAl alloy.

The Pd-Cr alloys develop a thin coherent, continuous coating of Cr_2O_3. A variety of other alloys containing oxide formers, especially the rare earth metals, are being examined to find compositions with even better resistance to oxidation and lower thermal coefficients of resistance.

GENERAL RULES CONCERNING ρ AND α

Matthieson: $\rho = \rho_o + \rho_T$

Dellinger: $\rho\alpha = \text{Constant} \quad \alpha = \frac{d\rho}{dT}$

Linde: $\Delta\rho \propto V_X^2$

V = valence
X = alloying element

Norbury: $\rho\alpha(N - N_X)^2$

N = atomic number
X = alloying element

Figure 1

HIGH-SPEED THERMAL CYCLE/ RESISTIVITY MEASUREMENT APPARATUS

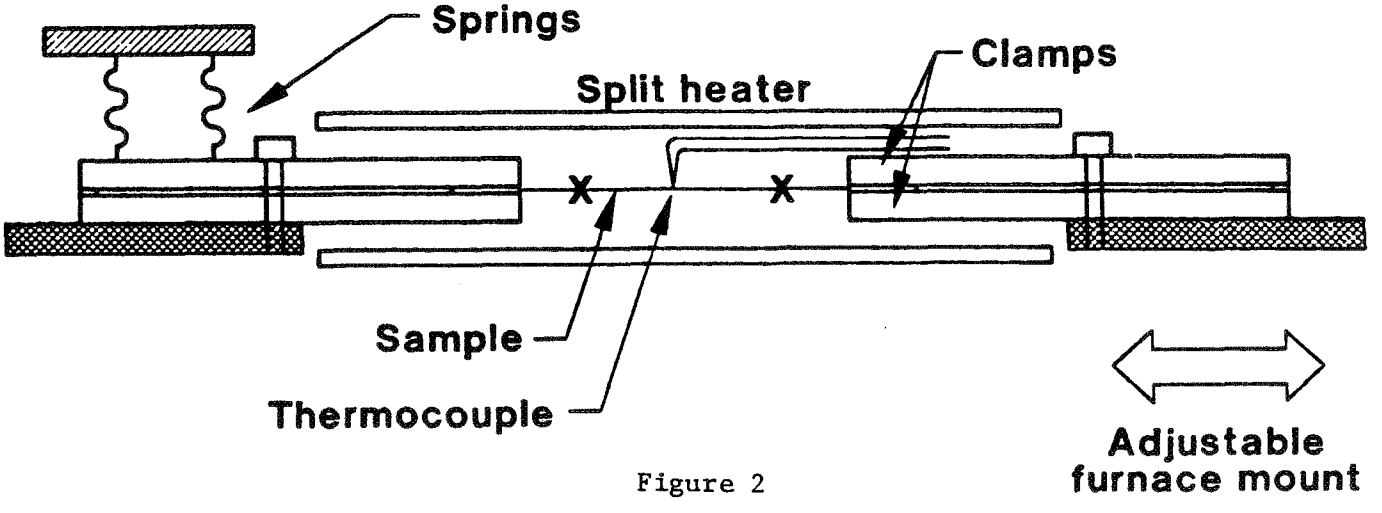

Figure 2

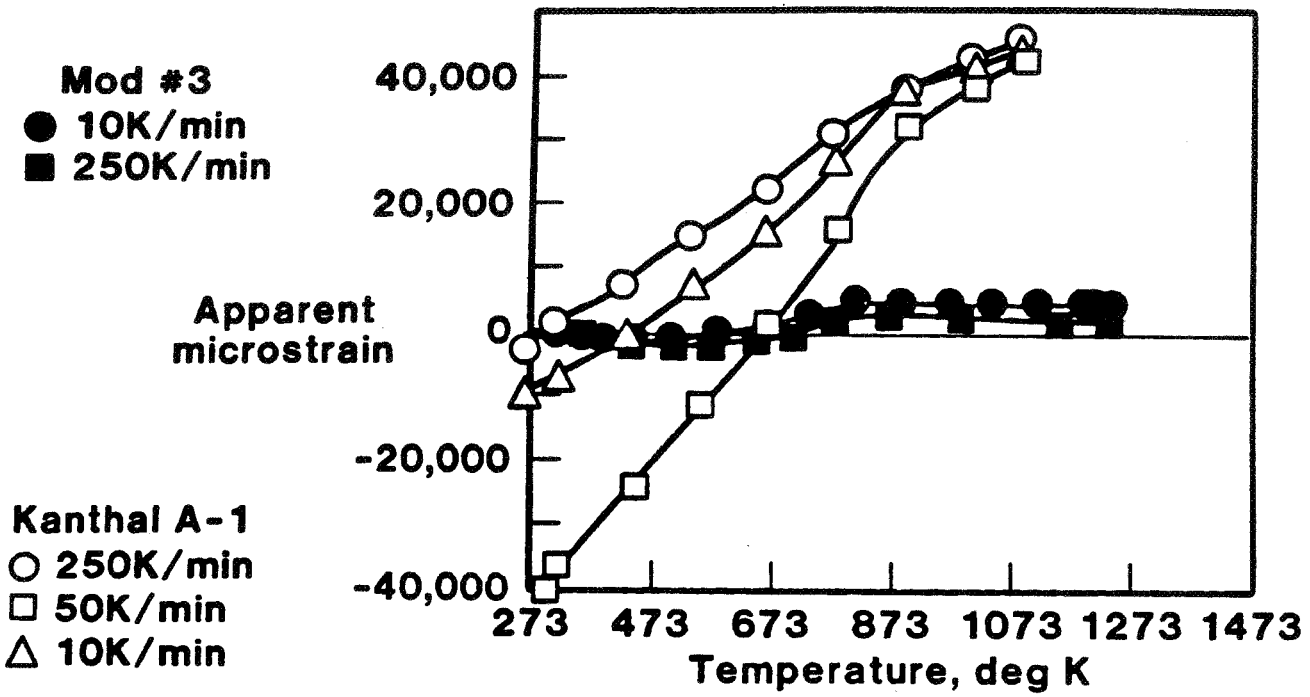

Figure 3

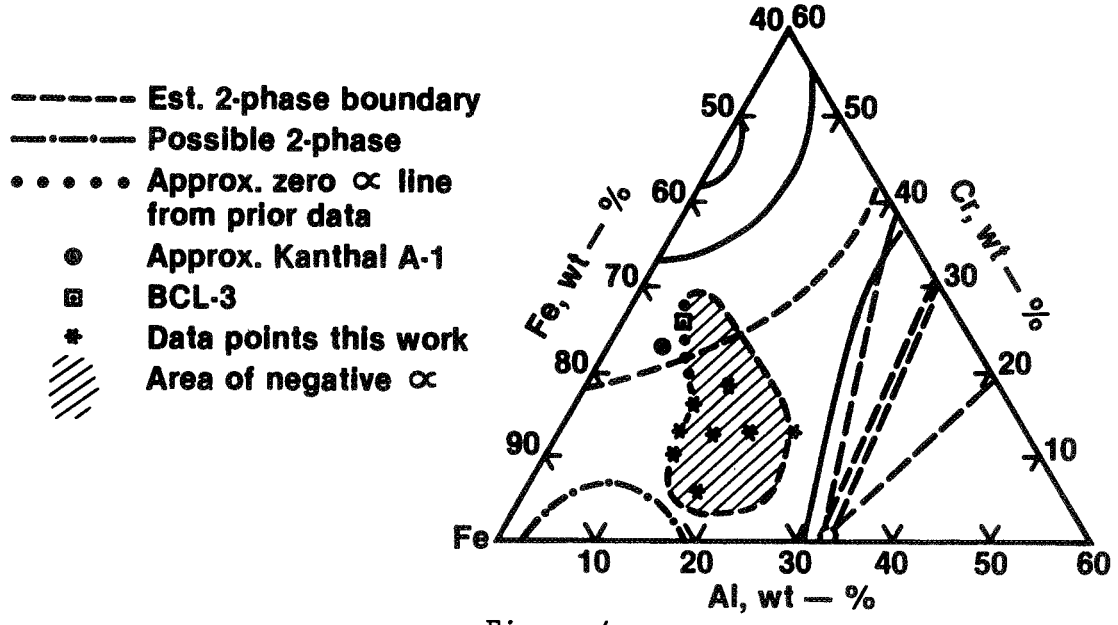

Figure 4

82 10 GR 1

DEMONSTRATION TEST OF BURNER LINER STRAIN MEASUREMENT SYSTEMS: INTERIM RESULTS*

Karl A. Stetson
United Technologies Research Center
East Hartford, Connecticut

Howard P. Grant
Pratt and Whitney Aircraft
East Hartford, Connecticut

Abstract

Work is in progress to demonstrate two techniques for static strain measurements on a jet engine burner liner. Measurements are being made with a set of resistance strain gages made from Kanthal A-1 wire and via heterodyne speckle photogrammetry. The background of the program is presented along with current results.

Introduction

A previous program (NAS3-22126) has resulted in identifying two potentially applicable methods for static strain measurement of the thermal deformations of jet engine burner liners. The first employs resistance strain gages made from Kanthal A-1 wire and the second is a form of photogrammetry based upon laser speckle photographs (specklegrams) of the surface under study. The photographs are made by illuminating the object with laser light and making photographic recordings on high resolution plates through a telecentric lens system. The coherence of laser light creates high contrast speckles in the image that move as if attached to the object surface. Strain is revealed as image magnification by photogrammetric comparison of pairs of specklegrams. The accuracy of this comparison is greatly enhanced by use of a heterodyne interferometer.

Both methods have features that are attractive as well as problematic. The wire gages provide continuous output in a conventional format and, because they are bonded to the actual object surface, are not influenced by rigid-body tilts and translations. On the other hand they are subject to failure, they can exhibit large and variable values of apparent strain, they have temperature limitations, they only measure strain at specific locations, and they can influence the mechanical behavior of the object. By comparison, speckle photogrammetry offers virtually no temperature restriction, allows continuous geometrical mapping of strain distributions, has an apparent strain equal to thermal expansion, and is noncontacting. Nonetheless, it only samples the object at discrete times, it can be disturbed by rigid-body motions, it requires optical access to the object surface, and it can be influenced by thermal inhomogeneities in the gas through which the object is viewed.

*This work is being performed under contract NAS3-23690.

Program Description

The current program combines both methods in a prototype study of combustor behavior. A JT12D combustor (see Fig. 1) has been modified for operation in the temperature range desired (Up to 950°K for the Kanthal gages and up to 1140°K for the photogrammetry). A section has been cut from the burner and instrumented with ten gages and seven thermocouples as shown in Fig. 2. A hole has been provided so that the louver lip may be photographed and included in the photogrammetric strain measurement. The gaged section has been put through temperature calibration tests to predetermine the apparent strains of the gages. Reference gages have also been tested on a constant strain bar to determine the gage factor as a function of temperature. The section of the burner was then welded back into place and the burner installed in the test stand.

A window was provided in the test cell as shown in Fig. 3 through which the burner is illuminated and photographed. Figure 4 shows the layout of the optical components. A pulsed laser provides illumination of about 1 msec duration with adequate energy to expose the plates. The system is operated remotely from the control room.

During the actual test runs, specklegram data is recorded in the form of photographic exposures at designated times, while strain gage data is recorded continuously as electrical signals. To maintain correlation between the speckle patterns of successive photographs, the burner is heated isothermally by increasing the inlet air temperature until spontaneous ignition is possible. After ignition, various cycles can be simulated by variation of the fuel flow. After testing is complete, both strain gage and specklegram data are processed to obtain strain information.

Processing for the strain gage data consists primarily of numerical correction for apparent strain and gage factors. Processing for the specklegram data consists of developing the photographic plates and evaluating them on an interferometric comparator. The number of locations on the photographs at which two-dimensional strain data may be obtained is limited by the time available for data processing. Strains are to be measured, therefore, only at the ten gage locations and at ten additional locations including the louver lip. Thermocouple readings will be used to correct for thermal expansion and provide thermomechanical strain.

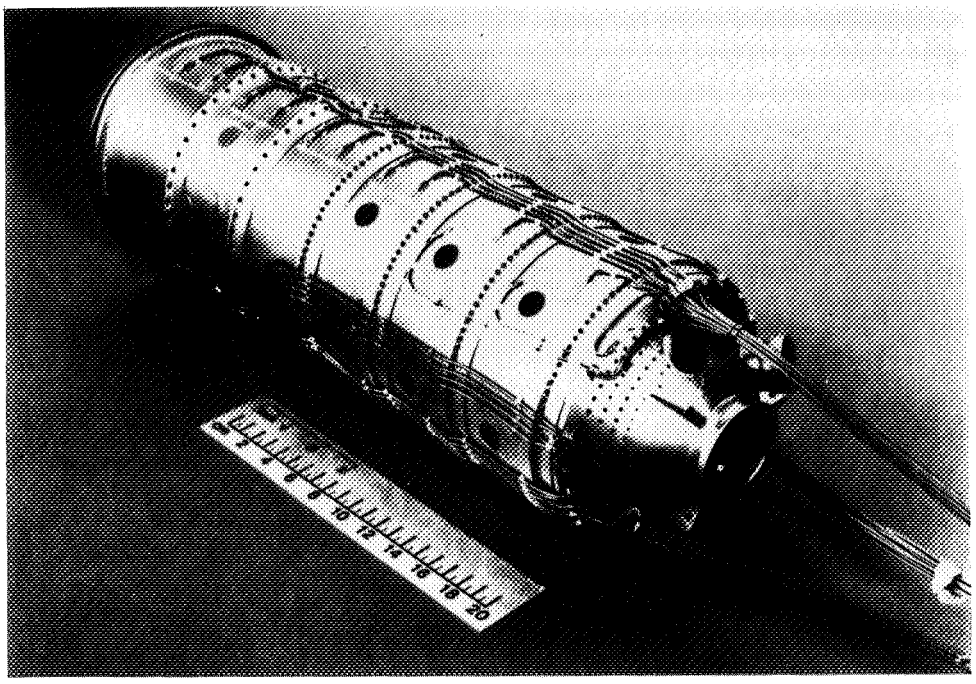

FIG. 1

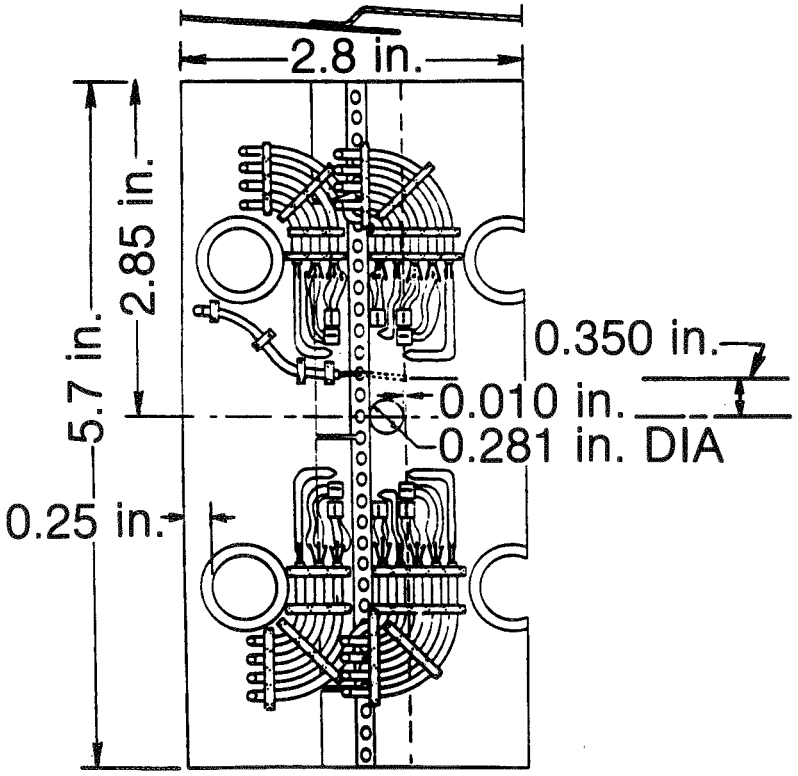

FIG. 2

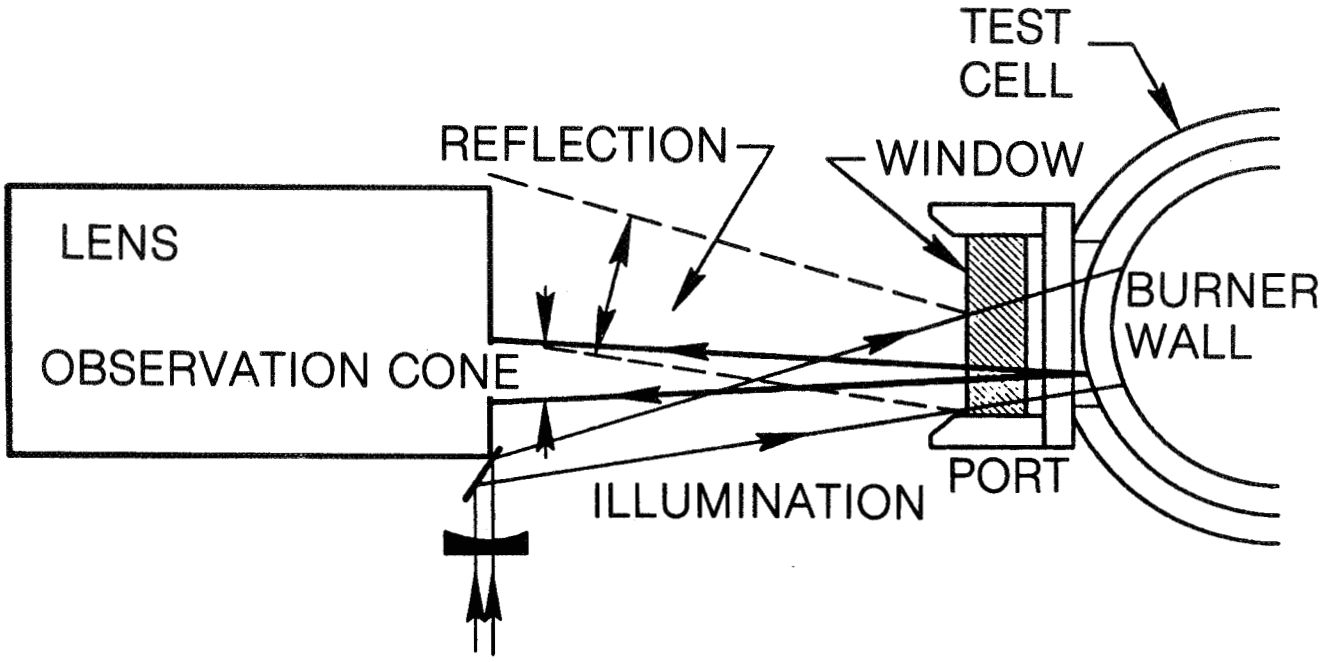
TEST
CELL
REFLECTION
WINDOW
LENS
BURNER
WALL
OBSERVATION CONE
PORT
ILLUMINATION

FIG. 3

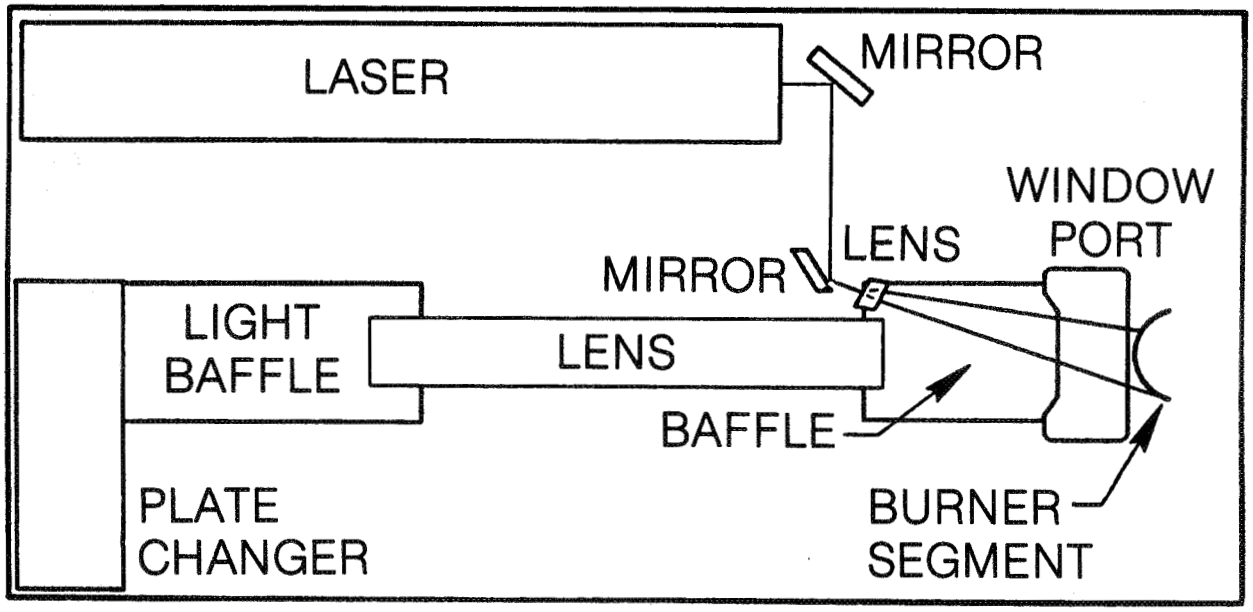
LASER
MIRROR
WINDOW
PORT
LENS
MIRROR
LIGHT
BAFFLE
LENS
BAFFLE
PLATE
CHANGER
BURNER
SEGMENT

FIG. 4

D7

DEVELOPMENT OF HEAT FLUX SENSORS FOR TURBINE AIRFOILS AND COMBUSTOR LINERS

William H. Atkinson
Pratt & Whitney Aircraft Group
Engineering Division

This paper briefly describes the work performed under two contracts: NAS3-23529, "Turbine Blade and Vane Heat Flux Sensor Development"; and a pre-HOST effort, NAS3-22133, "Advanced High Temperature Heat Flux Sensor Development". The objective of each of these contracts is to develop heat flux sensors for use on gas turbine engine hot section components.

The design of durable turbine airfoils that use a minimum amount of cooling air requires knowledge of the heat loads on the airfoils during engine operation. Measurement of these heat loads will permit the verification or modification of the analytical models used in the design process and will improve the ability to predict and confirm the thermal performance of turbine airfoil designs. Heat flux sensors for turbine blades and vanes must be compatible with the cast nickel-base and cobalt-base materials used in their fabrication and will need to operate in a hostile environment with regard to temperature, pressure and thermal cycling. There is also a need to miniaturize the sensors to obtain measurements without perturbing the heat flows that are to be measured.

At the start of the turbine blade and vane program, a literature search and a survey of commercially available sensors were conducted to determine the current state of the art for heat flux sensors. These investigations revealed that there were no existing sensors which met the geometrical and environmental requirements of the blade and vane heat flux measurements. An effort was then initiated to develop feasible sensor designs for turbine blade and vane applications. Several concepts were chosen for further consideration:

- o embedded thermocouple sensors using the airfoil wall as a thermal barrier,
- o Gardon gage sensors fabricated into the airfoil wall,
- o several types of transient sensors.

Sensor concepts that were only suitable for transient testing were subsequently dropped from consideration because of the complexity of introducing sufficiently rapid transient conditions into the hot side heat transfer coefficient or into the airfoil coolant during actual engine testing.

Figure 1 is a schematic of the embedded thermocouple sensor. This type of one dimensional steady state sensor determines the heat flux by measuring the temperature drop across a thermal barrier. In this case, the airfoil wall itself acts as the thermal barrier. The Gardon gage sensor is shown schematically in figure 2. This type of steady state sensor determines the heat flux from the temperature rise due to radial conduction from the insulated section of the hot side of the airfoil wall. Both these sensors have been optimized for steady state conditions but may also be used as transient heat flux sensors.

A series of thermoelectric tests were conducted on blade and vane alloys to determine the suitability of these materials as thermoelectric elements. The use of the airfoil material in the thermoelectric circuit gives a direct differential output and reduces the number of wires required, minimizing the potential for temperature perturbations caused by the presence of the wires. All of the

superalloys tested were found to produce positive thermoelectric outputs with temperature when paired with platinum. These thermoelectric outputs were stable throughout four thermal cycles and several hours of thermal soaking. Alumel was selected as the preferred thermoelectric material because of the relatively high voltage output, availability and low cost. Millivolt outputs versus temperature of the various superalloys when paired with Alumel are presented in figure 3.

The sensor designs were analyzed for thermal performance using a three dimensional finite difference heat transfer program (TCAL) developed at Pratt & Whitney Aircraft. This program determined the thermal perturbations caused by the presence of the sensor and the theoretical outputs to be expected from the sensor. This information was used to calculate the anticipated error in the heat flux indicated by the sensor compared with the heat flux that existed in the unperturbed airfoil.

Both the embedded thermocouple and Gardon gage sensor designs were fabricated into first stage turbine blade halves. For the embedded thermocouple sensors, grooves were eloxed into the inner and outer airfoil surfaces. The thermocouples were installed in the grooves using a wedge wire technique, and the surface of the installation was smoothed off. Figures 4 and 5 show the interior and exterior walls of a typical installation. The blade halves were then welded together and the assembled blade is shown in figure 6.

For the Gardon gage sensors, a cavity was eloxed into the interior wall of the blade half and a groove was eloxed to route the leadwire away from the sensor. To minimize the number of grooves required, the Gardon gage sensor used a three wire swaged lead. The thermocouple junctions were made in the cavity by resistance welding, and the leadwire was installed in the groove using a wedge wire technique. The cavity was then filled with a ceramic cement to provide oxidation and mechanical protection for the thermocouple wires and to restore the aerodynamic integrity of the internal blade wall. Figure 7 shows the completed Gardon gage sensor on the interior blade surface.

A calibration fixture, shown in figure 8, was designed and fabricated for the calibration of airfoil-mounted heat flux sensors. This fixture is mounted below a quartz lamp bank heat source, shown in figure 9. The fixture allows positioning of the airfoil so that the surface of the heat flux sensor is normal to the incident radiation. The surface of the airfoil is coated with material having a known and stable absorptance and emittance. The incident radiation is measured with a reference Hy-Cal asymptotic calorimeter. This same test apparatus is used for thermal cycle tests and thermal soak tests as well as the calibration tests.

Data from the calibration of a typical embedded thermocouple sensor are shown in figures 10 and 11. Figure 11 shows that sensor sensitivity (sensor output/heat flux transmitted) varies with temperature. This would be expected because of variation in the thermal conductivity of the blade material and the thermoelectric output with temperature. If these factors are analytically accounted for, the sensor output can be normalized to an 1150 K sensor reference temperature. The normalized data for this sensor are presented in figures 12 and 13. Similarly, data for a typical Gardon gage sensor are presented in figures 14 and 15. These data normalized to an 1150 K sensor reference temperature are shown in figures 16 and 17.

Several sensors were subjected to thermal cycling tests, in which the sensors were rapidly heated to near maximum temperature and heat flux, held at this condition for one minute, cooled rapidly to near ambient temperature and held there

for three minutes. The normal test program was 50 thermal cycles. Calibration data for a typical sensor before and after the thermal cycle test are shown in figure 18. Thermal soak tests were also conducted on several sensors in which the sensor was held at near maximum temperature and heat flux for a period of 10 hours. Calibration data for a typical sensor before and after the thermal soak test are shown in figure 19.

The sensors developed under the first phase of the turbine blade and vane heat flux sensor program have been shown to be capable of measuring the heat loads on turbine airfoils with an accuracy of ±10 percent, and have withstood thermal cycling and thermal soak conditions that are to be expected to be representative of a gas turbine engine environment. A second phase of this program will demonstrate a wide variety of heat transfer measurement methods on a simple test piece in an atmospheric combustor rig. This work, just recently initiated, will consist of running a cylinder in cross flow behind a laboratory combustor rig. The first portion of this work will be to characterize the combustor exit as fully as possible with respect to temperature, pressure and velocity, including the spatial and temporal variations of these quantities. Various types of heat flux sensors and other heat flux measurement instrumentation will be mounted in cylindrical test sections and tested behind the combustor. This instrumentation will include both transient and steady state sensors as well as instrumentation for measuring dynamic gas and metal temperatures. The results of the various measurement techniques will be correlated and compared with the analytically predicted heat flux levels.

Under a pre-HOST NASA contract (Contract NAS3-22133, "Advanced High Temperature Heat Flux Sensor Development", from the NASA LeRC Instrumentation R&D Branch) described in Reference 1, high temperature steady state heat flux sensors were designed and fabricated for use in combustor liners. There were three sensor designs generated:

- o the laminated sensor,
- o the Gardon gage sensor,
- o the embedded thermocouple sensor.

Figure 20 shows a schematic representation of each of these sensors. The sensors were subjected to laboratory testing consisting of calibrations, thermal cycle tests and thermal soak tests. The test results on these sensors were presented at the 1982 HOST Contractor's Workshop.

In a continuation of that contractual effort, a combustor liner has been instrumented with eight heat flux sensors and is ready to be tested in a high pressure combustor facility. There are three Gardon gage sensors, three embedded thermocouple sensors and two laminated sensors mounted in the combustor liner. An overall view of the cold side of the liner is shown in figure 21, and a close up view of the cold side of two of the sensors is shown in figure 22. The hot side of one of the sensors, presented in figure 23, shows the resistance weld around the periphery of the sensor that was used to fasten the sensor into the liner wall. After the sensors were installed into the liner, a functional check was performed to verify that they were still operational. The liner will be run as a part of the test sequence on NASA Contract NAS3-22392, "Broad Specification Fuels Program".

These high pressure combustor tests will also include two radiometer probes for measuring the radiative portion of the total heat load. These two radiometers, a porous plug radiometer probe developed at Pratt & Whitney Aircraft and a commercially available Medtherm radiometer probe, are shown in figure 24. The porous

plug radiometer probe has a field of view nearly 180 degrees while the Medtherm radiometer has a 50 degree field of view. During the test, the two radiometers will be mounted on opposite walls facing each other as shown in figure 25. In this configuration, both probes will view the same volume and, hence, the signals should correlate. It is anticipated that the two probe locations will be interchanged during the test program to eliminate any rig bias. It is hoped that the data from these tests will help clarify some of the wide angle and narrow angle radiometer data taken in other test programs.

As a result of the two contracts for heat flux sensor development, high temperature steady state heat flux sensors have been fabricated for use on turbine blades and vanes and on combustor liners. The use of these sensors in upcoming test programs will provide detailed information on the heat loads on hot section components, and will represent a significant advance in the modeling and prediction of the heat transfer characteristics of gas turbine engines.

REFERENCE

1. Atkinson, W. H.: and Strange, R.R.: "Development of Advanced High-Temperature Heat Flux Sensors: NASA CR-165618: September 1982.

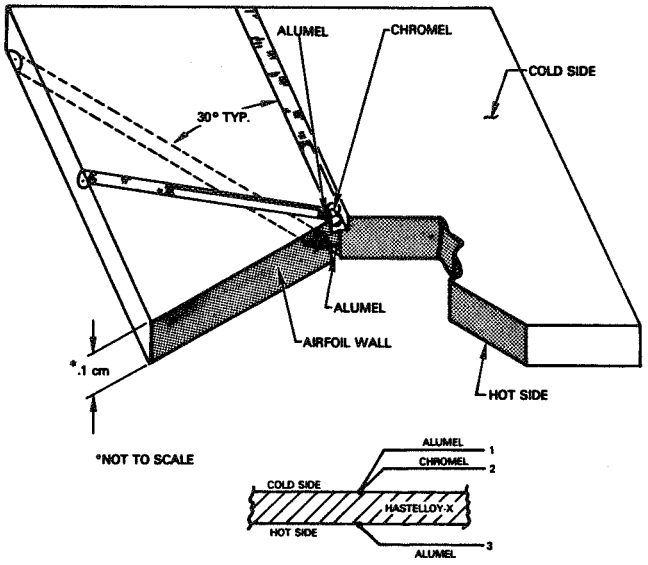

Figure 1 Schematic of Embedded Thermocouple Sensor

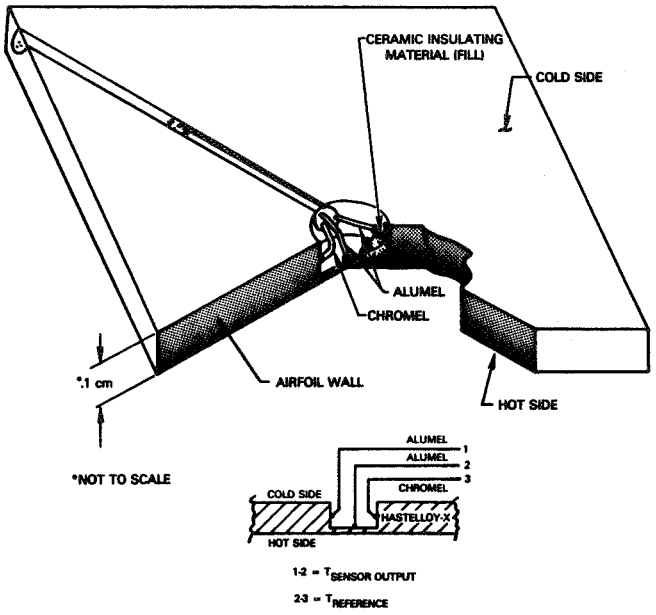

Figure 2 Schematic of Gardon Gage Sensor

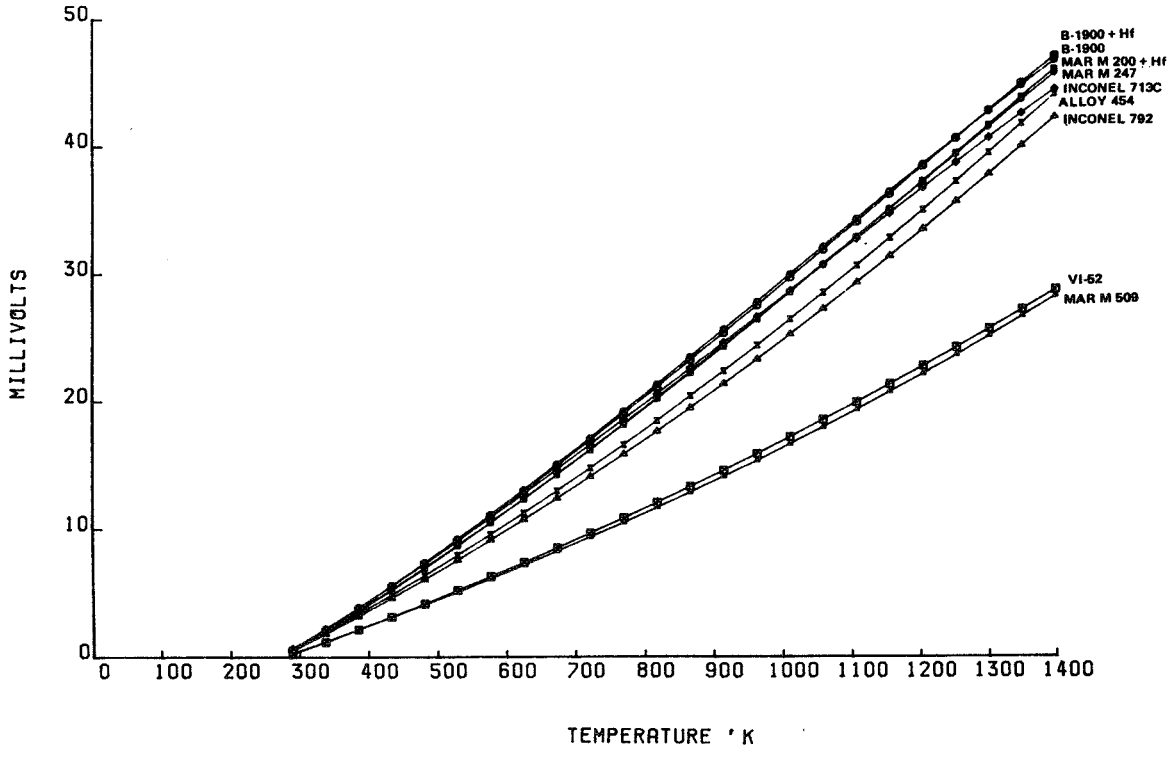

Figure 3 Plot of Thermoelectric Output of Superalloys versus Alumel

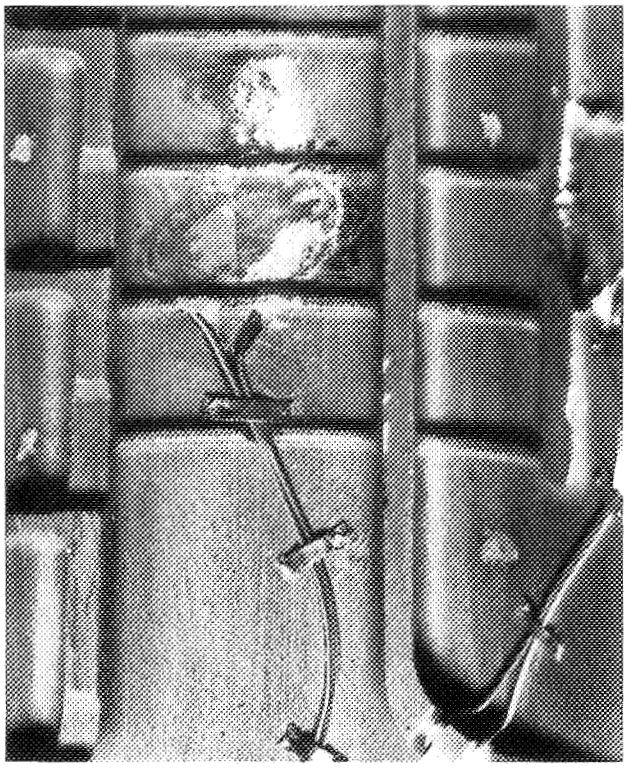

Figure 4 View of Interior Wall of Embedded Thermocouple Sensor

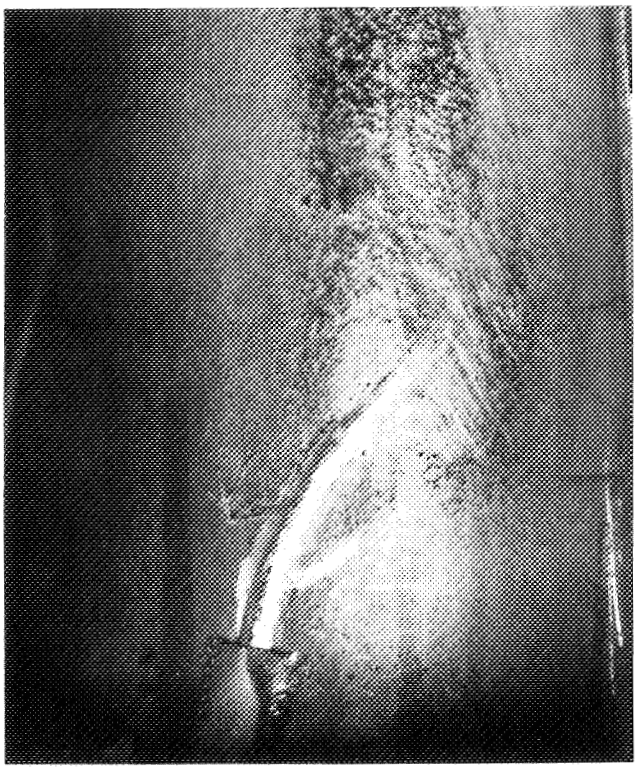

Figure 5 View of Exterior Wall of Embedded Thermocouple Sensor

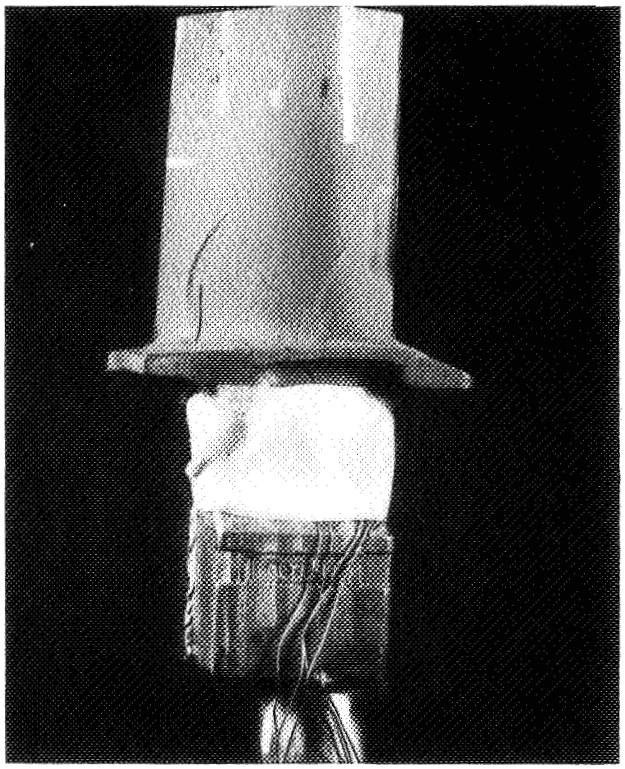

Figure 6 View of Assembled Embedded Thermocouple Instrumented Blade

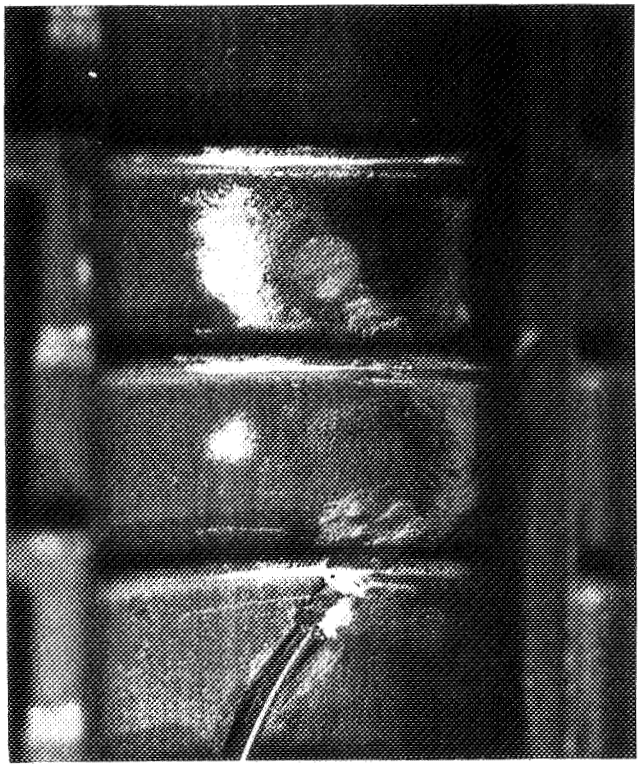

Figure 7 View of Interior Wall of Gardon Gage Sensor

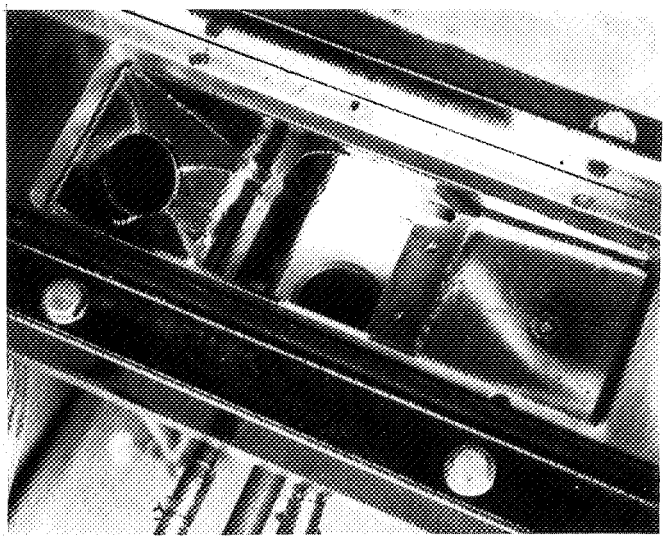

Figure 8 View of Calibration Fixture

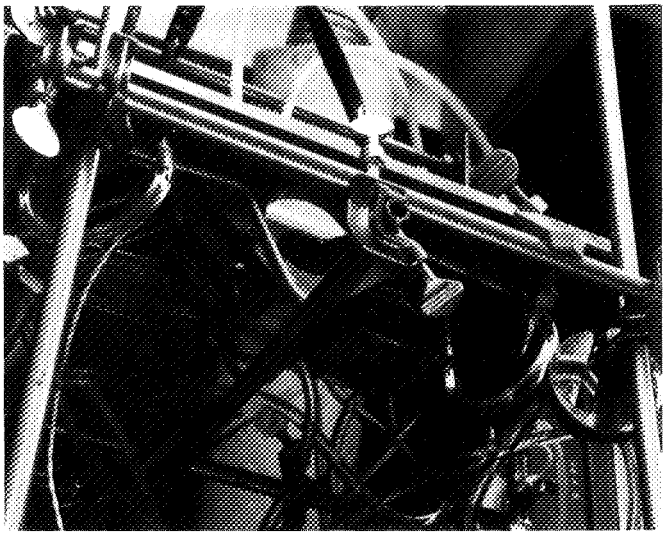

Figure 9 View of Calibration Setup

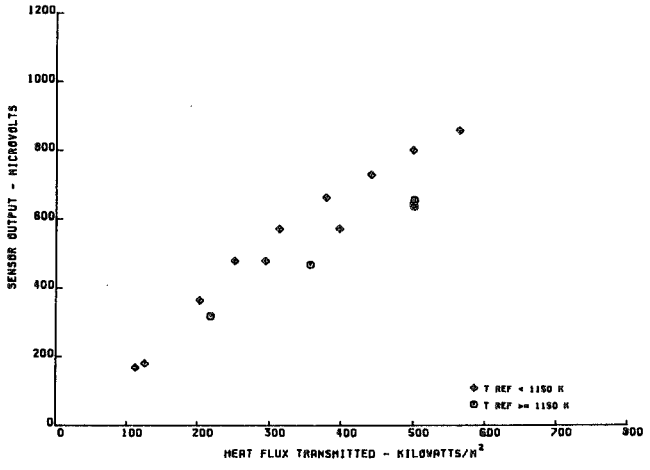

Figure 10 Plot of Output versus Heat Flux for Embedded Thermocouple Sensor

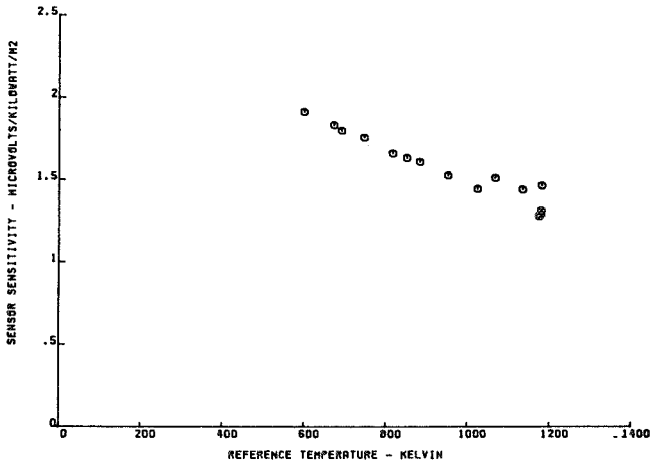

Figure 11 Plot of Sensitivity versus Temperature for Embedded Thermocouple Sensor

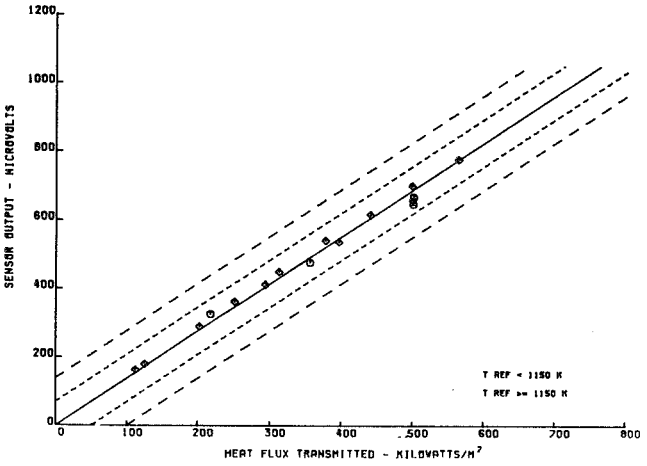

Figure 12 Plot of Normalized Output versus Heat Flux for Embedded Thermocouple Sensor

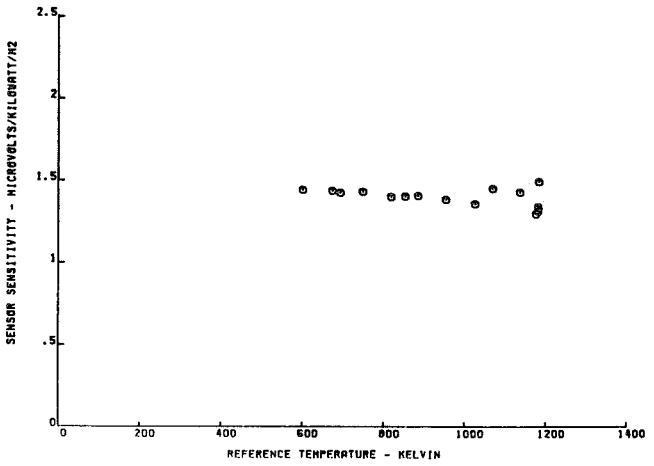

Figure 13 Plot of Normalized Sensitivity versus Temperature for Embedded Thermocouple Sensor

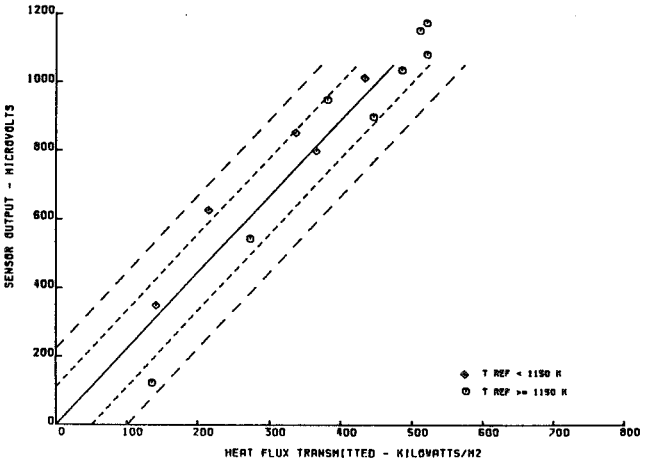

Figure 14 Plot of Output versus Heat Flux for Gardon Gage Sensor

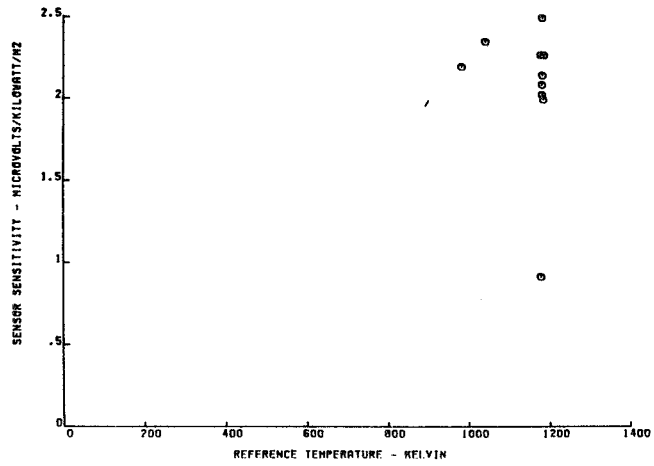

Figure 15 Plot of Sensitivity versus Temperature for Gardon Gage Sensor

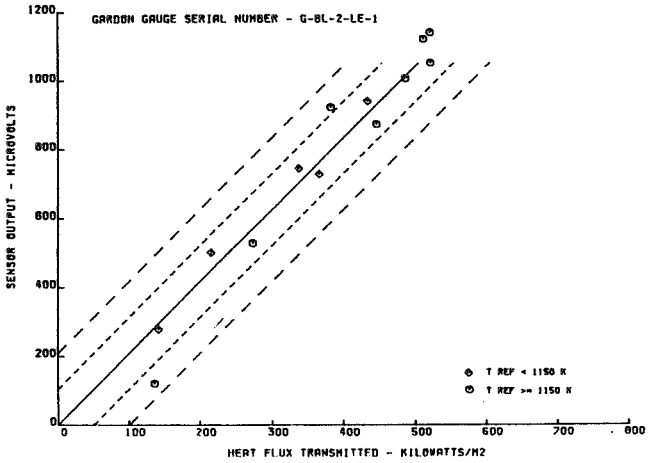

Figure 16 Plot of Normalized Output versus Heat Flux for Gardon Gage Sensor

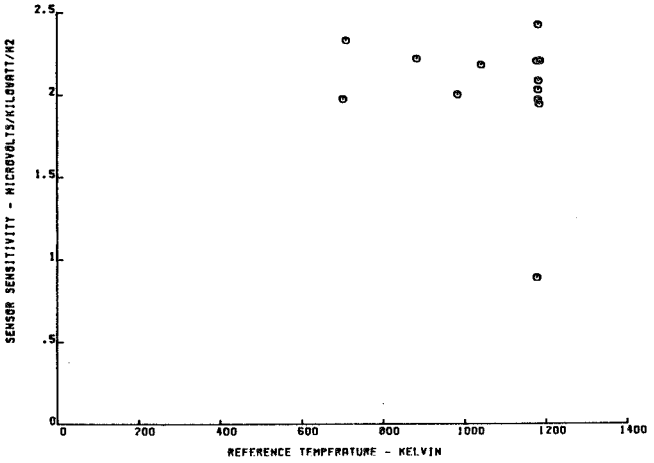

Figure 17 Plot of Normalized Sensitivity versus Temperature for Gardon Gage Sensor

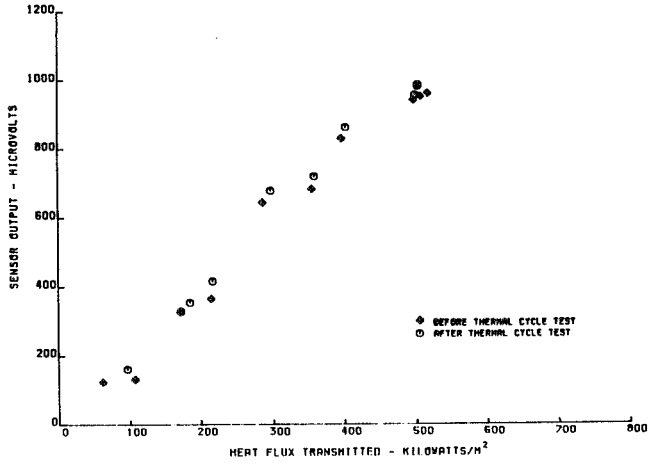

Figure 18 Plot of Data before and after Thermal Cycle Test

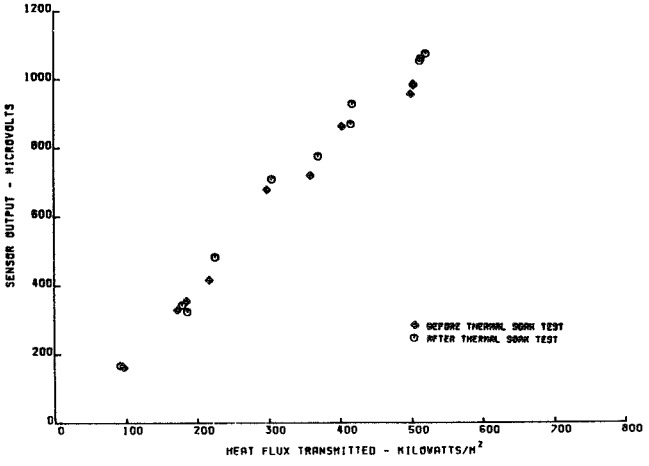

Figure 19 Plot of Data before and after Thermal Soak Test

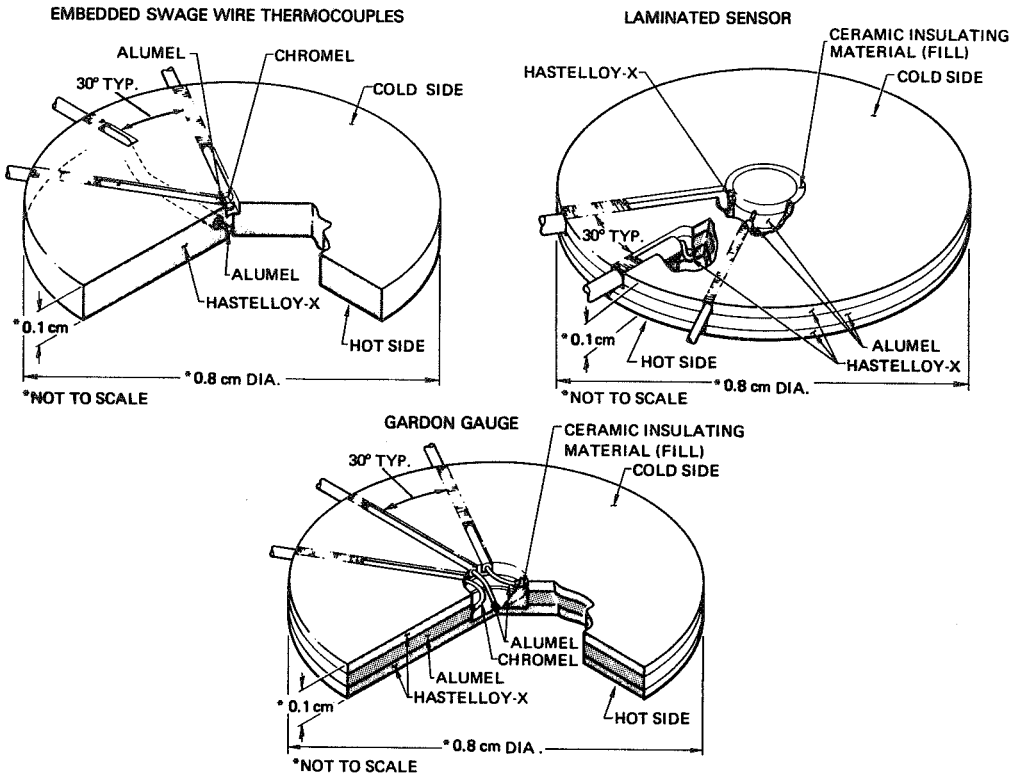

Figure 20 Schematic Representation of Combustor Liner Sensors

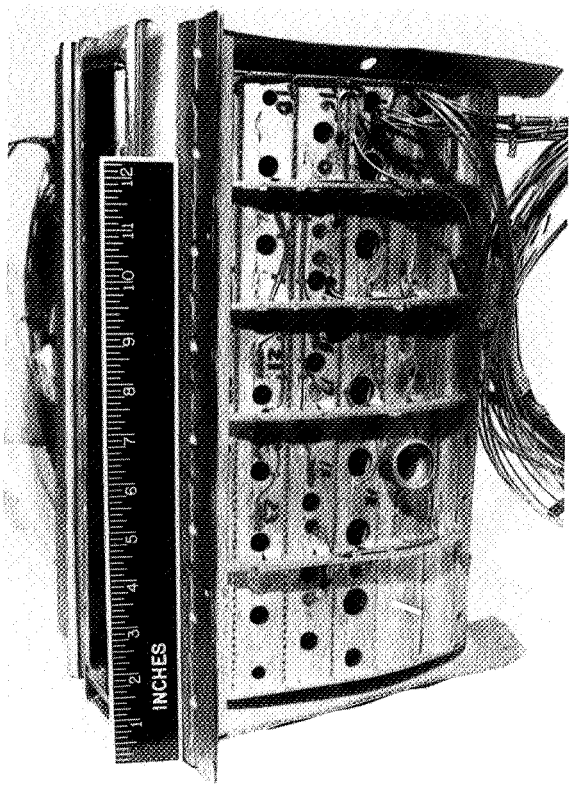

Figure 21 View of Cold Side of Instrumented Combustor Liner

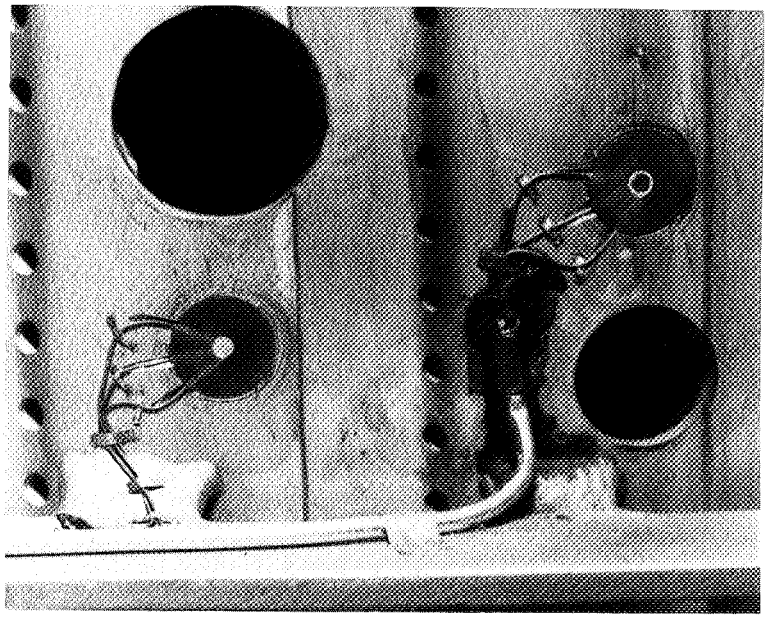

Figure 22 Close up View of Cold Side of Two Combustor Liner Heat Flux Sensors

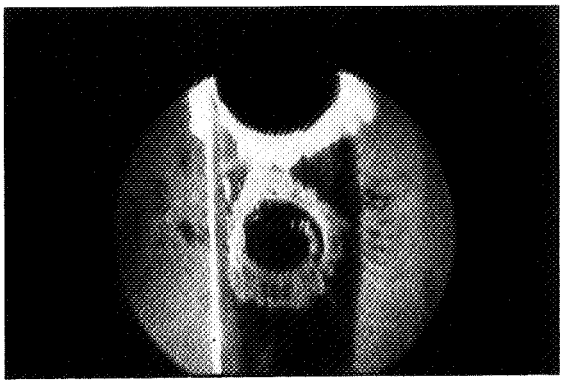

Figure 23 Close up View of Hot Side of Combustor Liner Heat Flux Sensor

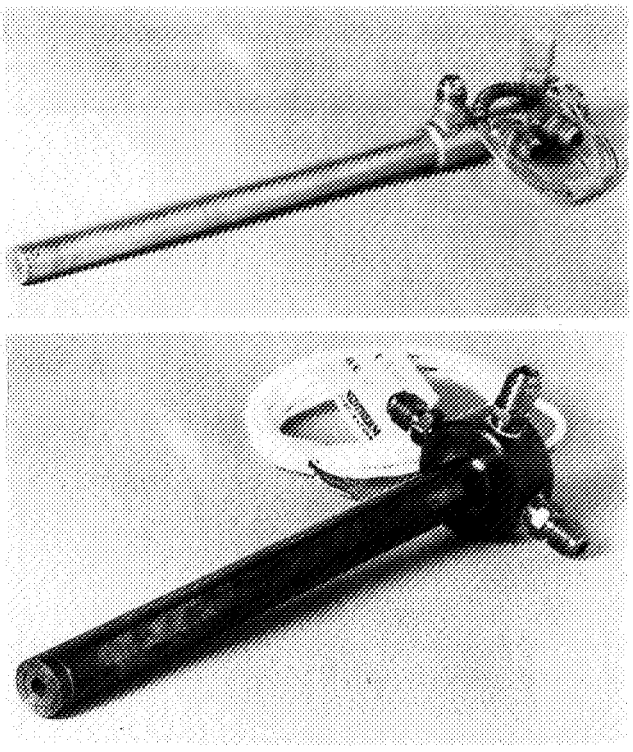

Figure 24 View of Porous Plug and Medtherm Radiometer Probes

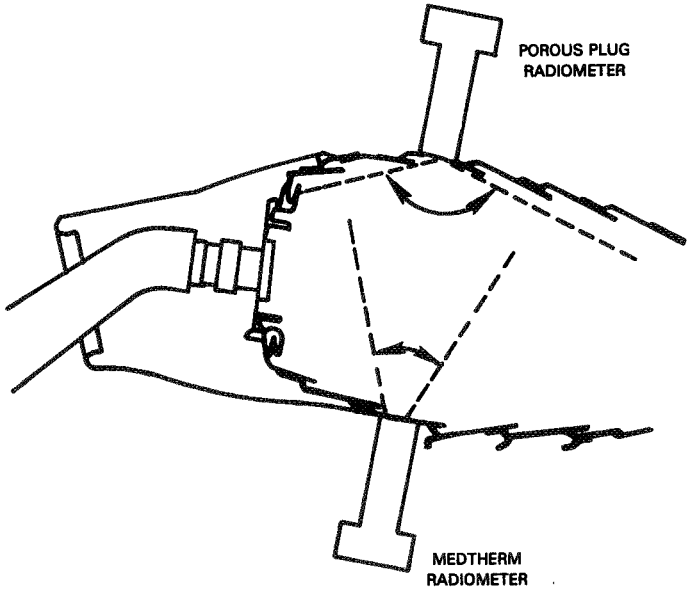

Figure 25 Schematic Representation of Radiometer Installation

Page intentionally left blank

D8

LASER ANEMOMETRY FOR HOT SECTION APPLICATIONS

Richard G. Seasholtz, Lawrence G. Oberle, and Donald H. Weikle
National Aeronautics and Space Administration
Lewis Research Center

INTRODUCTION

The objective of this in-house program is to develop laser anemometers (LA's) for use in the study of the hot section components of turbomachinery. Specifically, laser anemometers are being developed for use in the 50.8-cm (20-in.) diameter warm turbine and high-pressure turbine (HPT) facilities at Lewis. This paper presents a brief review of the status of the program along with some preliminary data taken in an open-jet burner.

A stepwise approach is being followed which builds on the experience gained in the development of laser anemometer systems for cold-flow turbomachinery facilities (refs. 1 and 2). The procedure being followed for the development of the hot section laser anemometer systems is

(1) establish measurement objectives for each facility--parameters to be measured and accuracies
(2) develop an analytical model for the complete LA systems
(3) perform necessary experiments to provide data not otherwise available; e.g., seed properties, surface relectivity, and window contamination
(4) experimentally verify the model using the open-jet burner facility
(5) optimize LA system design to give desired accuracies in minimum run time.

MEASUREMENT OBJECTIVES

The measurement objectives for both the warm turbine and the high pressure turbine facilities are to measure the following parameters with the given accuracies: mean velocity, 1 percent; flow angle, 1°; turbulence intensity, 10 percent; and turbulence scale, 20 percent. Also, it is desirable that these measurements be made to within 2 mm of the end walls. Finally, because of the high cost of operating these facilities, the LA systems must be designed to take these data in a minimum of experimental run time.

OPEN JET BURNER

An open-jet burner facility is being used as a test bed for the development and testing of all components of the laser anemometer system--optics, traversing hardware, seed generators, and windows. Furthermore, the extensive software needed for control and data acquisition will be written and tested in this facility before the system is installed in the turbine facilities, thus minimizing the amount of expensive debugging in the turbine facilities.

The open-jet burner facility consists of a general purpose laboratory combustor (fig. 1) and associated controls. The mixing and flow in this combustor closely approximate those of many conventional gas turbine combustors and the critical features of the combustion chemistry are reproduced. The

fuel (Jet A) is introduced at the front of the combustor by a pressure atomizing fuel nozzle. The combustion is stabilized in the forward section of the combustor by developing a strong, swirl stabilized recirculation zone. The hot combustion gases are cooled by dilution jets which are located at the back of the combustor. The primary and secondary jets have independent air supplies to permit adjustment of the velocity and temperature profiles at the exit. The ignitor, a flame monitor, and instrumentation ports are mounted in an instrumentation ring located between the primary and secondary sections. Seed particles are introduced through a tube mounted in one of the instrumentation ports. The 50.8-mm (2-in.) diameter exhaust can be operated over a temperature range of 1000 to 1600 K (1300° to 2500° F) at Mach numbers of 0.2 to 0.8.

OPTICAL CONFIGURATION

Several types of optical designs are being considered. The primary design is a conventional single component dual-beam fringe-type configuration as illustrated in figure 2. The other types of laser anemometers under consideration are

(1) a two-spot time-of-flight LA, which offers the ability to measure smaller particles than a fringe LA but suffers from low data rates in highly turbulent flow.

(2) a new design time-of-flight system developed under Grant NAS 3-2 at Case Western Reserve University (ref. 3). This configuration using four elliptical spots should give data rates similiar to a fringe system, but should be significantly more sensitive.

To illustrate the effect that various optical system parameters have on the performance of a fringe-type LA we can write the expression for the lower bound of the variance of the velocity measurement for a single particle (ref. 4) as

$$\sigma_{mv}^2 = \frac{8}{\pi^{1/2}} \left(\frac{hc}{\eta\lambda\sigma\Omega}\right) \frac{\Gamma_o}{P^2} \frac{v^3 w_o^3}{N^2 + 18/\pi^2} \tag{1}$$

where Γ_o represents the background light flux; v, the velocity; $2w_o$, the diameter of the probe volume; P, the laser power; N, the number of fringes; h, Planck's constant; c, the velocity of light; λ, the wavelength of the laser light; η, the quantum efficiency of the photodetector; Ω, the solid angle of the light collection optics; and σ, the light-scattering cross section of the particle. Equation (1) shows that to reduce the error for a given measurement it is desirable to

(1) have particles with a large light-scattering cross section (yet small and light enough to follow the flow, (e.g. about 1 micrometer diameter for most turbomachinery flows)

(2) have small f number optics (i.e. larger Ω)that captures as much of the light scattered from the particle as possible

(3) have a small probe volume with many fringes

(4) minimize the amount of stray background light (flare)

Note that the fringe spacing for a given velocity is constrained by the frequency responses of the photodetector and the signal processor (typically about 200 MHz). For example, with a 500-m/sec flow velocity resulting in a

150-MHz Doppler frequency, the fringe spacing is $v/f = 3.3$ micrometers. The minimum probe volume diameter $2w_0$ is then set by the number of cycles required by the signal processor. If 10 cycles are required, the minimum probe volume diameter would be 33 micrometers for this example.

The final focusing lens is a critical element of the optical system because it not only determines the minimum size of the probe volume, but it also determines how well the scattered light can be focused at the field stop. The field stop (a pinhole aperture usually located in front of the photodetector) acts as a spatial filter that prevents light scattered from surfaces near the probe volume (flare) from reaching the photodetector, thus reducing the r_0 term in equation (1). This ultimately determines how close to the end walls and blades that measurements can be made. The lens selected for the warm turbine system is a three-element, air-spaced, f/2.5 design, with a 100-mm clear aperture and a 235-mm back focal length.

Another consideration in determining the time required to measure turbulent flow parameters to the required accuracy is that velocity measurements taken within the correlation time of the flow are not independent. As shown in reference 5 the variance in the measurement of the mean velocity is

$$\sigma^2_{\overline{mv}} = \frac{2\tau_c}{T}\left[\frac{\sigma^2_{mv}}{2R\tau_c} + \sigma^2_v\left(1 + \frac{1}{2R\tau_c}\right)\right] \qquad (2)$$

where σ^2_{mv} is the variance of the individual particle velocity measurements (given by eq. (1)), T is the time over which the data is acquired, R is the mean data rate, σ^2_v is the variance of the flow fluctuations (the square of turbulence intensity), and τ_c is the flow correlation time. Thus, in addition to the data rate, the time scale and turbulence intensity of the flow must be known in order to estimate the data acquisition time. Note that increasing the data rate will not necessarily reduce the data acquisition time.

The selection of the type of optical configuration will be based on experimental evaluations to be made in the open-jet burner facility. The time required to measure the flow parameters given in the Measurement Objectives section along with the minimum distance that these measurements can be made from solid surfaces are the criteria that will be used to select the optical configuration.

TRAVERSING SYSTEM

The traversing system for the open jet burner facility is constructed using standard, commercially available linear actuators for XYZ motion of the optics package. A similar traversing system has been designed for the warm turbine system. A two-axis goniometer stage will be used to position a mirror located after the final focusing lens. This will permit the optical axis to be pointed along a radial line as well as slightly off the radial line to minimize shadowing caused by the shape of the turbine blades. A commercial controller is to be used for the actuators of the traversing systems; both local control and remote computer control via an RS-232 serial interface are available.

SEED PARTICLES

Particle characteristics necessary for hot section laser anemometry are primarily the same as ambient temperature laser anemometry with the exception that hot section particles must retain those characteristics at the high temperatures. A selected grade of alumina sized at 1.0 micrometer is being used initially. Other particles on hand for later trials are titanium dioxide, silicon carbide, hollow phenolic spheres, and Georgia clay.

A commercial aerodynamic particle sizing system is being used to presample the particles in use before a test and will be used to sample the exhaust products. This system consists of the particle sizer (ref. 6) along with a microcomputer, disk drive, and printer. The included software for this system is sufficient to analyze and graphically portray all the needed information on particles in the size range that we are using. The system can easily be calibrated with a selection of known particles. Samples of the alumina have been taken with the particle sizing system and the size distribution looks good for our use (fig. 3). No samples of this material have yet been acquired after going through the burner.

The particle generation system consists of a commercial, high volume, fluidized bed generator (ref. 7) as shown in figure 4. This system was selected so that we could be assured of high particle concentrations for present and future known applications. This system operates by injecting the alumina or other particles into a bed of brass beads (approx. diam 100 micrometers). As the bed of beads is fluidized and mixed the particles are deagglomerated and ejected from a 20-mm diameter nozzle.

Since we are restricted in the diameter of a penetration into the burner, we cannot achieve a sufficient flow rate to fluidize the brass beads without bypassing some of the particles. The concentration is sufficient using a 3-mm inlet into the burner when the particle generator is operating properly. We have had clogging problems and two failures in the mixer in approximately 40 hr of usage. The clogging problem may be caused by moisture in the alumina.

A seed injection probe has been designed for the warm turbine that can be remotely moved in the radial and circumferential directions. The range of movement of the seed injection probe takes into account the large turning angle (75°) of the stator.

WINDOWS

Gaining optical access to the stator and rotor passages of a turbine without modifying the flow is a challenging design problem even for cold flow at low pressures. The warm turbine facility will use two windows. One will cover the stator passage and the other the rotor passage. Only one window will be installed at a time. Each window will be curved to match the tip radius and will be mounted flush with the inside surface so the flow will not be disturbed. The window material is synthetic sapphire, selected for its strength at high temperature and good optical properties. Because of their curvature the windows will act as cylindrical lenses; the aberration introduced is minimized by making the windows relatively thin (about 3 mm). Compensating optics will be used to correct the remaining aberration.

One of the major concerns in the design of the LA for the turbine facilities is the unknown rate of contamination of the windows. It is expected that combustion products, lubricating oil, and seed material will be deposited on the window. Tests are being conducted in the open-jet burner facility to establish the contamination rate. Various means of keeping the window clean, such as using an air purge, will be examined. Window cleaning procedures will be studied to determine a practical means of cleaning the window without removing it from the turbine. A sapphire test window has been mounted on the traversing table and we will be watching the change in data rate during burner startup and as a function of time at various distances from the hot gases. The window will be examined after exposure to determine the type of contaminants. The type of contaminants and rate of buildup data can then be used to determine if a high-temperature, on-line window cleaning method is necessary and possible.

DATA PROCESSING AND EXPERIMENT CONTROL

In the laser anemometry program the computer has become a necessary tool, chiefly due to the requirement that data be obtained at rates exceeding 5 kHz and that the data be reduced, at least partially, on line. In addition to the data acquisition requirements, the computer will become the experiment controller, performing such housekeeping procedures as deciding when to move the optics into position, moving the optics, how long to take data, and which data to keep.

In order to meet these requirements, a computer with a large memory, a fast mass storage device, and control capabilities was purchased. The computer, a PDP 11/44, is now installed in the open-jet burner facility. Using the RSX-11M multitasking operating system, the PDP 11/44 will be able to run several on-line programs 'simultaneously': acquiring data, reducing and storing the acquired data, and presenting a preliminary data summary. In addition to the data acquisition and experiment control functions, the PDP 11/44 will be able to produce high quality on-line graphics, both on the terminal and on a graphics printer. A block diagram of this computer system is shown in figure 5.

Until the PDP 11/44 is operational, a small laboratory minicomputer is being used to take data with a program which controls the traversing system, takes up to 4000 data points, and draws a frequency (or velocity) histogram of the acquired data (figs. 6(a) and 6(d)). The data comes in from a counter-type signal processor, on a direct memory access (DMA) line, and is stored in memory as two 16-bit words per data point. The time-of-flight through the required number of fringes (time data) and the time between the present and most recent data point (TBD data) are both converted to a FORTRAN readable form. If desired, this data can then be stored on disk. Finally the program performs the necessary calculations to plot a frequency histogram.

Even though the on-line data reduction provides a measure of the average data rate, in order to properly evaluate the autocorrelation outputs (figs. 6(c) and 6(f)) a probability histogram of the time between data points is necessary (figs. 6(b) and 6(e)). Because the flow is randomly time-sampled, data points must occur relatively close together temporally (and therefore spatially) for the autocorrelation to be meaningful. If this occurs, as shown in both examples, data can then be autocorrelated to obtain a measure of the

turbulence scale. (The autocorrelation is calculated using the procedure given in ref. 8.) The data shown in figures 6(a) to (c) were taken in the potential core of a small air jet (turbulence intensity about 1.6 percent) and the data in figures 6(d) to (f) were taken in the mixing region of the open jet burner exhaust (cold flow), which had a much higher turbulence intensity (about 30 percent).

The on-line program has recently been modified to take velocity surveys; that is, to move the optics under program control, take data, and plot a profile of the velocity component chosen by the experimenter. Examples of radial surveys of mean axial velocity and turbulence intensity taken in the exhaust of the open-jet burner are shown in figure 7(a) for cold flow and figure 7(b) for hot flow.

Future modifications will allow the program to take data between the blades of a rotating turbine, and keep track of not only the position of the optics, but also the position of the turbine rotor with reference to a fixed point.

PLANS

We plan to install the laser anemometer system in the warm turbine facility during 1984 and make it operational in early 1985. Preliminary design work for the high-pressure turbine facility (HPT) window is now underway.

REFERENCES

1. Goldman, L. J. and Seasholtz, R. G., "Laser Anemometer Measurements in an Annular Cascade of Core Turbine Vanes and Comparison with Theory," NASA TP-2018, 1982.
2. Powell, J. A., Strazisar, A. J. and Seasholtz, R. G., "High-Speed Laser Anemometer System for Intrarotor Flow Mapping in Turbomachinery," NASA TP-2018, 1982.
3. Edwards, R. V., "Laser Anemometer Optimization," Presented at Turbine Engine Hot Section Technology (HOST) Workshop, NASA TM-83022, Cleveland, Ohio, October 19-20, 1982.
4. Lading, L., "The Time-of-Flight verses the LDA," Proceedings of the Third International Workshop on Laser Velocimetry, Purdue University, 1978.
5. Edwards, R. V. and Jensen, A. S., "Particle Sampling Statistics in Laser Anemometers: Sample and Hold Systems and Saturable Systems," J. Fluid Mech., vol. 133, 1983, pp. 397-411.
6. TSI, Inc. Model APS 33 Aerodynamic Particle Sizer Instruction Manual.
7. TSI, Inc. Model 9310 Fluidized Bed Aerosol Generator Instruction Manual, p. 2.
8. Smith, D. M. and Meadows, D. M., "Power Spectra from Random-Time Samples for Turbulence Measurements with a Laser Velocimeter," Proceedings of the Second International Workshop on Laser Velocimetry, Vol. 1, H. D. Thompson and W. H. Stevenson, eds., Bull. No. 144, Purdue Univ., 1974, pp. 27-44.

LABORATORY COMBUSTOR

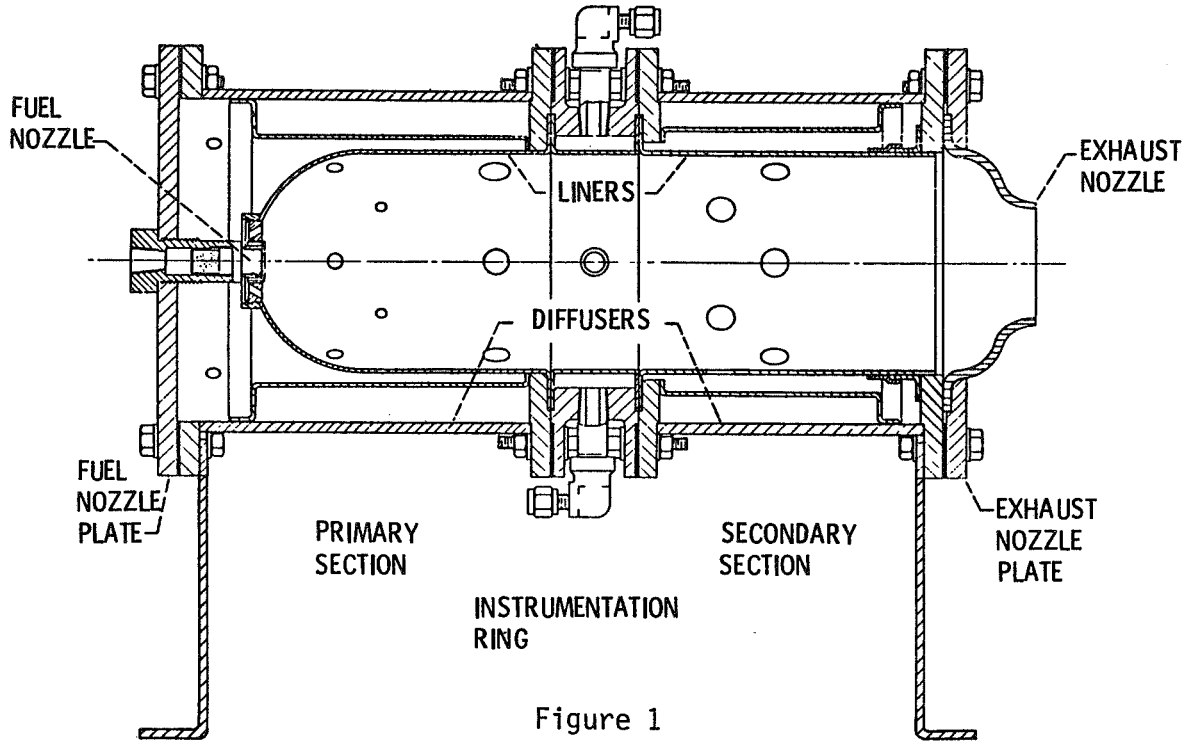

Figure 1

DUAL-BEAM FRINGE-TYPE LASER ANEMOMETER

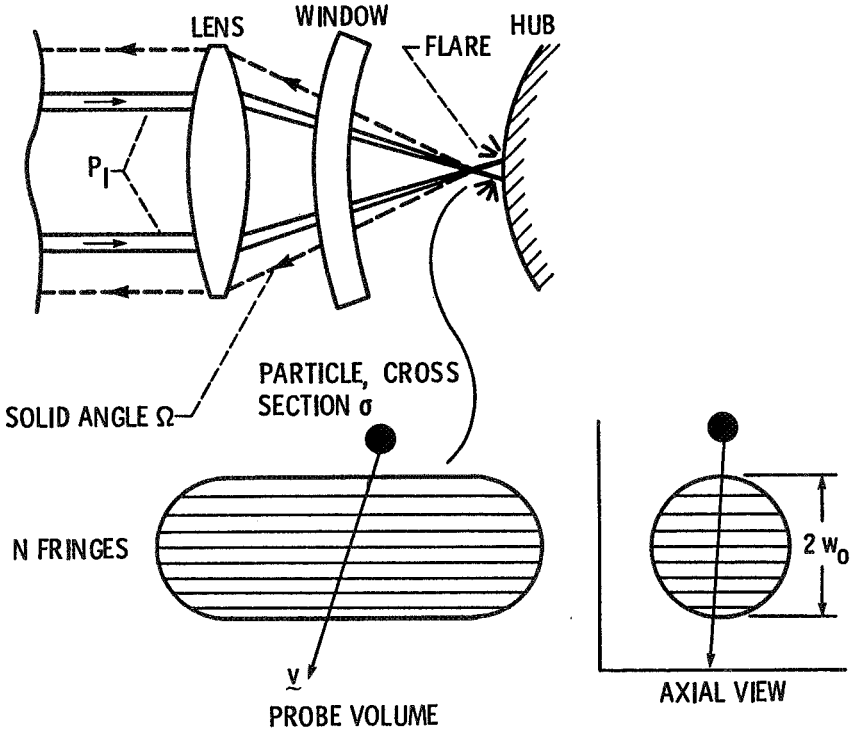

Figure 2

SIZE DISTRIBUTION OF ALUMINA POWDER

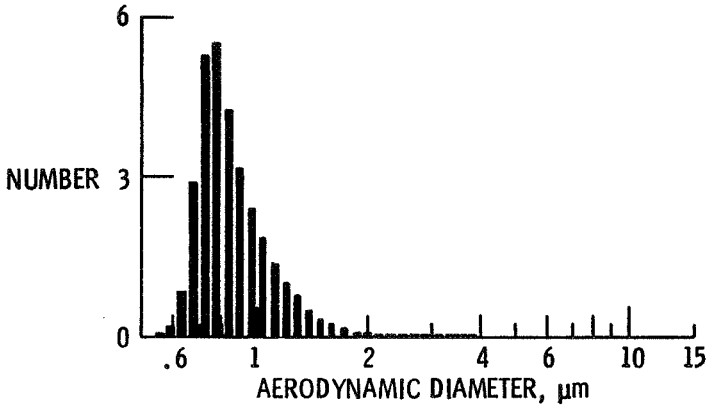

Figure 3

FLUIDIZED BED PARTICLE GENERATOR

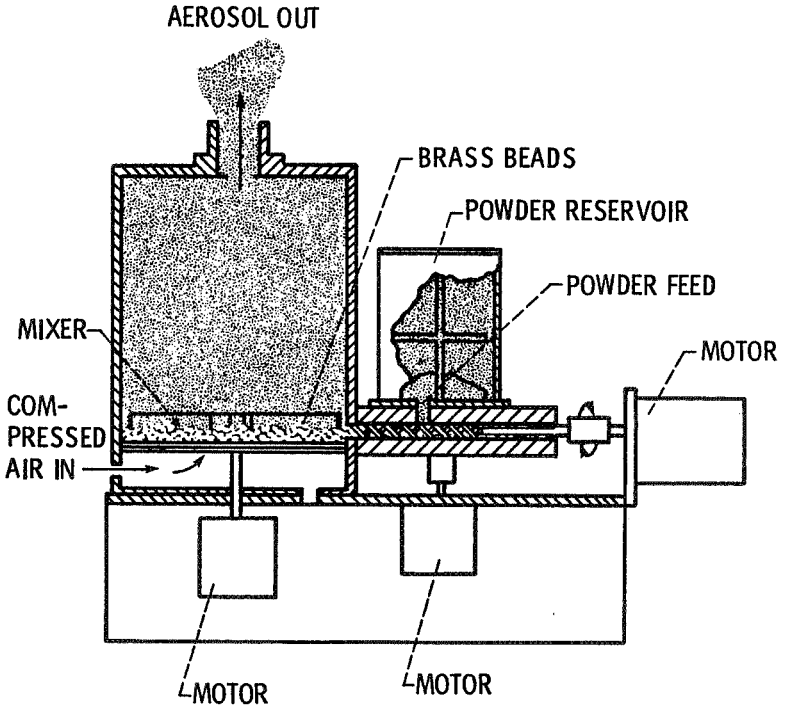

Figure 4

HOST LASER ANEMOMETRY SYSTEM

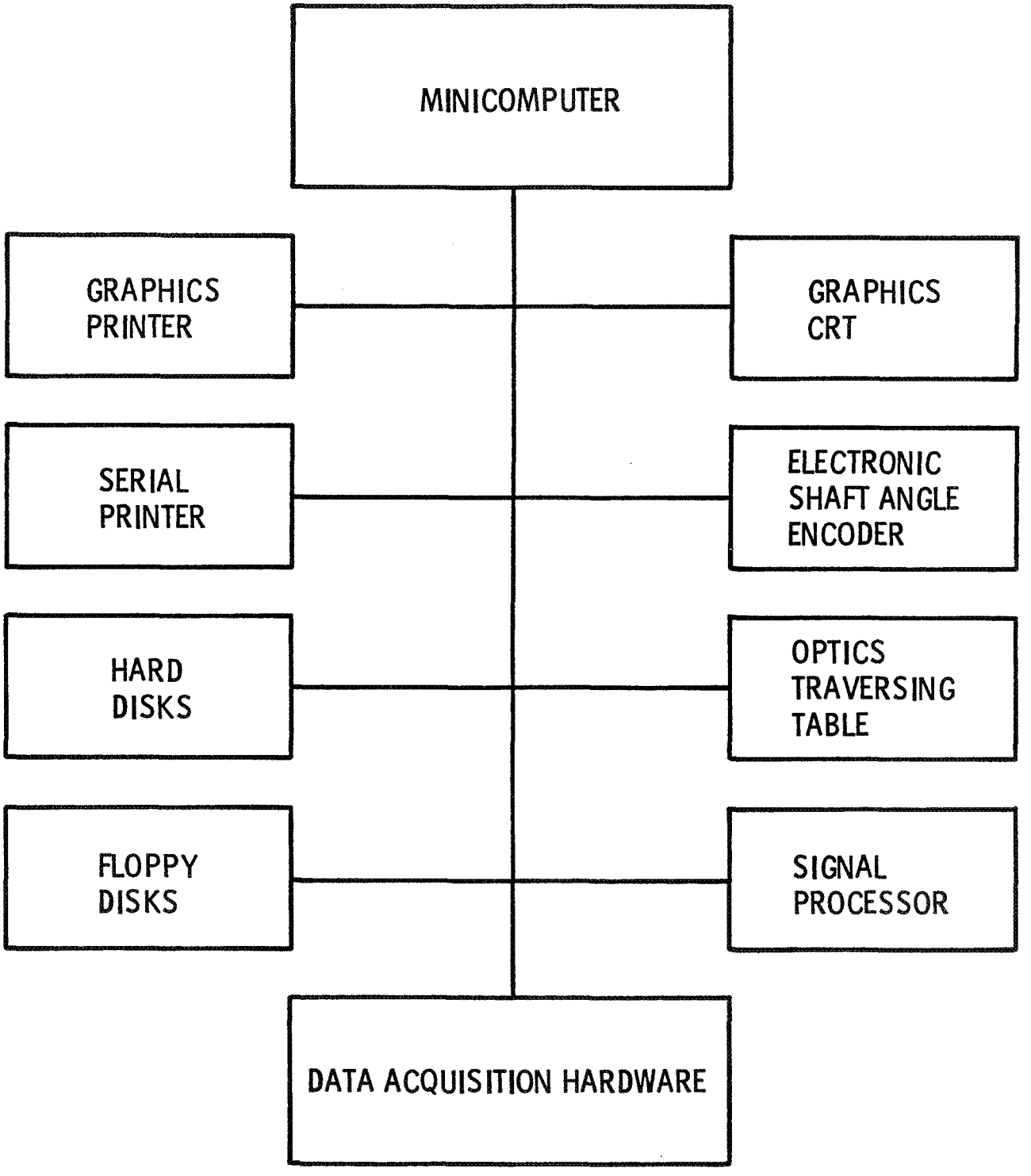

Figure 5

CRT DISPLAYS

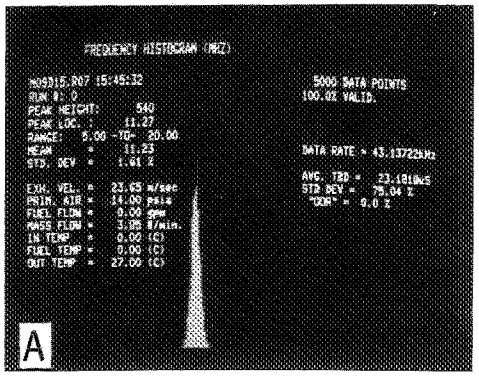

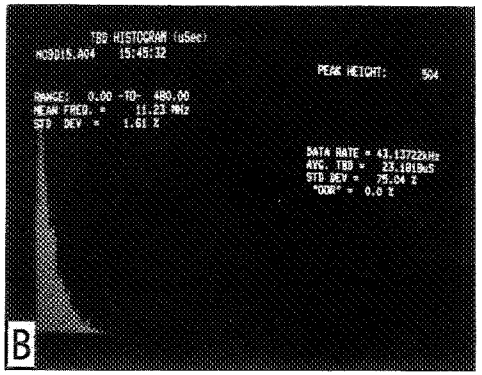

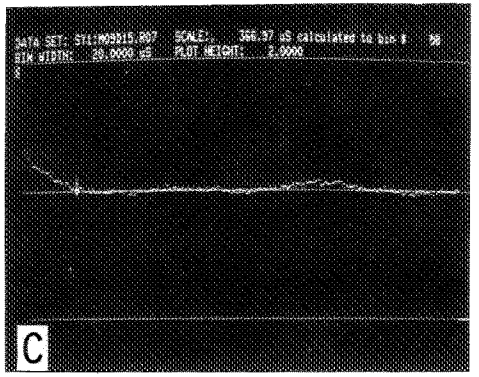

(A-C) LOW TURBULENCE CASE

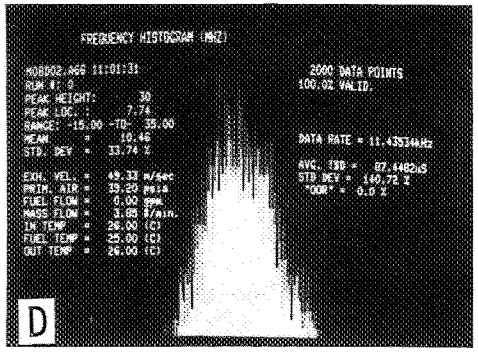

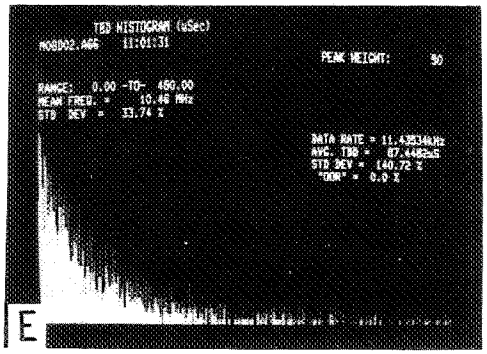

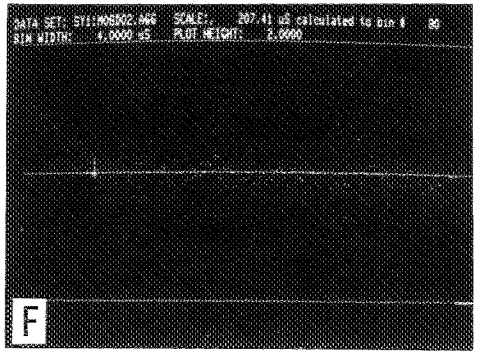

(D-F) HIGH TURBULENCE CASE

CS-83-2951

Figure 6

MEAN AXIAL VELOCITY AND TURBULENCE INTENSITY

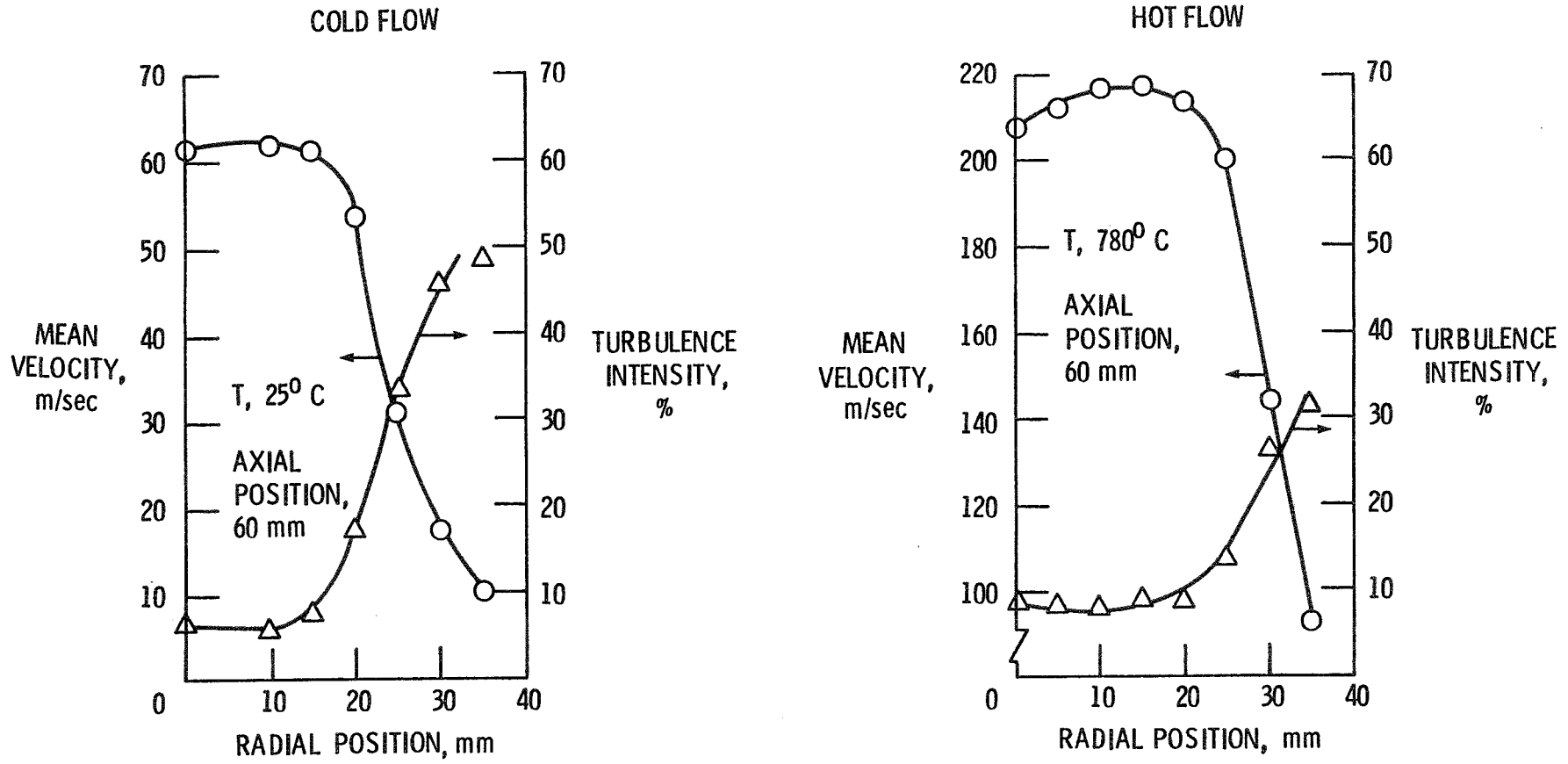

Figure 7

Page intentionally left blank

D9

TIME-OF-FLIGHT ANEMOMETER FOR HOT SECTION APPLICATIONS

Robert V. Edwards
Chemical Engineering Department
Case Western Reserve University

The purpose of this section of the project is to design, construct, and test laser anemometer configurations for Hot Section velocity measurements. Optimizing the laser anemometer system necessarily included the data processing algorithms used. It is felt that the requirements here are too demanding for standard laser anemometer systems.

Relevant Hot Section Properties

1) High temperature with possibility of large background radiation
2) Difficult optical access
3) Large flow velocity variation - especially in the rotating sections
4) Presence of solid surfaces that generate spurious reflections
5) Low seed particle density

In the past few years, the laser scattering group at Risø, Denmark, under the direction of Lars Lading, and the laser scattering group at Case Western Reserve University under Robert V. Edwards, have worked together to develop procedures for the optimal design of laser anemometry systems. The principles derived are being used to design the system for Hot Section measurements.

The system decided on is a so-called time-of-flight anemometer with elliptical spots. The version of the time-of-flight designed for this project contains two new features: 1) Elliptical spots - this gives the wide flow angle acceptance characteristics of a "fringe" anemometer combined with the superior spatial resolution of a time-of-flight anemometer. 2) The prototype for the Hot Section measurements uses a unique optical coding to transform the pulse into the optimal form for pulse position sensing. Heretofore, this required rather complex and inflexible electronic circuitry. This optical processor is intrinsically free from some of the errors to which the electronic circuits were prone.

Figure 1 is a photograph of the prototype optical system. The system is presently undergoing tests for accuracy and spatial resolution. The preliminary indications are that the system is capable of measurement within 300 μm of a surface. A better estimate of the spatial resolution will be possible only after we mechanically stiffen the system. It requires very tight tolerances on the optics.

A prototype has been built of an electronic signal processor for the anemometer. Figure 2 shows the signals generated to detect the pulse position. The zero crossing of the s-shaped pulses are used. A velocity histogram obtained using this system on a seeded flow in a small wind tunnel is shown in Figure 3.

The prototype system is being evaluated in terms of scale-up to a system capable of the desired hot stage measurements. In particular, the mechanical and optical requirements of the system are being evaluated.

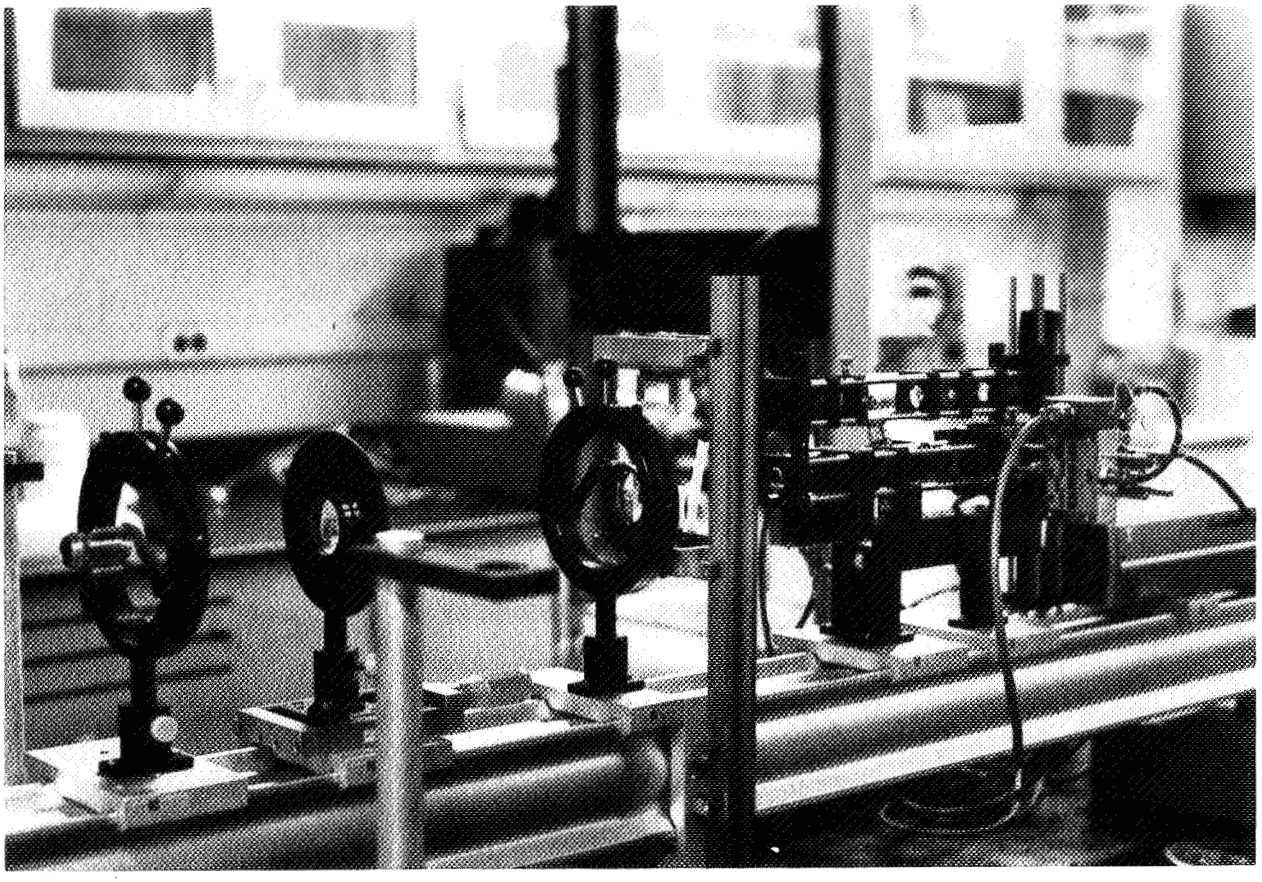

Figure 1: Prototype of Time-of-Flight Anemometer. It is constructed of commercial optical "breadboard" components.

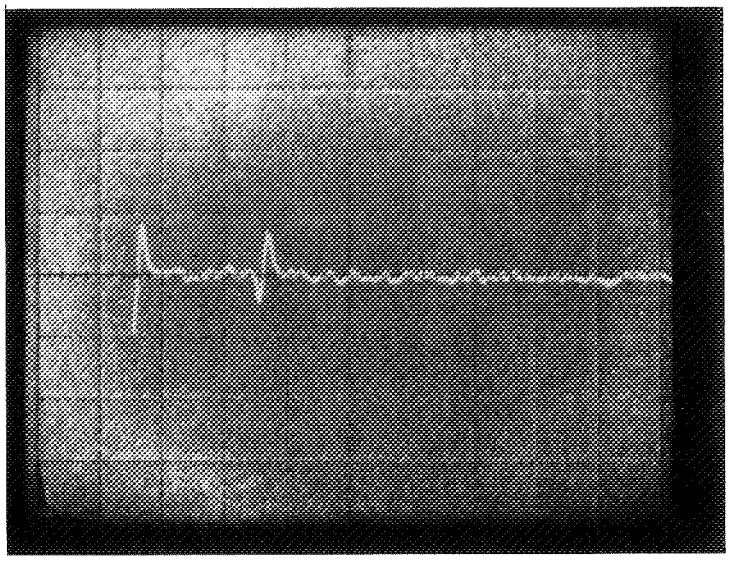

Figure 2: Oscilloscope trace of difference signal from the two photodetectors.

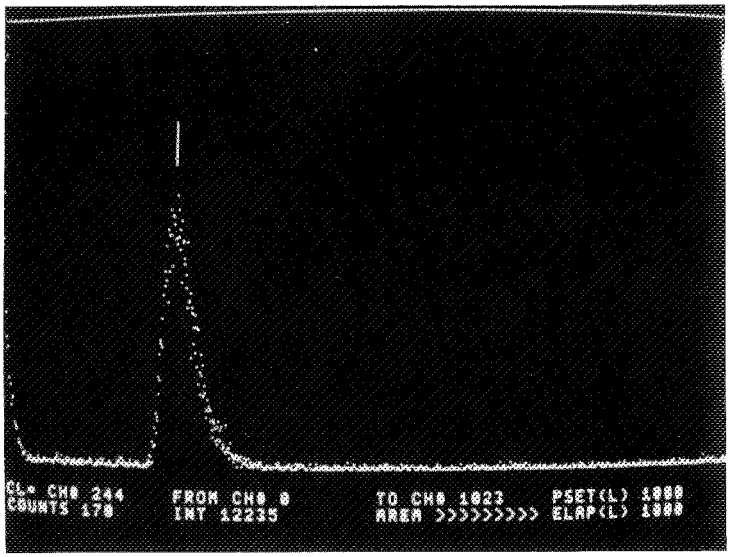

Figure 3: Velocity histogram obtained using new anemometer on air flow in a small wind tunnel. The pulse separation is converted to a pulse height and then stored on a pulse height analyzer.

Page intentionally left blank

D/0

TURBINE HEAT TRANSFER

John E. Rohde
National Aeronautics and Space Administration
Lewis Research Center
Cleveland, Ohio 44135

Improved turbine durability and performance and reduced development cost will all result from improved methods of predicting turbine metal temperatures. As you know, better metal temperature prediction methods require improvements in the methods of predicting the hot gas flow over the turbine airfoils and the cooling air flow inside the airfoil and in the methods of predicting the heat transfer rates on both the hot gas-side and coolant-side of the airfoil. The overall HOST Turbine Heat Transfer effort is directed at improving all four of these areas of concern.

Achievement of these improvements requires a rigorous and systematic research effort from both the experimental and analytical sides. The experimental approach being pursued starts with fundamental experiments using simple shapes and flat plates; progresses on to more realistic cold, warm, or hot cascades using airfoils; continues to progress on to more realistic warm turbine, large low-speed turbine, or transient turbine tests; and finally combines all the interactive effects in real-engine or real-engine type turbine tests. Analytical approaches being pursued also start with relatively simple mathematical models and progress to more realistic cases that include more interactive effects, and finally combines all the interactive effects of the turbine operating in the real engine environment.

The HOST Turbine Heat Transfer Subproject schedule showing the current activities is included in the attached figures. Each line on the figure represents a separate contract, grant, or NASA Lewis in-house effort. The dotted blocks indicate future potential contract or grant activities. Currently, contract and grant efforts are being conducted to obtain fundamental experimental data and to develop and/or assess analytical tools in all four areas of concern. These contract and grant activities will be discussed in detail later in this meeting by the respective principal investigators.

NASA Lewis in-house turbine research efforts are being pursued to obtain more realistic warm turbine and real-engine type turbine experimental data. The major turbine research parameters of interest that will be measured or determined to provide this better understanding of the aerothermal loads on air-cooled airfoils are the following:

1) local hot gas flow velocities and secondary flows,
2) local hot gas recovery temperature along the airfoil surfaces and other hot gas path surfaces,
3) local total and radiation heat fluxes to the airfoils and other hot gas path surfaces, and
4) local airfoil wall temperatures.

Very little or none of this type experimental research information exists with controlled warm or real-engine type conditions and known boundary conditions.

These in-house turbine research efforts will be conducted using the best available analyses to help define the test configurations, the types of research measurements, and for comparisons with the measured research results. Initially, analytical efforts will use the best available flow and heat transfer codes such as a twoor three-dimensional inviscid flow code and a two- or three-dimensional boundary layer heat transfer code. These analyses will be applied at the mid-span section and possibly at the hub and tip sections or other local zones of the hot gas flow path. More sophisticated three-dimensional viscous codes and three-dimensional viscous codes with boundary layer resolution will be used as they become available. These analytical efforts will be conducted using the best available source or sources in-house and on contract with industry and universities.

An Airfoil Metal Temperature Runoff effort is planned to start in 1985. This Airfoil Metal Temperature Runoff effort will be initiated using an all-impingement cooled static airfoil configuration and a multipass cooled rotating airfoil. Both of these air-cooled airfoils will use NASA conceived profiles and no film cooling initially. This program will provide engine manufacturers with an opportunity, through contracts and/or cooperative agreements, to assess and improve their analytical tools used to predict airfoil metal temperatures. The results of these assessments will be accumulated as an industry uncertainty band from the experimental data with the individual contributors predictions remaining known only to the individual contributor. Contracted contributors would be required to identify the analytical tools used and the uncertainty levels obtained.

ANALYTICAL TOOLS USED TO PREDICT AIRFOIL METAL TEMPERATURES

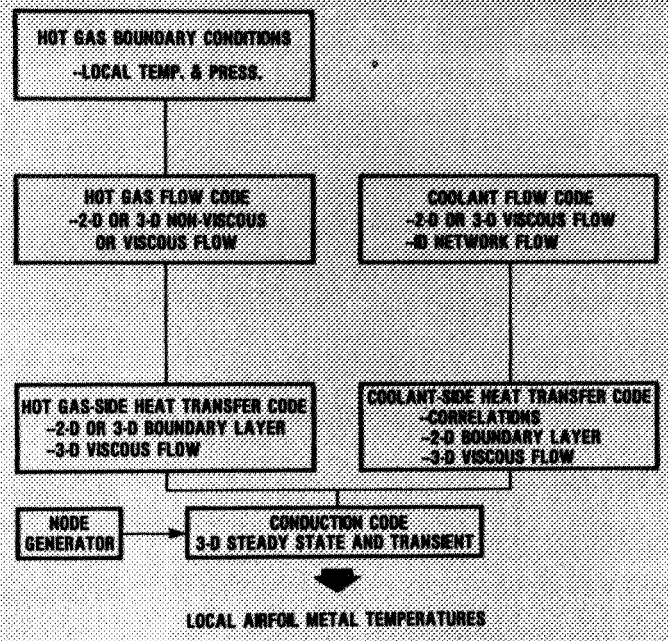

CD-83-13762

BUILDING BLOCK AEROTHERMAL TURBINE RESEARCH APPROACH

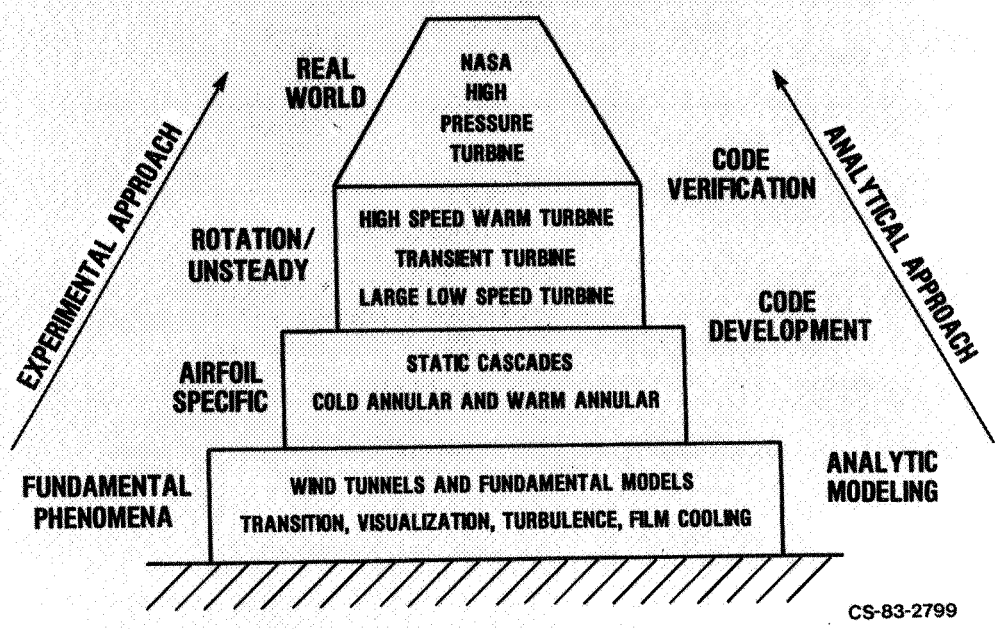

CS-83-2799

TURBINE HEAT TRANSFER SUBPROJECT SCHEDULE

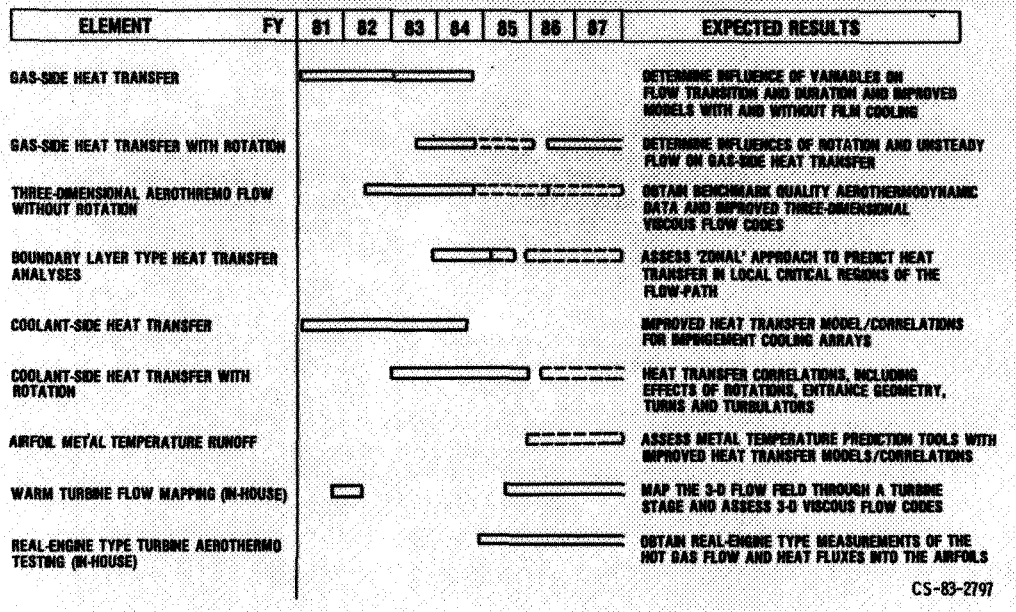
ELEMENT
FY
81
82
83
84
85
86
87
EXPECTED RESULTS
GAS-SIDE HEAT TRANSFER
DETERMINE INFLUENCE OF VARIABLES ON FLOW TRANSITION AND DURATION AND IMPROVED MODELS WITH AND WITHOUT FILM COOLING
GAS-SIDE HEAT TRANSFER WITH ROTATION
DETERMINE INFLUENCES OF ROTATION AND UNSTEADY FLOW ON GAS-SIDE HEAT TRANSFER
THREE-DIMENSIONAL AEROTHERMO FLOW WITHOUT ROTATION
OBTAIN BENCHMARK QUALITY AEROTHERMODYNAMIC DATA AND IMPROVED THREE-DIMENSIONAL VISCOUS FLOW CODES
BOUNDARY LAYER TYPE HEAT TRANSFER ANALYSES
ASSESS 'ZONAL' APPROACH TO PREDICT HEAT TRANSFER IN LOCAL CRITICAL REGIONS OF THE FLOW-PATH
COOLANT-SIDE HEAT TRANSFER
IMPROVED HEAT TRANSFER MODEL/CORRELATIONS FOR IMPINGEMENT COOLING ARRAYS
COOLANT-SIDE HEAT TRANSFER WITH ROTATION
HEAT TRANSFER CORRELATIONS, INCLUDING EFFECTS OF ROTATIONS, ENTRANCE GEOMETRY, TURNS AND TURBULATORS
AIRFOIL METAL TEMPERATURE RUNOFF
ASSESS METAL TEMPERATURE PREDICTION TOOLS WITH IMPROVED HEAT TRANSFER MODELS/CORRELATIONS
WARM TURBINE FLOW MAPPING (IN-HOUSE)
MAP THE 3-D FLOW FIELD THROUGH A TURBINE STAGE AND ASSESS 3-D VISCOUS FLOW CODES
REAL-ENGINE TYPE TURBINE AEROTHERMO TESTING (IN-HOUSE)
OBTAIN REAL-ENGINE TYPE MEASUREMENTS OF THE HOT GAS FLOW AND HEAT FLUXES INTO THE AIRFOILS
CS-83-2797

ANALYTICAL TOOLS USED TO PREDICT AIRFOIL METAL TEMPERATURES

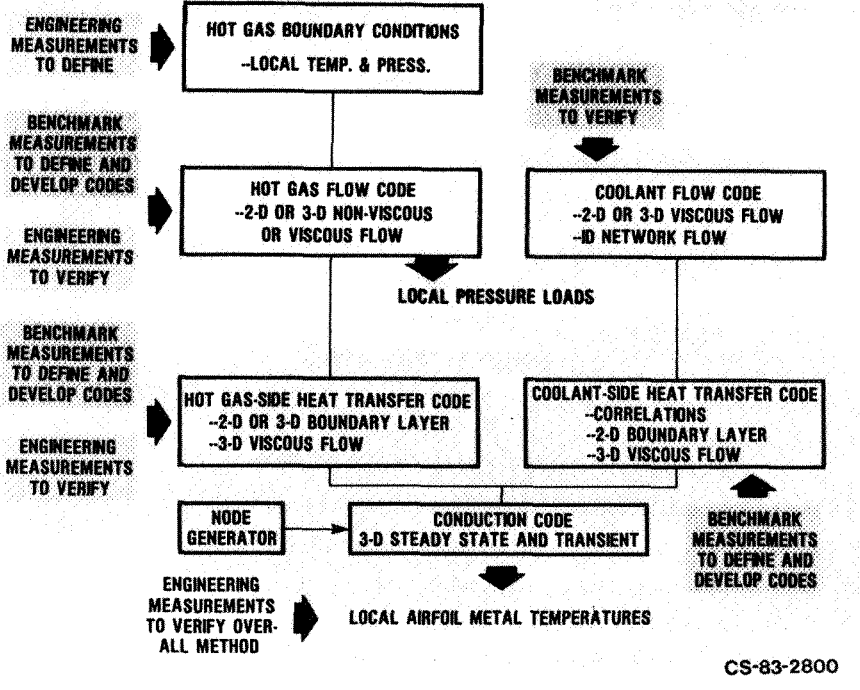
ENGINEERING MEASUREMENTS TO DEFINE
HOT GAS BOUNDARY CONDITIONS
--LOCAL TEMP. & PRESS.
BENCHMARK MEASUREMENTS TO VERIFY
BENCHMARK MEASUREMENTS TO DEFINE AND DEVELOP CODES
HOT GAS FLOW CODE
--2-D OR 3-D NON-VISCOUS OR VISCOUS FLOW
COOLANT FLOW CODE
--2-D OR 3-D VISCOUS FLOW
--1D NETWORK FLOW
ENGINEERING MEASUREMENTS TO VERIFY
LOCAL PRESSURE LOADS
BENCHMARK MEASUREMENTS TO DEFINE AND DEVELOP CODES
HOT GAS-SIDE HEAT TRANSFER CODE
--2-D OR 3-D BOUNDARY LAYER
--3-D VISCOUS FLOW
COOLANT-SIDE HEAT TRANSFER CODE
--CORRELATIONS
--2-D BOUNDARY LAYER
--3-D VISCOUS FLOW
ENGINEERING MEASUREMENTS TO VERIFY
NODE GENERATOR
CONDUCTION CODE
3-D STEADY STATE AND TRANSIENT
BENCHMARK MEASUREMENTS TO DEFINE AND DEVELOP CODES
ENGINEERING MEASUREMENTS TO VERIFY OVER-ALL METHOD
LOCAL AIRFOIL METAL TEMPERATURES
CS-83-2800

AIRFOIL METAL TEMPERATURE RUNOFF

GOAL: ASSESS AND IMPROVE ANALYTICAL TOOLS USED TO PREDICT AIRFOIL METAL TEMPERATURES

- ASSESS METAL TEMPERATURE PREDICTION USING AN ALL-IMPINGEMENT COOLED VANE WITH NO FILM COOLING INITIALLY
- REVISE ANALYTICAL TOOLS BASED ON REAL-ENGINE TYPE MEASUREMENTS OF THE LOCAL HOT GAS TEMPERATURES AND HEAT FLUXES AND REASSESS VANE METAL TEMPERATURE
- ASSESS METAL TEMPERATURE PREDICTION USING A MULTI-PASS COOLED BLADE WITH NO FILM COOLING INITIALLY

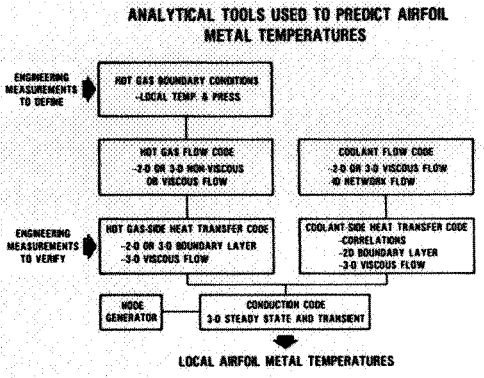
ANALYTICAL TOOLS USED TO PREDICT AIRFOIL METAL TEMPERATURES
ENGINEERING MEASUREMENTS TO DEFINE
HOT GAS BOUNDARY CONDITIONS -LOCAL TEMP. & PRESS
HOT GAS FLOW CODE -2-D OR 3-D NON-VISCOUS OR VISCOUS FLOW
COOLANT FLOW CODE -2-D OR 3-D VISCOUS FLOW -1D NETWORK FLOW
ENGINEERING MEASUREMENTS TO VERIFY
HOT GAS-SIDE HEAT TRANSFER CODE -2-D OR 3-D BOUNDARY LAYER -3-D VISCOUS FLOW
COOLANT-SIDE HEAT TRANSFER CODE -CORRELATIONS -2D BOUNDARY LAYER -3-D VISCOUS FLOW
MODE GENERATOR
CONDUCTION CODE 3-D STEADY STATE AND TRANSIENT
LOCAL AIRFOIL METAL TEMPERATURES

- REVISE ANALYTICAL TOOLS BASED ON REAL-ENGINE TYPE MEASUREMENTS OF THE LOCAL HOT GAS TEMPERATURES AND HEAT FLUXES AND REASSESS BLADE METAL TEMPERATURES

STATUS : MULITPLE CONTRACTS AND/ OR COOPERATIVE AGREEMENTS TO BE AWARDED IN 1985

CS-83-2801

Page intentionally left blank

D11

GAS FLOW ENVIRONMENTAL AND HEAT TRANSFER NONROTATING 3D PROGRAM

T. Geil and J. Steinhoff
University of Tennessee Space Institute

OBJECTIVES

The experimental contract objective is to provide a complete set of "benchmark" quality data for the flow and heat transfer within a "large" rectangular turning duct. These data are to be used to evaluate and verify three-dimensional internal viscous flow models and computational codes. The analytical contract objective is to select such a computational code and define the capabilities of this code to predict the experimental results. Details of the proper code operation will be defined and improvements to the code modeling capabilities will be formulated.

The experimental and analytical efforts are being conducted under a coordinated multiphase contract. Phase one, the current work, is the study of internal flow in a rectangular, square cross-sectioned, 90° bend turning duct, and is planned as a 28 month investigation which started in April, 1982. Phase one is divided into the following five tasks: I. Design and Fabrication, II. Experimental Velocity Measurements, III. Experimental Heat Transfer, IV. Theoretical Analysis and Data Comparison, V. Reporting and Technical Data. Future work to be performed at NASA's option includes the investigation of flow over an airfoil cascade, with and without film cooling, inside the turning radius of the duct.

Separate but coordinated experimental and analytic approaches are in progress to attain the contract objectives.

APPROACH, EXPERIMENTAL

The experimental facility design features modular tunnel components which allow flow measurements every 15° in the 90° bend. The 25.4 cm (10 in) square cross section tunnel is designed with a 13 to 1 area ratio bell mouth contoured to provide uniform flow velocity and is powered by a variable speed, six-bladed fan. (See Figures 1 and 2). The tunnel is designed for incompressible flow and will produce Reynolds numbers of 0.2 to 2.0 X 10^6 at the entrance of the 90° bend for tunnel velocities of 6 to 30 m/sec (20 to 100 ft/sec). These two flow conditions provide laminar and fully turbulent boundary layer profiles at the entrance to the 90° bend. The facility is also designed for adiabatic wall testing with large thermal gradients in the air stream. Heated air will be provided by electric resistance heaters sized so that 100 KW will produce a minimum of 110°C (200°F) temperature increase in the air stream.

The primary instrumentation is designed for non-intrusive flow measurements utilizing a three-dimensional, laser velocimeter (LV) and wall static pressure and heat flux gages. The LV utilizes two color beams and Bragg diffraction beam splitting/frequency shifting to separate the three simultaneous, orthogonal, vector velocity components. The LV signal processors determine the digital values of velocity from the seed particles crossing the laser beam probe volume. To improve and speed up digital data acquisition, the LV processors are designed around an S-100

Work done under NASA contract NSA3-23278.

bus Z-80 microprocessor which provides on-line, near-real time data reduction. This on-line data reduction capability will be used to assess the adequacy and precision of the data as it is acquired and recorded for off-line detailed analysis. Typical data output is shown in Figure 3. To qualify the measurements as "benchmark" data, the LV data will be compared with both pitot probe and hot wire anemometer measurements for flow conditions which permit comparisons.

CURRENT RESULTS AND PLANS, EXPERIMENTAL

All experimental hardware and instrumentation systems have been designed, fabricated, assembled, installed and checked out. Only the air heater remains to be fabricated, and only the heat flux measurement system remains to be checked . Extensive tunnel flow quality surveys have been completed in the inlet section following "benchmark" calibration of the LV system, pitot-static, and hot wire anemometer. All three measurement systems were calibrated against reference standards and were found to agree within $\pm$ 1% on the entrance section velocity. The LV system was calibrated with a spinning disk reference velocity at 20 m/sec. The pitot-static pressures were read on a precision slant manometer with 13mm of H_2O full scale. The hot-wire system was calibrated in a reference nozzle flow at 30.5 m/sec. Velocity surveys taken 50.8 cm (20 in) behind the bell mouth exit showed flat velocity profiles $\pm$ 0.5% mean velocity outside of the boundary layer. Laminar and turbulent boundary layers were measured at velocities of 4.5 m/sec and 19.4 m/sec, respectively as shown in Figure 4. Most significant finding was that the LV and hot-wire turbulence intensity measurements agreed within 10% or nominally 1% turbulence intensity. The mill bed traverse system has demonstrated repeated accuracy of $\pm$ 0.1mm on all three axis of movement. Both LV and probe positions are controlled by the computer driven mill bed.

Development of the flow seeding system was successfully completed during the LV system checkout. Phenolic micro-ballons of 2-5 micron size are sprayed in a slurry of alcohol and water into the air stream in front of the bell mouth. Uniform seed distribution was obtained in the test section with this system.

The experimental effort is progressing toward completion of flow measurements at the seven stations in the 90^{o} duct for the unheated flow. A minimum of 300 spatial points in the duct half-plane are being surveyed for mean velocity, unsteady velocity and total pressure at each station. After completion of the unheated flow surveys at two Reynolds numbers, scheduled for 1 December 1983, the air heater and tunnel insulation will be installed for the adiabatic wall testing during the winter months when lower ambient temperatures will reduce tunnel wall temperatures. The experimental phase of this effort is scheduled for completion in May, 1983.

APPROACH, ANALYTICAL

The analytical approach involves, first, selecting a computer code capable of solving the Navier Stokes equations with turbulence models for three dimensional internal flow, and adapting it to the experimental geometry and flow conditions. After this, calculations are to be made for laminar flow conditions for unheated flow. Analysis of these calculations will define the grid size and stretching factors required for adequate resolution as well as the values of time steps and smoothing factors required for convergence. Also, any output and graphics capability required for comparison with data is to be developed during this phase. The adequacy of the code with respect to the differencing scheme, adaptability and convergence will be decided in this phase, by comparisons with published experimental and computational data and by grid sensitivity studies.

The next phase of the effort involves computation of heated laminar flows with adiabatic wall conditions. This calculation is important for determining maximum wall temperatures to be expected in the experiment. It will also be important in determining whether for the temperatures planned, the velocities will deviate sufficiently from the unheated case to provide an interesting flow.

The third phase involves detailed comparison with experiment for laminar flows with and without heat added. The resolution of the computer code will be the main aspect tested here. The heated case will involve adiabatic wall conditions.

The fourth phase involves computing turbulent flows corresponding to actual experimental conditions, with and without heat added. Particular attention will be paid to the treatment of heat transport in the turbulence model. Detailed comparisons with experiment will be made.

A final phase involves selective grid refinement in regions where high resolution is required so that a measure of the numerical truncation error can be obtained.

CURRENT RESULTS AND PLANS, ANALYTICAL

The code selected for the analytical study is a version of the Beam-Warming algorithm adapted to generalized coordinate systems by P. D. Thomas. It is very well documented and relatively easy to use. The original plan to use the "MINT" code developed by Briley and McDonald has not been followed due to our inability to obtain the code. Detailed comparisons of the results of our code, for a laminar flow case, with published results of the MINT code have been made. For comparable grids the codes gave similar results. These results have also been compared to published experimental results as shown in Figure 5. This comparison indicated a discrepency which appeared to be due to lack of adequate resolution in the computed results for both codes. This discrepency has been investigated by grid refinement studies. Further, the effect of the grid stretching factors on the solution has been determined. The time step size and smoothing factors have been determined which approximately optimize convergence for this case. A graphical display program has been written and used to simulate streamlines in the flow as shown in Figure 6. These results have been qualitatively compared with preliminary experimental results in a 1/3 scale duct.

A heated laminar flow case with adiabatic wall conditions was then computed. It was determined that the wall temperature at a point near the end of the bend would be close to the maximum inlet temperature, which occurs at the center of the duct. Computed total temperature profiles are shown in Figure 7. This result is important in determining the maximum allowable inlet temperature. For the temperature profile considered, which was close to that planned in the experiment, it was also determined that the velocity profiles would differ significantly from those of the unheated flow. Thus, the heated flow experiment would result in a qualitatively different flow, for the planned inlet temperatures, and the experiment would give useful results.

Currently, we are running unheated turbulent flow cases. Preliminary results are being studied to determine the sensitivity of the results to the turbulence model parameters. Detailed comparisons with experiment will be made for the laminar cases, with and without heating, as soon as they are available. We will then proceed with the comparisons for turbulent flow and additional grid refinement studies.

Experimental Facility

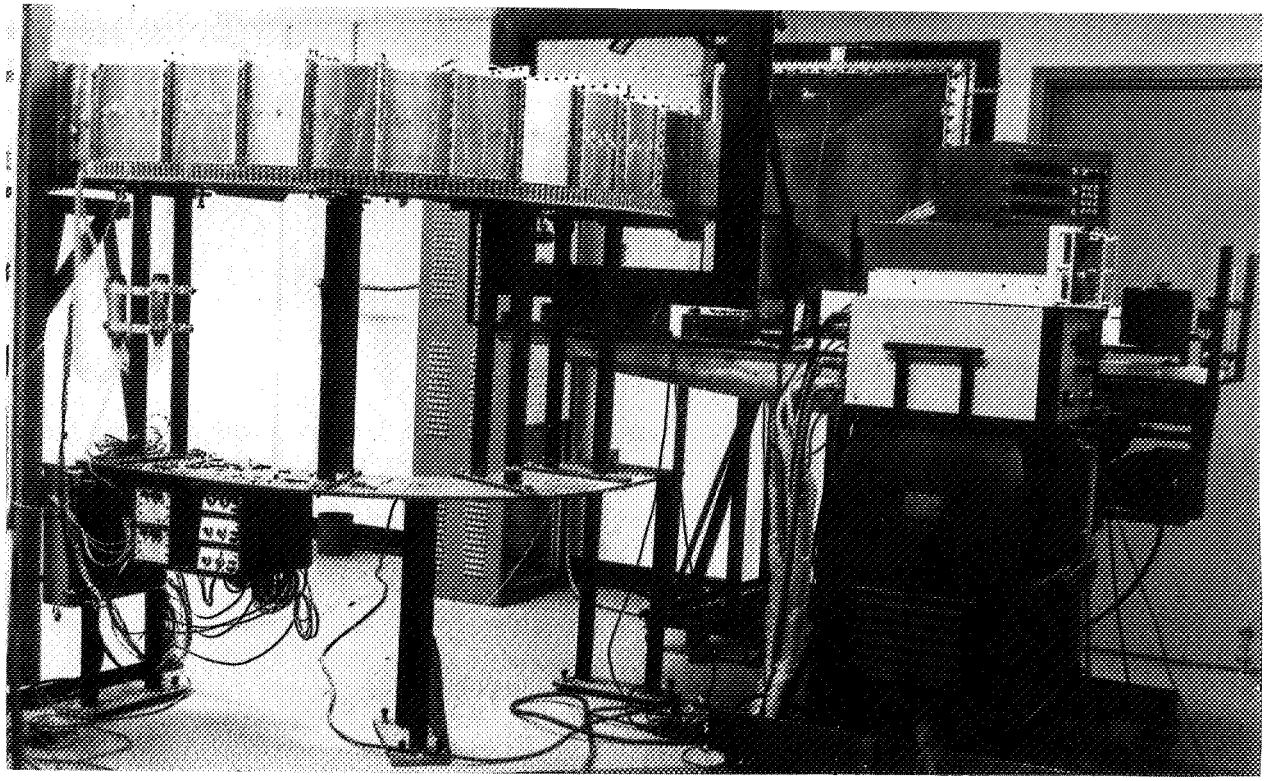

Figure 1.

LV and Pressure Instrumentation Detail

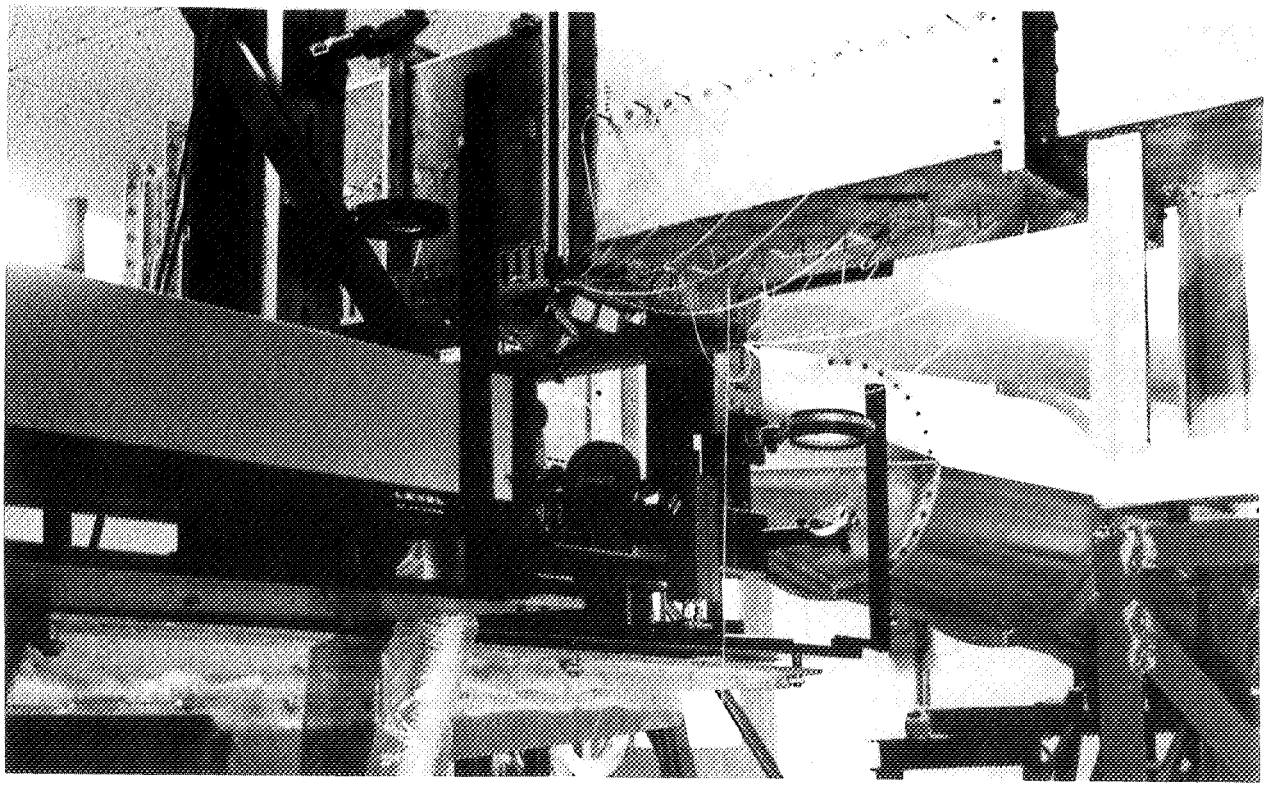

Figure 2.

Typical On-Line Data Display

	X Axial	Y Crosswise	Z Spanwise	Active modes
	(Active)	(Active)	(Active)	
Long Fringe Count	8	8	8	
Short Fringe Count	5	5	5	
Precount	2	3	3	
Clock Frequency	100.00	100.00	100.00	
High Pass Filter	1.2207E-02	2.0000E-01	1.0000E-01	XYZ
Fringe Period	46.100	36.030	15.360	
Maximum Aperiodicity	4.0000E+00	4.0000E+00	4.0000E+00	PRINT
Bias Frequency	-.60	.30	.23	PLOT
Platform position	-.0180	-.0100	-.0100	HDCOPY
Timer Rate	1.0E+03			
Sample Size	400			
Run Number	6			

		X	Y	Z
Vrms = 19.71	V	= 19.69	= .7315	= -.1691
SIGMArms = .3668	SIGMA	= .3660	= .2300	= 6.1734E-02
% = 1.862	%	= 1.859	% = 31.44	% = 36.50
Accepted = 271		= 348	= 326	= 381
Aperiodicity failures		= 52	= 74	= 19
High pass filter failures		= 0	= 0	= 0
Frequency		= .1729	= .2797	= .2410
Correlation Coefficient		= 5.42758E-02		
Covariance		= 2.82059E-04		

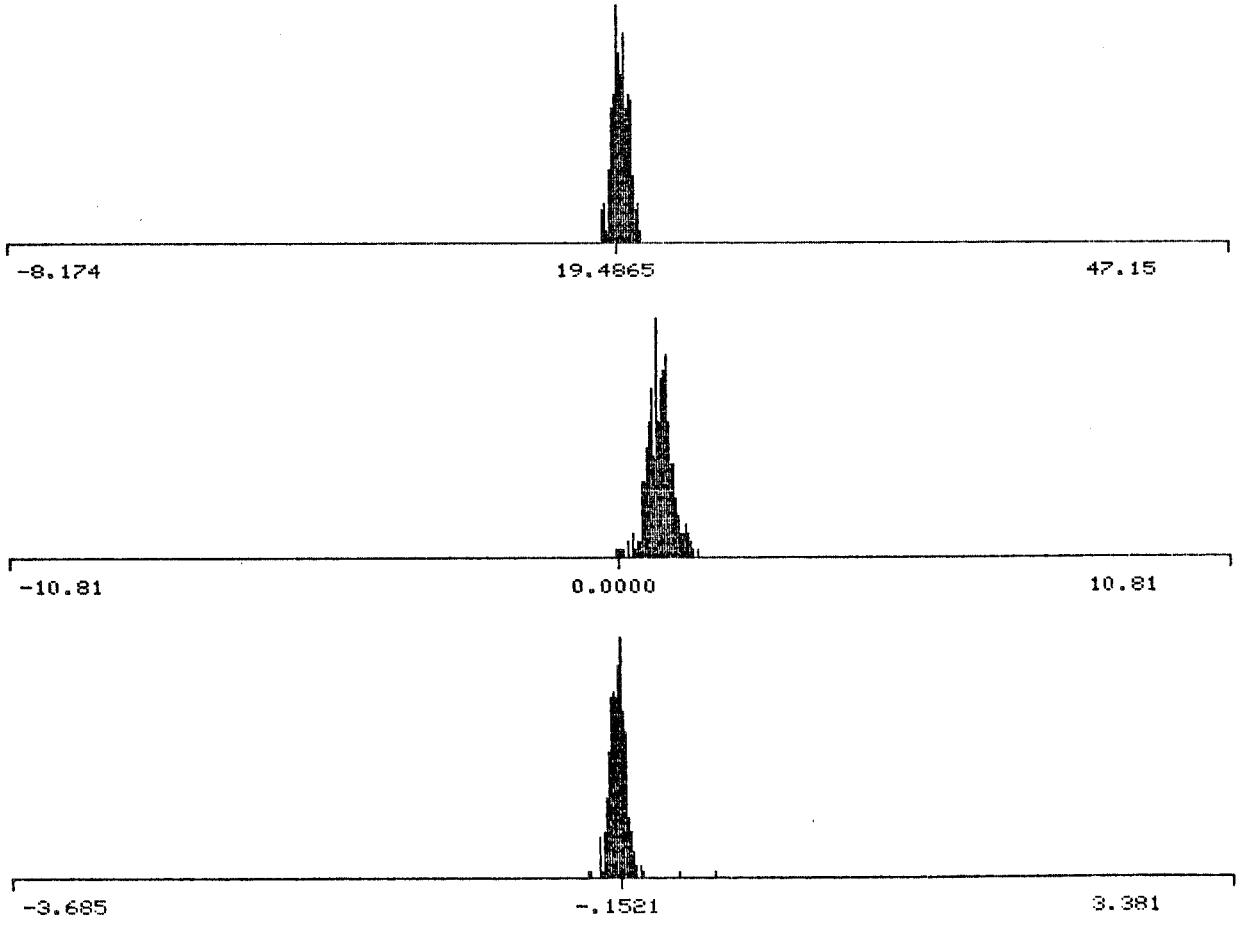

Figure 3.

Entrance Region Boundary Layer Profiles

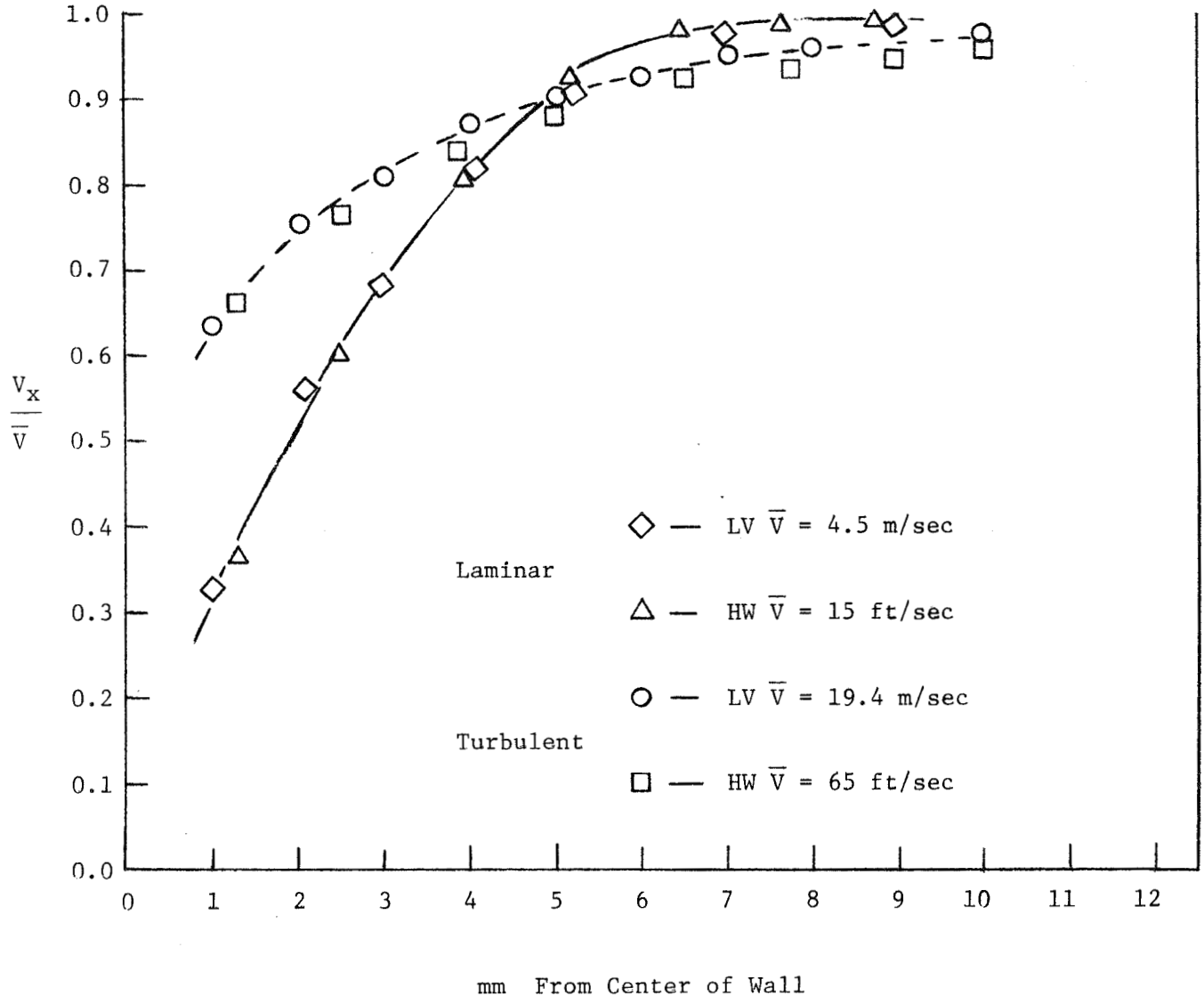

Figure 4

Axial Velocity Comparison Analytic/Experimental

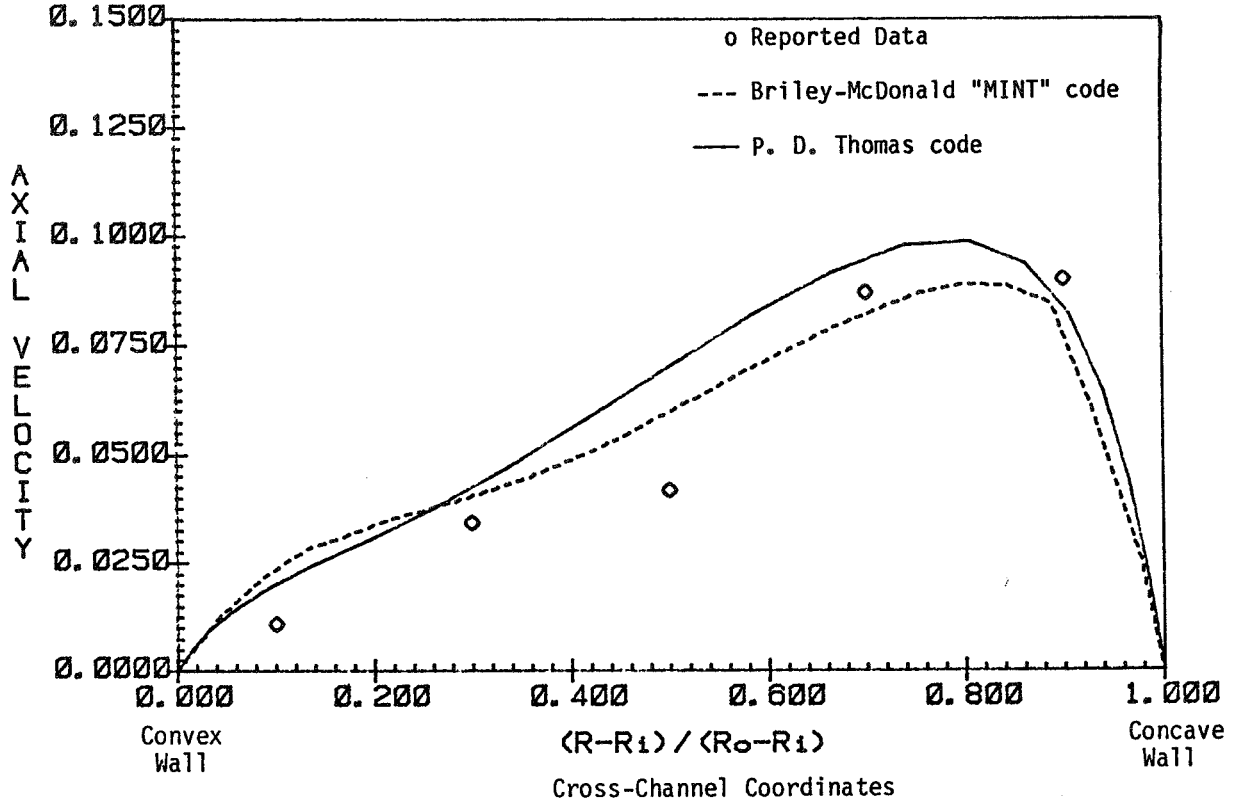

Figure 5.

Streamline Trace for Laminar Flow

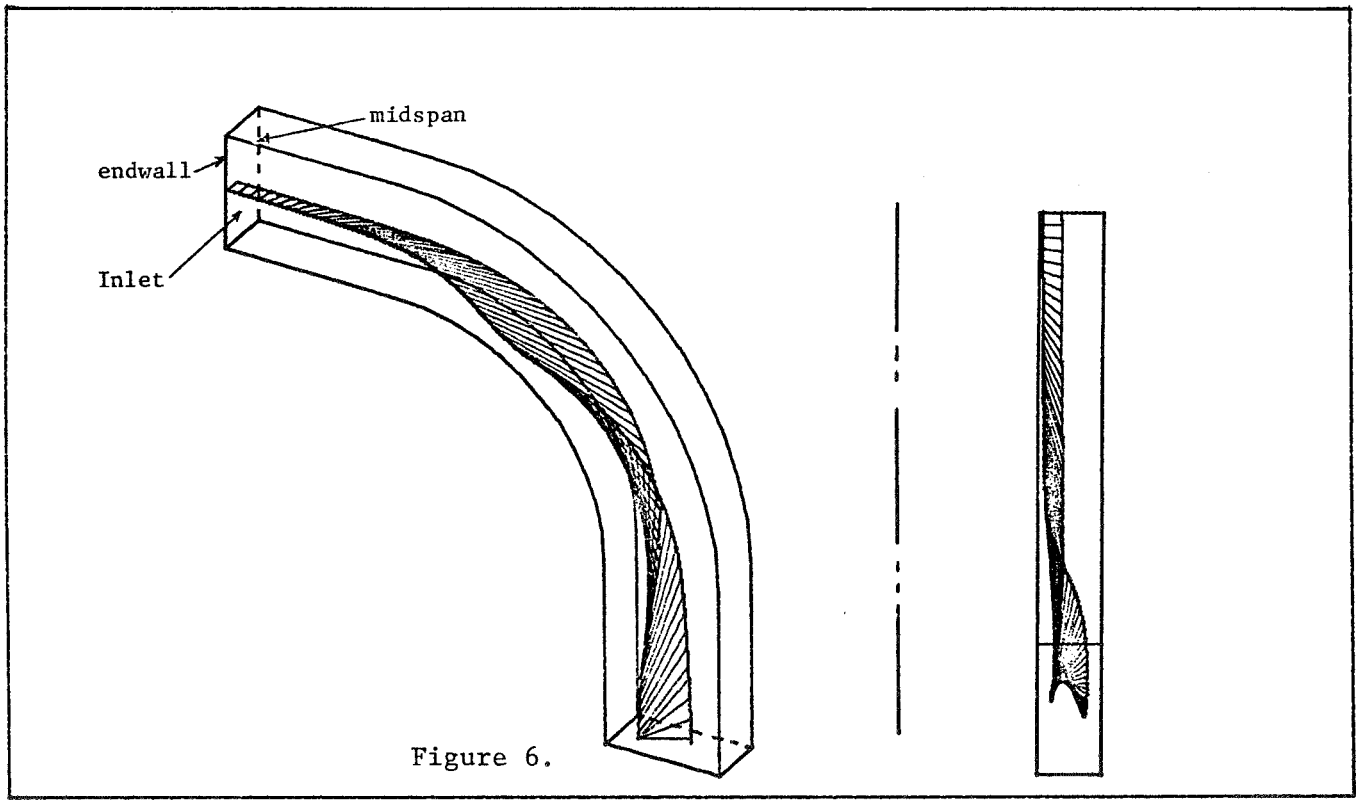

Figure 6.

Total Temperature Profile at Bend Exit
Laminar Flow, Adiabatic Wall

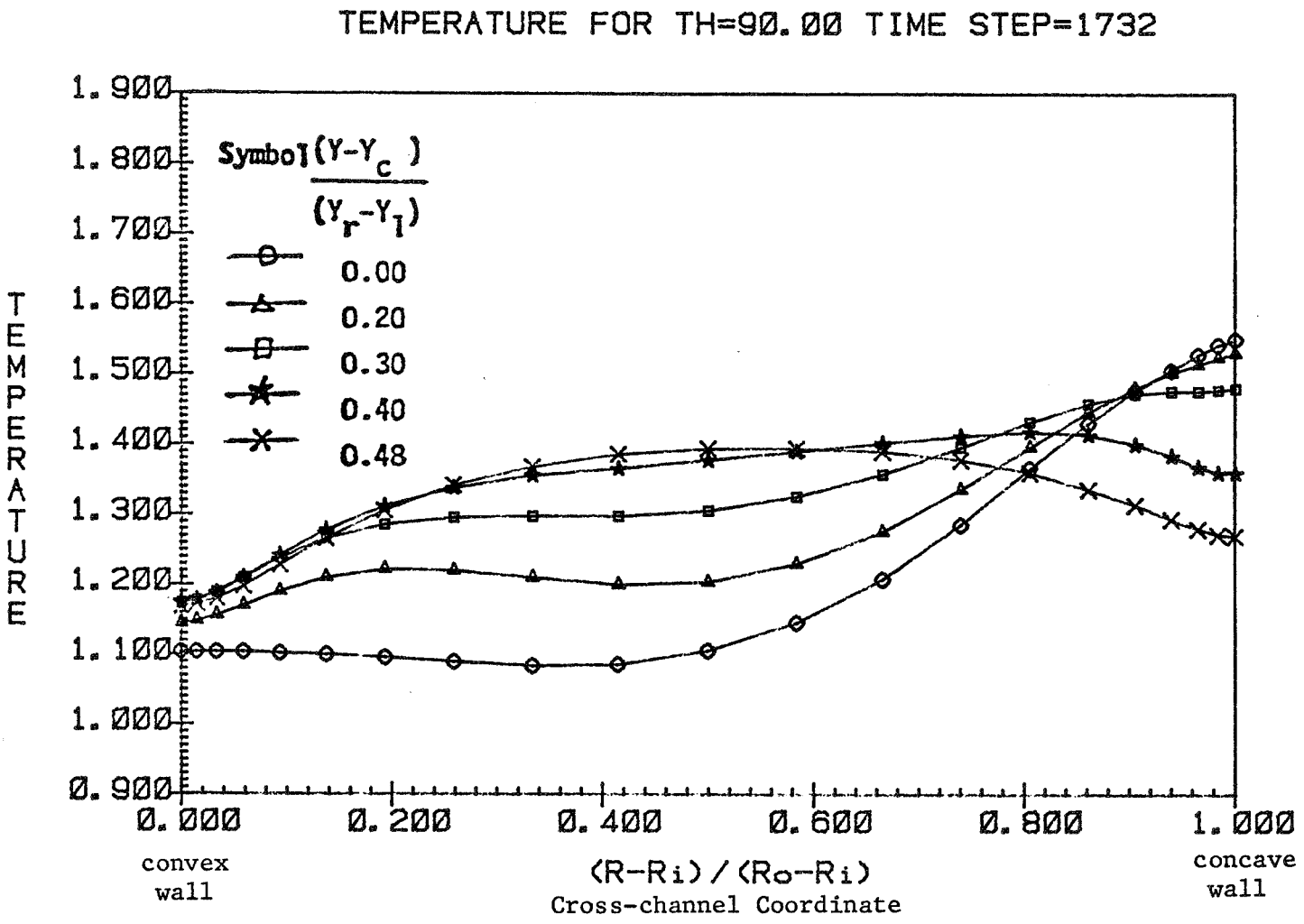

Figure 7.

D12

GAS SIDE HEAT TRANSFER

Larry D. Hylton
Allison Gas Turbine Operations
General Motors Corporation

Improvements in methods for predicting heat transfer rates on the hot gas side of turbine airfoils are necessary for improved turbine durability and performance. The development and verification of improved analytical models requires a systematic, closely coupled experimental and analytical program.

Work in this area has been performed under two contracts. The first, NAS 3-22761, addressed the problem of the prediction of hot gas side heat transfer rates to internally cooled (non-film cooled) airfoils. This effort was completed this year. The second contract, NAS 3-23695, is currently underway and will investigate the effect of leading edge "showerhead" film cooling on downstream heat transfer rates.

The objectives of the first contract were to assess the capability of currently available modeling techniques to predict airfoil surface heat transfer distributions in a 2-D flow field, acquire experimental data as required for model verification, and to make and verify improvements in the analytical models.

Two data sets, Turner (ref. 1) and Lander (ref. 2), were selected from the literature for use in evaluating existing models. Two additional airfoils were chosen for cascade testing under this contract. These airfoils, designated the Mark II and C3X, are representative of highly loaded, low solidity airfoils currently being designed. The aerodynamic configurations of the two vanes were carefully selected to emphasize fundamental differences in the character of the suction surface pressure distributions and the consequent effect on surface heat transfer distributions. Cross sections of the four airfoils and the grid used to make inviscid flow predictions for each airfoil are shown in figure 1. Note the significant variation in airfoil geometry. This variation was intended to provide a significant test of the analytical models. Predicted surface pressure distributions for the four airfoils are shown in figure 2.

The two heat transfer cascades tested were run in the Allison Aerothermodynamic Cascade Facility (ACF). The facility, described in figure 3, provides the capability of obtaining both heat transfer and aerodynamic measurements at simulated engine conditions. The experimental measurements were made in moderate-temperature, three-vane cascades under steady-state conditions. The principal independent parameters (Mach number, Reynolds number, turbulence intensity, and wall-to-gas temperature ratio) were varied over ranges consistent with actual engine operation, and the test matrix was structured to provide an assessment of the independent influence of each parameter. The test matrix over which both cascades were operated is shown in figure 4. Data was obtained at two exit Mach numbers, 0.9 and 1.05, and over a range of exit Reynolds numbers from $1.5X10^6$ to $2.5X10^6$. The inlet turbulence intensity, Tu, and wall-to-gas temperature ratio, T_w/T_g, were also varied.

The method employed in the facility to obtain airfoil surface heat transfer measurements is shown schematically in figure 5. Basically, the exterior of the airfoil is instrumented with grooved surface thermocouples with this data serving

as the exterior boundary condition input to a finite element analysis. The internal boundary conditions are calculated heat transfer coefficients in the internal cooling holes. These values are calculated from measurements of the coolant temperature, pressure and flowrate. The instrumented airfoil also contains static pressure taps, thus permitting simultaneous measurement of the surface pressure and heat transfer distributions. A typical set of data for the C3X cascade illustrating the effects of exit Reynolds number on the heat transfer distribution is shown in figure 6. Note that the heat transfer measurement technique provides sufficient detail to clearly see the effect of Reynolds number on transition on the suction surface. Data from the two cascades, coupled with that from the literature cases, provide a data base covering a wide range of operating conditions and geometries and thus present a significant test for the predictive capabilities of the analytical methods.

The analytical methods development program consisted of two separate phases. In the first phase, the literature was reviewed to establish general candidate methods that were characteristic of current methodology incorporated within actual gas turbine preliminary design systems. As a result of this survey, three 2-D boundary layer methods were chosen: an integral method, a finite difference (differential) method with a zero-equation mixing length hypothesis turbulence model, and the same differential method with a two-equation turbulence model. The literature was thoroughly reviewed to obtain relevant airfoil heat transfer experimental data to use in a general evaluation of the three selected boundary layer methods. The data sets were selected based on relevance to realistic gas turbine environments (i.e., Reynolds number effects, free-stream turbulence effects, strong pressure gradient effects, etc.). Analytical/numerical solutions were compared with experimental results. Based on the findings of this first phase general methods evaluation process, the differential method with zeroth order turbulence modeling was selected for the second phase of the analytical program. The literature was further reviewed for models that had the potential of treating the airfoil heat transfer problem more realistically. A number of transition process models, free-stream turbulence augmentation models, and a single explicit longitudinal surface curvature correction model were selected for evaluation. Various single and/or combined model solutions were evaluated using data from four different airfoil experiments. This evaluation process eventually led to a final "gas turbine airfoil specific" modeling effort which resulted in an effective viscosity formulation that, when implemented, gave better overall solutions than any literature modeling approach tested previously.

Figures 7a and 7b respectively show the unmodified and modified suction surface heat transfer predictions for three different operating conditions using the STAN5 boundary layer code for the Lander airfoil. Increasing run numbers correspond to increased inlet or exit Reynolds number and free-stream turbulence intensity. The experimental data are represented as symbols. Lander's data are important in that they illustrated nominally laminar heat transfer augmentation attributed to free-stream turbulence effects, as well as Reynolds number effects related to transition origin. As shown in figure 7, the augmentation phenomenon is predicted significantly better by the final model.

Figures 8a and 8b show the unmodified and modified solutions compared with the data of Turner. The significance given to Turner's data was that they isolated the effects of free-stream turbulence. Figure 8a shows only one solution because the original unmodified method did not account for the effects of free-stream turbulence. As can be seen in figure 8b, the modified solutions give a very good representation of the pressure surface experimental data. The modified suction surface solutions give reasonable trends up to the point where a transition process is indicated by the experimental data. Overall, the modified solutions are a significant improvement

over the unmodified solution, represent the pressure surface data very well, and provide qualitatively good trends for the suction surface.

Unmodified and modified predictions of the characteristic Reynolds number effects in the Mark II cascade are compared with the data in figures 9a and 9b, respectively. It should be pointed out that the analytically predicted stagnation point was displaced approximately 5% (0.05) of pressure surface distance toward the pressure surface away from the extreme forward point on the airfoil, which was used as the datum (0) in these figures. The stagnation point corresponds to the predicted inviscid flow solution zero velocity location on the pressure surface. Note that this does not correspond to the highest local value of measured heat transfer in the leading edge region. Both the modified and unmodified solutions reflect the proper trends moving away from the stagnation point. The absence of solutions beyond 0.2 normalized surface distance on the suction surface indicates that all solutions encountered separation due to the presence of a suction surface shock at the location. No attempt was made to restart the solutions downstream of the shock. Overall, the modified solutions are able to qualitatively and quantitatively predict the pressure surface data reasonably well and yield much better predictions than the unmodified solutions, which predicted pressure surface transition.

In a manner similar to the Mark II comparative studies, the experimental results for the C3X cascade were also simulated numerically and the predictions are shown in figure 10. Figures 10a and 10b show both unmodified and modified solutions at three different Reynolds number conditions. Qualitatively, the modified pressure surface solutions represent a substantial improvement over the original (unmodified) approach. However the quantitative predictions (using the modified procedure) begin to deviate significantly from the data along the aft portions of the surface. The suction surface predictions of both the unmodified, figure 10a, and the modified, figure 10b approaches yield quantitatively acceptable results for some of the cases, but the indicated suction surface transition process (i.e., gradual transition) is better represented by the modified solutions.

Finally, in response to the objectives of this program, a recommended procedure was developed for constructing a viable, 2-D airfoil external convective heat transfer method for gas turbine design systems, including the specification of boundary conditions, initial conditions, and preferred definitions of effective viscosity determined here to be most suitable for gas turbine preliminary design applications.

The analytical and experimental work performed under contract NAS 3-22761, including the recommended design procedure, are reported in detail in NASA CR 168015 (ref. 3) which was published in May, 1983.

Work on the second contract, NAS 3-23695, began earlier this year. This effort is intended to extend the work performed under the first contract in two respects. First, the analytical boundary layer analysis and experimental cascade studies of the first contract will be extended to include a leading edge showerhead film cooling array. Secondly, recognizing the long term limitations of the boundary layer approach, an analytical effort was added to investigate the application of a Navier-Stokes solver to the turbine cascade problem. This effort was subcontracted to Scientific Research Associates, Inc. (SRA) and will utilize their MINT code.

The boundary layer efforts are structured similar to the first contract. Namely the STAN5/STANCOOL type approach to making heat transfer predictions for airfoils with leading edge film cooling will be evaluated and modified as required to improve

heat transfer predictions. These modifications will then be validated by comparisons with experimental data acquired under the contract.

The experimental program utilizes the C3X cascade from the original contract. The center, instrumented airfoil was replaced with one containing five rows of film cooling holes in the leading edge region. Figure 11 illustrates the original airfoil with the radial cooling holes and finite element grid shown. The new film cooled airfoil was modified in the leading edge region as shown in figure 12. Downstream of the region shown in figure 12 the cooling hole geometry and instrumentation is identical to the non-film cooled airfoil tested under the first contract. Heat transfer measurements will be made downstream of the film cooling array. No heat transfer measurements will be made within the array. By using a modified airfoil of the same profile as one of the two tested under the original contract, a good non-film cooled baseline will have been established, and fully qualified cascade hardware and experimental techniques will be employed to maximum advantage.

The analytical efforts on the Navier-Stokes MINT code are intended to provide a major step toward developing an analytical tool capable of predicting the flow and heat transfer in a full 3-D turbine cascade. Initial efforts on the MINT code will be performed on a 2-D version. The "C" grid generator previously used in the program will be replaced with an "O" grid generator. Due to its construction, the "C" grid requires a cusped trailing edge. In solving the transonic turbine problem, the trailing edge geometry appears to be very important. In preliminary calculations with the "C" grid, discrepancies between predictions and experimental data in the trailing edge region are thought to be a result of the cusped trailing edge approximation. The addition of the "O" grid generator to the program should enhance its capabilities.

The 2-D version of the code with the "O" grid generator will be used to make predictions for the cascades tested under the first contract. The comparison of the predictions with the data will serve as verification of the code modifications. Following these comparisons the code will be extended to handle the full 3-D case and a sample calculation for a 3-D cascade will be made. The final modification scheduled to be made to the code is the incorporation of a film cooling-trailing edge blowing capability into the code. Following completion of all modifications to the code, SRA will assist NASA personnel in running demonstration cases with the code on the NASA Lewis computer.

Progress on the second contract has been made on both analytical efforts and on the experimental effort. The boundary layer analytical efforts have concentrated on evaluating the STAN5/STANCOOL programs abilities to predict heat transfer to circular cylinders. This is the initial step in predicting the airfoil leading edge film cooling problem. Comparisons of the predictions for both solid cylinders and film cooled cylinders were made with the data in reference 4. Based on these results efforts are currently underway to make modifications to the models to improve their capabilities.

Progress on the MINT code includes installation and checkout of the program on the NASA Lewis computer. In addition, the "O" grid generator has been developed and sample "O" grids have been constructed. Efforts on verifying the capabilities of the program with the "O" grid generator by comparing predictions with cascade data sets are currently underway.

Under the experimental phase of the contract the new C3X airfoil containing the leading edge "showerhead" film cooling array, has been designed, fabricated,

instrumented and installed in the cascade. Preliminary testing of the cascade has started. Technical efforts on this program are scheduled to be completed by May, 1984.

REFERENCES

1. Turner, A. B.: Local Heat Transfer Measurements on a Gas Turbine Blade, Jour. of Mechanical Engng. Sciences, Vol. 13, 1971, pp. 1-12.

2. Lander, R. D.: Effect of Free-Stream Turbulence on the Heat Transfer to Turbine Airfoils, Tech. Rept. AFAPL-TR-69-70, Air Force Systems Command, Sept. 1969.

3. Hylton, L. D.; Mihelc, M. S.; Turner, E. R.; Nealy, D. A.; and York, R. E.: Analytical and Experimental Evaluation of the Heat Transfer Distribution Over the Surfaces of Turbine Vanes, Detroit Diesel Allison Report EDR 11209, NASA CR-168015, May 1983.

4. Luckey, D. W.: Stagnation Region Gas Film Cooling: Spanwise Angled Injection from Multiple Rows of Holes, PhD Thesis, Purdue University, 1980.

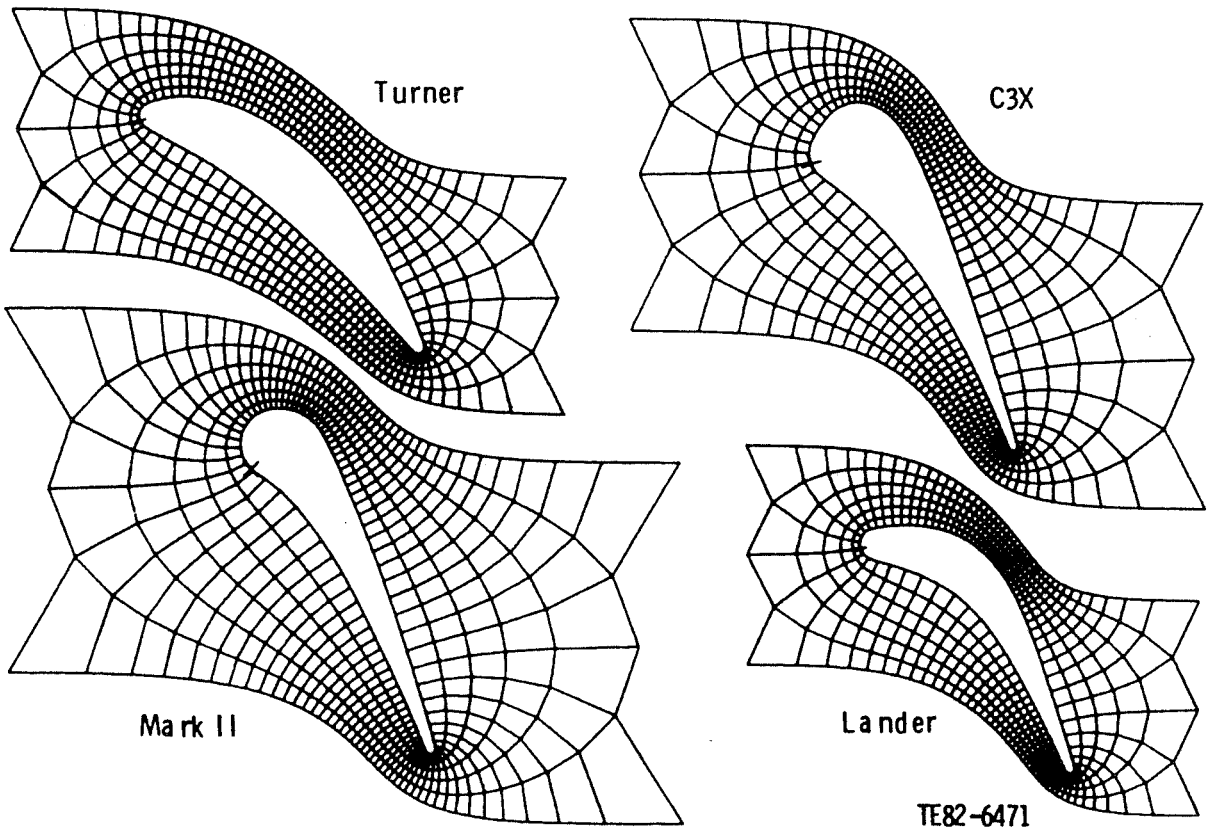

Figure 1. Airfoil profiles with inviscid flow analysis grid.

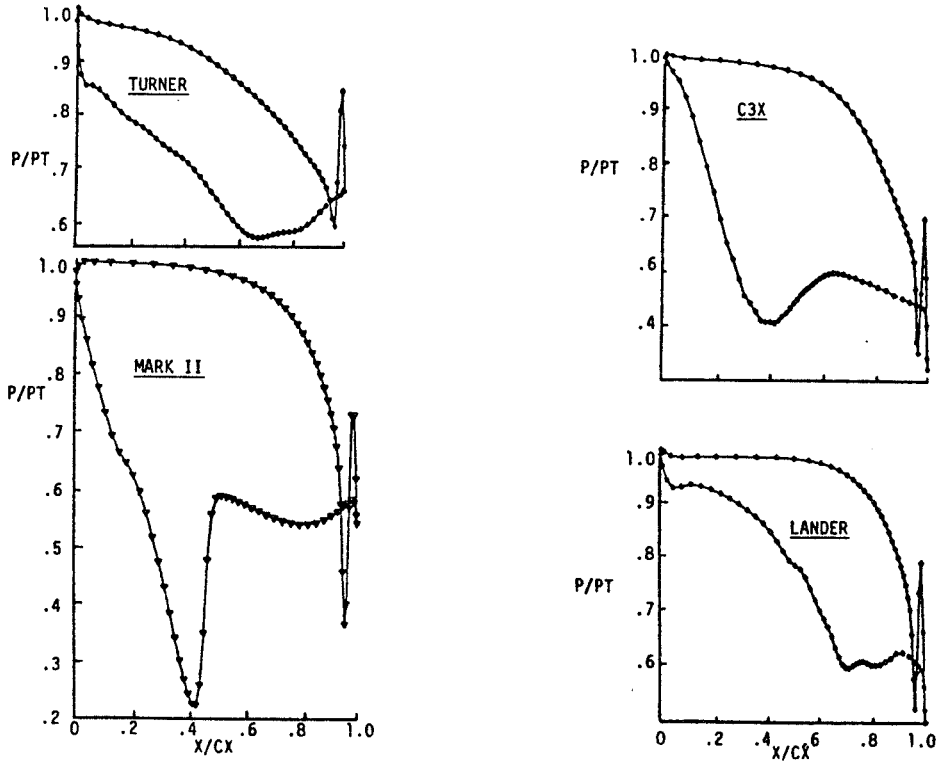

Figure 2. Airfoil predicted pressure distribution.

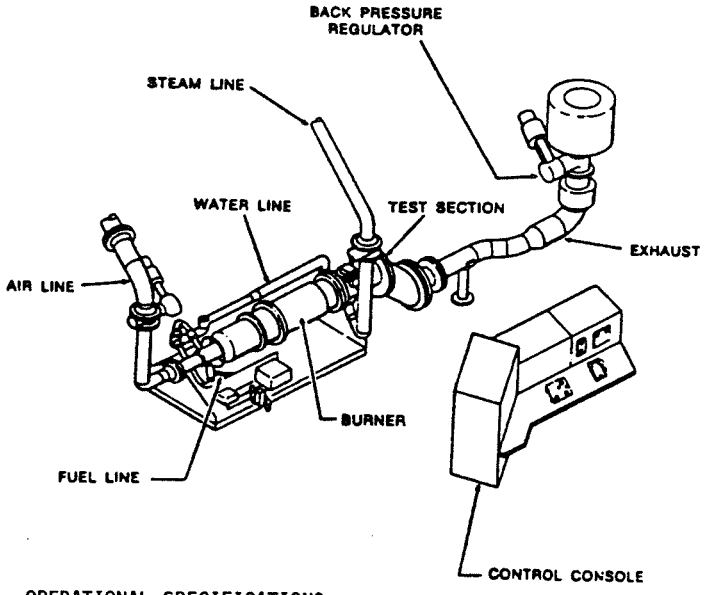

OPERATIONAL SPECIFICATIONS

AIR SUPPLY	9.5 LB/SEC AT 105 PSIA OR 5.0 LBM/SEC AT 245 PSIA
INLET PRESSURE	20 PSIA TO 245 PSIA
STAGNATION TEMPERATURE	400°F TO 3200°F
PRIMARY FUEL	NATURAL GAS

OPERATIONAL PHILOSOPHY

- TWO-DIMENSIONAL LINEAR CASCADE
- PROVIDES HEAT TRANSFER AND AERODYNAMIC DATA SIMULTANEOUSLY
- OPERATED AT SIMULATED ENGINE CONDITIONS
  - REDUCED TEMPERATURE
  - REDUCED PRESSURE
  - SCALED-UP AIRFOIL GEOMETRY
  - HIGH FREESTREAM TURBULENCE
- WIDE OPERATING RANGE
  - REYNOLDS NUMBER CONTROL
  - EXIT MACH NUMBER CONTROL
  - WALL-TO-GAS TEMPERATURE RATIO CONTROL
  - INLET TURBULENCE INTENSITY CONTROL
- HIGH DENSITY INSTRUMENTATION
  - UP TO 300 TEMPERATURES
  - UP TO 288 PRESSURES
- DEDICATED FACILITY COMPUTER
  - COMPUTER CONTROLLED DATA ACQUISITION
  - ONLINE DATA ANALYSIS

Figure 3. Allison Aerothermodynamic Cascade Facility

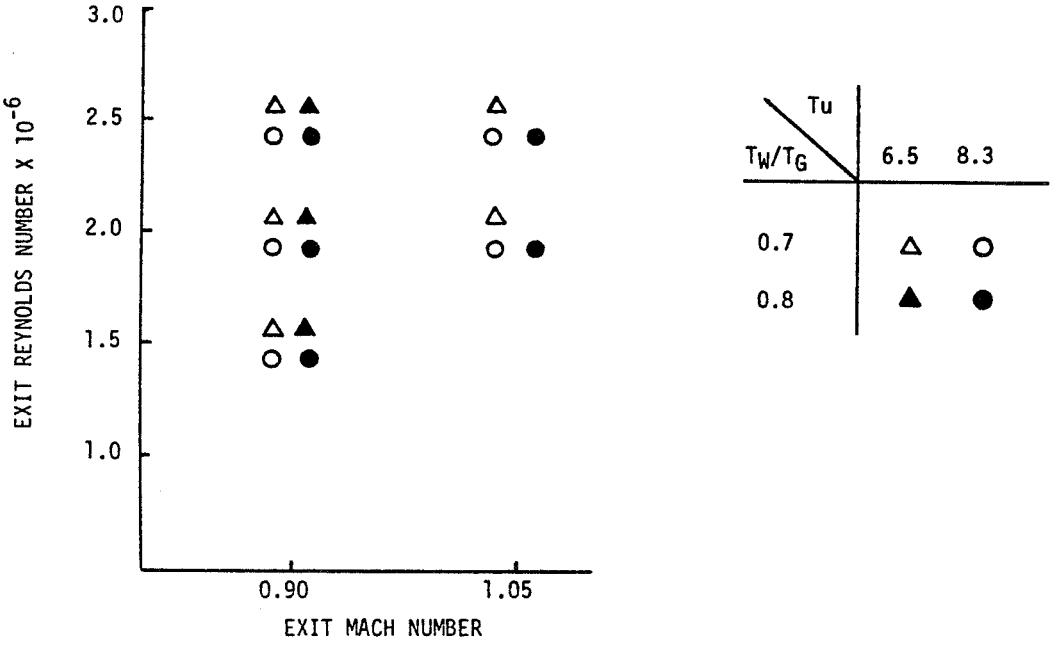

Figure 4. Cascade test matrix.

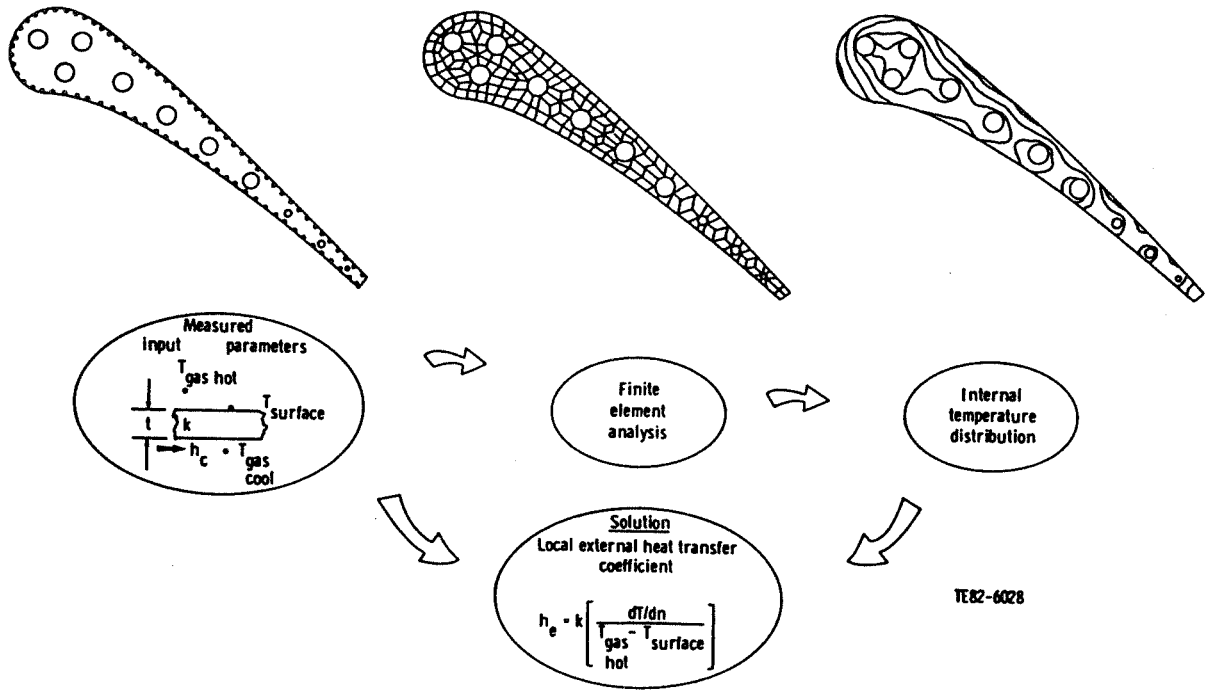

Figure 5. Heat transfer measurement technique.

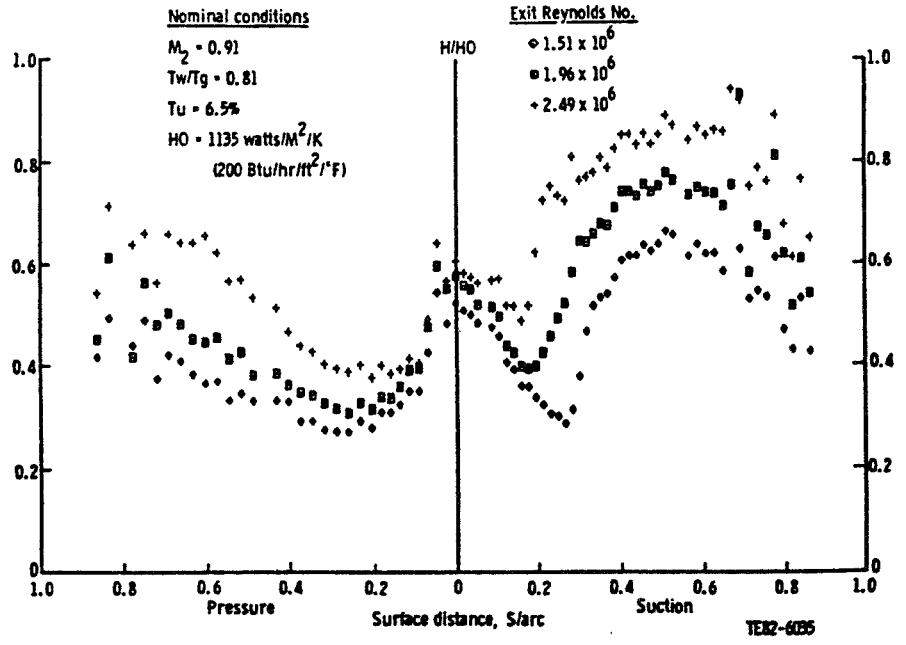

Figure 6. Reynolds number effect on surface heat transfer distribution for C3X airfoil.

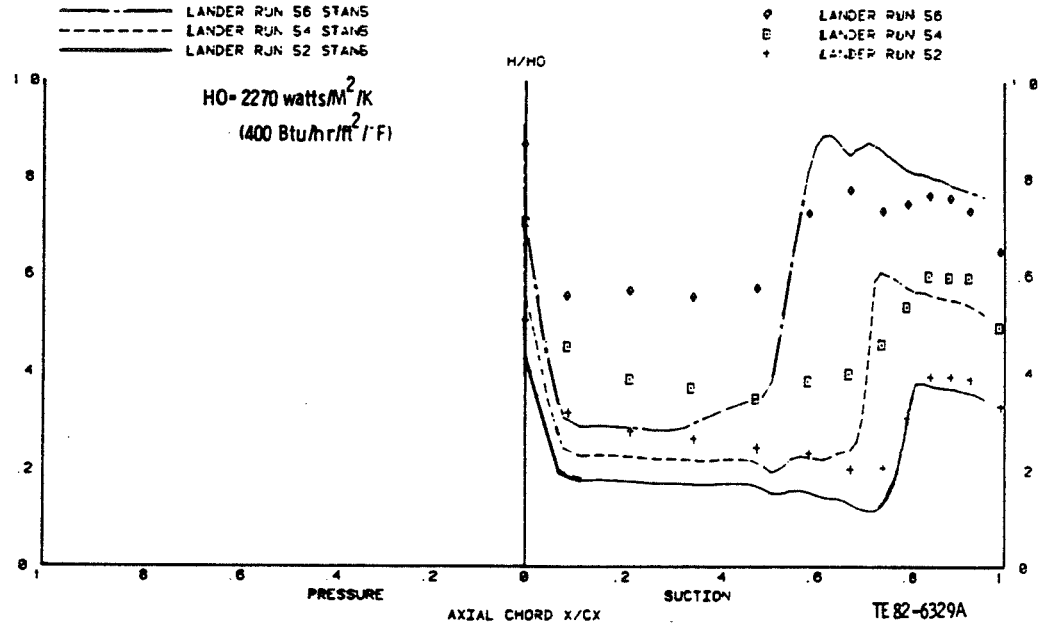

(a) Unmodified STAN5 results

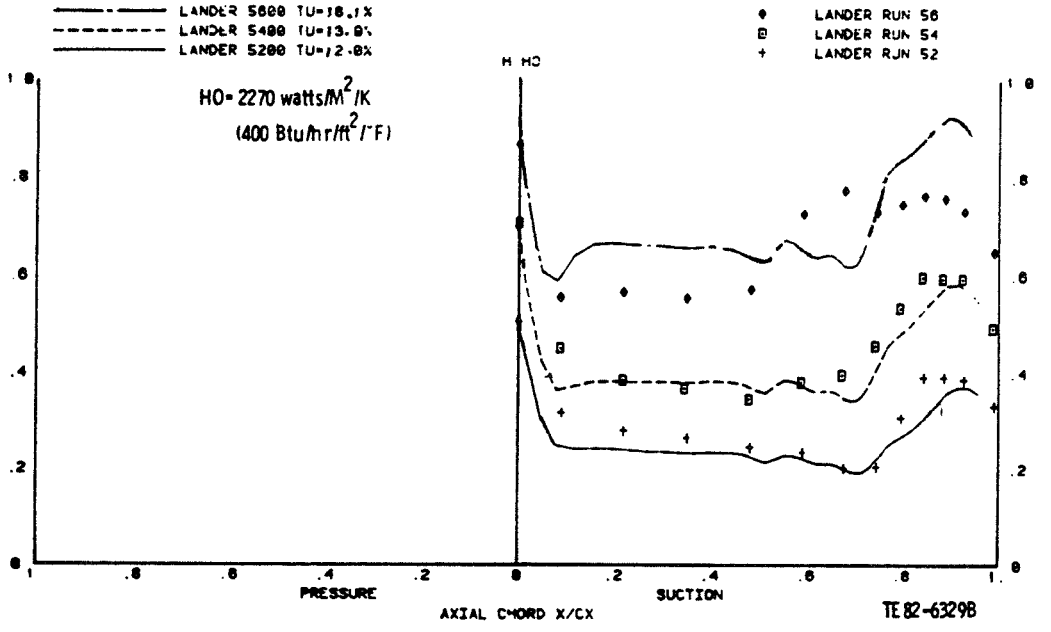

(b) Modified STAN5 results

Figure 7. STAN5 solutions compared with Lander airfoil suction surface experimental heat transfer coefficient data illustrating the combined effects of varying Reynolds number and free-stream turbulence intensity.

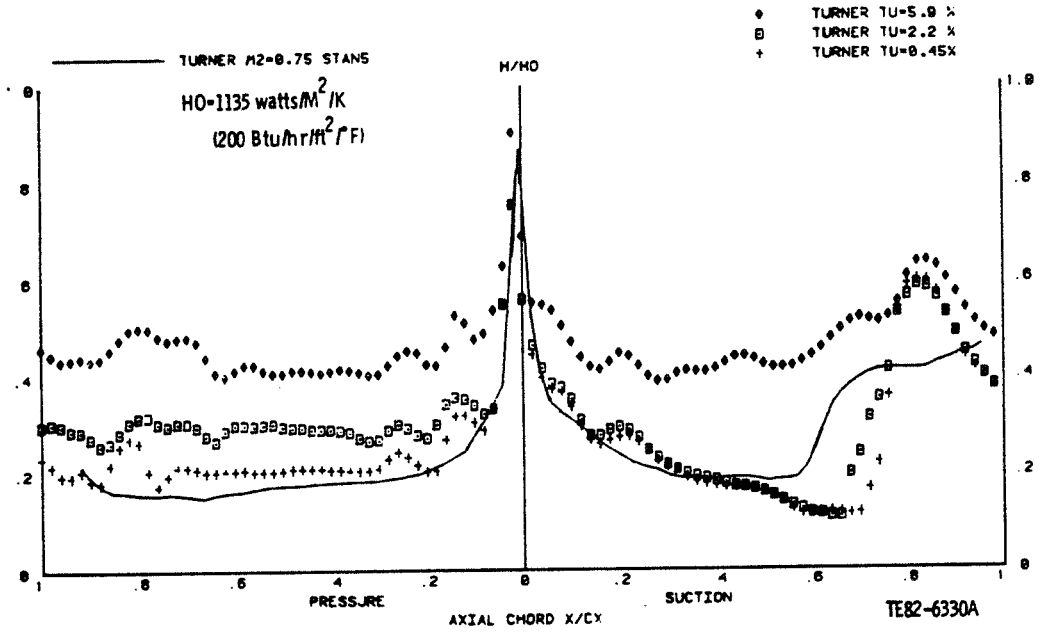

(a) Unmodified STAN5 results

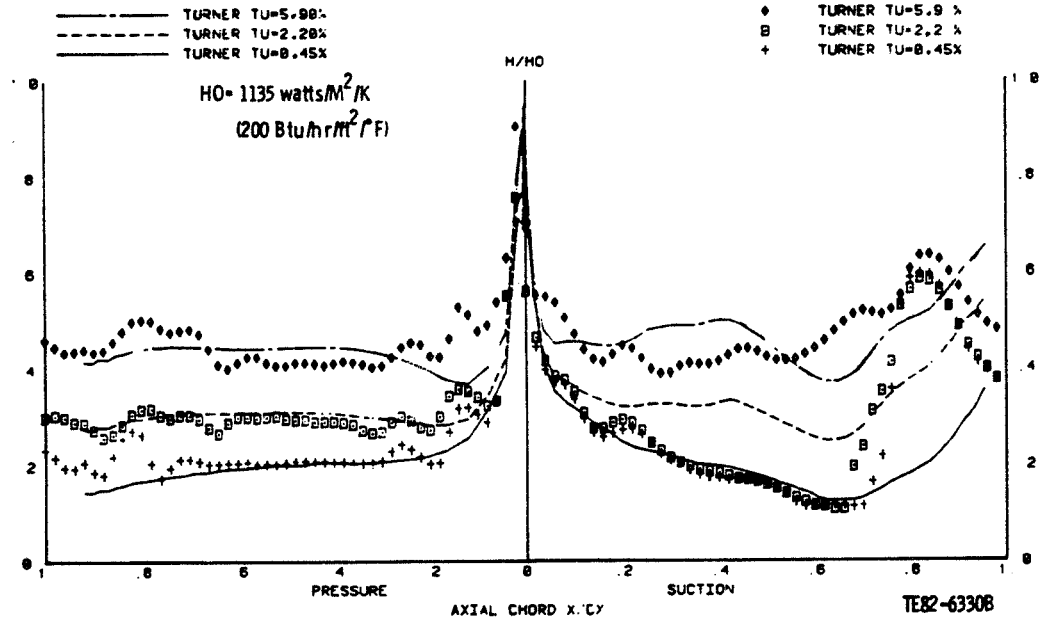

(b) Modified STAN5 results

Figure 9. STAN5 solutions compared with Turner airfoil experimental heat transfer coefficient data illustrating the effects of varying free-stream turbulence intensity.

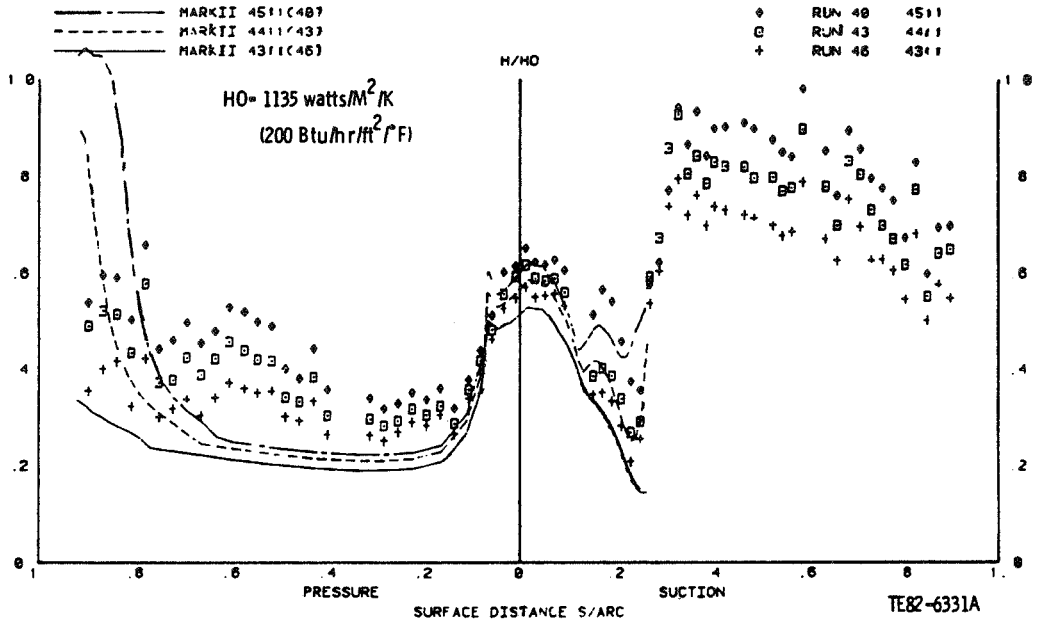

(a) Unmodified STAN5 results

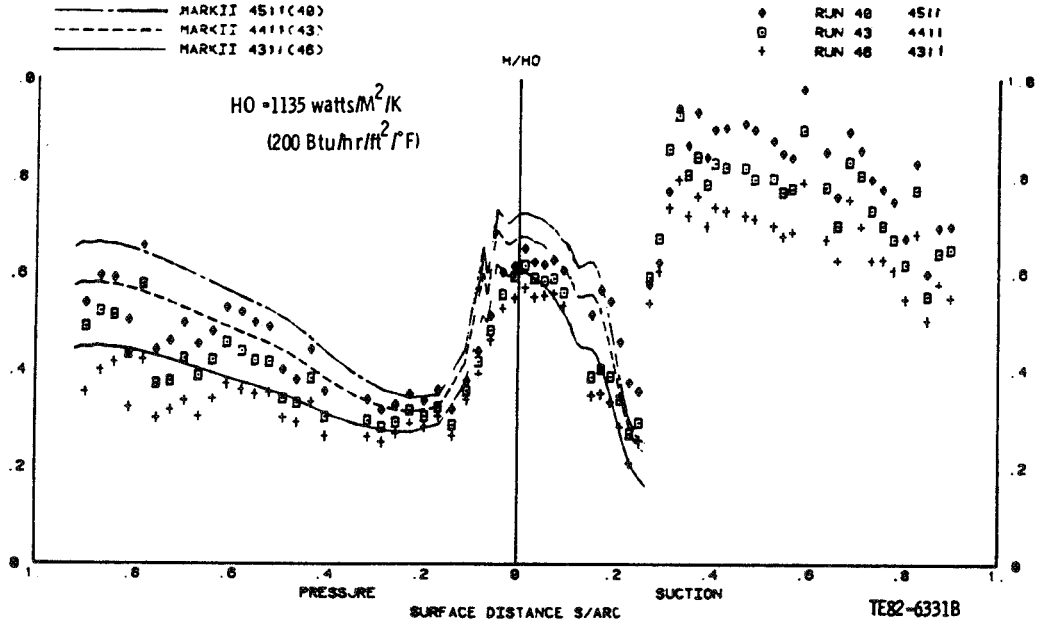

(b) Modified STAN5 results

Figure 9. STAN5 solutions compared with Mark II airfoil experimental heat transfer coefficient data illustrating the effects of varying exit Reynolds number.

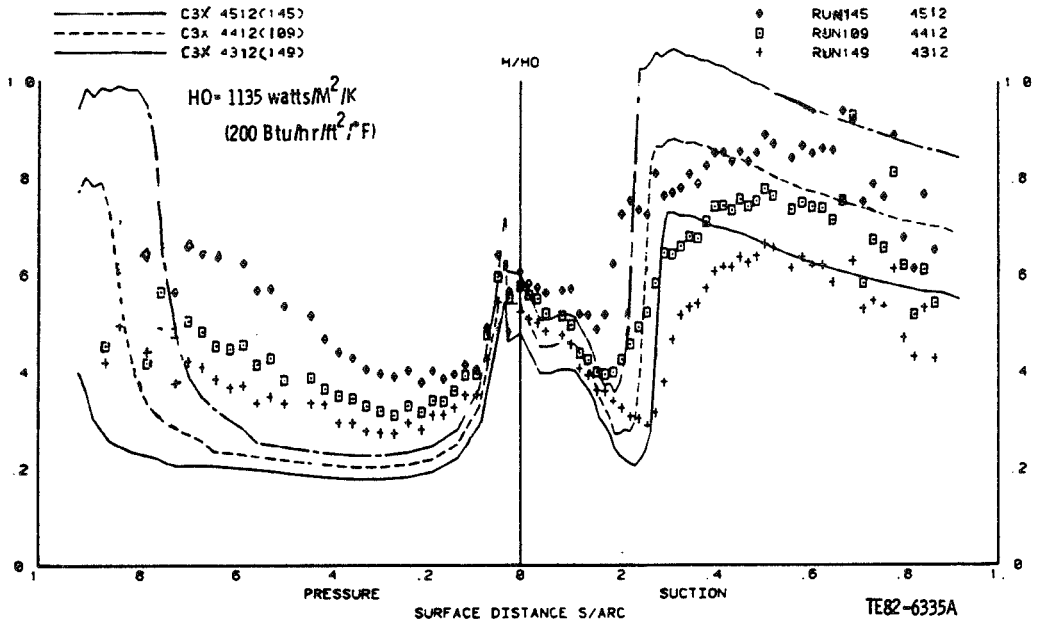

(a) Unmodified STAN5 results

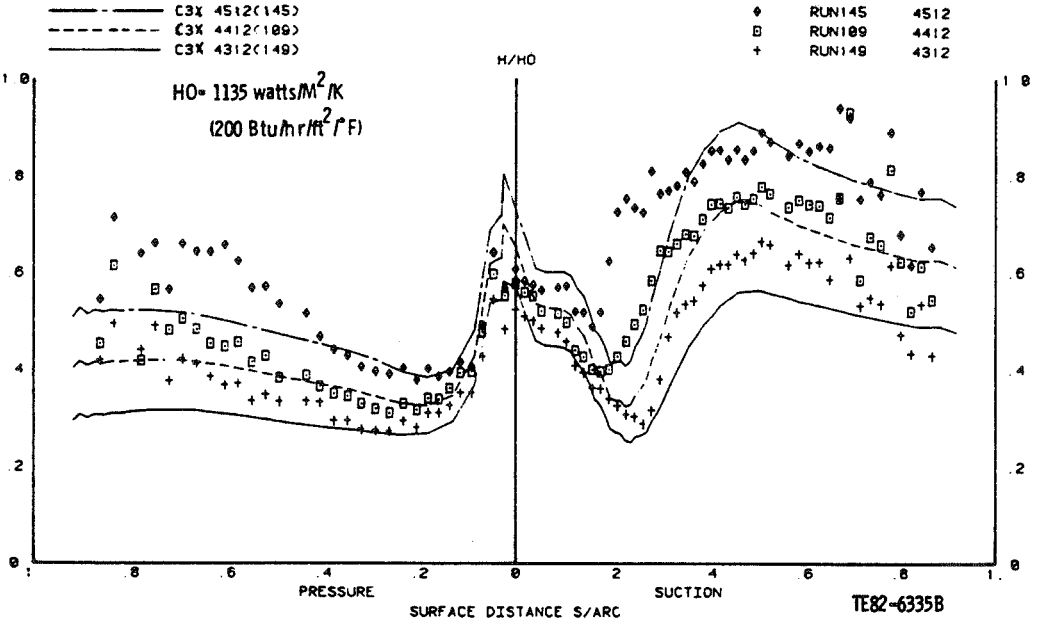

(b) Modified STAN5 results

Figure 10. STAN5 solutions compared with C3X airfoil experimental heat transfer coefficient data illustrating the effects of varying Reynolds number.

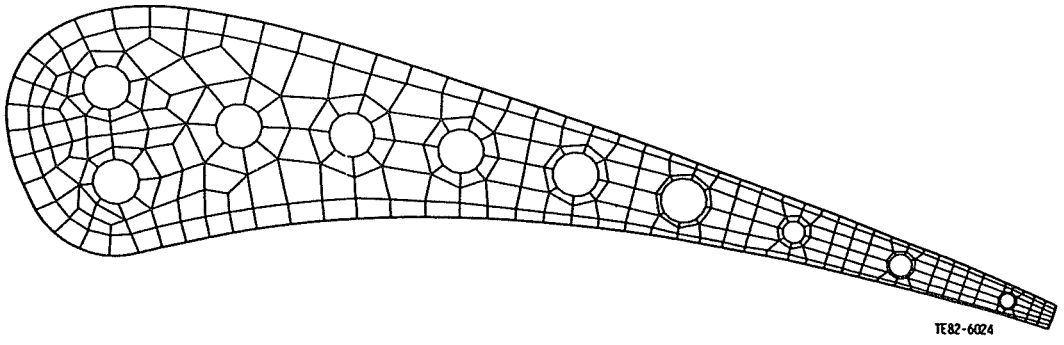

Figure 11. C3X airfoil cross section with finite element grid and cooling hole locations for contract NAS 3-22761.

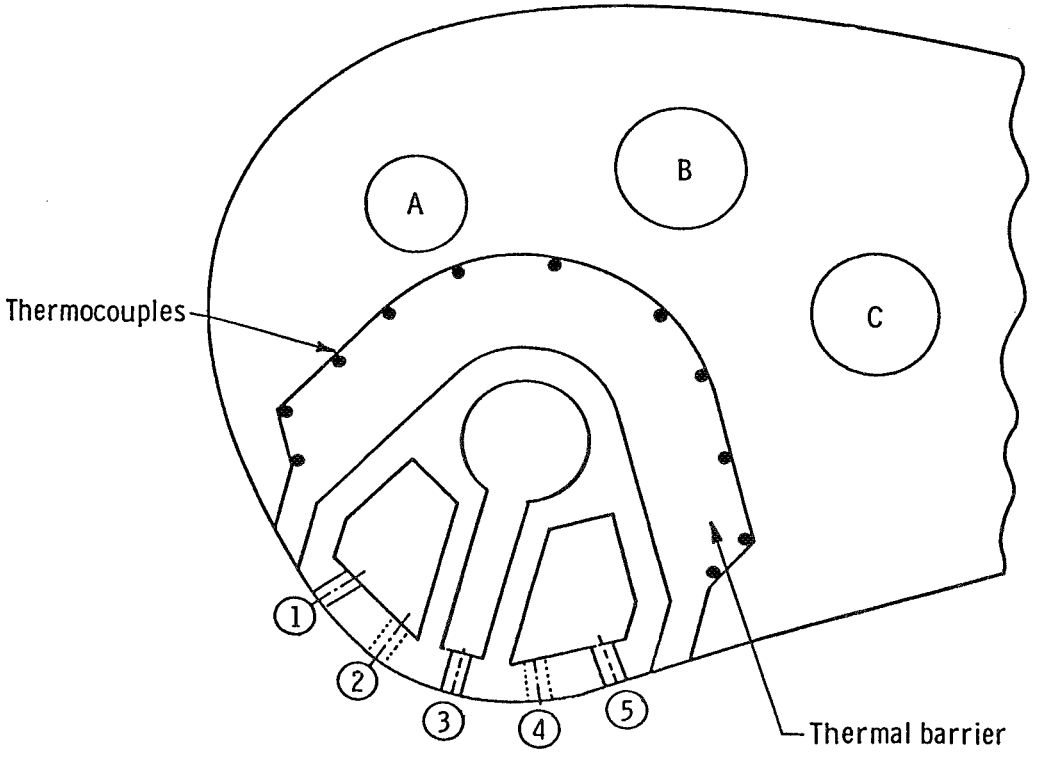

Figure 12. Modified leading edge region of C3X airfoil for film cooling studies in contract NAS 3-23695.

Page intentionally left blank

D/3

Assessment of a 3-D Boundary Layer Code to Predict Heat Transfer and Flow Losses in a Turbine*

Veer N. Vatsa
United Technologies Research Center

The prediction of the complete flow field in a turbine passage is an extremely difficult task due to the complex three-dimensional pattern which contains separation and attachment lines, a saddle point and horseshoe vortex (Fig. 1). Whereas, in principle such a problem can be solved using full Navier-Stokes equations, in reality methods based on a Navier-Stokes solution procedure encounter difficulty in accurately predicting surface quantities (e.g. heat transfer) due to grid limitations imposed by the speed and size of the existing computers. On the other hand the overall problem is strongly three-dimensional and too complex to be analyzed by the current design methods based on inviscid and/or viscous strip theories. Thus there is a strong need for enhancing the current prediction techniques through inclusion of 3-D viscous effects. A potentially simple and cost effective way to achieve this is to use a prediction method based on three-dimensional boundary layer (3-DBL) theory. The major objective of this program is to assess the applicability of such a 3-DBL approach for the prediction of heat loads, boundary layer growth, pressure losses and streamline skewing in critical areas of a turbine passage. A brief discussion of the physical problem addressed here along with the overall approach is presented in the following paragraphs.

In the present investigation, zonal concepts are utilized to delineate regions of application of 3-DBL theory--these being the endwall, suction and pressure surfaces. Each of the regions selected for this investigation has some unique features. For example, the experimental data of Ref. 1 for the surface streamline pattern (Fig. 2a) and the corresponding Stanton (St) number distribution (Fig. 2b) for the endwall region of a planar cascade displays strong three-dimensional effects due to sweeping of the boundary layer across the passage from the pressure to the suction surface. A modified version of the 3-DBL code of Ref. 2, named "TABLET" (Three- Dimensional Algorithm for Boundary-Layer Equations in Turbulent Flows) will be used to analyze the viscous flow downstream of the attachment line between the pressure and suction surface junctures in the endwall region.

The second region of interest is the turbine blade suction surface. As shown in Fig. 3a, the growth of endwall boundary layers produces inward deflection of the streamlines along the suction surface. Thus strong crossflow velocities are induced from the endwall region towards midspan and the flow becomes progressively more three-dimensional as the trailing-edge is approached. The effect of cross flow induced three-dimensionality is also clear from the measured St number distributions (Ref. 1) shown in Fig. 3b. The "TABLET" code will be used to analyze the flow and predict the effect of streamline convergence on St number distributions in the region which lies downstream of the leading-edge and between the separation line and midspan.

---

*This work was sponsored by NASA-Lewis Research Center under Contract NAS3-23716.

The final region of interest is the pressure side of the blade. Here, the three-dimensionality in the flow is induced by a different mechanism altogether--namely, that of blade rotation. A typical streamline pattern on the pressure surface of a rotating blade obtained from Ref. 3 is presented in Fig. 4, where a strong outward radial flow was encountered. Due to the lower flow velocities in the viscous-layer, the flow close to the wall is skewed outwards more than the inviscid flow. The flow downstream of the leading-edge and away from the hub will be analyzed to assess the "TABLET" code for predicting radial outflow of surface streamlines due to blade rotation effects.

The computer code "TABLET" being used in this investigation solves the finite-difference form of the compressible 3-DBL equations (including the energy equation) in a nonorthogonal surface coordinate system. An efficient, implicit, fully coupled finite-difference solution procedure is employed. Boundary conditions are obtained from experimental data to eliminate errors associated with inviscid approximations. Starting solutions along two inflow boundaries (selected from close examination of data) are obtained by solving the appropriate limiting form of the 3-DBL equations. Sample solutions obtained to date will be described in the next few paragraphs.

The first test case for this investigation was selected to establish the accuracy of the present 3-DBL code for analyzing passage flows. For this reason, the flow in a 60 deg curved duct, for which an extensive set of data is available in Ref. 4, was computed using the "TABLET" code. The schematic of the flow problem along with the nomenclature and locations of the measuring stations is shown in Fig. 5. The two inflow boundaries for this problem were selected to be along line A and along the radial line at Station 1. Streamwise velocity profiles along these inflow boundaries were generated from Whitfield's wall-wake correlation (Ref. 5) which uses experimentally measured values of the skin friction coefficient, momentum-thickness-Reynolds number and shape factor as input. Cross-flow velocity profiles along the inflow boundaries were generated from Mager's (Ref. 6) cross-flow representation using measured skewing of surface streamlines. The "TABLET" code has been used to compute the viscous flow on the upper wall of the curved duct from Station 1 to Station 15 in the streamwise direction and from the pressure side A to the suction side E in the spanwise direction. The predicted values for all the integral properties and the skin friction coefficient compare very well with the measured data. A typical comparison from this study is presented in Fig. 6 where the surface streamline skewing angle, β_w, is shown. This figure clearly indicates that relatively large skewing of surface streamlines, typically encountered in turbine passage flows, can be accurately predicted using the present 3-DBL analysis.

The next test case chosen for this study is the flow in the endwall region of a turbine passage. The surface streamline pattern and St number distribution for this case have already been shown in Figs. 2(a) and (b). Figure 7a shows the schematic diagram of the computational mesh which consists of boundary fitted lines at constant percentage pitch locations and vertical lines at constant percentage axial locations. The upstream inflow boundry is selected to be the line at 10 percent chord distance downstream of the leading edge and the pressure side inflow boundary is taken to be along the intersection of endwall and pressure surfaces (Fig. 7a). Locally similar solutions are used along these inflow boundaries to generate the starting profiles. Since the location and extent of the transition zone is not known for this problem, a preliminary case has been run by assuming that the flow is fully laminar in the leading-edge region and it transits to turbulent flow instantaneously at the second streamwise mesh point (x/Bx = 0.105). The computed Stanton

(St) number distribution at x/Bx = 0.2, 0.4, 0.6 and 0.8 is shown in Fig. 7b along with the measured data. The predicted values of St number display the correct qualitative variation when traversing from pressure side to suction side over the region considered here. Keeping in mind the fact that no attempt has been made to modify the turbulence model, the present results are very encouraging. A sensitivity study will be conducted to determine the effect of changes in transition location and turbulence model on the St number distribution in the near future.

It is planned to use the "TABLET" code for predicting the viscous flow on the suction surface of the blade to study the effect of streamline convergence on heat transfer. Finally, this code will be used to predict the skewing of surface streamlines on the pressure surface of the rotating turbine blade of Ref. 3, to complete the assessment of the applicability of the 3-DBL theory for analyzing viscous flow in a turbine passage.

References

1. Graziani, R. A., Blair, M. F., Taylor, J. R. and Mayle, R. D.: An Experimental Study of Endwall and Airfoil Surface Heat Transfer in a Large Scale Turbine Blade Cascade. Trans. of ASME, J. of Eng. for Power, Vol. 102, No. 2, April 1980, pp. 257-267.

2. Vatsa, V. N. and Davis, R. T.: The Use of Levy-Lees Variables in 3-D Boundary Layer Flows. NASA CR-112315, January 1973.

3. Dring, R. P. and Joslyn, H. D.: Measurements of Turbine Rotor Blade Flows. ASME Gas Turbine Conference, New Orleans, LA, Measurement Methods in Rotating Components of Turbomachinery, pp. 51-58.

4. Vermeulen, A. J.: Measurements of Three-Dimensional Turbulent Boundary Layers, Ph.D. Thesis, Dept. of Engineering, University of Cambridge, England, November 1971.

5. Whitfield, D. A.: Analytical Description of the Complete Turbulent Boundary Layer Velocity Profile. AIAA Journal, Vol. 17, No. 10, October 1979, pp. 1145-1147.

6. Mager, A.: Generalization of Boundary-Layer Momentum Integral Equations to Three-Dimensional Flows Including those of Rotating Systems, NACA Report 1067 (1951).

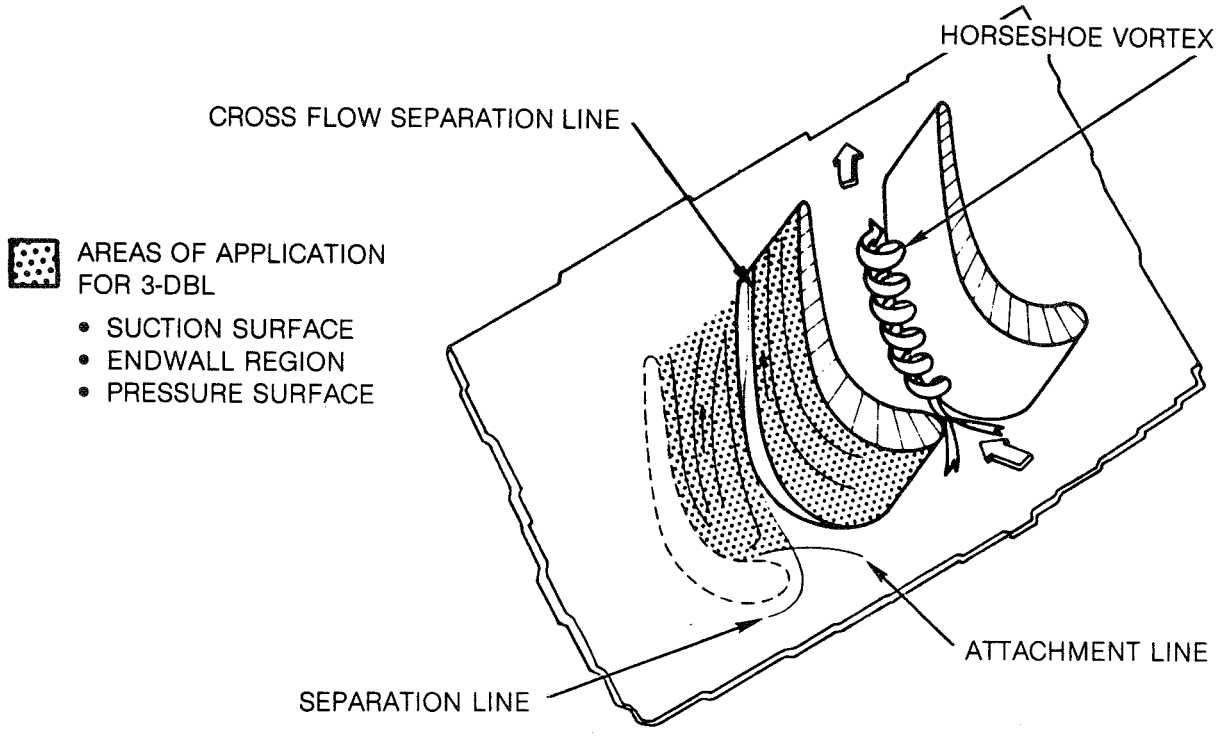

Fig. 1. Schematic of Flow in a Turbine Passage

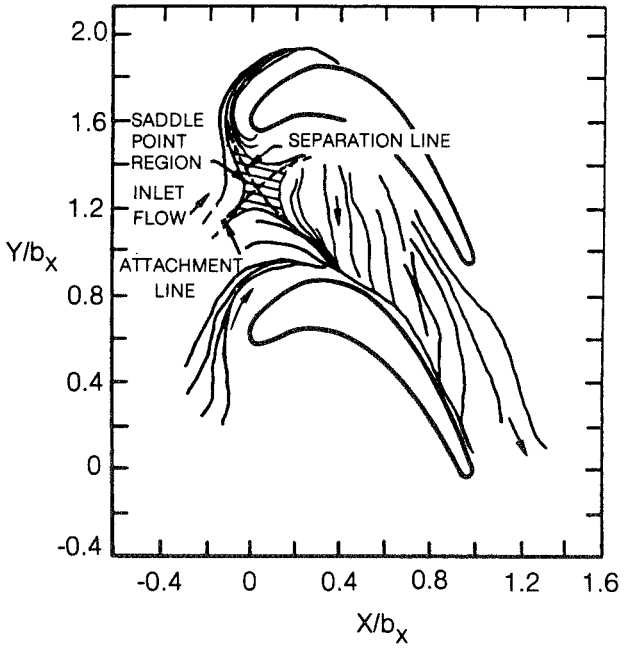

Fig. 2a. Endwall Surface Limiting Streamlines

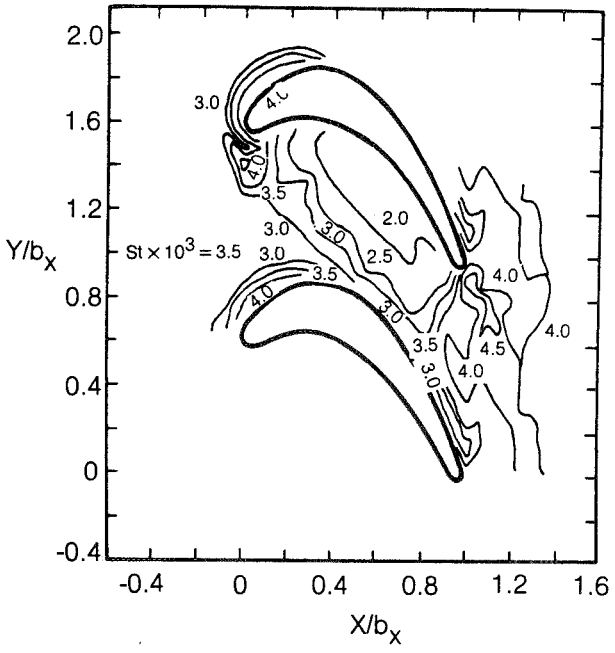

Fig. 2b. Endwall Stanton Number Contours

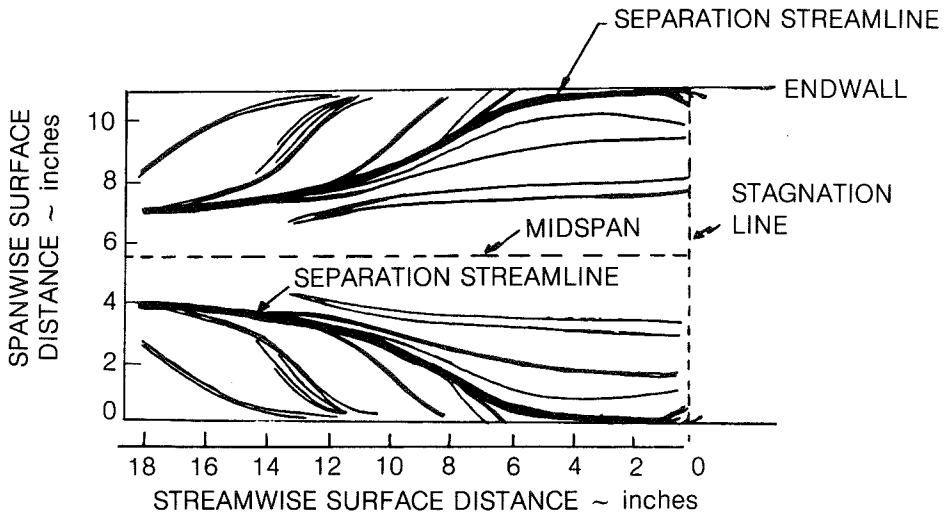

Fig. 3a. Blade Suction Surface Limiting Streamlines

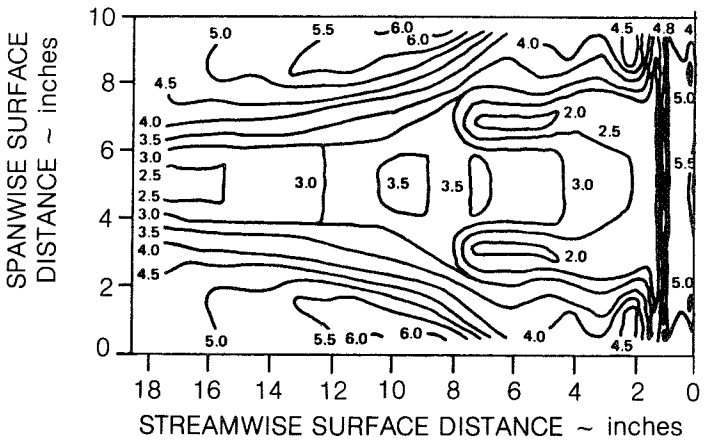

Fig. 3b. Blade Suction Surface Stanton Number Contours

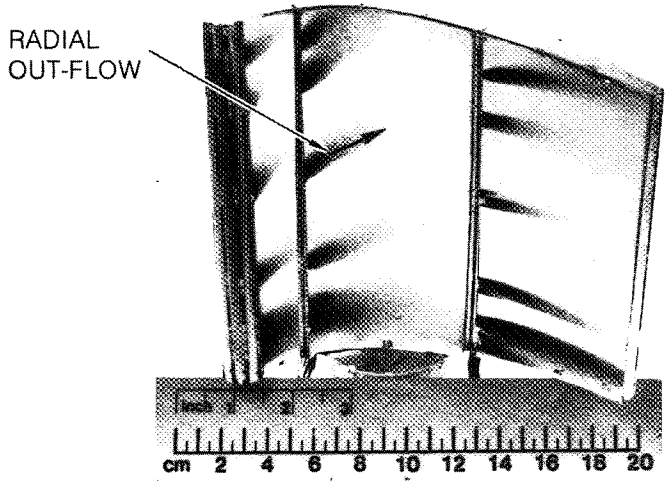

Fig. 4. Pressure Surface Limiting Streamlines

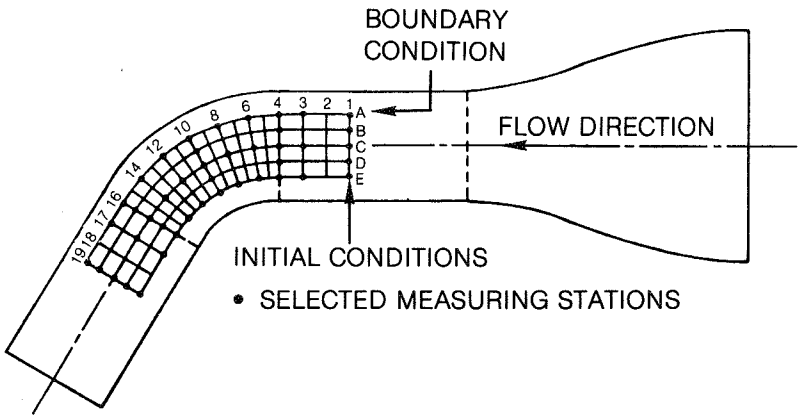

Fig. 5. Schematic of Experimental Setup for Flow in a Curved Duct

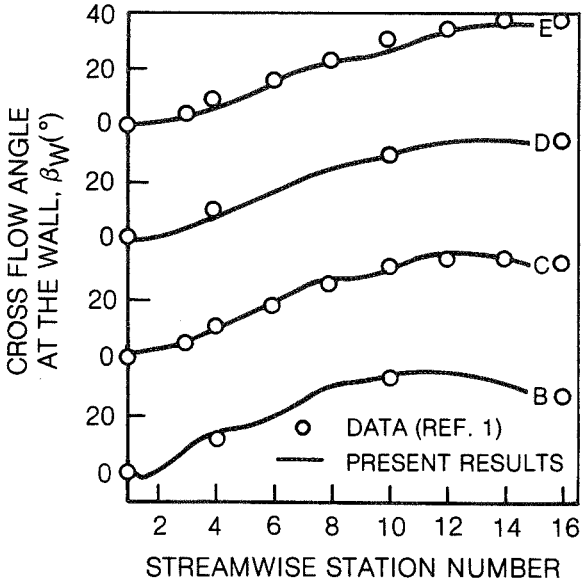

Fig. 6. Wall Cross Flow Angle Distribution for Flow in a Curved Duct

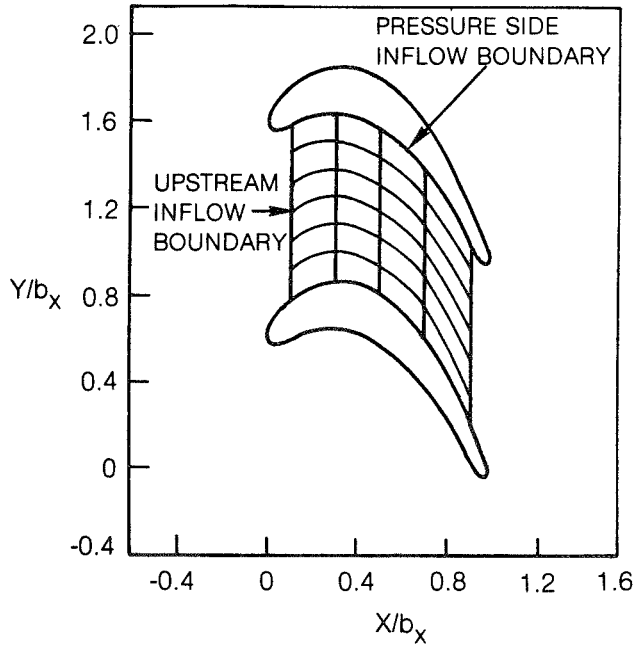

Fig. 7a. Schematic Diagram of Endwall Computational Region

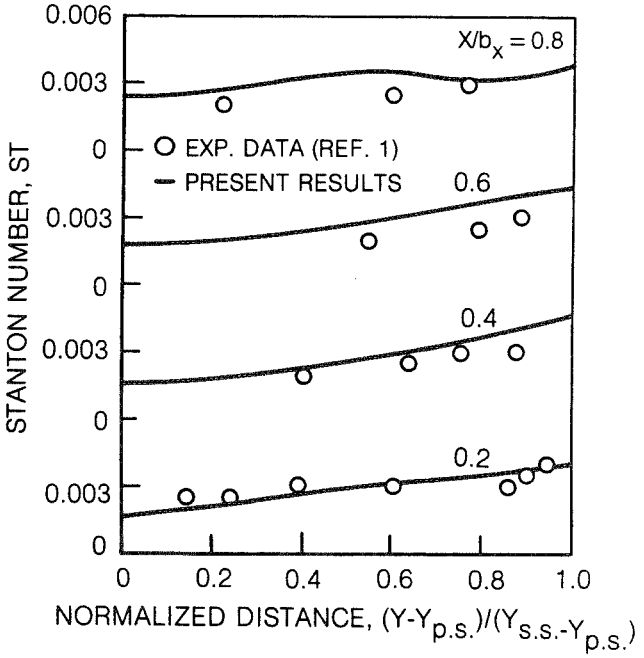

Fig. 7b. Comparison of Endwall Stanton Number Distributions

D4

GAS-SIDE HEAT TRANSFER WITH ROTATION

Robert P. Dring
United Technologies Research Center

The primary basis for heat transfer analysis of turbine blades is experimental data obtained in linear cascades. These data have been very valuable in identifying the major heat transfer and fluid flow features of a turbine airfoil. The question of major interest is how well all of these data translate to the rotating turbine blade. It is known from the work of Lokay and Trushin (ref. 1) that average heat transfer coefficients on the rotor may be as much as 40 percent above the values measured on the same blades non-rotating. Recent work by Dunn and Holt (ref. 2) supports the Russian conclusion. What is lacking is a set of data from a rotating system which is of sufficient detail as to make careful local comparisons between static cascade and rotor blade heat transfer. In addition, data is needed in a rotating system in which there is sufficient documentation of the flow field to support the computer analyses being developed today. A second major question is the influence, if any, of the first stator row on the heat transfer of the second stator row after the flow has passed through the rotor.

The first objective of the present program, is to obtain a detailed set of heat transfer coefficients along the midspan of a blade in a rotating turbine. The turbine stage to be examined is that of Dring et al. (ref. 3), as shown in figure 1. Aerodynamic testing of this stage has already been conducted to document, among other things, the impact of rotor-stator interaction on the airfoil unsteady pressure distributions. The time averaged and unsteady pressure envelopes are shown in figure 2. The rotor heat transfer data are to be such that they can be compared directly with data taken in the static cascade experiment of Graziani et al. (ref. 4), as illustrated in figure 3. The data are also to be compared to some standard analysis of blade boundary layer heat transfer which is in use today. In addition to providing this all-important comparison between rotating and stationary data, this experiment should provide important insight to the more elaborate full three-dimensional programs being proposed for future research. A second program objective is to obtain a detailed set of heat transfer coefficients along the midspan of a stator vane located in the wake of a full upstream turbine stage. Particular focus here is on the relative circumferential location of the first and second stators. The final program objective is to improve the analytical capability to predict the experimental data.

The program is divided into two phases. The first phase is designed to provide a high density of high accuracy heat flux measurements on both the pressure and suction surfaces of a rotating turbine blade, figure 1. The program will include two rotor-stator spacings to assess the influence of rotor-stator interaction as in the experiment of Dring et al. (ref. 3). It will also include both positive and negative incidence as well as the design incidence. Finally, the first phase program will include comparison of the data with static cascade data, figure 3, and with a common boundary layer heat transfer analysis. The second phase will be designed to provide

a high density of high accuracy heat flux measurements on both the pressure and suction surfaces of a second stator row turbine vane. The program will be run at one of the rotor-stator spacings used in the first phase. It will include, at minimum, four different circumferential positionings of the first stator row relative to the second stator row. In addition, the second phase will include an analysis to describe the experimental phenomena of both phases, which will improve the current ability to predict turbine midspan airfoil heat transfer.

REFERENCES

1. Lokay, V. I.; and Trushin, V. A.: Heat Transfer from the Gas and Flow-Passage Elements of a Rotating Gas Turbine. Heat Transfer - Soviet Research, Vol. 2, No. 4, July 1970.

2. Dunn, M. G.; and Holt, J. L.: The Turbine Stage Heat Flux Measurements. Paper No. 82-1289, AIAA/ASME 18th Joint Propulsion Conference, 21-23, June 1982, Cleveland, Ohio.

3. Dring, R. P.; Joslyn, H. D.; Hardin, L. W.; and Wagner, J. H.: Turbine Rotor-Stator Interaction, Trans. ASME, Jour. Eng. for Power, Vol. 104, October 1982, pp. 729-742.

4. Graziani, R. A.; Blair, M. F.; Taylor, J. R.; and Mayle, R. E.: An Experimental Study of Endwall and Airfoil Surface Heat Transfer in a Large Scale Turbine Blade Cascade. Trans. ASME, Jour. Eng. for Power, Vol. 102, No. 2, April 1980, pp. 257-267.

OBJECTIVES

- **Turbine rotor heat transfer data**
- **Rotor-stator interaction (ΔX)**
- **Comparison with cascade data**
- **Second stator heat transfer data**
- **Stator-stator interaction (ΔCirc)**
- **Quasi-steady and/or unsteady boundary layer analysis**

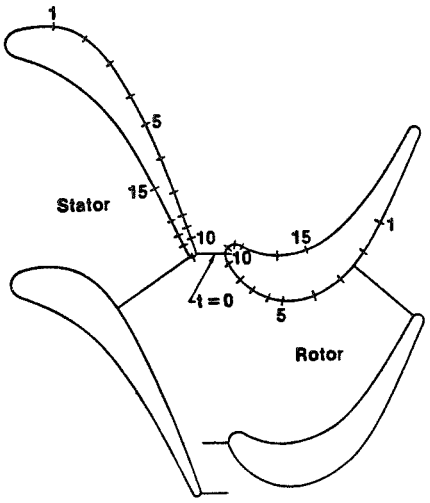

FIGURE 1. TURBINE STAGE AT 15% GAP (Ref. 3)

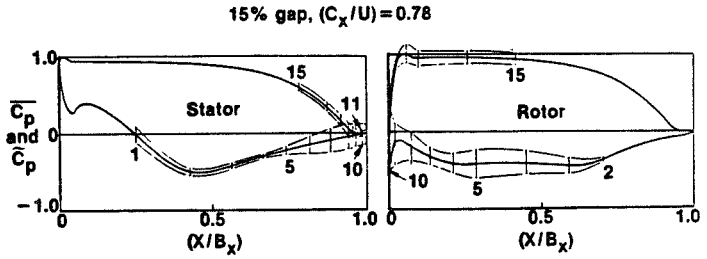

FIGURE 2. UNSTEADY PRESSURE ENVELOPES (Ref. 3)

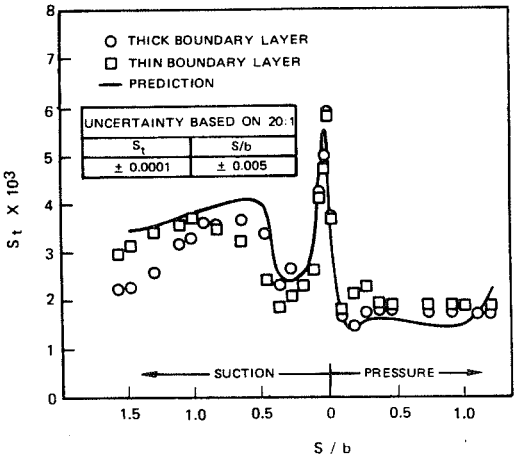

FIGURE 3. MEASURED AND PREDICTED MIDSPAN HEAT TRANSFER DISTRIBUTIONS (Ref. 4)

Page intentionally left blank

D15

COOLANT PASSAGE HEAT TRANSFER WITH ROTATION
A Progress Report on the Computational Aspects

L. D. Aceto, Program Manager
G. J. Sturgess, Presenter
Pratt & Whitney Engineering, Pratt & Whitney Aircraft Group

Turbine airfoils are subjected to increasingly higher heat loads which escalate the cooling requirements in order to satisfy life goals for the component materials. If turbine efficiency is to be maintained, however, cooling requirements should be as low as possible. To keep the quantity of cooling air bounded, a more efficient internal cooling scheme must be developed. One approach is to employ airfoils with multi-pass cooling passages that contain devices to augment internal heat transfer while limiting pressure drop. (fig. 1).

Design experience with multi-pass cooling passage airfoils has shown that a surplus of cooling air must be provided as a margin of safety. This increased cooling air leads to a performance penalty. Reliable methods for predicting the internal thermal and aerodynamic performance of multi-pass cooling passage airfoils would reduce or eliminate the need for the safety margin of surplus cooling air.

The objective of the program is to develop and verify improved analytical methods that will form the basis for design technology which will result in efficient turbine components with improved durability without sacrificing performance. The objective will be met by: 1) establishing a comprehensive experimental database that can form the basis of an empirical design system. 2) developing computational fluid dynamic techniques, and 3) analyzing the information in the database with both phenomenological modeling and mathemetical modeling to derive a suitable design and analysis procedure.

Currently, a design phase has been completed which defined a rotating experiment to simulate blade passage cooling. Models of blade internal geometries will be studied. The first model with instrumented smooth wall legs has been designed and is being fabricated. It is scheduled for testing in December, 1983. The subsequent models will have "rough" walls and will address passage aspect ratio changes. These tests will generate a database for the development of a design system.

The prediction of local coolant side heat transfer coefficients and coolant temperature rise and pressure drop in the cooling passages is difficult because of the three dimensional, elliptic nature of the flow, the effects of rotation, and the complex turbulence promoting devices. The analytical approach under consideration is based on the 3D-TEACH computer code being developed for gas turbine combustor applications by Pratt & Whitney Aircraft, (ref. 1).

The 3D-TEACH code is a generalized aerothermal fluid dynamic solver for three-dimensional, elliptic, turbulent, steady flows. The approach stays within the framework of continuum mechanics and uses a statistical description of turbulence, coupled with the accepted Eulerian description provided by the Navier-Strokes equations of motion. Closure to the resulting time-mean equations is provided by turbulence modeling of the eddy viscosity type. The modeled partial differential

equations are manipulated into a general form that permits a single solution algorithm to be used for a numerical procedure. A hybird (upwind/central) finite differencing scheme is used to discretize the equations.

A version of the 3D-TEACH code has been modified to calculate fluid flow and heat transfer in rotating passages. In order to be able to apply the code with confidence to the experimental data generated in this program, it is essential to assess the suitability of the physical modeling used. To do this, the code is being exercised in flow situations similar to the turbine airfoil application, but simpler in nature. Such a procedure enables the weaknesses, if any, to be identified easily.

To test the behavior of the modified momentum equations flow in a rotating multi-pass passage (figure 1), was calculated. Flow patterns are made visible by the use of streak lines. Figure 2 shows flow at 600 RPM (0·174 Rossby Number) in two cross-sections of the passage. The development of a vortex pair in the outflow (away from axis of rotation) leg due to Coriolis forces can be seen clearly. The action of the sharp turns is to coalesce these vortices into a single vortex that dominates flow in the inflow leg. The observed behavior appears sensible.

The quantitative behavior in rotation was examined through reference 2. For example, a comparison of velocity profiles for the duct rotating at 165 R.P.M. is given in figure 3. Streakline flow visualization shows also the development of Coriolis vortices in the duct.

The ability of the code to calculate heat transfer in a rectangular duct with a sharp 180 degree bend was examined through reference 3. A comparison of calculated and measured Nusselt numbers for the various zones through the passage is given in figure 4 at two Reynolds numbers.

The behavior of the code thus far is pleasing, and the results of the comparisons with the verification experiments is very encouraging. Further investigations of these and other suitable experiments will continue to build confidence in the code. Use of more sophisticated turbulence modeling will also be explored. The developed code will then be applied to the measurements to be made as part of this program.

REFERENCES

1. Sturgress, G. J., "Aerothermal Modeling - Phase I Final Report," NASA Rept. CR. 168202, May 1983.

2. Moon, I.M., "Effects of Coriolis Force on the Turbulent Boundary Layer in Rotating Fluid Mechanics," M.I.T. Gas Turbine Lab. Report No. 74, June 1964.

3. Metzger, D. and Sahm, M., "Measured Heat Transfer in Smooth Rectangular Ducts with 180 Degree Sharp-Corners Turns," Arizona State University Tech. Rept. ERC-R-83003, January 1983.

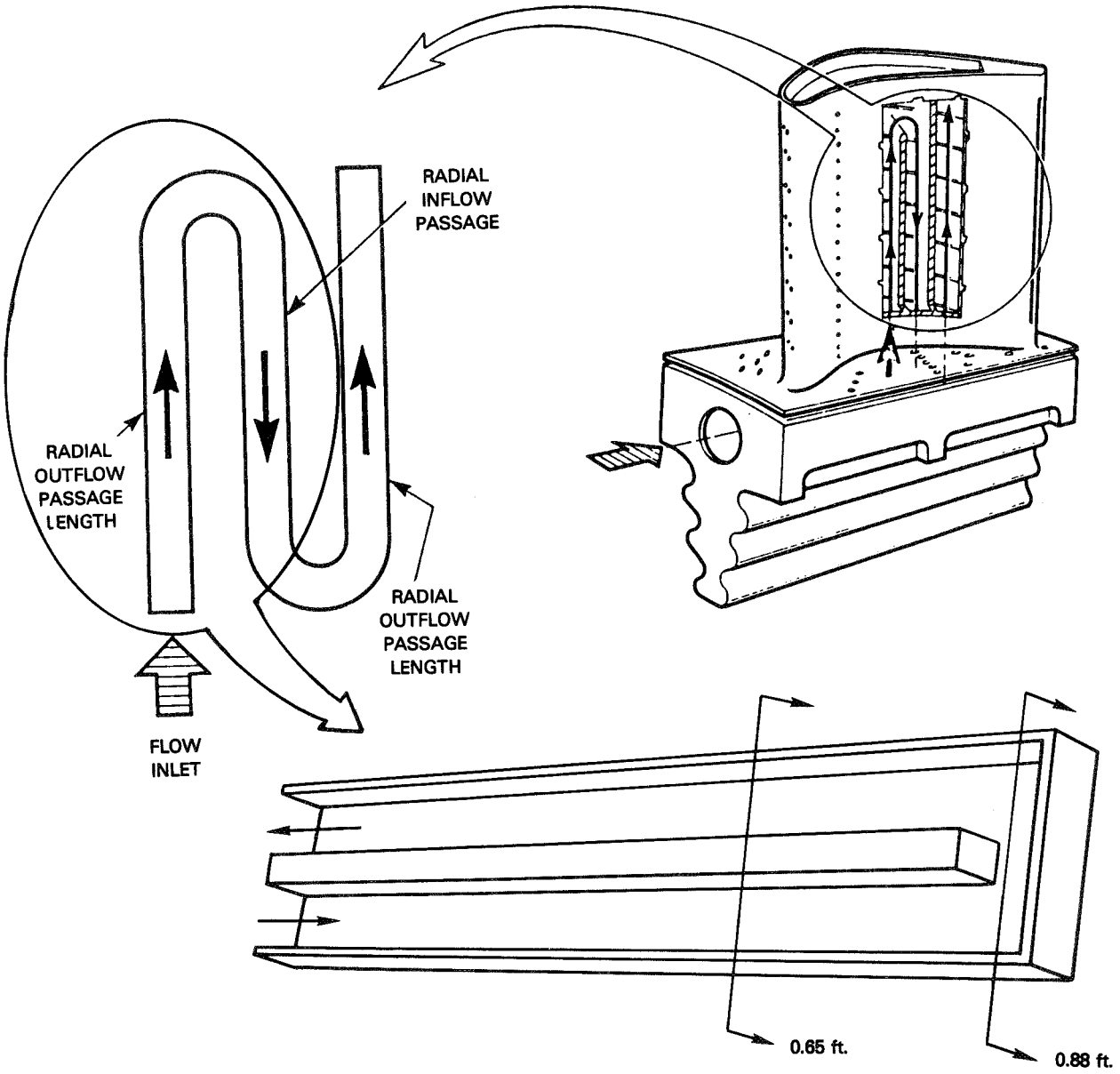

Figure 1 Schematic Of Coolant Passage

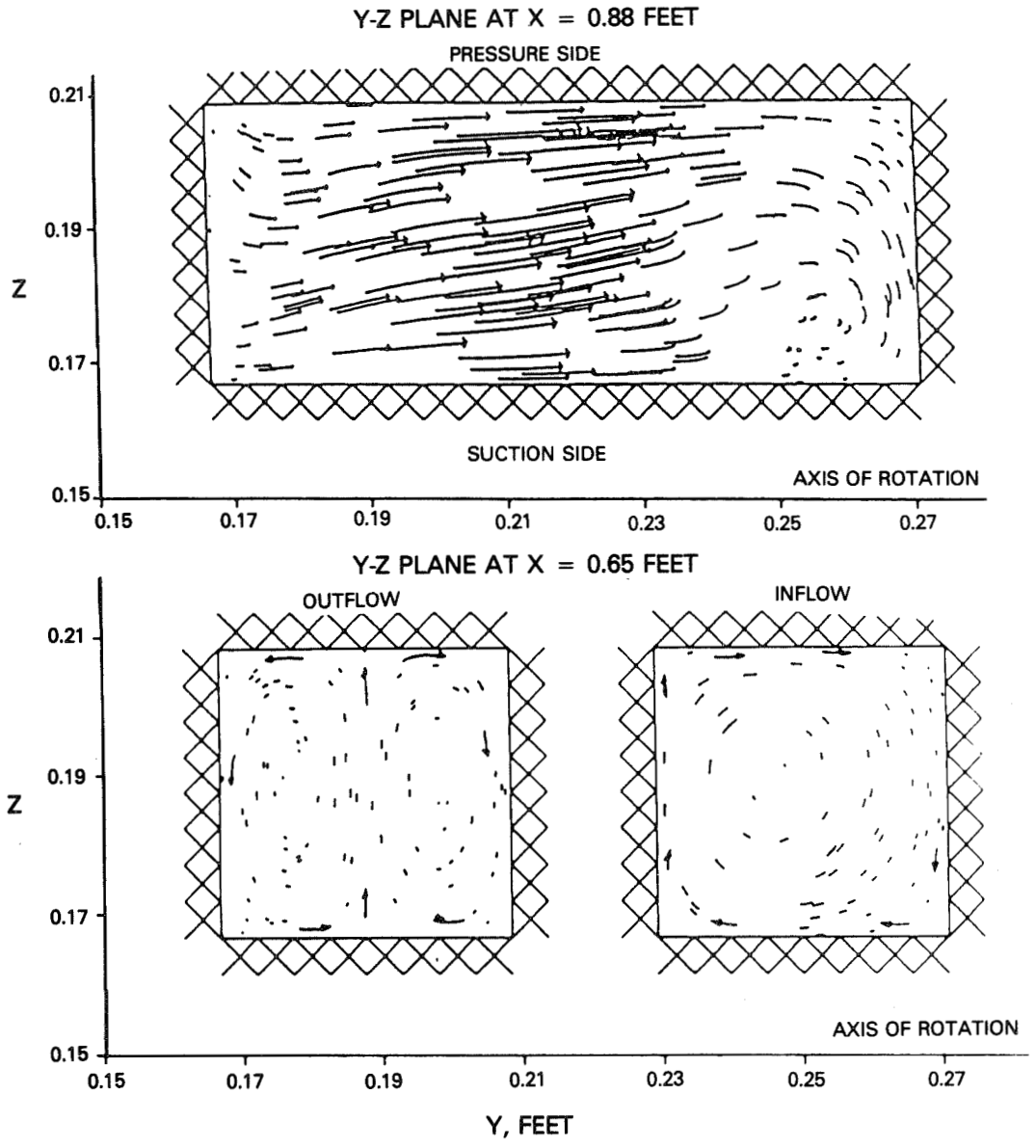

Figure 2 Test Of Momentum Equations Rotation at 600 R.P.M.

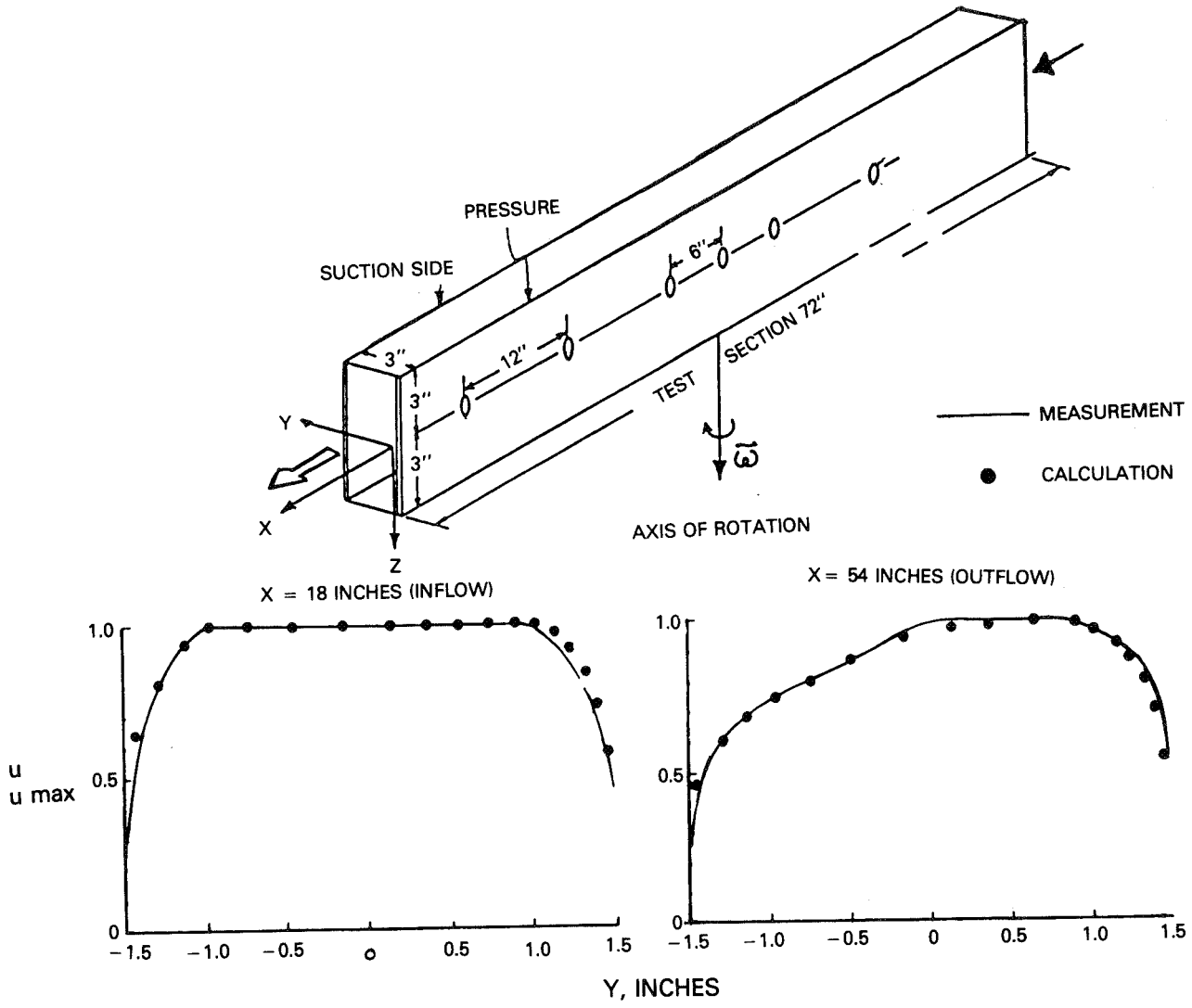

Figure 3 Axial Velocity Profile Development at 165 R.P.M. For Moon's Experiment

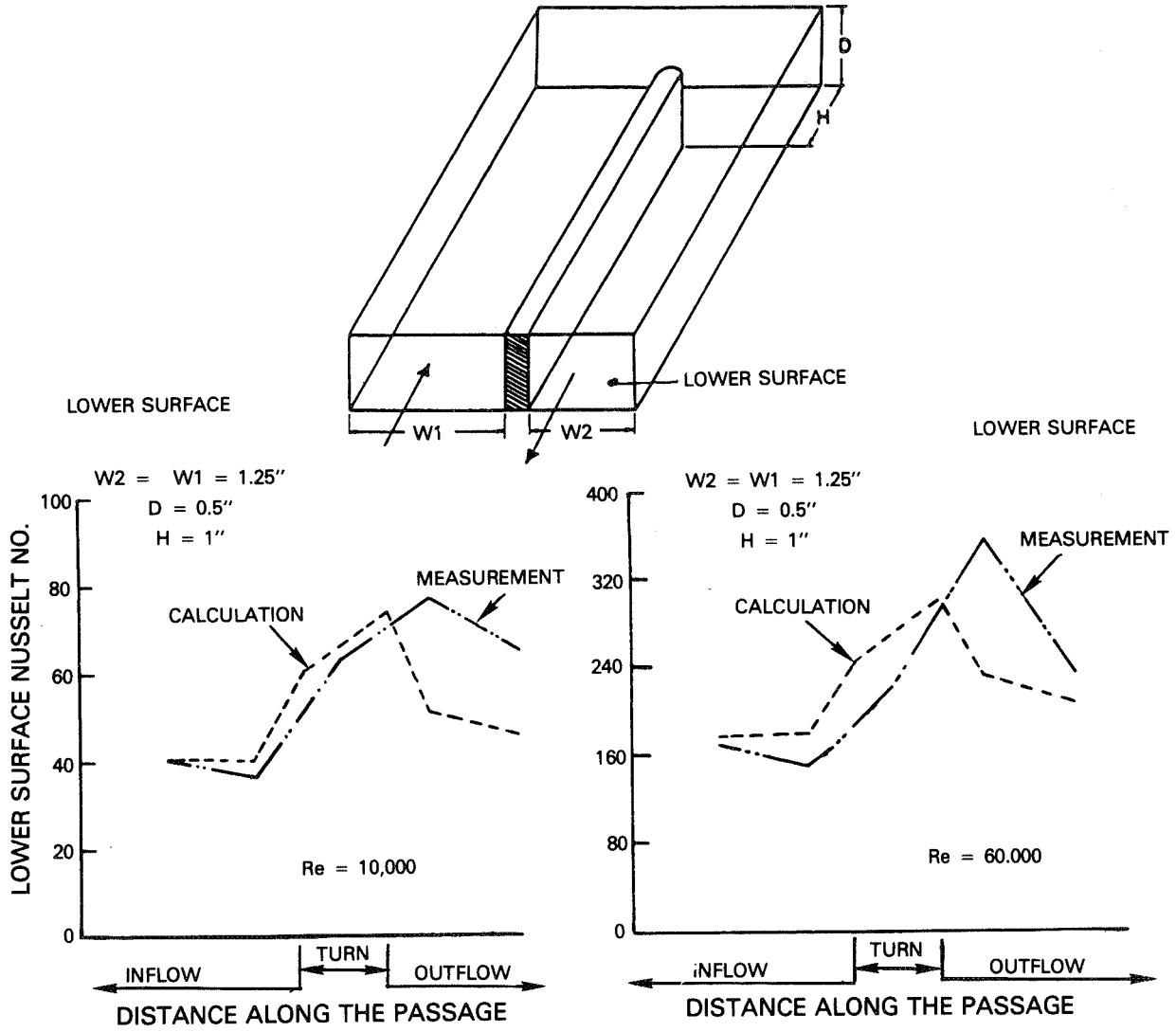

Figure 4 Heat Transfer In 180° Sharp Bend For Metzger's Experiment

D16

JET ARRAY IMPINGEMENT HEAT TRANSFER CHARACTERISTICS

L.W. Florschuetz and D.E. Metzger
Department of Mechanical and Aerospace Engineering
Arizona State University

Two-dimensional arrays of circular air jets impinging on a heat transfer surface parallel to the jet orifice plate are considered. The jet flow, after impingement, is constrained to exit in a single direction along the channel formed by the jet orifice plate and the heat transfer surface. In addition to the crossflow which originates from the jets following impingement, an initial crossflow is present which approaches the array through an upstream extension of the channel (fig. 1). The configurations considered are intended to model the impingement cooled midchord region of gas turbine airfoils in cases where an initial crossflow is also present (fig. 2). A major objective is determination of the effect of initial crossflow air temperature relative to jet array air temperature on impingement surface heat fluxes.

Earlier work in this NASA sponsored project was directed at modeling uniform arrays in cases where an initial crossflow is not present. In those cases, referred to here as noninitial crossflow geometries, there was an endwall or upstream edge to the channel positioned one-half a streamwise hole spacing upstream of the first spanwise row of holes in the array. Note that with the initial crossflow geometry (fig. 1), the special case of zero initial crossflow ($m_c = 0$) is identical to the noninitial crossflow case except for the presence of the upstream channel endwall in the latter case.

In this extended abstract, nomenclature and definition of parameters is first indicated for the more general initial crossflow case. Then the main features of the prior noninitial crossflow studies are briefly summarized. The current status of the initial crossflow work is then discussed.

Consider a uniform rectangular array of circular jet orifices with an inline hole pattern (figs. 1 and 3). Consider further the heat flux, q, at the impingement surface, averaged across the span, but resolved in the streamwise direction to a region of width x_n, centered opposite an arbitrary spanwise row of holes within the array at location x. It is desired to express q as a function of parameters associated with the entire array. Assume constant fluid properties, negligible viscous dissipation, a uniform impingement surface temperature, T_s, an adiabatic jet orifice plate surface at the jet exit plane, and a fully developed channel flow at the entrance to the array (x = 0) with a mixed-mean temperature T_c. Then, at the specified x

$$q = f\ (\underbrace{m_j,\ m_c}_{\text{flow}},\ \underbrace{T_j,\ T_c,\ T_s}_{\text{temperature}},\ \underbrace{x_n,\ y_n,\ z,\ d,\ L}_{\text{geometry}},\ \underbrace{\mu,\ k,\ c_p}_{\text{fluid}})$$

or in one possible dimensionless form, at x/L,

$$\frac{q \cdot d}{k(T_s - T_j)} = f[m_c/m_j,\ \overline{\overline{Re}}_j,(T_c-T_j)/(T_s-T_j),\ x_n/d, y_n/d, z/d,\ L/x_n,\ Pr]$$

In this form the dependent parameter, which has the form of a Nusselt number, incorporates a heat transfer coefficient defined as $q/(T_s-T_j)$ with the jet temperature T_j as the characteristic fluid temperature. With this definition the Nusselt number is not independent of the temperature differences of the problem, since it still depends on the initial crossflow temperature ratio $(T_c-T_j)/(T_s-T_j)$. In spite of the restrictions imposed, there are still eight independent dimensionless parameters, nine including the specified x/L. Note that one of these is L/x_n which is just the number of spanwise rows in the array.

Still considering q in terms of parameters associated with the entire array, an alternate formulation is

$$q = f(m_j,\ m_c,\ T_{aw},\ T_s,\ x_n,\ y_n,\ z,\ d,\ L,\ \mu,\ k,\ c_p)$$

where

$$T_{aw} = f(m_j,\ m_c,\ T_j,\ T_c,\ x_n,\ y_n,\ z,\ d,\ L,\ \mu,\ k,\ c_p)$$

Then in dimensionless form

$$Nu = \frac{q \cdot d}{k(T_s-T_{aw})} = f(m_c/m_j,\ \overline{\overline{Re}}_j,\ x_n/d,\ y_n/d,\ z/d,\ L/x_n,\ Pr) \qquad (1)$$

and

$$\eta = \frac{T_{aw}-T_j}{T_c-T_j} = f(m_c/m_j,\ \overline{\overline{Re}}_j,\ x_n/d,\ y_n/d,\ z/d,\ L/x_n,\ Pr) \qquad (2)$$

This formulation, employing the adiabatic wall temperature, has the advantage that the heat transfer coefficient, $q/(T_s-T_{aw})$, and Nusselt number are rendered independent of the temperature differences of the problem. But, unless $T_c=T_j$, the additional dependent parameter η is also needed. This Nusselt number and the corresponding η are a function of seven independent dimensionless parameters, eight including the specified x/L.

At this point the possibility of representing q as a function of parameters associated only with a given spanwise row is considered (fig. 4). Here, it is assumed that the dependence of q on the velocity and temperature distribution at the control surface (channel cross-section) immediately upstream of the row may be represented in terms of a single velocity and a single temperature parameter, denoted by G_c and T_c. Then in dimensionless form one may write

$$Nu = \frac{q \cdot d}{k(T_s-T_{aw})} = f(G_c/G_j,\ Re_j,\ x_n/d,\ y_n/d,\ z/d,\ Pr) \qquad (3)$$

and

$$\frac{T_{aw}-T_j}{T_c-T_j} = f(G_c/G_j,\ Re_j,\ x_n/d,\ y_n/d,\ z/d,\ Pr) \qquad (4)$$

In general, of course, q will depend on the velocity and temperature distributions over such a control surface, which, in turn, depend on the history of the mixing jet

flows and crossflows upstream of the control surface. However, the above approximation, if shown to be adequate, admits the possibility of applying measurements obtained for uniform array geometries to heat transfer opposite individual rows of nonuniform array geometries.

Results based on an extensive series of tests for a range of uniform array geometries in noninitial crossflow configurations using air as the working fluid are reported in tabular and graphical forms in references 1, 2 and 3 in terms of the parameters of equation (1), except for m_c/m_j which is not a relevant parameter in noninitial crossflow cases. Results were obtained for every geometry tested with Nu resolved in the streamwise direction to at least x_n, and in most cases to $x_n/3$. Correlations, in algebraic form, for Nu (resolved to x_n) expressed in terms of parameters associated with a single spanwise row as in equation (3), are reported in references 4 and 5. In these references, a theoretically based flow distribution model is also presented and validated by comparison with measured flow distributions for these noninitial crossflow cases. The validated flow model was used in developing the correlations referred to above. Results for nonuniform arrays in noninitial crossflow configurations have also been obtained and compared with the uniform array data and the correlation based on that data (ref. 6). Examples are shown in figure 5.

One of the more extensive prior heat transfer studies of two-dimensional arrays of circular jets was reported in reference 7. The studies completed under the present project go substantially beyond prior work, and provide a much more complete understanding of the problem as well as needed design information. The main features of the present project which had not been addressed in prior work may be summarized as follows: (1) streamwise spatial resolution of at least x_n for all geometries tested; (2) observations of ''damped'' periodic streamwise variations of heat transfer coefficients along entire array with spatial resolution of $x_n/3$; (3) detailed verification of validity of geometric scaling; (4) rectangular arrays, i.e., not restricted to $x_n/y_n = 1$; (5) staggered as well as inline hole patterns; (6) correlation for streamwise local application developed in algebraic form; (7) nonuniform as well as uniform array geometries tested; (8) experimentally validated theoretical flow distribution model developed for both uniform and nonuniform array geometries; (9) applicability of uniform array data and correlation to nonuniform arrays examined; (10) effect of confined crossflow on jet orifice discharge coefficients; (11) effects of initial crossflow rate and temperature, currently in progress, discussed further below.

An example of heat transfer characteristics with initial crossflow, specified in terms of array parameters as in equations (1) and (2), is shown in figure 6 for the B(5,4,3)I geometry (i.e., B-size plenum, $x_n/d=5$, $y_n/d=4$, $z/d=3$, Inline hole pattern). The corresponding flow distribution is shown in figure 7. Additional such results are reported in reference 6.

Nusselt numbers specified in terms of parameters at an individual spanwise row, as in equation (3), are illustrated in figure 8. The presence of initial crossflow extends the data point range of G_c/G_j beyond the maximum values existing for the noninitial crossflow (or essentially identical zero initial crossflow) cases. The B(5,4,2)I geometry (upper plot in fig. 8) clearly shows that a minimum value of Nu may occur at a certain G_c/G_j. A point is reached where the jet no longer effectively impinges on the surface, but the Nusselt number increases with the increasing crossflow velocity. The prior noninitial crossflow correlation (refs. 4 and 5) though shown extrapolated beyond the range of G_c/G_j on which it was based,

appears to be reasonably consistent with the data points until the increase in Nusselt number begins, except for several data points from the first and second spanwise rows of the array.

Dimensionless adiabatic wall temperatures specified in terms of parameters at an individual spanwise row, as in equation (4), are illustrated in figures 9 and 10. In figure 9, $T_{m,n}$, the mixed-mean total temperature, was used as the characteristic crossflow temperature, T_c, immediately upstream of a given row. Figure 10 shows data for the same cases, but with $T_{aw,n-1}$, the adiabatic wall temperature opposite the row immediately upstream of the row in question, used to represent T_c. It is not clear at this writing whether either of these approaches will prove to be of general utility over a range of geometries. This question is currently being studied. In some instances the dimensionless adiabatic wall temperature at the first row or two, like the Nusselt number, clearly does not follow the general trend of the data points. This is because the relationship between q and T_s at the impingement surface opposite a given row clearly must depend on the details of the velocity and temperature distributions over the channel cross-section immediately upstream of the row. These distributions at downstream rows may differ considerably from those at the first several rows of an initial crossflow array, and their effects cannot necessarily be represented accurately by a single crossflow velocity and a single temperature parameter.

REFERENCES

1. Florschuetz, L.W., Metzger, D.E., Takeuchi, D.I. and Berry, R.A., Multiple Jet Impingement Heat Transfer Characteristics - Experimental Investigation of Inline and Staggered Arrays with Crossflow, NASA Contractor Report 3217, January 1980.

2. Metzger, D.E., Florschuetz, L.W., Takeuchi, D.I., Behee, R.D. and Berry, R.A., ''Heat Transfer Characteristics for Inline and Staggered Arrays of Circular Jets with Crossflow of Spent Air,'' ASME Journal of Heat Transfer, Vol. 101, 1979, pp. 526-531.

3. Florschuetz, L.W., Berry, R.A. and Metzger, D.E., ''Periodic Streamwise Variations of Heat Transfer Coefficients for Inline and Staggered Arrays of Circular Jets with Crossflow of Spent Air,'' ASME Journal of Heat Transfer, Vol. 102, 1980, pp. 132-137.

4. Florschuetz, L.W., Truman, C.R. and Metzger, D.E., ''Streamwise Flow and Heat Transfer Distributions for Jet Array Impingement with Crossflow,'' ASME Journal of Heat Transfer, Vol. 103, 1981, pp. 337-342.

5. Florschuetz, L.W., Metzger, D.E., and Truman, C.R., Jet Array Impingement with Crossflow - Correlation of Streamwise Resolved Flow and Heat Transfer Distributions, NASA Contractor Report 3373, January 1981.

6. Florschuetz, L.W., Metzger, D.E., Su, C.C., Isoda, Y. and Tseng, H.H., Jet Array Impingement Flow Distributions and Heat Transfer Characteristics - Effects of Initial Crossflow and Nonuniform Array Geometry, NASA Contractor Report 3630, November 1982.

7. Kercher, D.M. and Tabakoff, W., ''Heat Transfer by a Square Array of Round Air Jets Impinging Perpendicular to a Flat Surface Including the Effect of Spent Air,'' ASME Journal of Engineering for Power, Vol. 92, No. 1, January 1970, pp. 73-82.

NOMENCLATURE (includes symbols not explicitly defined in text or figures)

C_D = jet plate discharge coefficient
c_p = constant pressure specific heat
f = friction coefficient
G_c = crossflow mass velocity based on channel cross-sectional area
G_j = jet mass velocity based on jet hole area
h = heat transfer coefficient at impingement surface, $q/(T_s-T_{aw})$
k = thermal conductivity
m_c = initial crossflow rate
m_j = total jet flow rate
μ = dynamic viscosity
Pr = Prandtl number
q = heat flux at impingement surface
Re_j = jet Reynolds number, $G_j d/\mu$
T_{aw} = adiabatic wall temperature (with subscript n, denotes location opposite spanwise row number n)
T_c = characteristic temperature of initial crossflow or of crossflow within array depending on context
T_j = characteristic temperature of jet flow
$T_{m,n}$ = crossflow channel mixed-mean temperature upstream of spanwise row n
T_s = heat transfer surface temperature

Superscript

$(\overline{})$ = overbar refers to mean value over jet plate

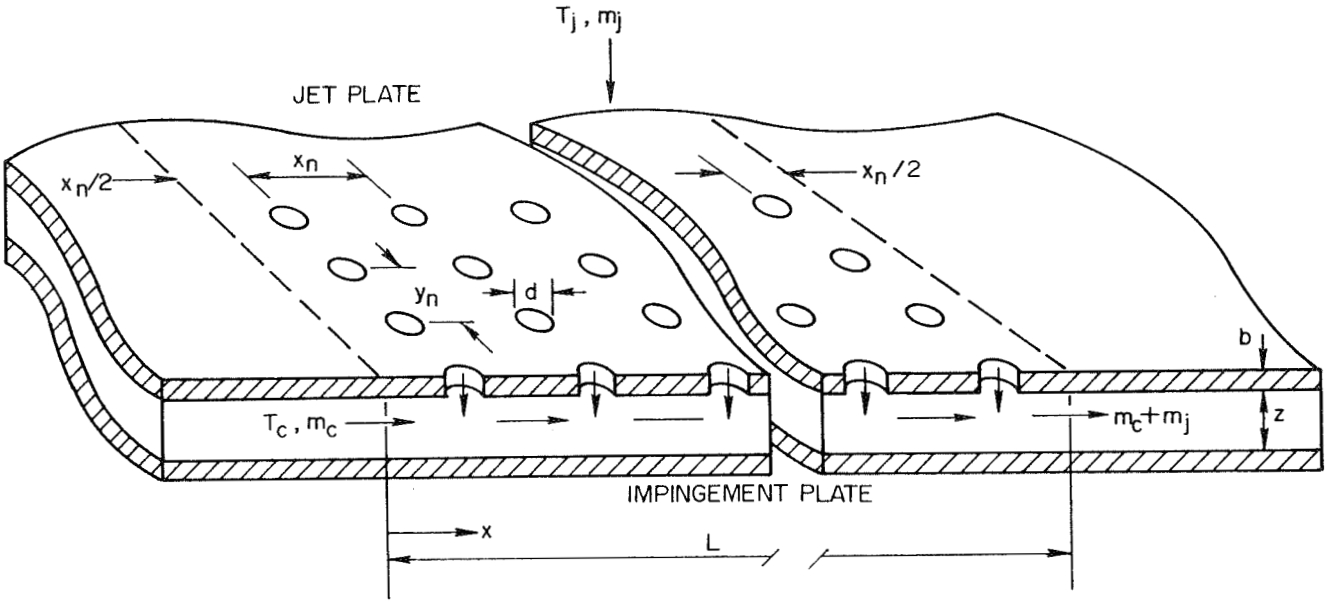

Figure 1. Basic test model geometry with initial crossflow.

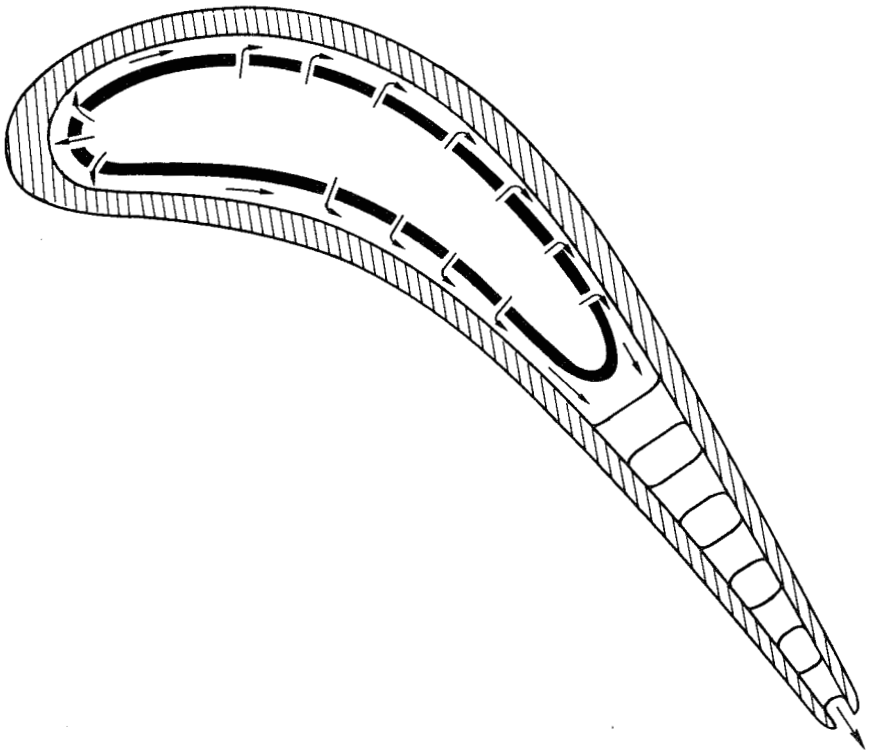

Figure 2. Impingement cooled airfoil - midchord jet arrays subject to initial crossflow.

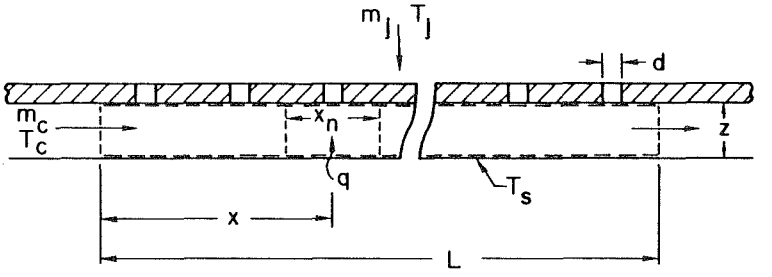

CONSIDER AT SPECIFIED x

$$q = f(m_j, m_c, T_j, T_c, T_s, x_n, y_n, z, d, L, \mu, k, c_p,)$$

FLOW TEMPERATURE GEOMETRY FLUID

THEN POSSIBLE DIMENSIONLESS FORM AT SPECIFIED x/L IS

$$\frac{q \cdot d}{k(T_s - T_j)} = f\left[m_c/m_j, \overline{Re}_j, (T_c - T_j)/(T_s - T_j), x_n/d, y_n/d, z/d, L/x_n, Pr\right]$$

Figure 3. Possible formulation of streamwise resolved impingement surface heat transfer characteristics in terms of array parameters.

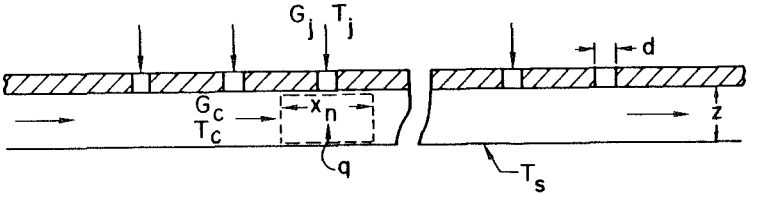

CONSIDER

$$q = f(G_c, G_j, T_{aw}, T_s, x_n, y_n, z, d, \mu, k, c_p)$$

WHERE

$$T_{aw} = f(G_c, G_j, T_j, T_c, x_n, y_n, z, d, \mu, k, c_p)$$

DIMENSIONLESS FORM

$$\frac{q \cdot d}{k(T_s - T_{aw})} = f(G_c/G_j, Re_j, x_n/d, y_n/d, z/d, Pr)$$

$$\frac{T_{aw} - T_j}{T_c - T_j} = f(G_c/G_j, Re_j, x_n/d, y_n/d, z/d, Pr)$$

Figure 4. Possible formulation of streamwise resolved impingement surface heat transfer characteristics in terms of individual spanwise jet row parameters.

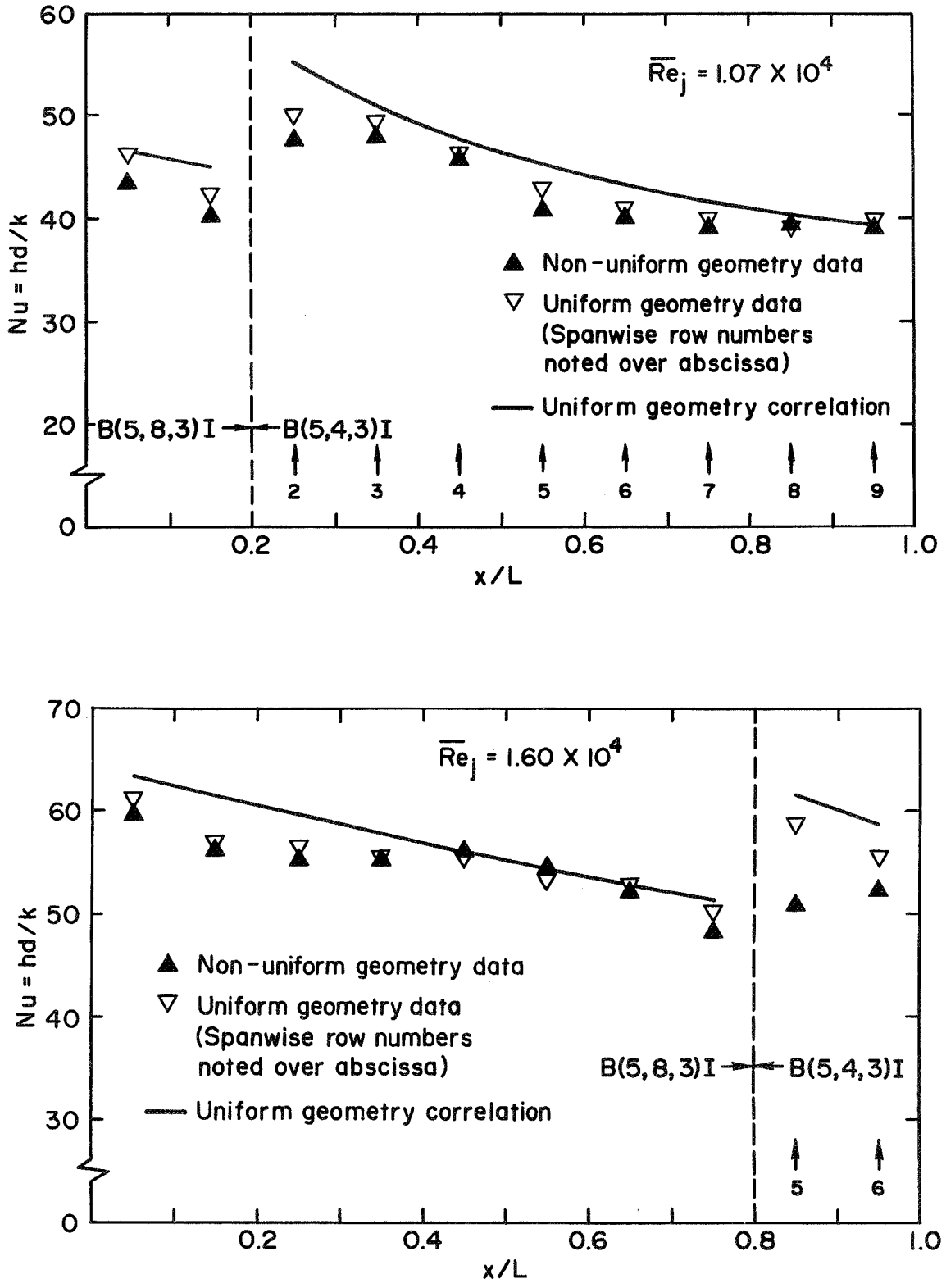

Figure 5. Examples of nonuniform array geometry Nusselt numbers compared with uniform array data and correlation.

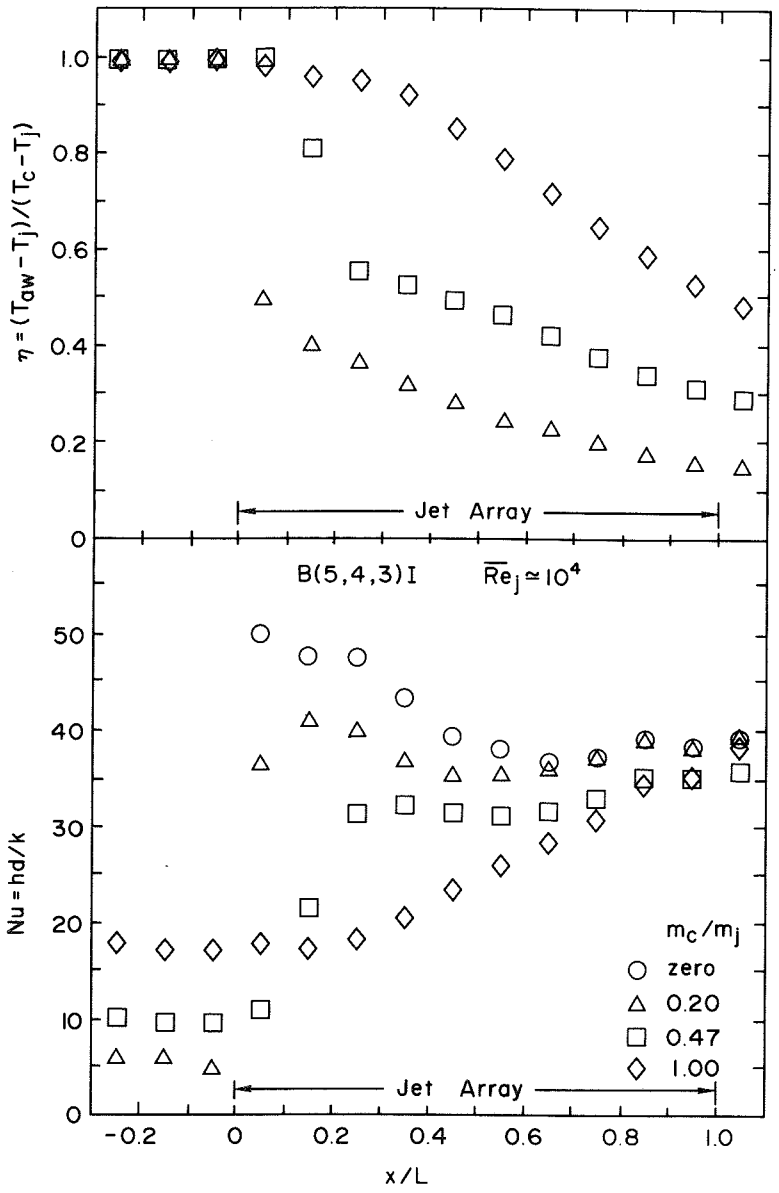

Figure 6. Examples of streamwise profiles of initial crossflow Nusselt numbers (Nu) and dimensionless adiabatic wall temperatures (η) specified in terms of array parameters.

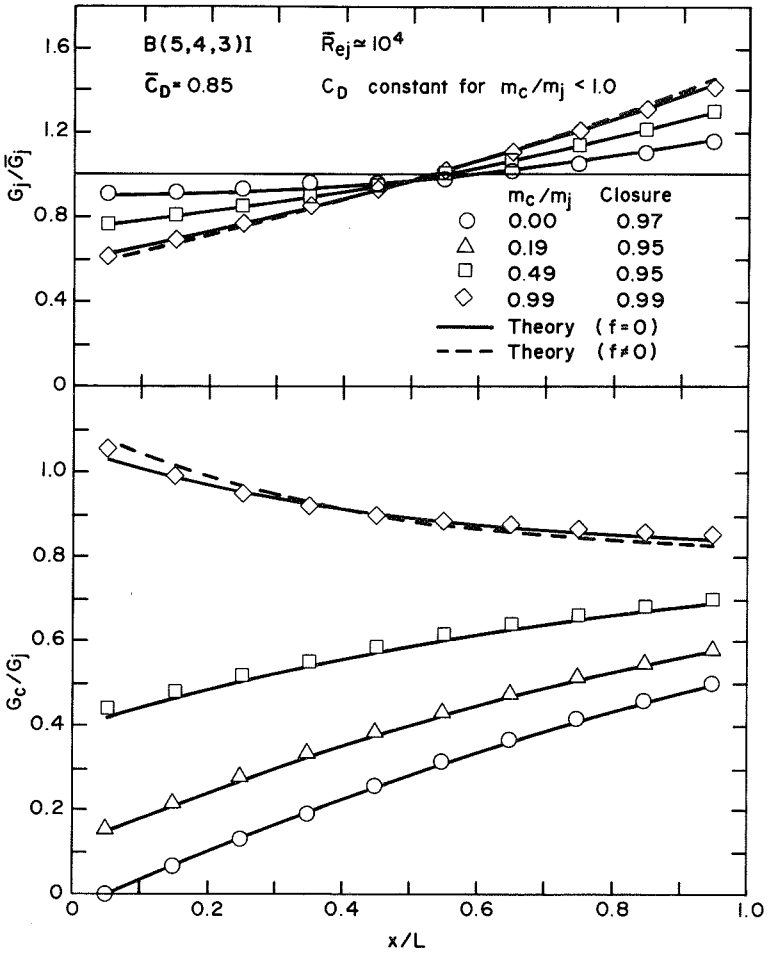

Figure 7. Examples of flow distributions with initial crossflow for array geometry of figure 6.

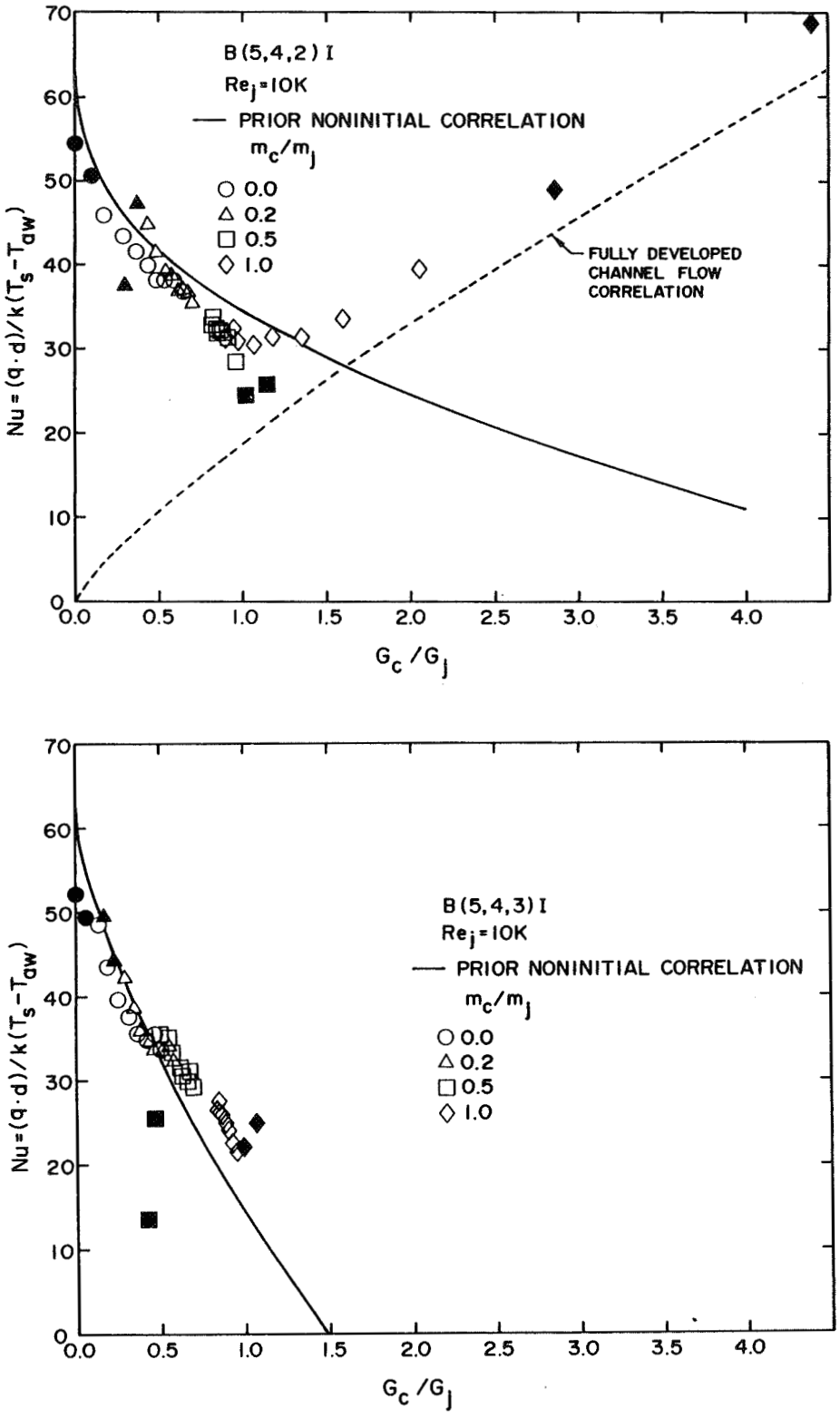

Figure 8. Examples of streamwise resolved Nusselt numbers as a function of individual spanwise row cross-to-jet mass velocity ratios. Solid symbols denote data from first and second upstream rows of array.

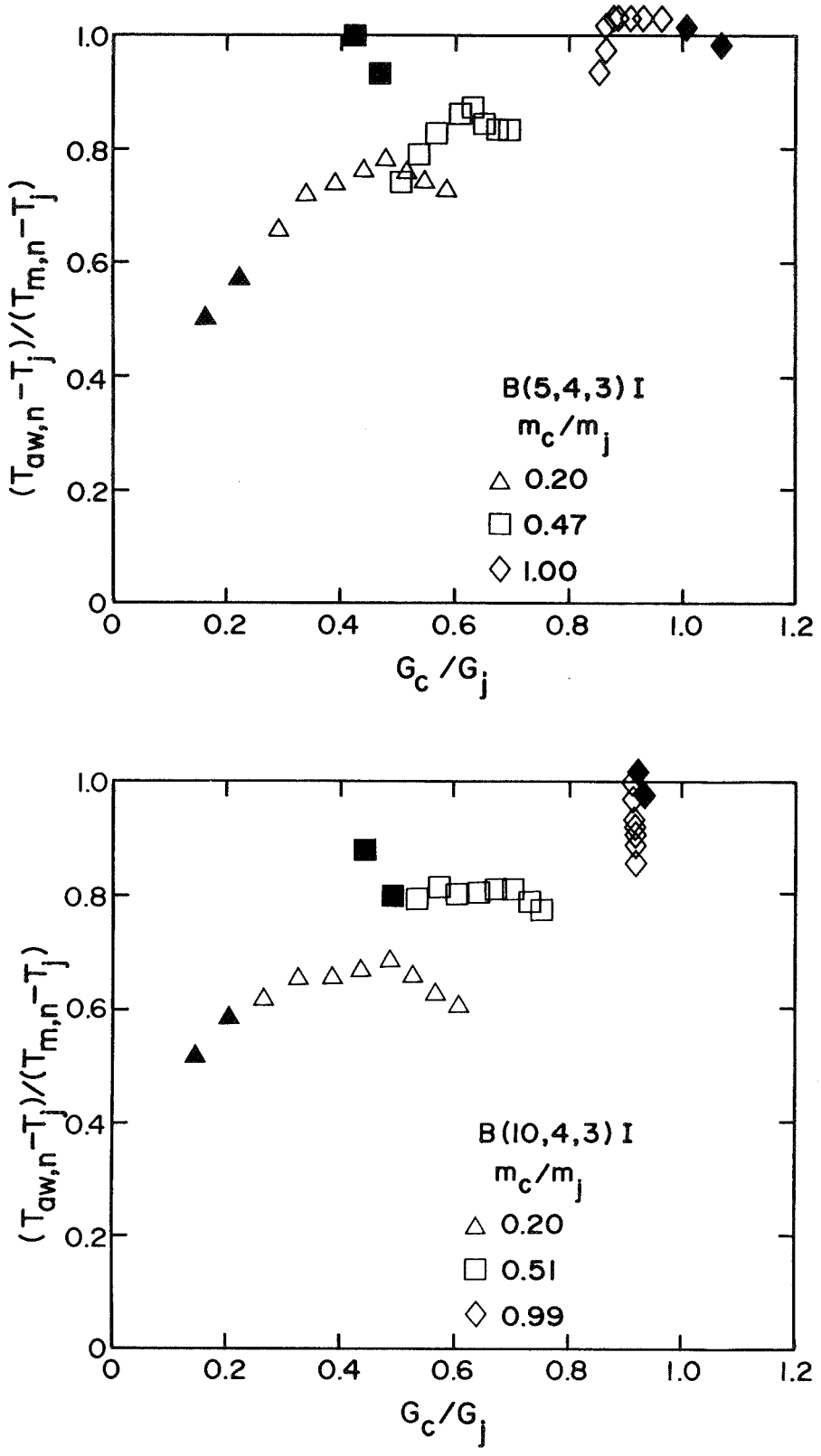

Figure 9. Examples of dimensionless adiabatic wall temperature as a function of individual spanwise row cross-to-jet mass velocity ratio, using mixed-mean total temperature upstream of row as characteristic crossflow temperature. Solid symbols denote data from first and second rows of array.

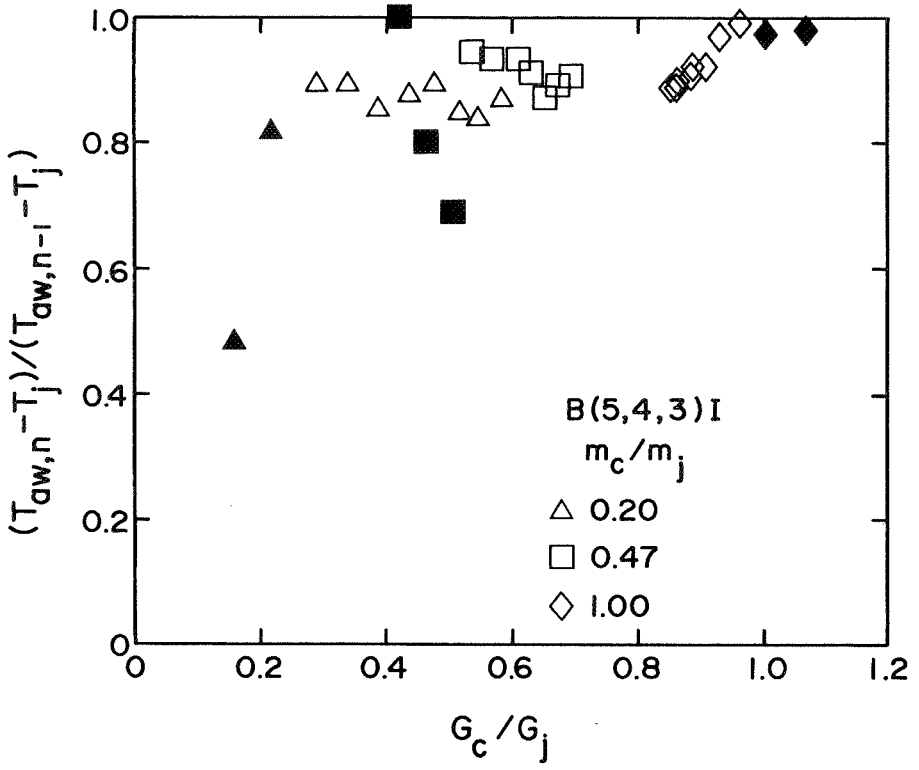

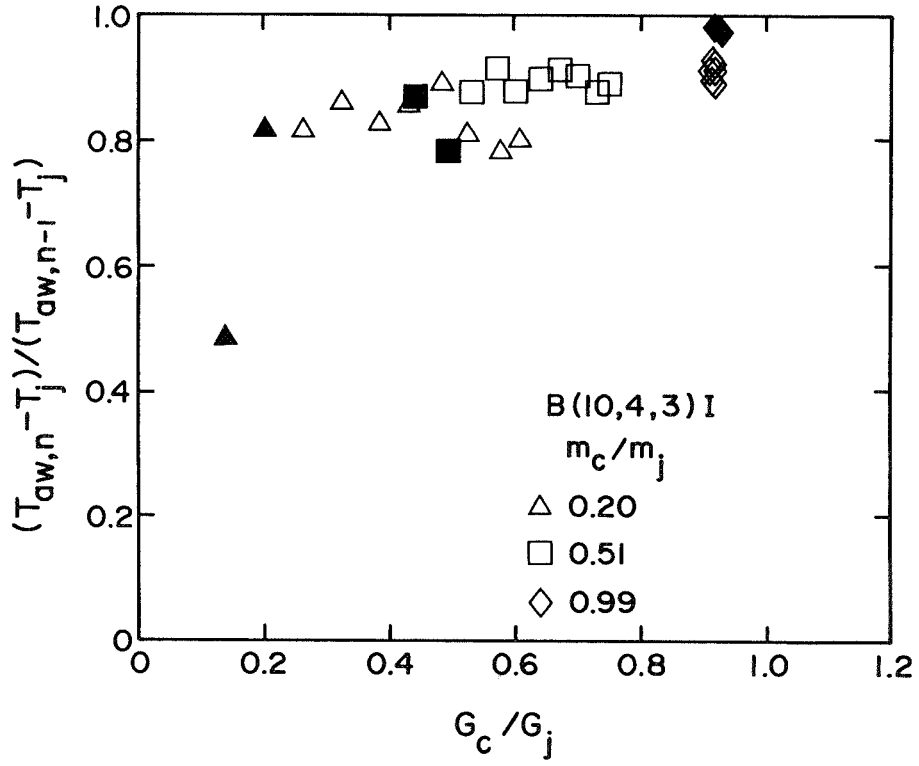

Figure 10. Examples of dimensionless adiabatic wall temperature as a function of individual spanwise row cross-to-jet velocity ratio, using adiabatic wall temperature at upstream row as characteristic crossflow temperature. Solid symbols denote data from first and second rows of array.

D17

COMBUSTION HOT SECTION TECHNOLOGY

David B. Ercegovic

Propulsion Laboratory
AVARDCOM Research and Technology Laboratories
Lewis Research Center
Cleveland, Ohio

The overall objective of the Turbine Engine Hot Section Technology Combustion Project is to develop and verify improved and more accurate analysis methods for increasing the ability to design with confidence the combustion system for advanced aircraft turbine engines. The analysis methods developed will be generically applicable to combustion systems and not restricted to one specific engine or manufacturer.

This project's approach was to first assess and evaluate existing combustor aerothermal analysis models by means of a contracted effort initiated during FY '82. This evaluation effort has assessed and quantified known models' strengths and deficiencies. The results of this assessment will be summarized later in this report by the three contractors Garrett, General Electric and Pratt and Whitney Aircraft who conducted this independent evaluation. A balanced contract and in-house program will then be conducted to support, focus, and accelerate the development of new methods to more accurately predict and model the physical phenomena occurring within the combustor. This program will include both analytical and experimental research efforts in the areas of aerothermal modeling and liner cyclic life.

During FY '84 the Aerothermal Modeling Program - Phase II will be initiated, which is expected to have contracted model development efforts in the areas of improved numerical methods for turbulent viscous flows, flow interactions, and fuel spray flow-field interactions. A Phase III effort is planned to address remaining model deficiencies. The primary in-house effort in this area will be the determination of high pressure flame radiation characteristics in a full annular combustor. This experiment will be conducted in the NASA LeRC High Pressure Facility with the results compiled into a comprehensive flame radiation and liner heat flux model.

In the area of liner cyclic life, HOST is engaged in a co-operative effort with Pra-t and Whitney Aircraft to develop a test apparatus to economically determine combustor thermal strains and cyclic life. This test apparatus will be run in-house at NASA LeRC and will be the test vehicle for many of the advanced high temperature instruments developed under HOST sponsorship. The fundamental data generated in this project will be used to assess and further develop current analytical liner life programs.

COMBUSTION

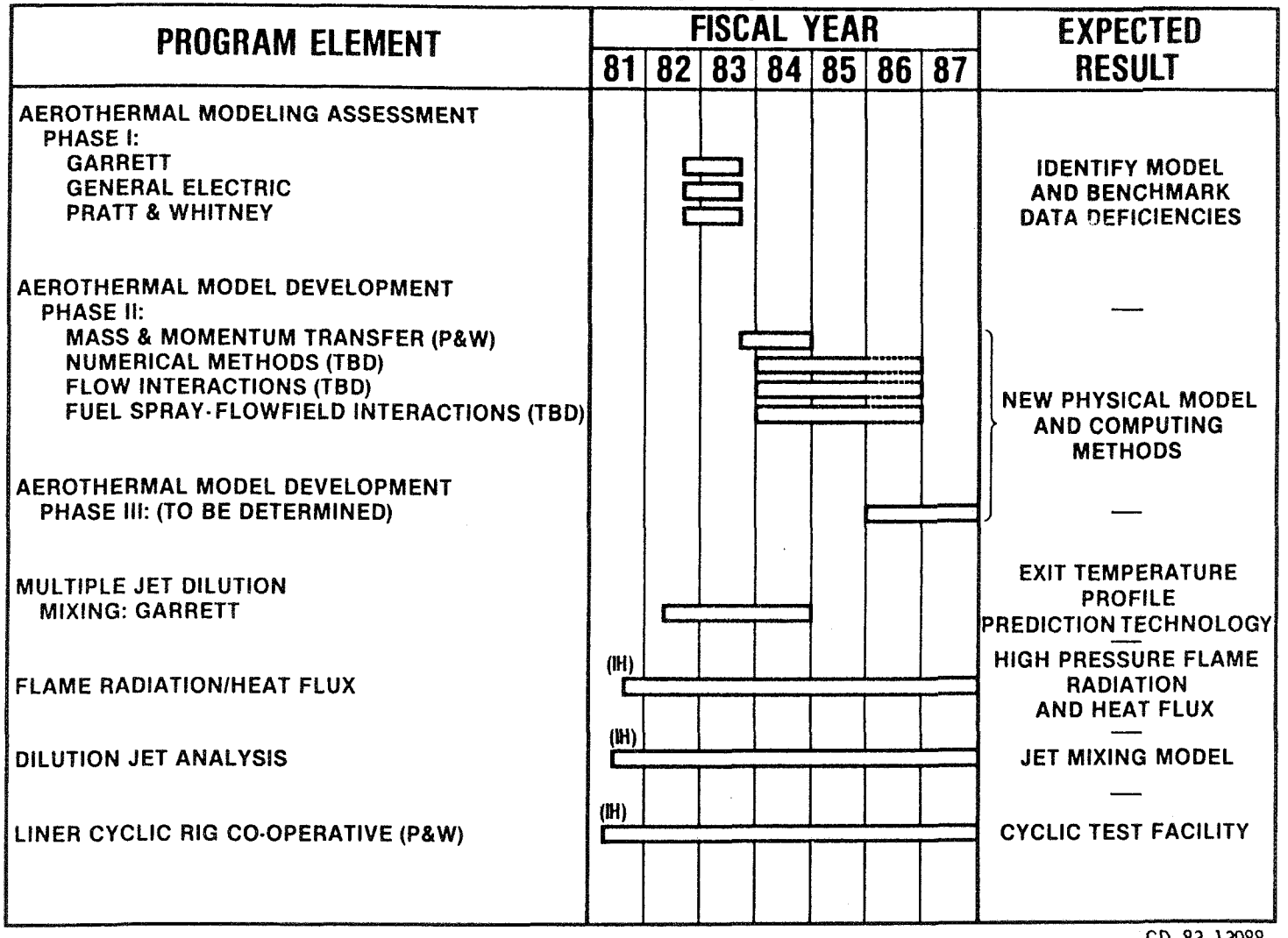

CD-83-13988

AEROTHERMAL MODELING PROGRAM - PHASE I

R. Srinivasan, R. Reynolds, K. Johnson, and H. Mongia
Garrett Turbine Engine Company

The main objective of the NASA-sponsored Aerothermal Modeling Program, Phase I, was to assess current aerothermal submodels used in the Garrett Turbine Engine Company (GTEC) analytical combustor models.

A number of "benchmark" quality test cases were selected after an extensive literature survey (ref. 1). The selected test cases, including both nonreacting and reacting flows, were broadly divided into the following categories:

- Simple flows
- Complex nonswirling flows
- Swirling flows
- Dilution jet mixing in confined crossflows.

These test cases were used to assess the following submodels separately and jointly for various combustion processes:

- k-ϵ model of turbulence and algebraic stress model, with and without various corrections, including low Reynolds number and Richardson number corrections
- Scalar transport models
- Multistep kinetic schemes
- Turbulence/chemistry interaction
- Spray combustion.

Based upon the Phase I work, the following assessments of the submodels were made:

- The k-ϵ model and its modifications give good correlations for
  - Simple flows
  - Far-field regimes of nonswirling/swirling flows involving regions of recirculation
  - Non-recirculating swirling flows
  - Outer regions of strong swirling flows.

- These models give reasonable correlations for
  - Nonswirling recirculating flows excluding the vicinity of any attachment point
  - Confined disk flow with a central jet
  - Shear layer of strong swirling flows
  - Confined swirler with hub and shroud expansions.

The k-ϵ model and its modifications predict only the trends in recirculation zones of swirling flows and confined swirler flows without outer expansion.

The Reynolds stresses predicted by the algebraic stress model (ASM) correlate well for simple flows. The ASM correctly predicts the normal stresses in nonswirling recirculating flows. The ASM predictions give reasonable correlations for:

- Shear stresses in nonswirling recirculating flows
- Normal stresses in swirling flows.

For predicting the scalar transport, the k-ϵ model with constant Prandtl number gives good correlation where the gradient diffusion approximation is valid. The algebraic scalar transport model is a promising approach and more validation efforts are needed.

On the turbulence/chemistry interaction models, the following general conclusions were made:

- Both two-step and four-step kinetic schemes show promise
- A modified eddy breakup model can easily be extended to multi-step kinetic schemes
- Bilger's two-reaction-zone model gives good results for jet flames, but requires more work.

When dilution jet mixing was considered, the three-dimensional analytical model had the following characteristics:

- Slightly underpredicted jet penetration
- Centerline temperatures predicted well
- Transverse mixing predictions slower than data
- Effect of S/D, H/D, J on mixing predicted correctly (where D = geometric orifice diameter, H = local duct height at the survey plane, J = jet versus mainstream momentum ratio, S = orifice spacing)

- Good correlation for jet injection from
  - One wall
  - Both walls - inline orifices
  - Both walls - staggered orifices

The following general conclusions were derived from the Phase I work (ref. 2):

- An accurate numerical scheme should be developed to minimize numerical diffusion in the computations of recirculating flows
- Benchmark quality data should be generated under well defined environments for validating the various submodels used in gas turbine combustion analysis
- Although current aerothermal models make reasonable predictions, intensive model development and validation efforts should continue for the following submodels:
  - Algebraic stress model
  - Algebraic scalar transport model
  - Two-step and four-step schemes
  - Probability density function approach for a two-step scheme
  - Double-reaction-zone model.

REFERENCES

1. Srivatsa, S.K.; Srinivasan, R.; and Mongia, H.C.: Aerothermal Modeling Program, Phase I - Subtask 1.2 Report, Data Base Generation. Garrett Turbine Engine Company Report 21-4484, September 1982.

2. Srinivasan, R.; Reynolds, R.; Ball, I.; Berry, R.; Johnson, K.; and Mongia, H.: Aerothermal Modeling Program, Phase I, Final Report. Garrett Turbine Engine Company Report 21-4742, August 1983.

Page intentionally left blank

AMT 73
P153

AEROTHERMAL MODELING - PHASE I

A Closing Progress Report

G. J. Sturgess
Pratt & Whitney Engineering

The overall objective of the two-phase Aerothermal Modeling Program is to develop the computational fluid dynamics tools needed to improve the design, analysis and development process for the gas turbine engine combustion chamber. In the first phase, 1982 state-of-the-art models were evaluated, shortcomings were identified, and improvements to these models were recommended. The models were of steady-state, time-averaged formulation. It is planned to implement the recommendations made in the first phase as part of the second phase effort.

The results of the study highlighted the importance of inlet boundary conditions when making evaluations of the modeling by means of comparison with benchmark-quality experimental data (ref. 1). The study also revealed that the calculation accuracy was not independent of the numerics used in the solution procedure. It proved necessary to establish a hierarchy of physical models (fig. 1), whose realism must be improved in sequence.

It was found that relatively simple flows could be calculated with acceptable accuracy (fig. 2). However, there was less success with more complicated flows (fig. 3). Shortcomings were identified in the turbulence model with respect to swirling flows and flows with strong streamline curvature, and for calculation of turbulent mass transport (table 1).

The evaluation suffered from a serious lack of readily available and suitable benchmark quality experiments. Many experiments exist in the literature, but they frequently suffer from incomplete boundary conditions, lack of parametric variation of operating conditions, and clear delineation between the physical processes involved.

It was concluded that the current models are of qualitative accuracy only, and are therefore suitable for scale-up, perturbation, and diagnostic studies. In these roles they can serve as useful engineering tools. Further work is required to improve quantitative accuracy for the intended use.

Phase I has proved useful in that it has provided a detailed and systematic examination of the physical modeling used, and it has shown the weaknesses inherent in this modeling. It has also provided substantial insight into the powerful influences exerted on solution accuracy by the inlet boundary conditions, and the numerics used in the computer codes.

The study made it apparent that serious difficulties exist with the present generation of computational fluid dynamics codes for application to the combustor. These difficulties are not perceived as being fatal however. The economic and competitive driving forces in the industry that gave rise to the codes are still real and urgent, and the codes have indeed demonstrated great potential for productivity

improvement in addition to great technical capability. Ways to improve the existing methods exist, and others can be devised. There is no reason or need to abandon the effort. Improvement of the codes should be continued.

REFERENCES

1. Sturgess, G.J., Syed, S.A. and McManus, K.R., "Importance of Inlet Boundary Conditions for Numerical Sumulation (sic) of Combustor Flows," Paper No. AIAA-83-1263, AIAA/SAE/ASME 19th Joint Propulsion Conference, Seattle, Washington, June 27-29, 1983

HIERARCHY OF PHYSICAL MODELS

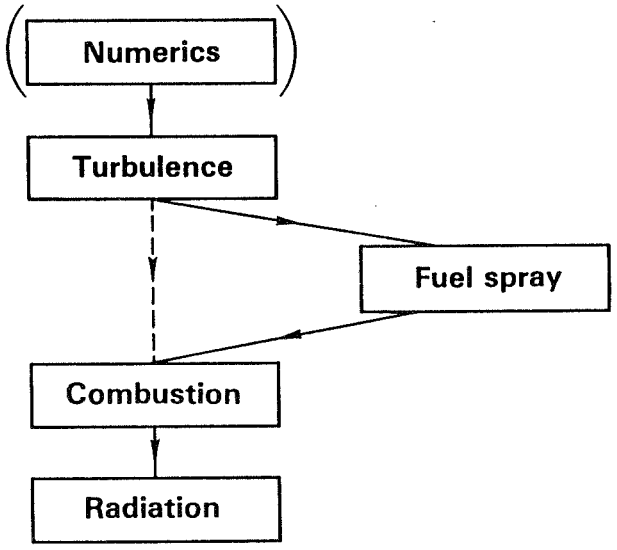

Figure 1

SIMPLE FLOWS WERE WELL-CALCULATED

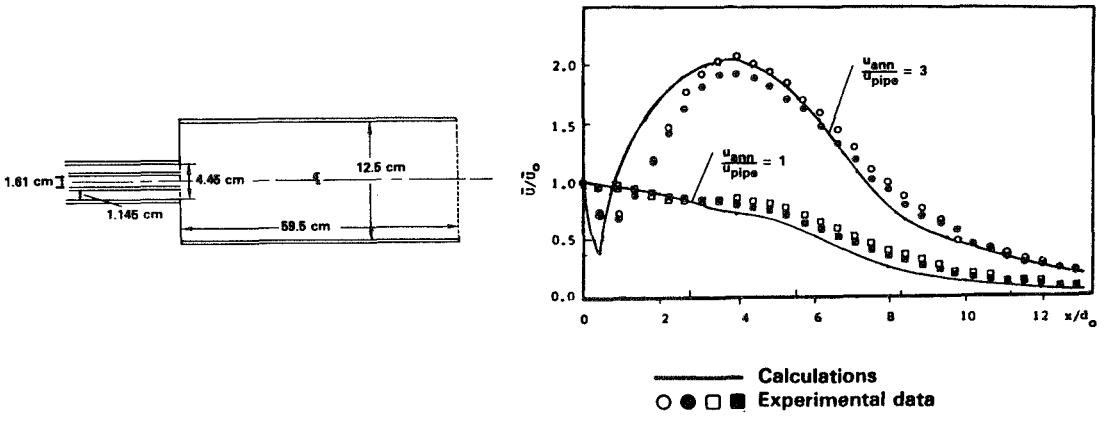

Figure 2

MORE COMPLEX FLOWS NOT CALCULATED AS WELL

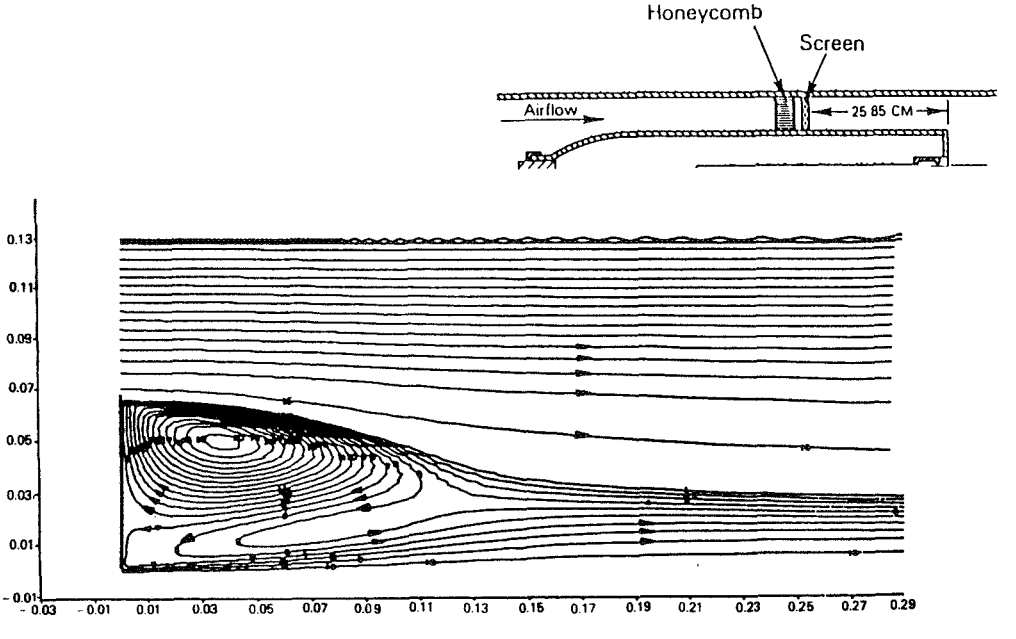

Reacting flow: 2 kg/sec. air, 16 kg/hr. propane

Figure 3

Table 1

USE OF CONSTANT TURBULENT SCHMIDT NUMBER APPEARS INAPPROPRIATE

Flow type	Characteristics	Schmidt No.
Boundary layers	Predominantly unidirectional	0.9
Round free jets	2-D, external entrainment	0.7
Simple recirculation zones	Simple stagnation points	0.5
Confined round jets	2-D, self-entrainment	0.7
Complex recirculation zones	2 or 3-D, multiple stagnation points, multiple recirculations	0.2

AEROTHERMAL MODELING PROGRAM

PHASE I

GENERAL ELECTRIC COMPANY

M.J. Kenworthy

The objective of this Phase I Aerothermal Modeling program was to identify deficiencies in the aerothermal models that are currently used or planned for use at General Electric in the design of gas turbine engine combustors. This effort was accomplished by assessing the predictions of the existing models with "benchmark" quaility test data. This effort, together with other similar efforts sponsored by NASA, was intended to help assess the current state of the art, and to define Phase II efforts needed to evolve improved and more advanced aerothermal analysis methods, increasing the ability to design improved high performance, durable combustors for advanced aircraft gas turbine engines.

This Phase I effort focused on the ability of the existing models to predict or analyze those features associated with durability. These primarily are: 1) the combustor liner metal temperature distribution, and 2) the combustor exit gas temperature patterns, which in turn affects the life of the downstream turbine components. Other features of interest to the combustor designer such as blowout limits and emissions do not directly affect design for durability.

Figure 1 shows schematically General Electric's calculation modules within the overall aerothermal model. Except for the internal flow module, the modules are well developed and have been in use for many years. The internal flow module is planned for use in the design process at General Electric after it has been developed and/or demonstrated to have useful accuracy. Thus, the assessment of the existing internal flow module constituted a major portion of the efforts.

The internal flow module, INTFLOW, contains two basic computing codes: 1) the code assembled by the Garrett Turbine Company under the Army sponsored Combustor Design Validation Program efforts, Reference 1, and the very similar code assembled by the Northern Research and Engineering Company, Reference 2. To help evaluate accurately the physical submodules and the numerical techniques within INTFLOW or under consideration for eventual incorporation in INTFLOW, the two-dimensional (planar or axisymmetric) research code, GETREF (General Electric Turbulent Reacting Flow) developed at General Electric was also utilized in the assessments.

Four axisymmetric benchmark experiments were chosen to assess the capabilities of available two-dimensional analysis methods. GETREC was used in conducting these assessments. This first experiment which was performed

at General Electric, involved detailed studies of an axisymmetric fuel jet burning in a coflowing air (Reference 3). The primary reasons for its selection are: 1) the removal of "numerical diffusion" errors since the governing equations become parabolic, and 2) the high quality LDV and spontaneous Raman scattering data available. An unambiguous evaluation of the turbulence chemistry interaction model was made which confirmed the model approach. In addition to this jet experiment, three other axisymmetric recirculating flow experiments were chosen: an isothermal annular dilution jet experiment (Reference 4), an isothermal double swirled pipe flow (Reference 5), and a bluff-body stabilized non-premixed flame (Reference 6). These provided checks of the model under progressively more complex circumstances. The results demonstrated the value of an algebraic stress model for modifying the K-ε turbulence model in the presence of swirl, and showed that the recirculation zone with heat release could be closely predicted.

For assessments of three-dimensional analysis capabilities, the aerodynamics of simple round dilution jet flows in a crossflow were studied. Data from Reference 7 were chosen for this examination. To provide data from more complex flowfields, a series of experiments were devised and conducted as part of this aerothermal modeling program which involved progressively more complex flows beginning with a row of jets in a crossflow followed by: opposing jets, alternate jets of different sizes, and then a second row of dilution jets with the two row pattern simulating the dilution pattern of one General Electric combustor. This was followed with experiments including swirl cups in the dome and heat release.

Assessments with INTFLOW began with variations of grid density and turbulence input parameters to examine agreement with the dilution jet in crossflow. Figure 2 shows the most detailed of the grids examined. Figure 3 compares measurements of jet penetration and temperature mixing with calculations achieved with the two basic codes within INTFLOW using identical input parameters. It is significant that this excellent agreement was achieved even though the two codes calculated different turbulence intensity levels throughout the flowfield. Also, difficulties were encountered in predicting all jet momentum ratios well with the same turbulence input parameters.

Figure 4 shows measurements from a F101 combustor sector compared with calculations. The overall pattern is reasonably predicted showing hottest regions concentrated between fuel nozzles. This calculation, utilized as input, measured flowfield conditions just downstream of the dome swirl cup.

While plausible looking results can be achieved with the INTFLOW module and agreement can be achieved after some educated selection of the inputs, predictions sufficiently accurate for aiding in design or development for enhancing durability have not yet been achieved within the limits of available (or even reasonable) computer storage. Improved numerics, reduced computation time, and better input information/techniques for the swirl cup fuel injector region are needed in addition to the improved physical modeling features demonstrated during this program.

References

1. Mongia, H.C., et.al., "Combustor Design Criteria Validation," USATL-TR-78--55A, 55B, 55C, February 1979.

2. "The Design and Development of Gas Turbine Combustors, Phase II Basic Computing System," Report No. 1420-3, Northern Research and Engineering Corporation.

3. Lapp, M., Drake, M.C., Penney, C.M., Pitz, R.W., and Correa, S.M., "Turbulent $CO/H_2/N_2$ Jet Diffusion Flame in Coflowing Air," DOE Contract Report DE-AC04-78 ET 13146, 1983.

4. Green, A., and Whitelaw, J.H., Measurements and Calculations of the Isothermal Flow in Axisymmetric Models of Combustor Geometries, J. Mech. Eng. Sci., Vol. 22, p. 119, 1980.

5. Vu, B.T., and Gouldin, F., Flow Measurements in a Model Swirl Combustor, AIAA Paper No. 80,007, 1980.

6. Lightman, A.J., Richmond, R.D., Magill, P.D., Krishnamurthy, L., Roquemore, W.M., Bradley, R.P., Stutrud, J.S., and Reeves, C.M., Velocity Measurements in a Bluff-Body Diffusion Flame, AIAA Fifteenth Thermophysics Conference, Snowmass, Colorado.

7. Walker, R.E., and Kors, D.L., "Multiple Jet Study Final Report," NASA CR 121217, June 1973.

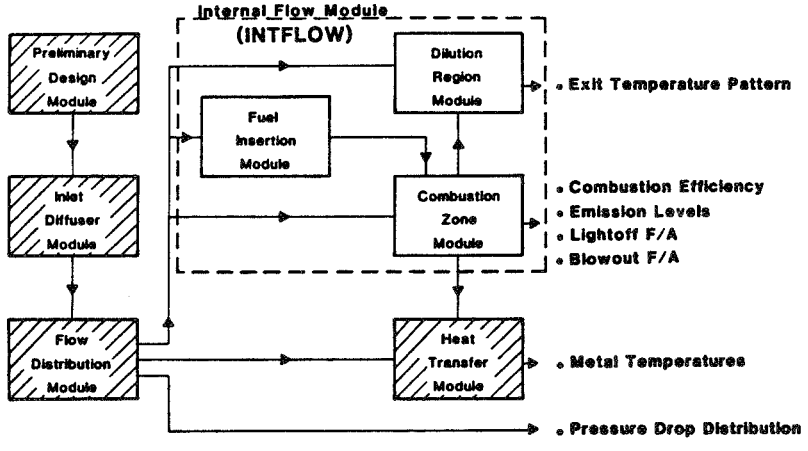
Internal Flow Module
(INTFLOW)
Preliminary Design Module
Inlet Diffuser Module
Flow Distribution Module
Fuel Insertion Module
Dilution Region Module
Combustion Zone Module
Heat Transfer Module
• Exit Temperature Pattern
• Combustion Efficiency
• Emission Levels
• Lightoff F/A
• Blowout F/A
• Metal Temperatures
• Pressure Drop Distribution
• Shaded boxes are modules in current use in combustor design and development work.
• Open boxes are modules in General Electric's aerothermal model planned for use in the future in design and development work after adequate accuracy is demonstrated or developed.

Figure 1. General Electric's Aerothermal Model.

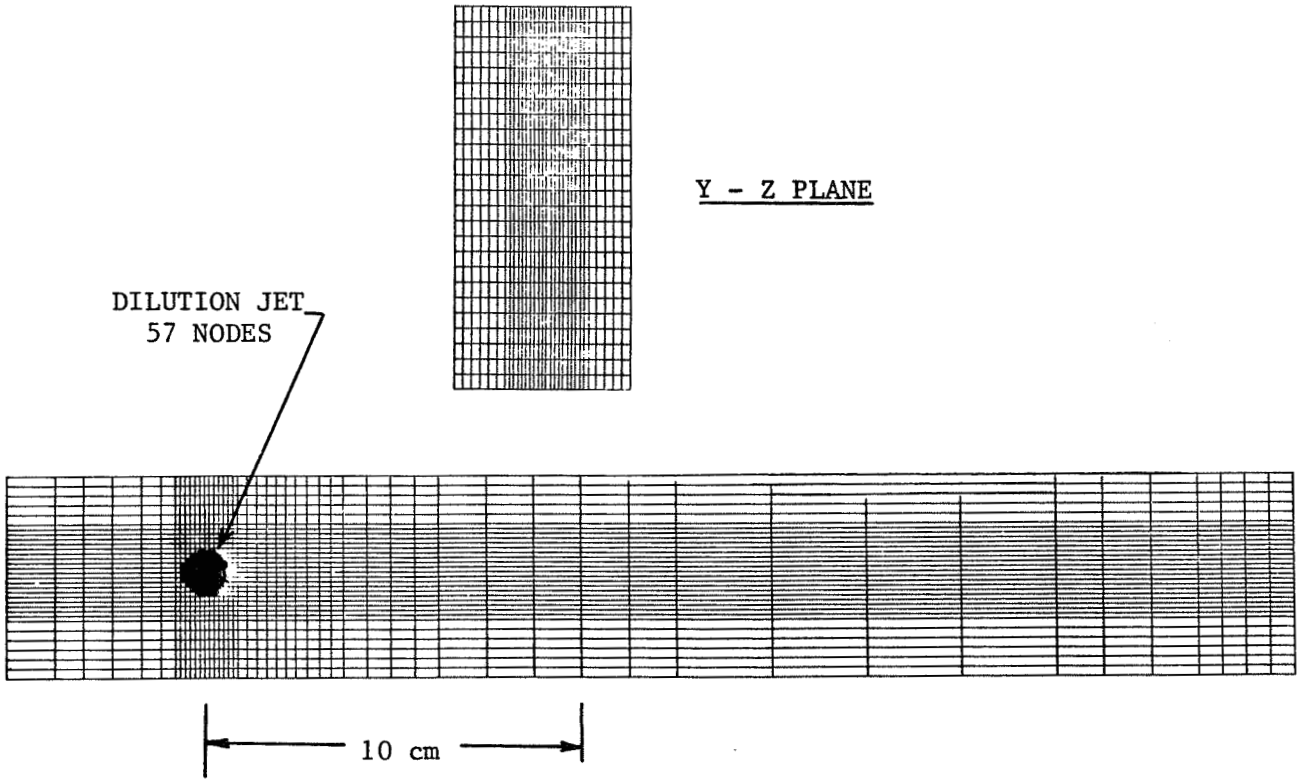

Figure 2. High Grid Density, 41,600 Nodes, for Dilution Jet Study.

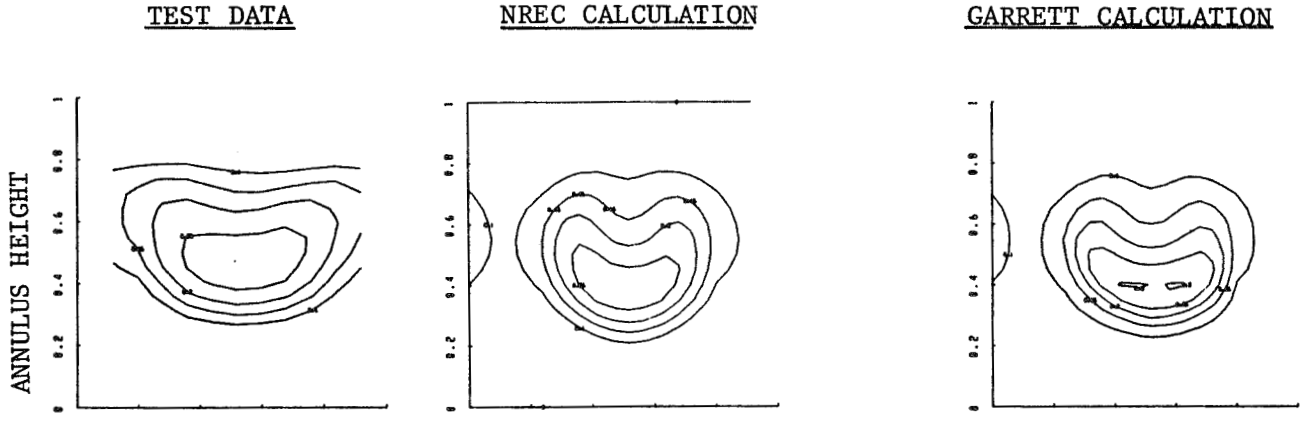

Figure 3. Comparison of Jet Penetration Temperature Contours of Two Basic Codes within INTFLOW with Measurements at 4 X/D Down-Stream of Jet.

INTFLOW CALCULATION

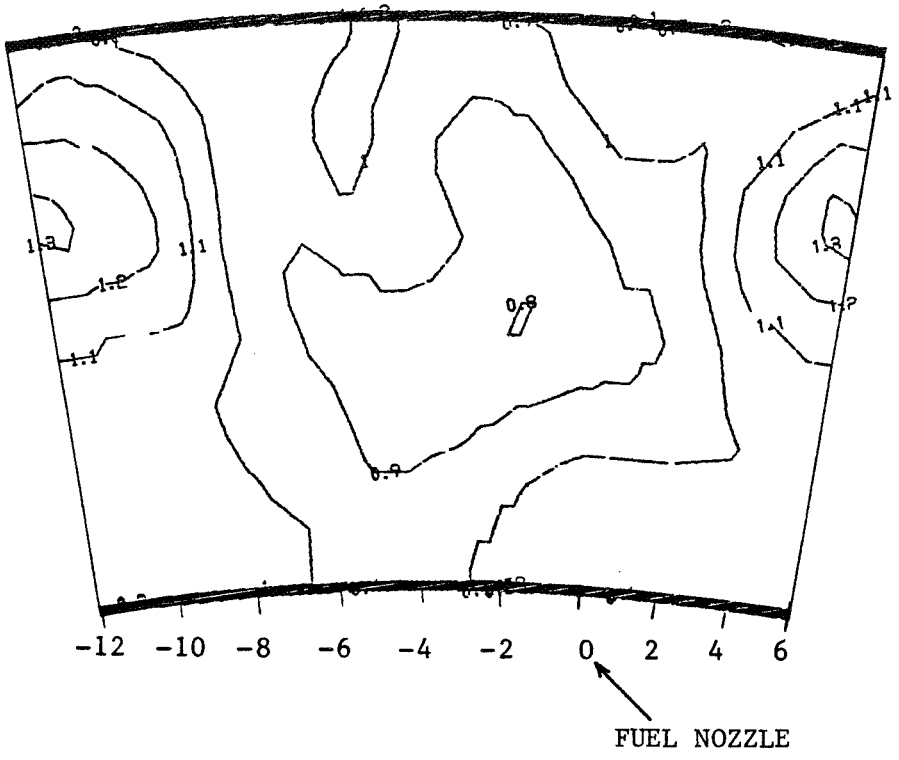

SECTOR MEASUREMENTS

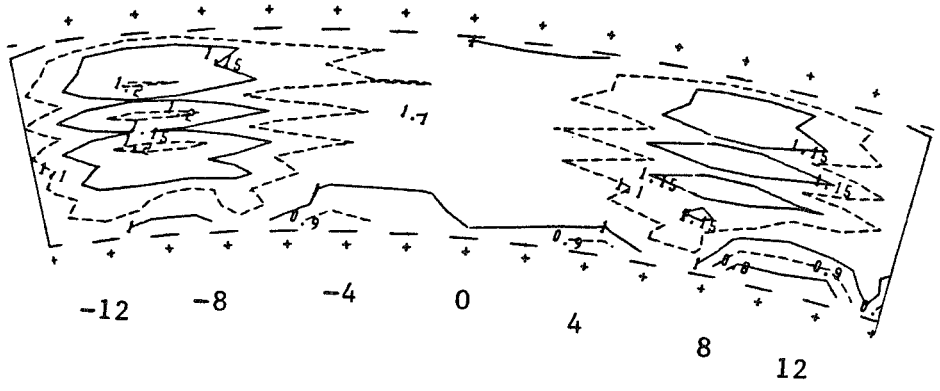

Figure 4. Comparison of F101 Sector Measurements with INTFLOW Using Cylindrical Wall Assumption.

Page intentionally left blank

DILUTION JET MIXING PROGRAM - PHASE II

R. Srinivasan, E. Coleman, K. Johnson, and H. Mongia
Garrett Turbine Engine Company

This program is a continuation of the ongoing program under NASA Contract NAS3-22110. In Phase I of this program, the dilution jet mixing study was limited to single-sided jet injections (ref. 1). The objectives of Phase II of the dilution jet mixing program are:

- Extend the data base on mixing a single-sided row of jets with a confined cross flow
- Collect data base on mixing a two-sided row of jets with a confined cross flow
- Develop empirical jet mixing correlations

The parameters investigated during Phase II of the program are:

- Circular versus square orifices, two-dimensional slot
- J, H/D, S/D (where D = geometric orifice diameter, H = local duct height at the survey plane, J = jet versus mainstream momentum ratio, S = orifice spacing)
- In-line and staggered orifice configurations
- Nonuniform cross-stream temperature and velocity profiles
- Cross-stream flow area convergence

Figure 1 shows a flow schematic of the dilution jet test rig. The mainstream temperature and velocity profiles can be tailored by adjusting the flow to the profile generator upstream of the test section. Dilution air enters the test section through sharp-edged orifices in the test section walls from the top, bottom, or both.

Figure 2 provides more detail on the test sections and orifice configurations used in this study. The height of the test section at the injection plane, Ho, was 10.16 cm for all tests. Orifice plate open areas were varied from 2.5 to 20 percent of the mainstream cross section at the injection location. The primary independent geometric variables are the orifice size and the spacing between adjacent orifices. These are conveniently expressed in dimensionless form as the ratio of the duct height to orifice diameter, Ho/D, and the ratio of the orifice spacing to duct height, S/Ho. The product of these ratios is the orifice spacing-to-diameter ratio, S/D.

Tests were performed with two-sided injection in convergent ducts having a convergence rate of 0.5 cm/cm. The tests were made in symmetric

as well as asymmetric convergent ducts with isothermal mainstream conditions.

The dilution jet mixing characteristics were determined by measuring temperature and pressure distributions with a vertical rake probe, positioned at different axial and lateral stations. This probe had 20 thermocouple elements, with a 20-element total pressure rake, and a 20-element static pressure rake located nominally 5 mm (0.05 Ho) on each side of the thermocouple rake. The center-to-center spacing between sensors on each rake was also 0.05 Ho.

The vertical rake probe was traversed over a matrix of 44 to 60 Z-X plane survey locations (where X is parallel to the duct axis; Y is parallel to the orifice centerline, radial direction; and Z is normal to the duct axis, transverse direction). The flow-field mapping in the Z-direction was done over a distance equal to one or one and a half times the hole spacing, S, at intervals of S/10. For most tests, the X-Y plane containing the orifice centerline (centerplane) was at the center of the span surveyed; i.e., data surveys were from midplane to midplane.

Measurements in the X-direction were made at up to 5 planes with $0.25 \leqslant X/Ho \leqslant 2$. Note that because the designers' objective was to identify dilution zone configurations to provide a desired mixing pattern within a given combustor length, the downstream stations of interest were defined in intervals of the duct height at the injection location, Ho, rather than at the orifice diameter, D.

The correlations developed by Holdeman and Walker (ref. 2) were found to be accurate for single-sided injections in Phase I of this program. However, these correlations were not adequate for two-sided injections. Improved accuracy was obtained with the new correlations de veloped in this program. Predictions for profiled mainstream test cases were obtained by superposition of mainstream temperature profiles and the NASA/Garrett correlations. These predictions were found to be good to first-order accuracy.

The NASA/Garrett correlations also include the effects of flow area convergence. However, further effort is needed to improve the accuracy of the correlations.

REFERENCES

1. Srinivasan, R.; Berenfeld, A.; and Mongia, H.C.: Dilution Jet Mixing Phase I Report. Garrett Turbine Engine Company Report 21-4302 (NASA CR-168031), November 1982.

2. Holdeman, J.D.; and Walker, R.E.: Mixing of a Row of Jets with a Confined Crossflow. AIAA Journal, Vol. 15, No. 2, February 1977.

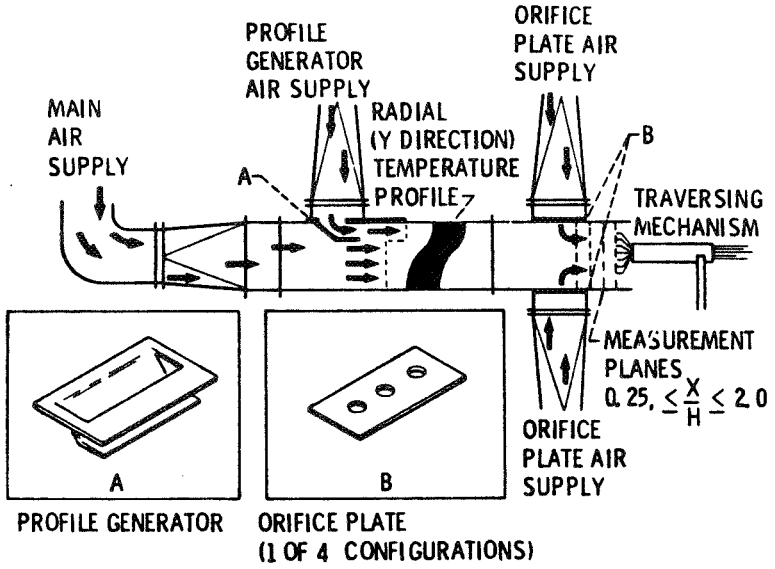

Figure 1. - Dilution Jet Mixing Flow Schematic.

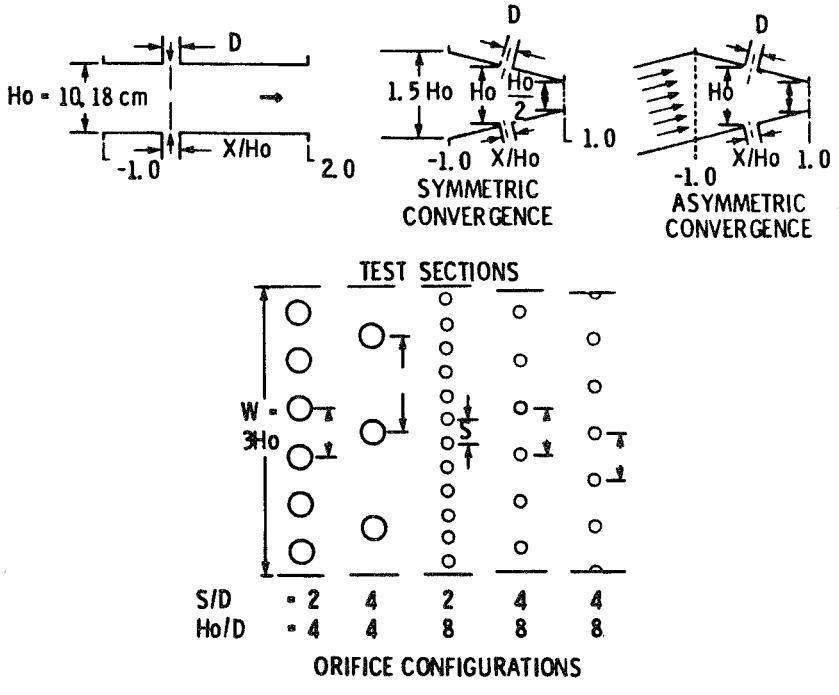

Figure 2. - Test Sections and Orifice Configurations.

Page intentionally left blank

MASS AND MOMENTUM TURBULENT TRANSPORT EXPERIMENTS

B. V. Johnson
United Technologies Research Center

An experimental study of mixing downstream of nonswirling (Ref. 1) and swirling coaxial jets discharging into an expanded duct is being conducted to obtain data for the evaluation and improvement of turbulent transport models currently used in a variety of computational procedures throughout the propulsion community for combustor flow modeling. The study uses laser velocimeter (LV) and laser induced fluorescence (LIF) techniques to measure velocities and concentration, hot film techniques to qualitatively determine the time dependent characteristics of the flow and the scale of the turbulent structure.

The combined LV and LIF measurement techniques are used to acquire simultaneous measurements of velocity and concentration of a trace material inserted into one fluid (Fig. 1). A two-color LV system was used to simultaneously measure two velocity components. Velocities in three directions, concentrations, momentum turbulent transport in three directions are obtained from a series of six measurements. The simultaneous data pairs are used to determine the mean r.m.s. deviation from the mean, the skewness and the kurtosis for the probability density functions of each data set (Fig. 2). These results can be compared with results from numerical codes or with a variety of existing or proposed turbulent transport models (Fig. 3).

Flow visualization studies and detailed laser velocimeter/laser induced fluorescence measurements have been conducted for nonswirling and swirling coaxial jets discharging into expanded ducts (Fig. 4). Typical results for the nonswirling flow condition are shown in Figs. 5 through 7. Turbulent transport results showed the existence of countergradient and mass trasnfer and nonisotropic turbulent transport diffusivity coefficients.

The current effort is directed toward determining length scale and dissipation rates used in the turbulent transport models. Hot film measurements of the axial velocity component will be used to obtain a velocity spectrum and an autocorrelation upstream of the inlet plane, near the inlet plane and at selected locations in several shear layers. Dissipation rates and integral length scales will be determined from these measurements using conventional approximations. These results can be compared with those calculated by the numerical codes. LV and LIF measurements will also be made to determine the effect of changing the inlet duct geometry on the near inlet turublent transport characteristics.

FIG. 1 SKETCH OF OPTICS ARRANGEMENT

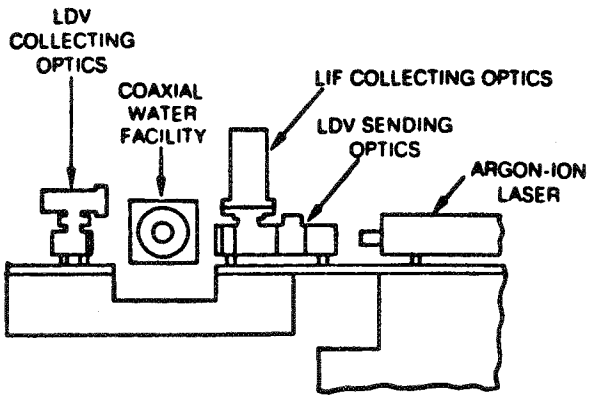

FIG. 2 **TURBULENT TRANSPORT MEASUREMENTS**

Data pairs	Prob. density functions	Properties determined
u, v	u, v, w	Mean value or transport rate
u, w	c	RMS deviation from mean
v, w	uv, uw, vw	Skewness of p.d.f.
u, c	uc, vc, wc	Kurtosis of p.d.f.
v, c		Correlation coefficients
w, c		

FIG. 4 SHEAR REGIONS OF COAXIAL JETS

a) NONSWIRLING FLOW

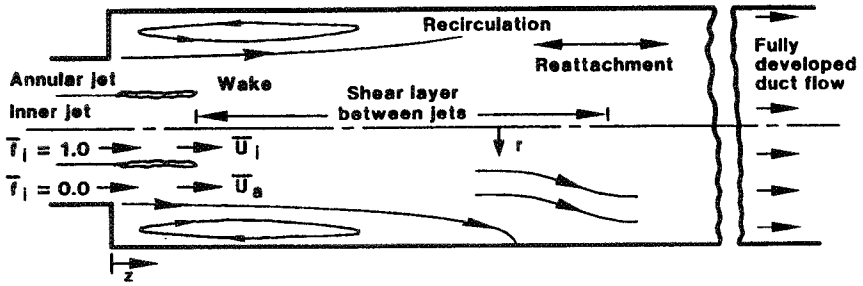

b) SWIRLING FLOW

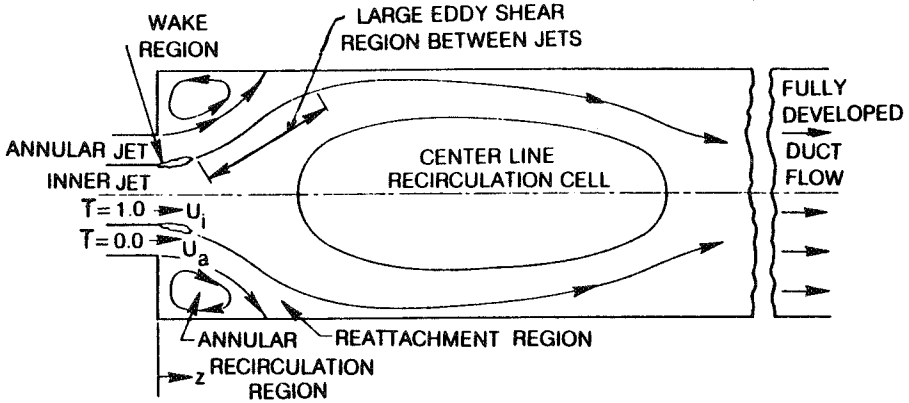

FIG. 3

TURBULENT TRANSPORT MODELS

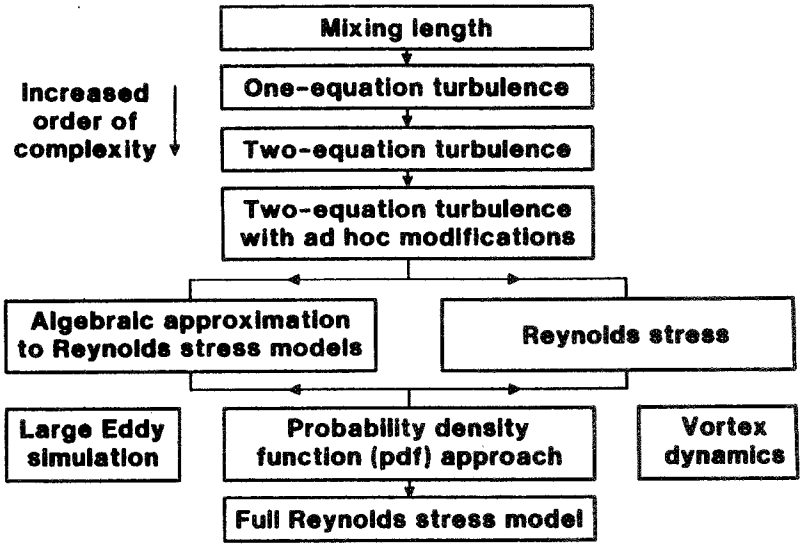

FIC. 5 MOMENTS OF TURBULENT MOMENTUM TRANSPORT PROFILES

θ = 0 DEG -○, 180 -●

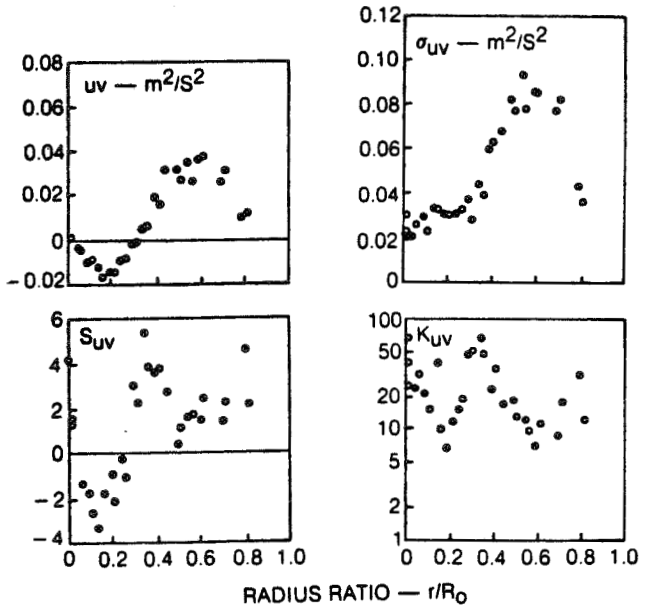

FIG. 6 MOMENTUM TURBULENT TRANSPORT ISOGRAM ($\overline{uv}$)

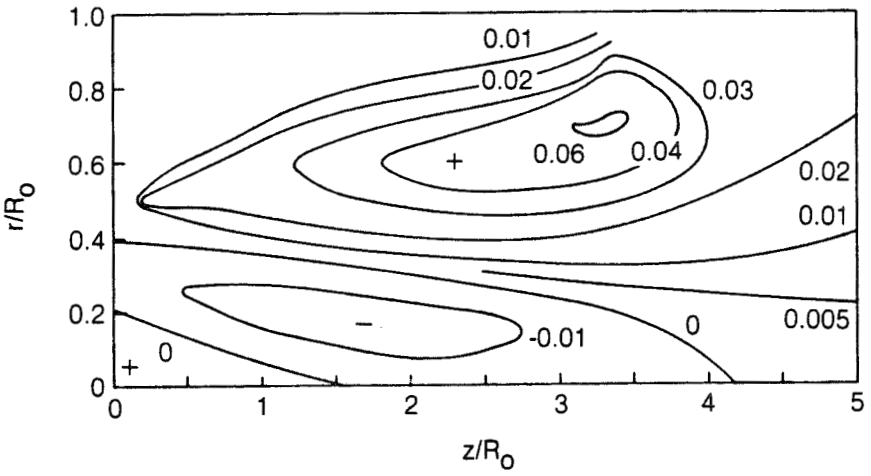

FIG. 7 CORRELATION COEFFICIENT FOR MOMENTUM TURBULENT TRANSPORT (R_{uv})

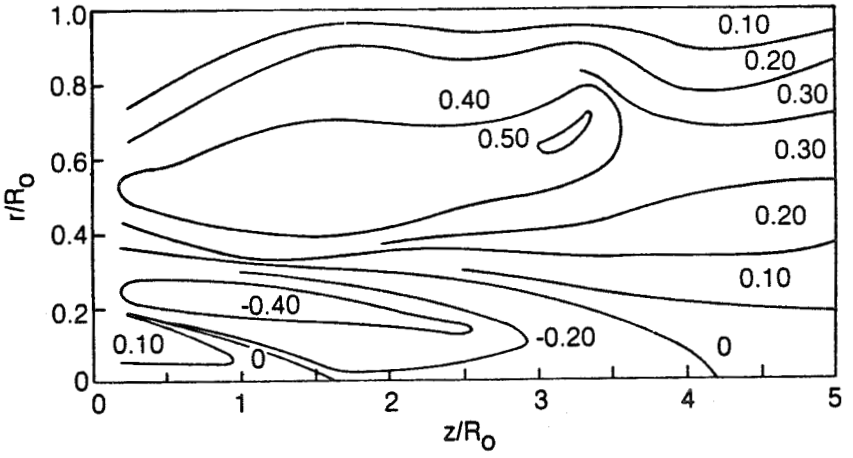

Page intentionally left blank

D18

HOST STRUCTURAL ANALYSIS PROGRAM

OVERVIEW

by

R. H. Johns, Subproject Manager

Hot section components of aircraft gas turbine engines are subjected to severe thermal-structural loading conditions, especially during the start-up and take-off portions of the engine cycle. The most severe and damaging stresses and strains are those induced by the steep thermal gradients induced during the start-up transient. These transient stresses and strains are also the most difficult to predict, in part because the temperature gradients and distributions are not well known or readily predictable, and also because the cyclic elastic-viscoplastic behavior of the materials at these extremes of temperature and strain are not well known or readily predictable.

A broad spectrum of structures-related technology programs is underway to address these deficiencies. The problems are being addressed at the basic as well as the applied level, including participation by industry and universities as well as in-house at NASA Lewis. In addition to the HOST structural analysis program, some related program elements are being supported through our Base R&T program.

One element of the structures program is developing improved time-varying thermal-mechanical load models for the entire engine mission cycle from start-up to shutdown. The thermal model refinements will be consistent with those required by the structural code including considerations of mesh-point density, strain concentrations, and thermal gradients. Models will be developed for the burner liner, turbine vane and turbine blade. One aspect of this part of the program is a thermal data transfer module recently developed which automates the transfer of temperatures from available heat transfer codes or experimental data sets to the structural analysis code. Another part of the program is an automated component-specific geometric modeling capability which will produce 3-D finite element models of the components. Self-adaptive solution strategies will be developed and included to facilitate selection of appropriate elements, mesh sizes, etc.

Another major part of the program is the development of new and improved nonlinear 3-D finite elements and associated structural analysis programs, including the development of temporal elements with time-dependent properties to account for creep effects in the materials and components. Two contracts were recently signed to accomplish these developments. Improved constitutive modeling methods to facilitate improved prediction of cyclic thermomechanical viscoplastic material behavior are also under development. Experimental facilities to aid in developing and verifying theories and models are currently being established in-house at Lewis.

Further explanation and details about the various structures program elements mentioned above are given in the following write-ups.

STRUCTURAL ANALYSIS...IT'S ROLE IN HOST

GOAL:

DEVELOP AND VALIDATE INTEGRATED TIME-VARYING THERMOMECHANICAL LOAD MODELS, COMPONENT-SPECIFIC AUTOMATED GEOMETRIC MODELING AND SOLUTION STRATEGY CAPABILITIES, AND ADVANCED INELASTIC ANALYSIS METHODS INCLUDING PLASTICITY AND CREEP EFFECTS FOR NONLINEAR ANISOTROPIC FINITE ELEMENT STRUCTURAL ANALYSIS AND DESIGN COMPUTER CODES FOR TURBINE ENGINE HOT SECTION COMPONENTS

PROGRAM INTEGRATION

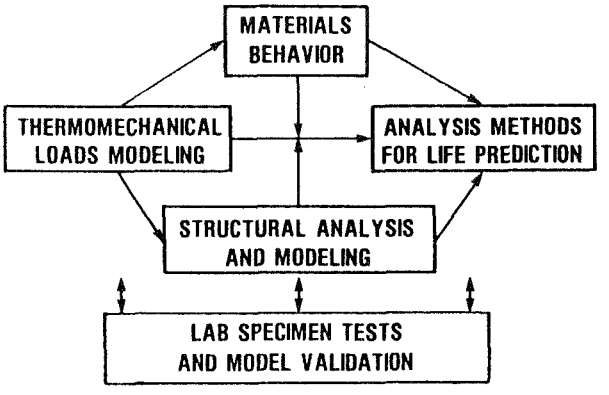
MATERIALS BEHAVIOR
THERMOMECHANICAL LOADS MODELING
ANALYSIS METHODS FOR LIFE PREDICTION
STRUCTURAL ANALYSIS AND MODELING
LAB SPECIMEN TESTS AND MODEL VALIDATION

PROGRAM ELEMENTS:

- THERMAL/STRUCTURAL DATA TRANSFER MODULE
- THERMAL/MECHANICAL LOAD/MISSION AND COMPONENT-SPECIFIC STRUCTURAL MODELS
- 3-D INELASTIC ANALYSIS METHODS
- BURNER LINER CYCLIC RIG (STRUCTURAL ASPECTS)
- HIGH TEMPERATURE STRUCTURES LABORATORY

CS-83-0643

HOST

STRUCTURAL ANALYSIS PROGRAM

OBJECTIVE:

TO DEVELOP AND VALIDATE INTEGRATED TIME-VARYING THERMAL/MECHANICAL LOAD MODELS, COMPONENT-SPECIFIC AUTOMATED GEOMETRIC MODELING AND SOLUTION STRATEGY CAPABILITIES, AND ADVANCED INELASTIC ANALYSIS METHODS AND CONSTITUTIVE MODELS, INCLUDING PLASTICITY AND CREEP EFFECTS, FOR NONLINEAR, ANISOTROPIC, FINITE ELEMENT STRUCTURAL ANALYSIS AND DESIGN COMPUTER CODES.

STRUCTURAL ANALYSIS

PROGRAM ELEMENT	FISCAL YEAR 81	82	83	84	85	86	87	EXPECTED RESULT
THERMAL DATA TRANSFER		(C)						COMPUTER MODULE LINKING THERMAL AND STRUCTURAL ANALYSES
COMPONENT SPECIFIC MODELING			(C)			▼		COMPONENT-RELATED, TIME VARYING, THERMAL-MECHANICAL LOAD HISTORY & GEOMETRIC MODELS
3-D INELASTIC ANALYSIS			(C)		▼			ADVANCED 3-D INELASTIC STRUCTURAL/ STRESS ANALYSIS METHODS AND SOLUTION STRATEGIES
LINER CYCLIC RIG		(IH)						BURNER STRUCTURAL/LIFE EXPERIMENTS
HIGH-TEMPERATURE STRUCTURES LAB			(IH)					INTEGRATED EXPERIMENTAL /ANALYSIS RESEARCH
MATERIAL BEHAVIOR TECHNOLOGY		(IH)						CONSTITUTIVE THEORY & MODELING METHODS

HOT SECTION COMPONENTS REQUIRING 3-D INELASTIC ANALYSIS

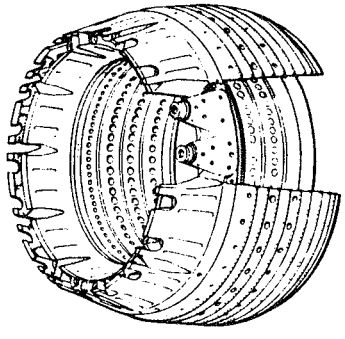

COMBUSTOR LINER

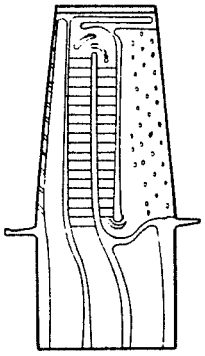

TURBINE BLADE

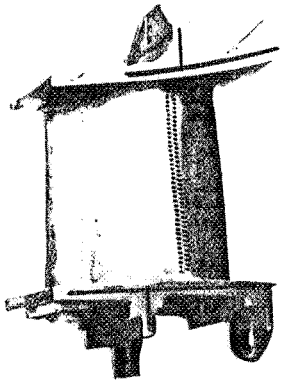

TURBINE VANE

CS-83-0641

BURNER LINER THERMAL LOAD TRANSFER MODULE (HOST)

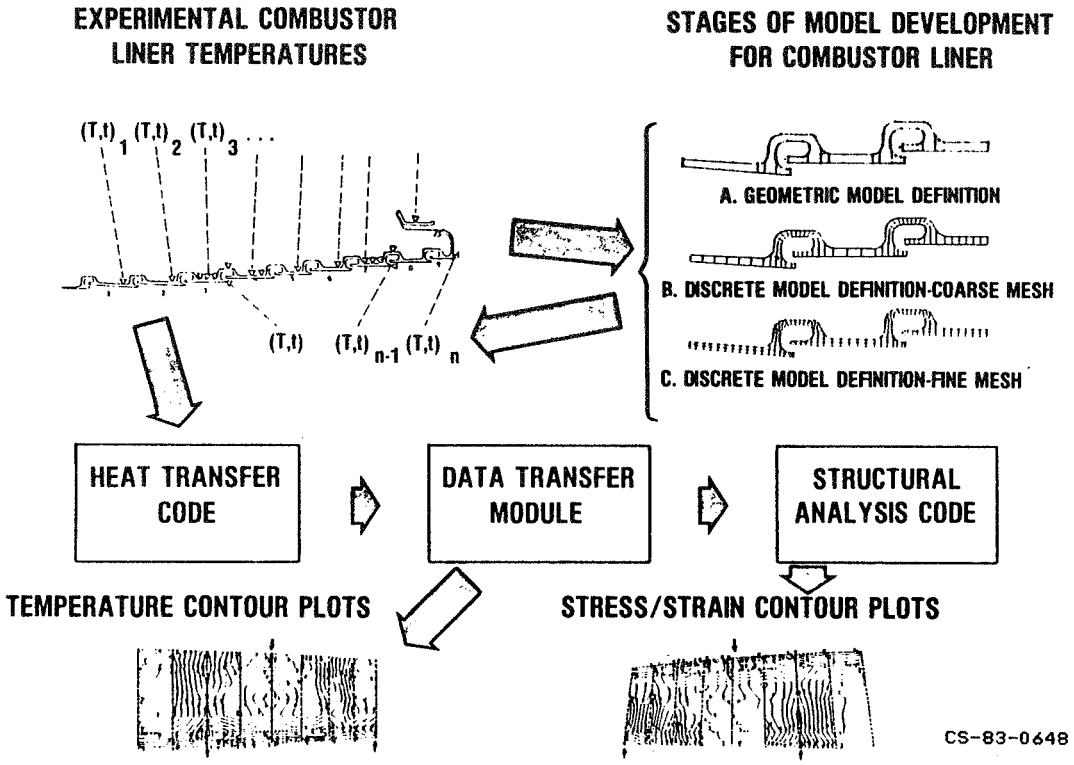

COMPONENT—SPECIFIC MODELING (HOST)

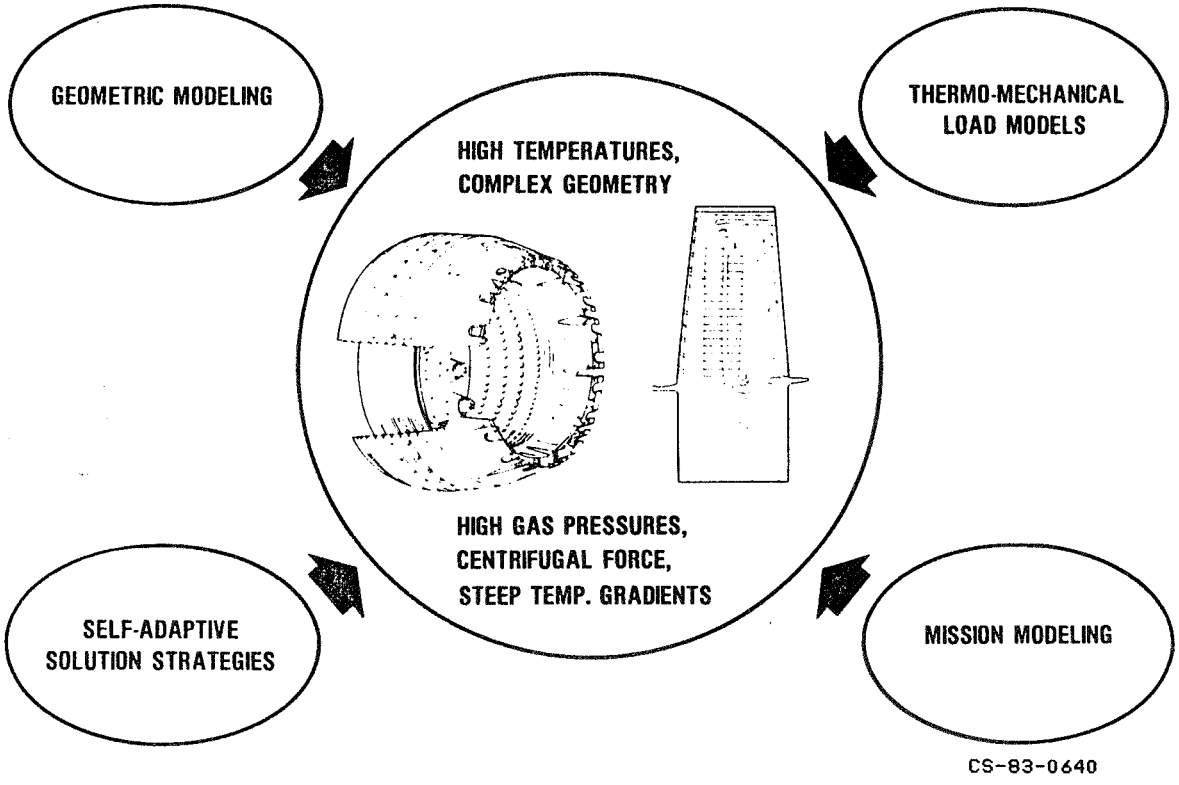

3-D INELASTIC ANALYSIS (HOST)

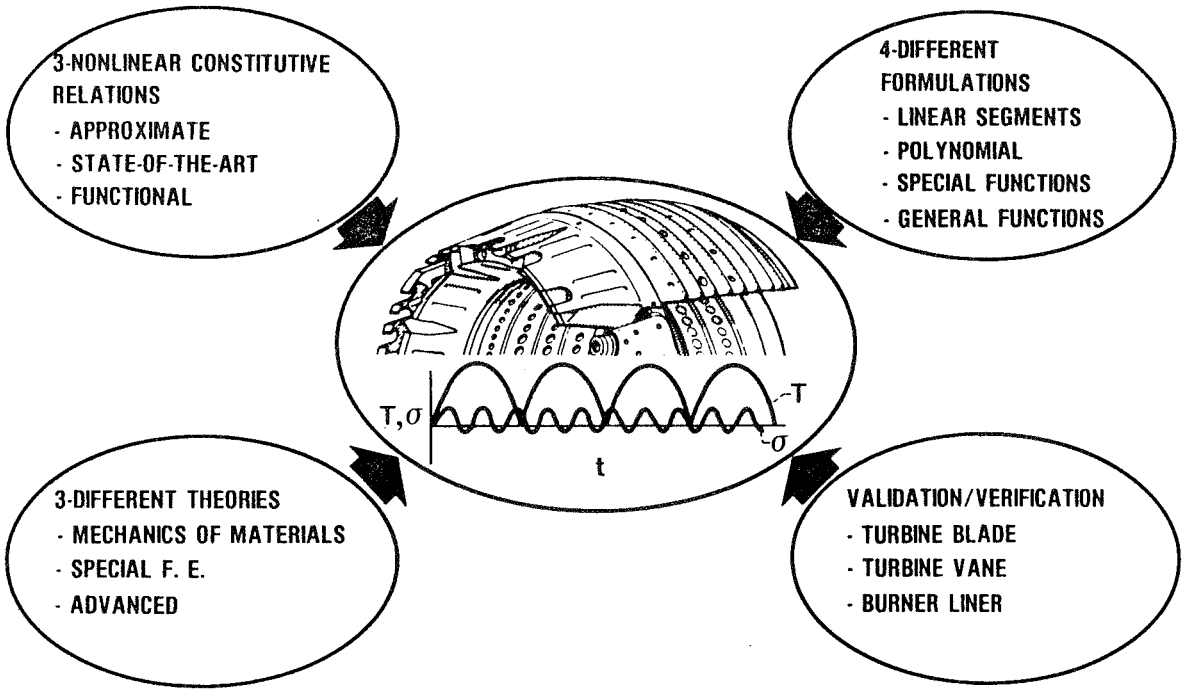

CS-83-0639

AUTOMATED HIGH TEMPERATURE STRUCTURES RESEARCH LABORATORY

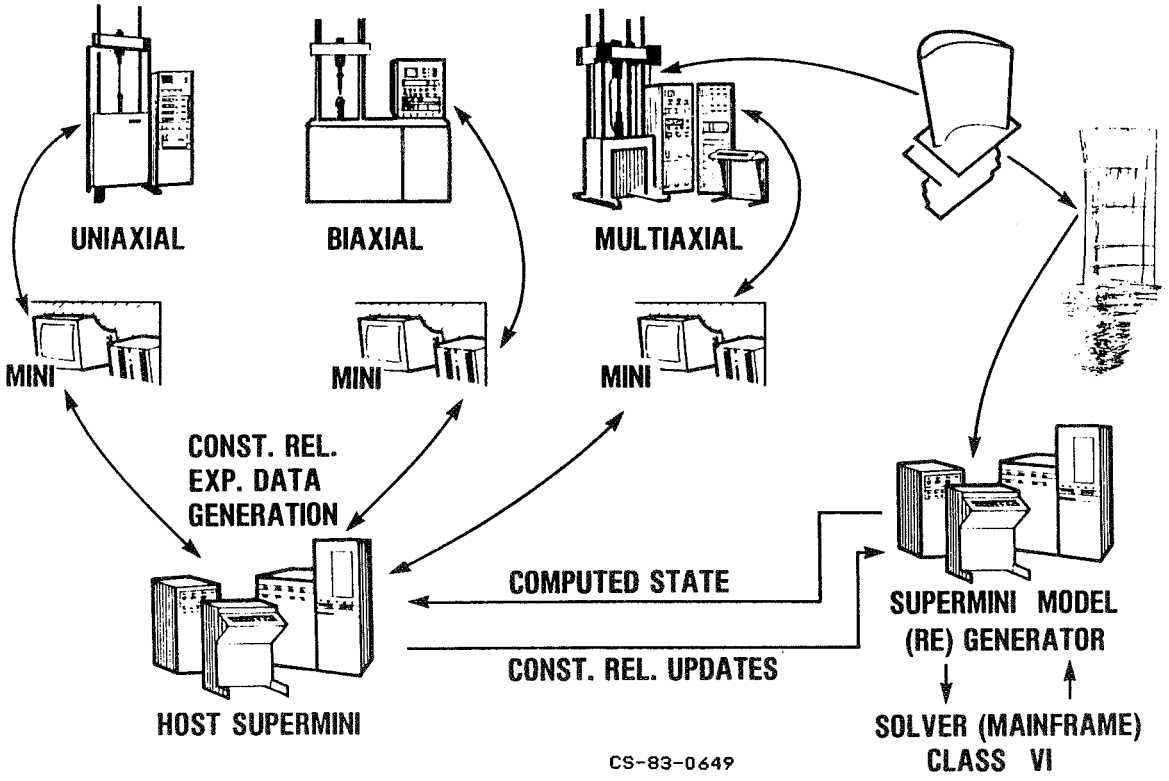

CS-83-0649

TURBINE ENGINE HOT SECTION TECHNOLOGY
STRUCTURES ANALYSIS SESSION

AGENDA

OVERVIEW	R. H. JOHNS, LeRC
THERMAL/STRUCTURAL DATA MODULE	R. J. MAFFEO, G.E.
COMPONENT SPECIFIC MODELING	M. L. ROBERTS, G.E.
3-D INELASTIC ANALYSIS METHODS	E. S. TODD, P & W
3-D INELASTIC ANALYSIS METHODS	R. L. McKNIGHT, G.E.
LINER CYCLIC LIFE RIG	R. L. THOMPSON, LeRC
QUARTZ LAMP RIG	D. F. SCHULTZ, LeRC

D19

BURNER LINER THERMAL/STRUCTURAL LOAD MODELLING

R. J. Maffeo
General Electric Company
Aircraft Engine Business Group

The objective of this program is to develop a thermal data transfer computer program module for the Burner Liner Thermal-Structural Load Modelling Program. This will be accomplished by (1) reviewing existing methodologies for thermal data transfer and selecting three heat transfer codes for application in this program, (2) evaluating the selected codes to establish criteria for developing a computer program module to transfer thermal data from the heat transfer codes to selected stress analysis codes, (3) developing the automated thermal load transfer module, and (4) verifying and documenting the module.

In aircraft turbine engine hot section components, cyclic thermal stresses are the most important damage mechanism. Consequently, accurate and reliable prediction of thermal loads is essential to improving durability. To achieve this goal, a considerable effort over the past 20 years has been devoted to the acquisition of engine temperature test data, as well as the development of accurate, reliable, and efficient computer codes for the prediction of steady-state and transient temperatures and for the calculation of elastic and inelastic cyclic stresses and strains in hot section components. There is a need for continued development of these codes, because the availability of more accurate analysis techniques for complex configurations has enabled engine designers to use more sophisticated designs to achieve higher cycle efficiency and reduce weight.

It has become apparent in recent years that there is a serious problem of interfacing the output temperatures and temperature gradients from either the heat transfer codes or engine tests with the input to the stress analysis codes. With the growth in computer capacity and speed and the development of input preprocessors and output postprocessors, the analysis of components using hundreds and even thousands of nodes in the heat transfer and stress models has become economical and routine. This has exacerbated the problem of manual transfer of output temperatures from heat transfer nodes to stress analysis input to where the engineering effort required is comparable to that required for the remainder of the analysis. Furthermore, a considerable amount of approximation has been introduced in an effort to accelerate the process. This tends to introduce errors into the temperature data which negates the improved accuracy in the temperature distribution achieved through use of a finer mesh. There is, then, a strong need for an automatic thermal interface module.

The overall objectives of this thermal transfer module are that it handle independent mesh configurations, finite difference and finite element heat transfer codes, perform the transfer in an accurate and efficient fashion and that the total system be flexible for future applications.

Based on our study of existing thermal transfer modules, and our experience with our two-dimensional in-house transfer code, three levels of program development criteria were identified.

Work done under NASA contract NAS3-23272.

Level I contains the general criteria which must be satisfied for a usable product. These include:

- -Independent Heat Transfer and Stress Model Meshes
- -Accurate Transfer of Thermal Data
- -Computationally Efficient Transfer
- -User Friendly Program
- -Flexible System

Level II contains specific criteria which must be satisfied to meet requirements associated with gas turbine applications, such as:

- -Internal Coordinate Transformations
- -Automatic Exterior Surfacing Techniques
- -Geometrical and Temporal Windowing Capability

Level III has criteria which are desirable but not necessary. Total automation of these could be accomplished in future enhancements of the transfer code. Items that fall in this area include:

- -Automatic Scaling of Temperatures Based on Engine Power Setting
- -Altered Stress Geometry
- -Automatic Handling of Temperature Discontinuities

All of the Level I and Level II criteria have been developed and implemented into the thermal load transfer code. This code is being used at General Electric and has been used in conjunction with a three-dimensional model of a combustor liner for the verification phase of this contract. The existing transfer module can process heat transfer results directly from the MARC and SINDA programs and will output temperature information in the forms required for MARC and NASTRAN. The input and output routines in the module are very flexible and could easily be modified to except data from other heat transfer codes and format data to other stress analysis codes.

This thermal load transfer module has been shown to efficiently and accurately transfer thermal data from dissimilar heat transfer meshes to stress meshes. The fundamental part of the code, the 3D search, interpolation and surfacing routines, have much more potential. They form an outstanding foundation for automatic construction of embedded meshes, local element mesh refinement, and the transfer of other mechanical type loading.

Problem

- Large Heat Transfer/Stress Models
- Different Mesh Densities
- Finite Difference vs Finite Element Codes
- Thermal Transfer Time Consuming and Error Prone

Objectives

- Transfer Temperatures From a Heat Transfer Study to a Stress Analysis
  - Independent Meshes
  - Accurate/Efficient Transfer
  - Flexible

Objective

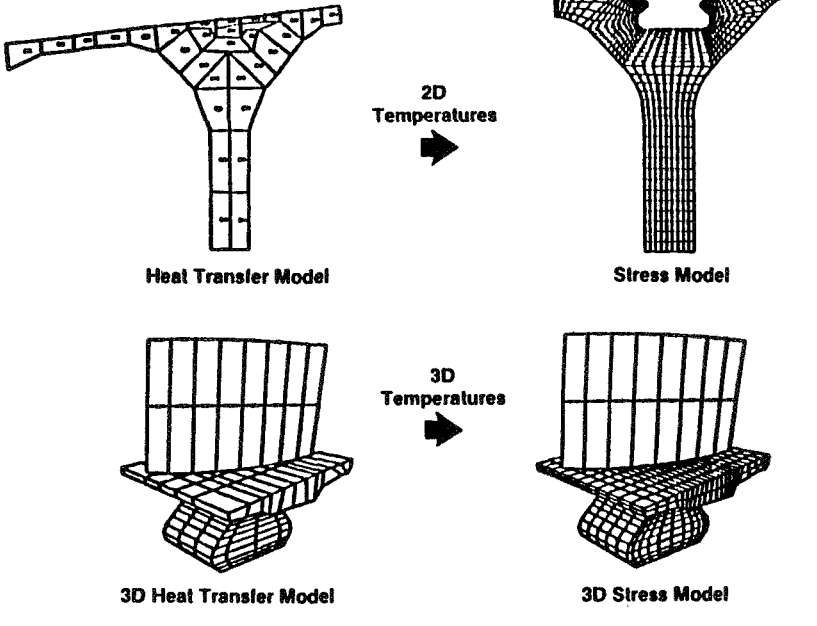

Thermal Transfer Module

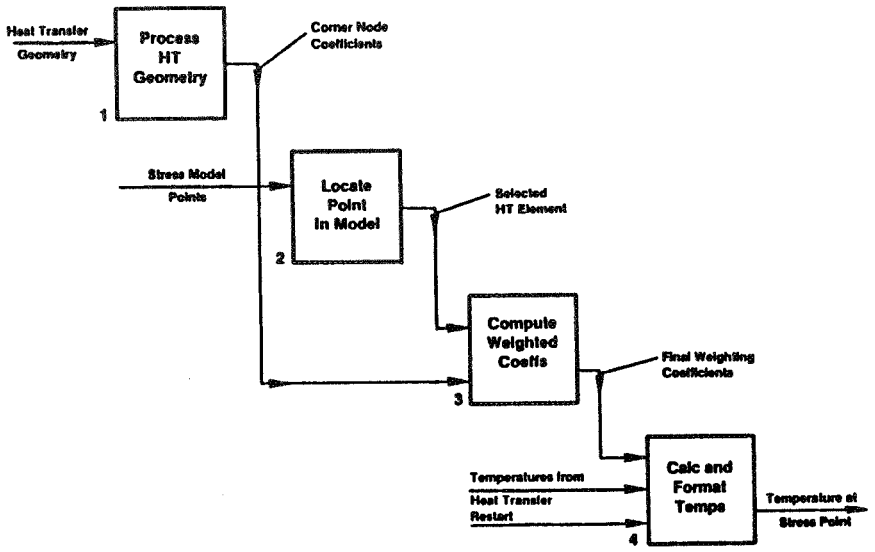

Overall System

Enhanced Program Features

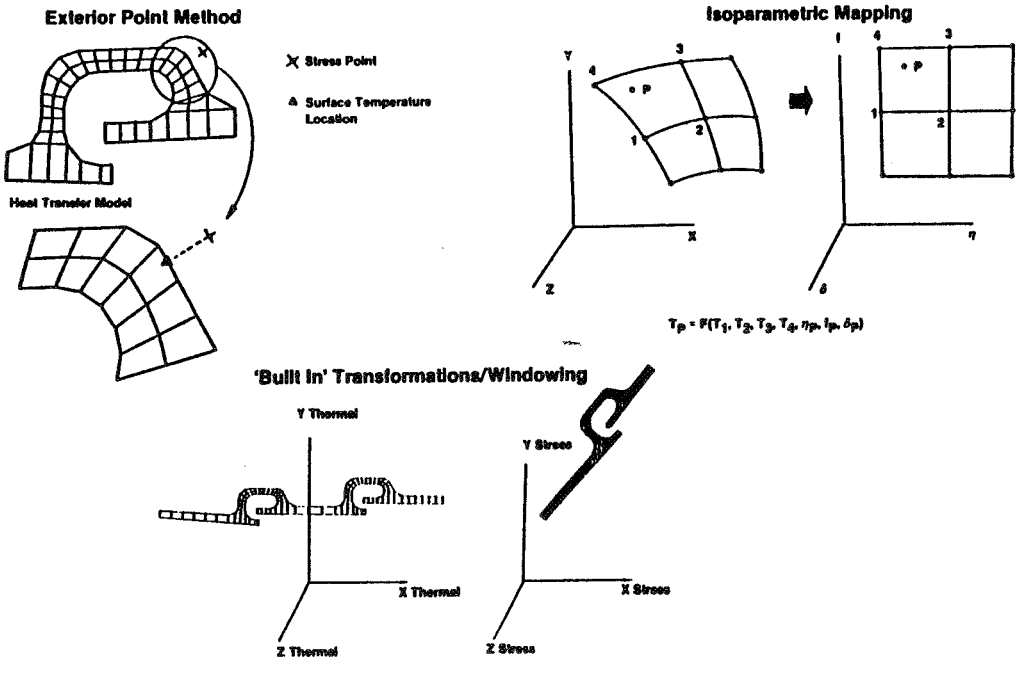

Verification Study

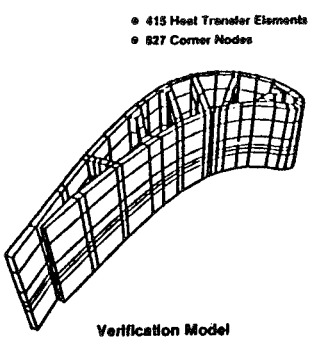

Verification Model

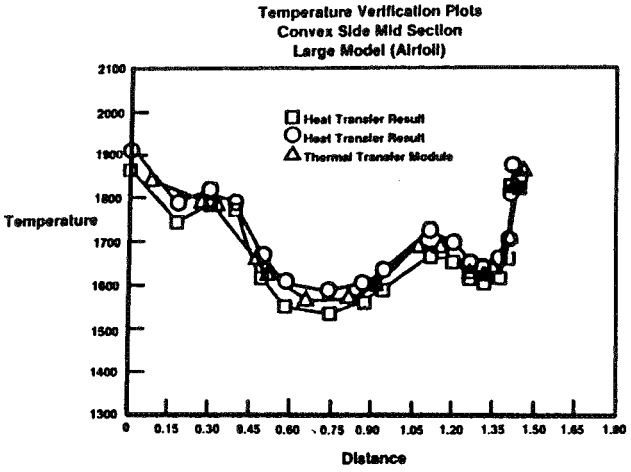

Future Applications

Automatic Boundary Condition Assignment

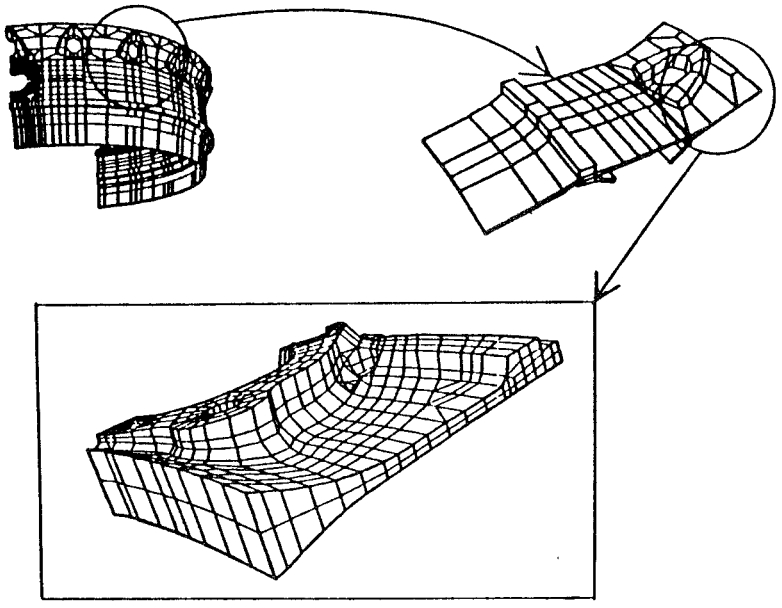

Page intentionally left blank

D20

COMPONENT-SPECIFIC MODELING*

M. L. Roberts
General Electric Company

Introduction

Modern jet engine design imposes extremely high loadings and temperatures on hot section components. Fuel costs dictate that minimum weight components be used wherever possible. In order to satisfy these two criteria, designers are turning toward improved materials and innovative designs. Along with these approaches, however, they must also have more accurate, more economical, and more comprehensive analytical methods.

Numerous analytical methods are available which can, in principle, handle any problem which might arise. However, the time and expense required to produce acceptable solutions is often excessive. This program addresses this problem by setting out a plan to create specialized software packages, which will provide the necessary answers in an efficient, user-oriented, streamlined fashion. Separate component-specific models will be created for burner liners, turbine blades, and turbine vanes using fundamental data from many technical areas. The methods developed will be simple to execute, but they will not be simple in concept. The problem is extremely complex and only by a thorough understanding of the details can the important technical approaches be extracted. The packaging of these interdisciplinary approaches into a total system must then conform to the modular requirements for useful computer programs.

Objective

The overall objective of this program is to develop and verify a series of interdisciplinary modeling and analysis techniques which have been specialized to address three specific hot section components. These techniques will incorporate data as well as theoretical methods from many diverse areas, including cycle and performance analysis, heat transfer analysis, linear and nonlinear stress analysis, and mission analysis. Building on the proven techniques already available in these fields, the new methods developed through this contract will be integrated to provide an accurate, efficient, and unified approach to analyzing combustor burner liners, hollow air-cooled turbine blades, and air-cooled turbine vanes. For these components, the methods developed will predict temperature, deformation, stress, and strain histories throughout a complete flight mission.

Background

This program, to a great extent, will draw on prior experience. This base of experience is invaluable for understanding the highly complex interactions among all the different technical disciplines as well as for estimating the importance of different engine parameters. In particular, there are four specific areas in which experience will be especially beneficial.

*This work was done under NASA Contract NAS3-23687.

First, with the recent increases in fuel costs, greater emphasis has been placed on more accurate solutions for stresses and strains in order to understand and improve the durability and life of hot section components. Conventional linear elastic analyses are no longer sufficient; instead, they now provide the boundary values for more refined creep and plasticity calculations. These nonlinear analyses are now performed routinely as part of the design process at General Electric. This extensive experience with these plasticity and creep methods will contribute directly to developing component specific models.

Second, advances in 3-D modeling capability are being achieved by the concepts developed under the NASA-supported ESMOSS program. ESMOSS concepts will provide the basis to develop an efficient modeling system for geometric and discretized models of engine components.

Third, the NASA-funded Burner Liner Thermal/Structural Load Modeling Program will contribute strong support to this program. The specific area addressed, transfer of data from a 3-D heat transfer analysis model to a 3-D stress analysis model, will provide the background and framework for the data interpolation required for all thermomechanical models in this contract.

Fourth, over the past 10 years, General Electric has developed internally a family of computer programs: LASTS, OPSEV, and HOTSAM. These programs all have the common thread of using selected points from cycle data, heat transfer, and stress analyses, and a decomposition/synthesis approach to produce accurate values of temperature, stress, and strain throughout a mission. These programs are totally consistent with the overall objectives of this program, and represent a proven technology base upon which the component specific models will be developed. Significant advances to be made are the inclusion of nonlinear effects and the introduction of improved modeling and data transfer techniques.

Approach

The program is organized into nine tasks which can logically be separated into two broadly parallel activities (Figure 1). On the right of Figure 1 we have the Component Specific Thermo-Mechanical Load Mission Modeling path. Along this path a Decomposition/Synthesis approach will be taken. In broad terms this means developing methods to generate approximate numerical models for the engine cycle and the aerodynamic and heat transfer analyses needed to provide the input conditions for hot parts stress and life analysis.

The left path, Component Specific Structural Modeling will provide the tools to develop and analyse finite element nonlinear stress analysis models of combustor liners and turbine blades and vanes. These two paths are shown in more detail in Figures 2 and 3.

Software Development, Task IV consists of planning and writing the computer programs for both paths, with the necessary interconnections, using a structured, top down approach.

In the Thermomechanical Load Mission Modeling portion of the program (Figure 2) we will develop, in Task III, a Thermodynamic Engine Model which will generate the engine internal flow variables for any point on the operating mission. The method for doing this is described below. Task V will develop techniques to decompose

flight missions into characteristic mission segments. In Task VII a Thermomechanical Mission Model will be developed. This will use the flow variables from the Thermodynamic Model to determine metal temperature and pressure distributions for a representative combustor liner and turbine blade and vane.

Individual tasks for the Structural Modeling activity are shown in Figure 3. The requirements of Software Design, Task II, will be factored into Task VI, the evaluation of the structural analysis methods which were selected for evaluation in Task I. Task VIII will provide the capability for structurally modeling current state-of-the-art combustor liners and hollow turbine blades and vanes, given the defining dimensional parameters. These parameters will be chosen to facilitate parametric studies.

The component specific models will be developed in two steps. In the first a geometric model will be defined. In the application of the Component Specific Modeling Program this data will then be transferred to the Thermomechanical Load Mission Model to provide the geometry for determining component pressures and temperatures. Thus, a data transfer link will be developed to do this in Task IV, Software Development. The capability for generating from the geometric model a discretized, finite element model will also be part of Task VIII. At this point another link between the two paths will be needed to transfer the component temperatures and pressures from the Thermomechanical Load model to the finite element model, interpolating the data as needed to define nodal temperatures and pressures. This also will be completed in Task IV.

The final function in Task VIII will be the development of component-specific stress analysis models for the three components to perform cyclic elastic, plastic and creep analyses using loading conditions defined by the Thermomechanical Load Models Progress.

At this time considerable progress has been made on the Thermodynamic Engine Model. The model is being developed as a simple calculational tool which will take as inputs the three variables, altitude (h), Mach number (M) and power level (PL) for the allowed flight map of an engine, as shown in Figure 4. In addition, ambient temperature deviations from the standard atmosphere, airframe bleed air requirements and engine deterioration can also be included as part of the input to the Thermodynamic Model. For each input condition, specified by h, M and PL the Thermodynamic Engine Model will calculate gas weight flow ($\dot{w}$), temperature (t) and pressure (p) at selected aerodynamic engine stations, as needed to determine component thermal loadings. These stations are shown in Figure 5.

The technique for developing a Thermodynamic Engine Model is shown in Figures 6 and 7. The engine to be analyzed must be defined thermodynamically by an engine cycle deck (computer program) which can be run to generate the internal flow variables at the chosen aerodynamic stations (Figure 6). To encompass the complete engine operating map (Figure 4), 148 operating points are chosen and $\dot{w}$, t and p are calculated using the cycle deck for the selected stations, as well as N_1 and N_2, the fan and core speeds. From this station data an Engine Performance Cycle Map is constructed. This is essentially a set of three-dimensional data arrays which map the station data ($\dot{w}$, t, p, N_1 and N_2) on to the engine operating map (Figure 4). Given an arbitrary operating point defined by h, M and PL it is then, in principle, possible to interpolate on the Engine Performance Cycle Map to determine station data. In practice the station parameters are nonlinear functions of the input

parameters and considerable effort was needed to develop these multi-dimensional interpolations. The computer program used to generate the Engine Performance Cycle Map from the engine cycle desk output has been developed as part of Task III. The functioning of the Thermodynamic Engine Model is shown in Figure 7. Given an engine mission, as shown schematically in Figure 8 it can be defined by values of the input variables h, M and PL at selected times through the mission. Using these input variables and the Engine Performance Cycle Map an Interpolation Program, now being developed in Task III of this program, will calculate engine station parameters throughout the mission (Figure 7). These are then used to define Station Mission Profiles of $\dot{w}$, t, p, N_1, and N_2, as functions of time at each aerodynamic station. These Station Mission Profiles are become the input to the Thermomechanical Engine Model.

The Thermomechanical Model is less well developed at this time than the Thermodynamic Model. Its form will be based on types of correlations previously developed within General Electric. Figure 9 shows a representative correlation for a turbine vane. Metal temperatures at various points on the vane T_{VA} are correlated in terms of a vane overall cooling effectiveness, η, and station gas temperatures T_3 at compressor discharge, and T_4 at combustor discharge. Using the Station Mission Profiles it will be possible to calculate the temperatures at selected locations on each component as functions of time, given the input parameters h, M and PL that define the engine mission. These then will provide the boundary conditions for the component stress analyses.

On the Component Specific Structural Modeling path, concepts have been defined and are being implemented. Additional evaluations are needed, however, before they can be presented for discussion.

Conclusion

When completed this program will provide a stress analysis system for hot section parts that will allow the component designers to evaluate quickly the effects of mission variations, be easy to use, cost effective, and make a significant contribution to assessing hot section durability.

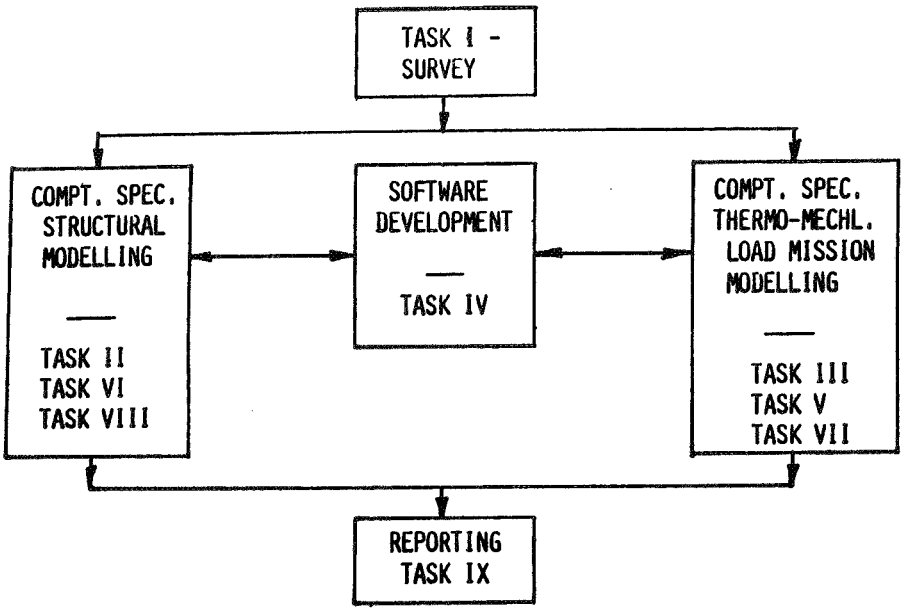

FIGURE 1. COMPONENT SPECIFIC MODELLING - BASE PROGRAM

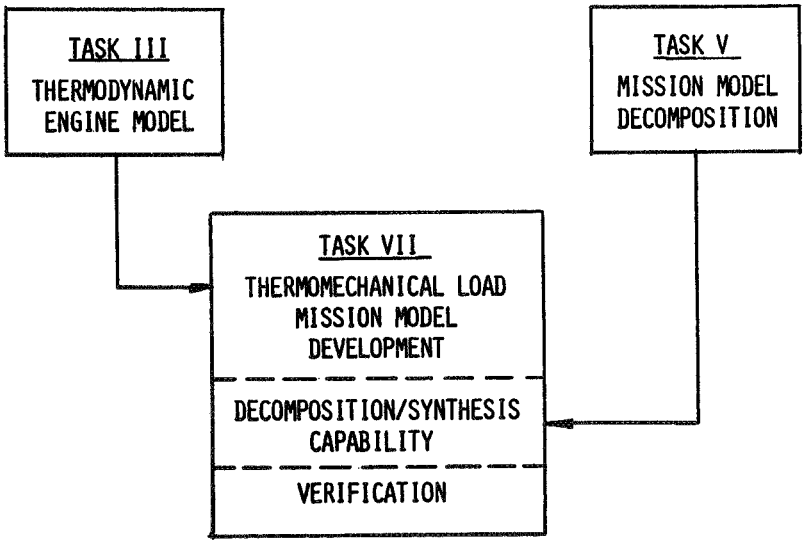

FIGURE 2. COMPONENT SPECIFIC
THERMOMECHANICAL LOAD MISSION MODELLING

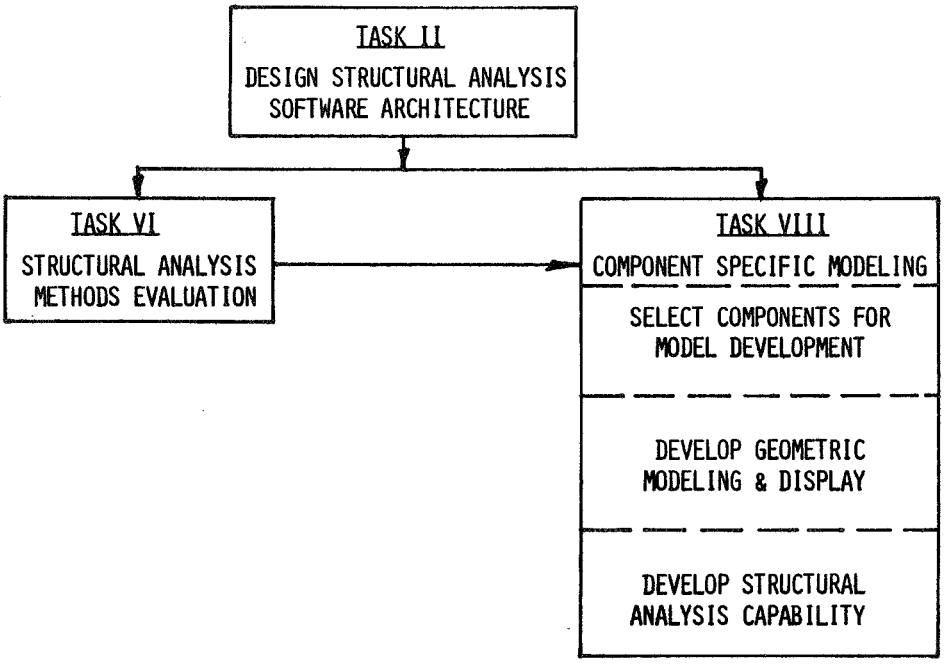

FIGURE 3. COMPONENT SPECIFIC STRUCTURAL MODELING

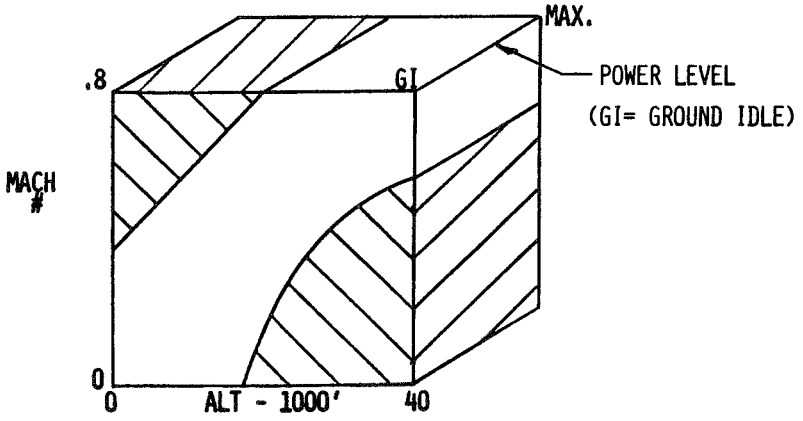

FIGURE 4. ENGINE OPERATING MAP

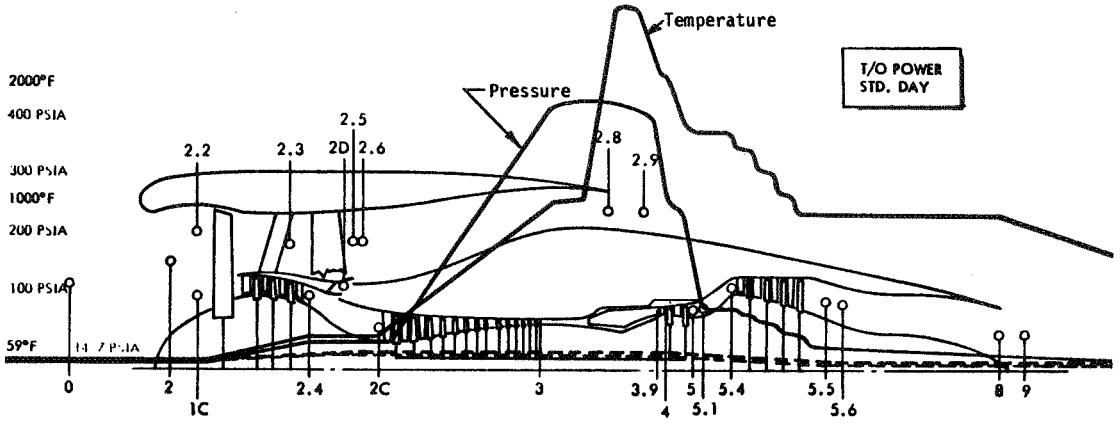

LEGEND:

0	AMBIENT	2C	HP COMPRESSOR INLET
2	ENGINE INLET	3	HP COMPRESSOR DISCHARGE
2.2	FAN TIP (BYPASS) STREAM INLET	3.9	HP TURBINE 1ST-STAGE NOZZLE INLET (W/O COOLING FLOW)
1C	FAN HUB (LP COMPRESSOR) STREAM INLET	4	HP TURBINE ROTOR INLET (W/ COOLING FLOW)
2.3	FAN DISCHARGE	5	HP TURBINE DISCHARGE (W/O COOLING FLOW)
2.4	LP COMPRESSOR DISCHARGE	5.1	HP TURBINE DISCHARGE (W/ COOLING FLOW)
2D	LP COMPRESSOR DISHCARGE BLEED PORT EXIT	5.4	LP TURBINE INLET (W/ COOLING FLOW)
2.5	BYPASS STREAM MIXING PLANE	5.5	LP TURBINE DISCHARGE (W/O COOLING FLOW)
2.6	BYPASS DUCT INLET (AFTER MIXING)	5.6	LP TURBINE DISCHARGE (W/ COOLING FLOW)
2.8	BYPASS DUCT JET NOZZLE THROAT	8	PRIMARY JET NOZZLE THROAT
2.9	BYPASS DUCT JET NOZZLE EXIT (COMPLETE EXPANSION)	9	PRIMARY JET NOZZLE EXIT (COMPLETE EXPANSION)

TEMPERATURE FAN ------ CORE ——— PRESSURE FAN ------ CORE ———

FIGURE 5. CF6 AERODYNAMIC STATIONS

T72-421-1

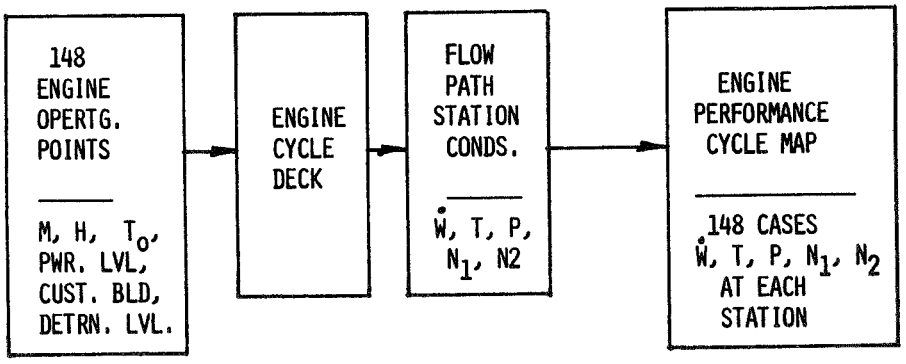

FIGURE 6. THERMODYNAMIC ENGINE MODEL CYCLE MAP GENERATION

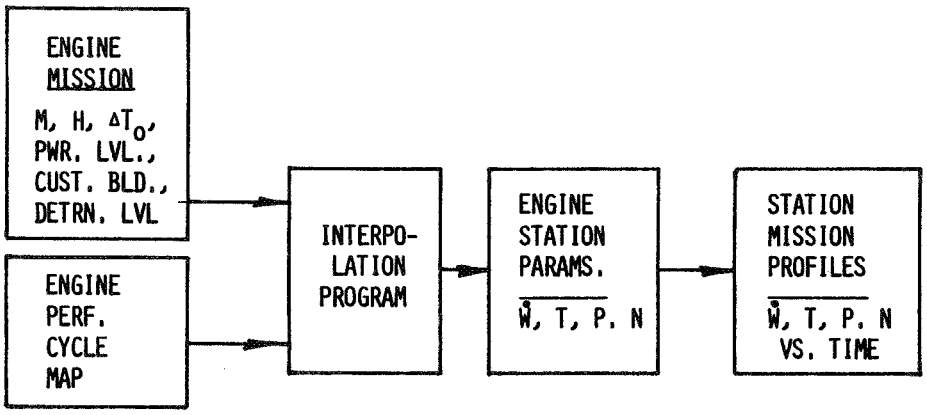

FIGURE 7. THERMODYNAMIC ENGINE MODEL

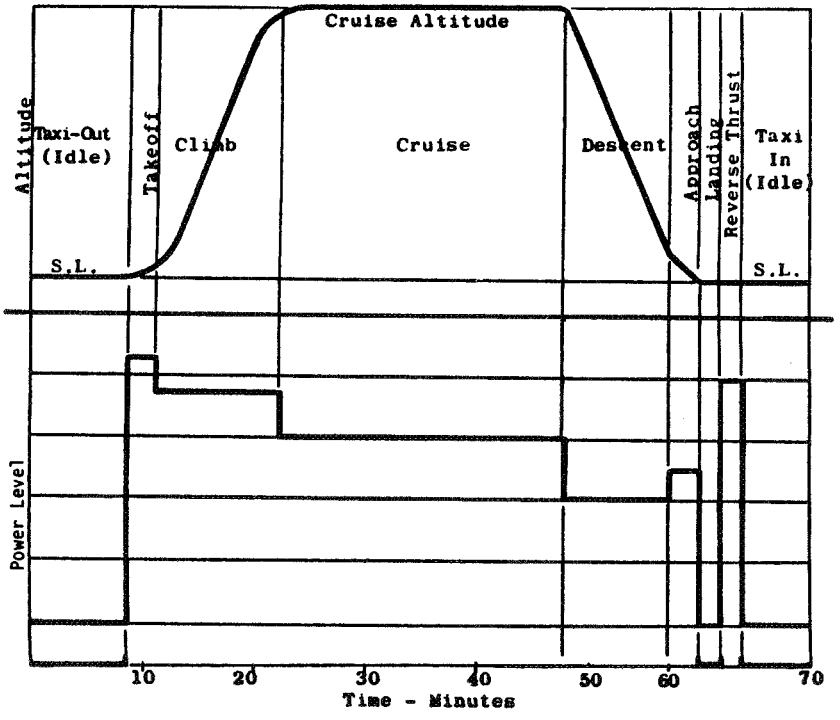

FIGURE 8. TYPICAL FLIGHT CYCLE

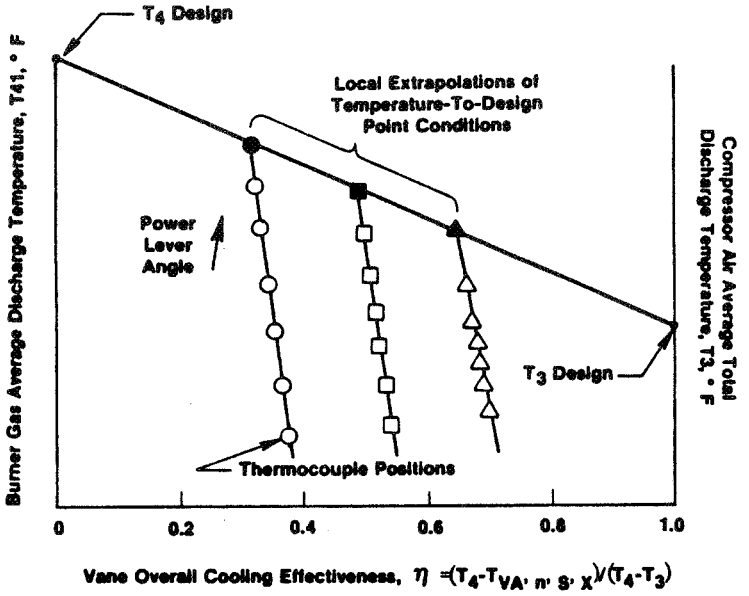

FIGURE 9. TURBINE VANE COOLING EFFECTIVENESS

Page intentionally left blank

D21

3D INELASTIC ANALYSIS METHODS FOR HOT SECTION COMPONENTS

L.T. Dame
R.L. McKnight
General Electric Company
Aircraft Engine Business Group

The objective of this research is to develop an analytical tool capable of economically evaluating the cyclic time-dependent plasticity which occurs in hot section engine components in areas of strain concentration resulting from the combination of both mechanical and thermal stresses. The techniques developed must be capable of accommodating large excursions in temperatures with the associated variations in material properties including plasticity and creep.

The overall objective of this proposed program is to develop advanced 3-D inelastic structural/stress analysis methods and solution strategies for more accurate and yet more cost-effective analysis of combustors, turbine blades, and vanes. The approach will be to develop four different theories, one linear and three higher order with increasing complexities including embedded singularities.

The objective will be achieved through a four-phase program consistent with the NASA Statement of Work.

In Task I, the linear formulation theory will be developed. These will consist of three linear formulation models in which stress, strain, and temperature are linear functions of the spatial coordinates; and the increments in loading, temperature, and time are linear. Three constitutive relations will be developed for these linear formulation models each capable of predicting elastic, plastic, thermal, and creep strains and cyclic effects. One constitutive relation will be approximate, one will be of the current genre, and one will be a unified theory.

In Task II, the polynomial formulation theory will be developed. These will consist of three polynomial formulation models in which stress, strain, and temperature are polynomial functions of the spatial coordinates, and the increments in loading temperature and time are quadratic. They will also accommodate two-intersecting embedded discontinuities. Three constitutive relations will be associated with these polynomial formulation models.

In Task IV, the special functions theory will be developed. These will consist of three special function formulation models in which stress, strain, and temperature are special functions of the spatial coordinates and the increments in loading, temperature, and time are special functions. These models will accommodate eight intersecting embedded similar discontinuities and have three associated constitutive relations.

In Task V, the general functions theory will be developed. These will consist of three general function formulation models in which stress, strain, and temperature are general functions of the spatial coordinates and the increments in loading, temperature, and time are general functions.

These models will accommodate eight intersecting embedded different discontinuities and have three constitutive relations associated with them. One of

the constitutive relations will be more complex than those used for the special functions theory.

Task III and VI are reporting requirements.

Work began on this program in April 1983. A literature survey was conducted in order to identify various solution techniques and constitutive models. In developing an economical computer tool it is essential to consider the interactions of solution technique, constitutive model, integration scheme, load incrementing, temperature incrementing, and time incrementing procedures.

For time dependent plasticity (or creep) problems the solution technique most commonly used in finite element codes is a constant stiffness scheme. Any economical scheme for thermo-mechanical cycling will of necessity require automatic time incrementing. Initially, the constitutive equation subroutines are being developed in the context of a finite element code with a constant stiffness iteration procedure, automatic time incrementing, linear variation of loads and boundary conditions and isothermal conditions. The introduction of time varying temperatures will require a modified solution procedure. The isothermal Bodner formulation has been implemented in a single element computer program and compared with test data and calculations in Reference 1.

In view of the increasing availability of vector processors, work is also underway to develop more efficient numerical procedures for solving sets of linear algebraic equations on such machines. Iterative procedures such as the Jacobi or Gauss-Seidel methods are more feasible with vector machines (Reference 2-3), especially if the stiffness matrix is stored in column form. Improvements in forming stiffness matrices may also be realized (Reference 4) which would greatly enhance the calculation time in tangent stiffness schemes. Eigenvalue calculation procedures may also be more economical using vector processors (Reference 5).

REFERENCES

1) Bodner, S.R., "Representation of Time Dependent Mechanical Behavior of Rene' 95 by Constitutive Equations", Technical Report AFML-TR-79-4114, Air Force Materials Laboratory, Wright-Patterson A.F.B., Ohio, August 1979.

2) Schonauer, W., "The Efficient Solution of Large Linear Systems, Resulting from the FDM for 3-D PDE's on Vector Computers", EDF-Bulletin De La Direction Des Etudes Et Des Recherches-Serie C - No. 1 - 1983.

3) Sameh, A., "An Overview of Parallel Algorithms in Numerical Linear Algebra", EDF - Bulletin De La Direction Des Etudes Et Des Recherches-Serie C - No. 1 - 1983.

4) Auguin, M., Boeri, F. and Jalby, W., "Etude de la Construction I'une Matrice de Rigidite Sur Une Architecture Multiprocesseur", EDF - Bulletin De La Direction Des Etudes Et Des Recherches - Serie C - No. 1 - 1983.

5) Barlow, R., Evans, D. and Shanehchi, "Programming Experience on Parallel Algorithms for the Eigenvalue Problem", EDF - Bulletin De La Direction Des Etudes Et Des Recherches - Serie C - No. 1 - 1983.

Page intentionally left blank

D22

3-D INELASTIC ANALYSIS METHODS FOR HOT SECTION COMPONENTS (BASE PROGRAM)

E. S. Todd
Pratt & Whitney Engineering

The objective of this program is to produce a series of new computer codes that permit more accurate and efficient three-dimensional inelastic analysis of selected hot section components - combustor liners, turbine blades and turbine vanes. The computer codes embody a progression of mathematical models and are streamlined to take advantage of geometrical features, loading conditions, and forms of material response that distinguish each group of selected components.

Software in the form of stand-alone codes and modules for use in General Purpose Structural Analysis (GPSA) programs will be provided by Pratt & Whitney Aircraft (P&WA) with assistance from three uniquely well qualified subcontractors: MARC Analysis Research Corporation (MARC), State University of New York at Buffalo (SUNY-B), and United Technologies Research Center (UTRC). Primary development of special finite element models will be accomplished by MARC, while mechanics of materials models and constitutive formulations will be assembled by UTRC. Development of advanced formulation (boundary element) models will be shared by P&WA and SUNY-B. Verification of the various analysis packages will be done by P&WA.

The technical effort of this program will be conducted over a period of twenty-four (24) months and will involve three (3) distinct tasks:

Task I - Linear Theory

Under this task a linear theory will be developed consisting of three linear formulation models: 1) mechanics of materials, 2) special finite elements, and 3) advanced formulation (boundary element) models. The linear theory is defined to mean that: 1) the stresses or strains and temperatures in the generic modeling region are linear functions of the spatial coordinates, and 2) the solution increments for load, temperature and/or time are extrapolated linearly from previous information. The emphasis in the linear theory for three-dimensional inelastic analysis will be on a methodology using a large number of generic modeling regions and a large number of increments, but simple calculations per increment.

Task II - Polynomial Theory

This task will involve the development of a polynomial theory consisting of three polynomial formulation models: 1) mechanics of materials, 2) special finite elements, and 3) advanced formulation (boundary element) models. The polynomial theory is defined to mean that: 1) the stresses or strains and temperatures in the generic modeling region are at least quadratic functions of the spatial coordinates, and 2) the solution increments for load, temperature and/or time are extrapolated at least quadratically from previous information. The emphasis in the polynomial theory for three-dimensional inelastic analysis will be on a methodology using a smaller number of generic modeling regions with two intersecting, embedded discontinuities and a smaller number of increments, but more complex calculations per increment than for

the linear theory (Task I).

Task III - Reporting Requirements

This task includes periodic technical, financial and schedular reporting and, at the conclusion of the technical effort, the submittal of a final Contractor Report.

Optional Program

An optional program, to be exercised at the discretion of the Government, will extend the base computer codes to include higher order representations of strain in space and time and to deal effectively with more complex collections of discontinuities such as cooling holes and coating cracks.

VALIDATION OF STRUCTURAL ANALYSIS METHODS USING BURNER LINER CYCLIC RIG TEST DATA

R. Thompson
National Aeronautics and Space Administration
Lewis Research Center
Cleveland, Ohio 44135

INTRODUCTION

The objectives of the HOST Burner Liner Cyclic Rig Test Program are basically threefold: (1) to assist in developing predictive tools needed to improve design analyses and procedures for the efficient and accurate prediction of burner liner structural response; (2) to calibrate, evaluate and validate these predictive tools by comparing the predicted results with the experimental data generated in the tests; and (3) to evaluate existing as well as advanced temperature and strain measurement instrumentation, both contact and non-contact, in a simulated engine cycle environment. The data generated will include measurements of the thermal environment (metal surface temperatures) as well as structural (strain) and life (fatigue) responses of simulated burner liners and specimens under controlled boundary and operating conditions. These data will be used to calibrate, compare and validate analytical theories, methodologies and design procedures, as well as improvements in them, for predicting liner temperatures, stress-strain responses and cycles to failure. Comparison of predicted results with experimental data will be used to show where the predictive theories, etc. need improvements. In addition, as the predictive tools, as well as the tests, test methods, and data acquisition and reduction techniques, are developed and validated, a proven, integrated analysis/experiment method will be developed to determine the cyclic life of a simulated burner liner.

TEST RIGS

Figure 1 includes a list of the test rigs under construction, with anticipated delivery dates and the basic specimens and burner liner components to be analyzed and tested in each rig. Flat plate specimens, with and without holes, will be tested in the Box Rig while tubular specimens, with and without holes, and subelements of burner liners will be tested in the Annular Rig. Each test will be increasingly more complex than the preceding one, both from the standpoint of geometry as well as the data acquisition and reduction requirements. Correspondingly, the structural analysis will become more complex in the progression of test configurations. For example, figure 2 shows the progression of flat plate specimens to be tested and structurally analyzed.

A schematic of the Box Rig, being fabricated in-house, is shown in figure 3. Four quartz lamps are used to heat the 8 x 5 x 0.05 inch flat plate specimens. Both water and air cooling are used. A viewing port provides for visual inspection of the specimen and data acquisition. Provisions for instrumentation include 30 thermocouples and 10 strain gage connections. Initially, the Box Rig will provide temperature and limited strain measurements using commercially available thermocouples and wire resistance strain

gages. But as advanced temperature and strain measurement instrumentation is developed and becomes available under the HOST program and elsewhere, the Box Rig will serve to evaluate the advanced instrumentation, for example, infrared thermal imaging camera for temperature mapping, thinfilm thermocouples and strain gages, laser speckle strain measurements, etc. The instrumentation with the greatest potential will then be installed and used on the Annular Rig.

A schematic of the Annular Rig is shown in figure 4. The test section, being built by P&W as part of a cooperative effort between NASA Lewis and P&W, has 112 quartz lamps to heat the 21-inch annular test specimen. The length of the heated portion of the test specimen is 10 inches. Both water and air cooling are used. Three active viewing ports are provided for visual inspection of the specimen and data acquisition. Seven quick disconnect instrumentation panels are shown in the figure. These panels provide for 100 thermocouple, 28 strain gage and 21 pressure transducer connections. Both the Box Rig and Annular Rig Test Programs will be conducted at NASA Lewis in ECRL-1.

Test conditions and variables to be considered in each of the test rigs and test configurations, and also used in the structural analysis, for validation of the predictive theories and tools will include thermal and mechanical load histories (simulating an engine mission cycle), different boundary conditions (fixed, free, etc.) a variety of specimen and subelement geometries (including advanced burner liner structural design concepts), different materials (initially Hastelloy-X will be used), various cooling schemes and cooling hole configurations, and the simulation of hot streaks. Based on these test conditions and test variables, test matrices for each rig and configuration will be developed with the intent to verify the predictive tools over as wide a range as is feasible, using the simplest of possible tests. Table I is a sample test matrix for a flat plate without holes.

EXPERIMENTS

To verify the feasibility of the tests and test rig designs, and identify potential test problems and analysis/experiment complications, a limited number of preliminary experiments were conducted and structural analyses performed using 5 x 8 x 0.05 inch Hastelloy-X flat plate specimens. The specimens were tested in the box rig shown in figure 5. Three quartz lamps, placed about 2 inches apart, center-to-center, about 1-1/2 inches from the reflector and about 1-1/2 inches below the test specimen, were used to heat the specimen. The lamps were air cooled through a manifold located at the bottom of the box. Air pressure for cooling the lamps ranged from 4 psi at the lowest power setting (30 W) to 60 psi at the maximum power (18 000 W) setting. The power was controllable in steps from 30 to 18 000 watts. No water cooling was provided in this rig. The top of the plate could be viewed through a cut-out in the top cover. Some of the more salient results of these tests are presented below.

The test specimen was held fixed between two identical frames by tightening 10 bolts, as shown in figure 6. The frames and specimen were positioned horizontally above the lamps and were held in place by leg supports (long bolts) which rested on the bottom of the box.

Both the frame and test specimen were instrumented. A total of 22 thermocouples (0.032-in.-diam. Chromel-Alumel) were mounted on the frame. Ten thermocouples were mounted on the specimens; three on the outer face (cool side) and seven on the inner face (hot side) exposed to the quartz lamps. The thermocouples were mounted along the two center axes of the plate. High-temperature resistance strain gages, BLH Model HT-12/2-5A, were mounted on two specimens. The strain gage is made of platinum-tungsten alloy and works for temperatures up to 1200° F. The locations of the thermocouples and strain gages on the frame and test specimen are shown in figure 7.

Three flat plate specimens without holes were tested. The first series of tests were conducted to verify that the rig was working properly, to verify the rigs performance capability and durability, and to observe the failure mode of the plate (buckling). The frame was instrumented with thermocouples but the plate was not. Temperature measurements of the frame indicated that depending on the rate at which the power was increased, the temperature difference between the top and bottom half of the frame could vary from 0 to 100° F at temperatures below 500° F (maximum frame temperature) to a maximum variation of 0 to 400° F at 1000° F and above. By increasing the power slowly, this difference could be controlled and kept to a minimum. The conclusion reached is that control of the frame temperature is needed to prevent buckling of the plate for a fixed edge boundary condition.

In the second series of tests, both temperature and strain measurements were obtained. Temperature variations on the plate and frame were recorded for several power settings. For a single power setting, representative plots of the plate and frame temperatures are shown in figures 8 and 9. The power level was stepped up from 375 volts (12 100 W) to 435 volts (15 500 W) and held constant for about 7 minutes. The delta increase in frame temperature ranged from 50° to 100° F whereas the delta increase in plate temperature ranged from 100° to 230° F. The initial maximum/minimum temperatures for the frame and plate were 510° (TC 12)/260° F (TC 4) and 1270° (TC 4)/830° F (TC 1), respectively. The final maximum/minimum temperatures for the frame and plate were 600°/310° F and 1500°/1000° F respectively. The frame temperature increased almost linearly with time while the plate temperature reached almost steady state conditions at about 2 minutes into the step increase in power. Contrary to our expectations, a non-uniform plate temperature was observed for this and all tests in the longitudial direction, while a more uniform temperature was observed across the plate (see figs. 8 and 9) for all tests. Through the thickness temperatures varied widely, ranging from 20° to 200° F. Unexplainably, the data show that the front half of the plate was much hotter than the back half of the plate (by about 530° F for data shown in fig. 9), and the front half of the frame (both bottom and top) was hotter than the back half (by about 100° F for the data shown in fig. 8) for all tests. The most obvious reasons for this anomaly were ruled out, such as a slopping plate, distance between lamps and test specimen, cooling air flow patterns, plugged air holes, and misalignment of the cooling air manifold. These tests showed: it was possible to control the plate temperature, both transient and steady state, by varying power settings and air flows; it was possible to achieve desired maximum/minimum temperatures in the plate, approximately 1700° F temperature at a power setting of 440 volts and a 900° F temperature at a power setting of 300 volts; it was possible to control the frame temperature to a degree; it was possible to control strains by varying both frame and plate temperatures for fixed edge boundary conditions; it was not possible to achieve uniform surface temperatures in the plate either in the horizontal or

longitudinal directions; it was not possible to achieve the desired or uniform through the thickness temperature gradients; and strain measurements were not obtained above 1200° F.

The primary objective of the third series of tests was to demonstrate whether or not a simulated engine mission cycle could be obtained. The test results showed that controlled complex, cyclic thermal cycles could be imposed on a flat plate specimen. Other than this, the test results obtained were similar to those obtained from the second series of tests.

ANALYSIS

A structural analysis of a flat plate specimen without holes was performed using MARC, a general purpose, nonlinear finite element structural analysis computer program. Walker's viscoplastic constitutive model was incorporated into MARC to account for the interaction between creep and plastic deformations.

The plate was analyzed using a four node plane stress element. The mesh configuration was set up so that direct comparisons could be made between models with a single hole and without a hole. The mesh configurations for these two models are shown in figure 10. The configurations are doubly symmetric, thus only a quarter of the plate is modelled.

A parametric study was conducted to examine different boundary conditions for a flat plate without holes. The results indicated that both the test specimen and frame would have to be analyzed together and that controlled, variable boundary conditions were necessary to reproduce the desired stress levels in the plate. Controlling the boundary conditions was done by providing truss members at the edges of the plate as shown in figure 11. By appropriately adjusting the temperature difference between the plate and the edge members, the stress levels can be varied in the plate. Thus, boundary conditions ranging from free edge (with the plate and edge bars at the same temperature) to fixed edge (with the edge bars kept at a reference temperature while the plate temperature is increased), as well as all intermediate conditions is possible. Further, depending on whether the edge bar temperatures lag behind the plate temperatures or vice versa, compression or tension may be produced in the plate. This reversal of stress would make it possible to trace hysteresis loops and thus study thermal ratcheting, compare experiment with predictions, etc.

A simulated engine mission cycle was studied assuming uniform temperatures in the plate and the edge bars, with a 5-percent temperature difference between the plate and frame as shown in figure 12. The initial temperature was set at 940° F and the cycle consisted of a 25-second ramp up to a maximum temperature of 1740° F, a 40 second hold time at this temperature level and a 30-second ramp down to a temperature of 940° F. Figure 12 shows the time variation of stress in element 18 (see fig. 10). The stress-strain variation for this element is plotted in figure 13. No direct comparisons could be made between this analysis and the experiments described earlier because of the nonuniformity of plate and frame temperatures obtained from the experiment.

CONCLUSIONS AND FUTURE RESEARCH

The preliminary experiments demonstrated the feasibility of the rig to achieve the desired plate temperatures, temperature gradients and cyclic thermal load histories, although uniform plate temperatures were not achieved. Finite element models of plates, with and without holes, and frames were generated and structural analyses were performed. However, a direct comparison between experiment and analysis could not be done because of the nonuniform plate temperatures obtained in the experiments.

The new Quartz Lamp Box Rig under construction has four quartz lamps, with a maximum power of 24 000 watts. This rig is expected to produce much more uniform plate temperatures than those obtained in the rig just described. In addition, computer controlled operation and data acquisition will allow for more accurate and extensive tests. The ESCORT II Data Acquisition System, available at Lewis, will be used for data acquisition and control of the experiment. The data obtained, both temperature and strain measurements, will be stored on tape for processing, reduction and analysis at a later date. Also, an infrared thermal video imaging system will be integrated into the system to obtain temperature maps of the plate.

The Annular Rig, as described earlier, under construction, will provide data on cylindrical shells and subelements of burner liners. The same features available for the Box Rig will be carried over to the Annular Rig. Preliminary structural analyses of plates and shells will be used to guide the direction of the experimentation in both the Box and Annular Rigs. Other analyses will be conducted to predict the material stress-strain response using the measured temperature distributions obtained from the tests. These analyses will provide a basis for comparing analytical predictions, for example, using several constitutive models, with the experimental data for validation and subsequent selection of improved analysis methods to predict, more efficiently and accurately, the structural response of burner liners.

TABLE I - SAMPLE TEST MATRIX FOR FLAT PLATE

TEST CONFIGURATION - FLAT PLATE WITHOUT HOLES

MATERIAL - HASTELLOY X

TEST NO.	TEMPERATURE STATE	TEMPERATURE HISTORY						BOUNDARY COND. FOR PLATE EDGES	NUMBER OF CYCLES (TIME BET. CYCLES, sec)
		RAMP UP		HOLD TIME		RAMP DOWN			
		TIME, sec.	TEMP., °F	TIME, sec.	TEMP., °F	TIME, sec.	TEMP., °F		
1	STEADY STATE-UNIFORM TEMP.	20	RT-600	300	600	--		FIXED EDGES	--
2	"	20	RT-800	300	800	--		"	--
3	"	20	RT-1000	300	1000	--		"	--
4	"	20	RT-1200	300	1200	--		"	--
5	"	20	RT-1400	300	1400	--		"	--
6	"	20	RT-1600	300	1600	--		"	--
7	"	20	RT-1800	300	1800	--		"	--
8	"	40	RT-1000	300	1000	--		"	--
9	"	40	RT-1400	300	1400	--		"	--
10	"	40	RT-1800	300	1800	--		"	--
11	"	60	RT-1000	300	1000	--		"	--
12	"	60	RT-1400	300	1400	--		"	--
13	"	60	RT-1800	300	1800	--		"	--
14	"	20	RT-1000	500	1000	--		"	--
15	"	40	RT-1000	500	1000	--		"	--
16	"	60	RT-1000	500	1000	--		"	--
17	"	20	RT-1400	500	1400	--		"	--
18	"	40	RT-1400	500	1400	--		"	--
19	"	60	RT-1400	500	1400	--		"	--
20	"	20	RT-1800	500	1800	--		"	--
21	"	40	RT-1800	500	1800	--		"	--
22	"	60	RT-1800	500	1800	--		"	--
23	CYCLE-	20	RT-1400	80	1400	20	1400-800	"	5
24	VARIABLE TEMP.	20	RT-1600	80	1600	20	1600-800	"	5
25	"	20	RT-1800	80	1800	20	1800-800	"	5
26	"	20	RT-1400	120	1400	20	1400-800	"	5 (60)
27	"	20	RT-1600	120	1600	20	1600-800	"	5 (60)
28	"	20	RT-1800	120	1800	20	1800-800	"	5 (60)
29	"	30	RT-1400	80	1400	30	1400-800	"	5 (60)
30	"	30	RT-1600	80	1600	30	1600-800	"	5 (60)
31	"	30	RT-1800	80	1800	30	1800-800	"	5 (60)
32	"	20	RT-1400	80	1400	20	1400-800	"	25 (60)
33	"	20	RT-1600	80	1600	20	1600-800	"	25 (60)
34	"	20	RT-1800	80	1800	20	1800-800	"	25 (60)
35	HOT STREAK (+50° F)					--			
36	UNIFORM TEMP.	20	RT-1000	300	1000	--		"	--
37	"	20	RT-1400	300	1400	--		"	--
38	"	20	RT-1800	300	1800	--		"	--
39	HOT STREAK (+50° F)								
40	CYCLIC TEMP.	20	RT-1400	80	1400	20	1400-800	"	5 (60)
41	"	20	RT-1600	80	1600	20	1600-800	"	5 (60)
42	"	20	RT-1800	80	1800	20	1800-800	"	5 (60)
43	HOT STREAK (+100° F)	20		80	1400	20	1400-800	"	5 (60)
44	CYCLIC TEMP.	20		80	1600	20	1600-800	"	5 (60)
45	"	20		80	1800	20	1800-800	"	5 (60)

COMPONENTS TO BE ANALYZED AND TESTED
IN HOST BURNER LINER CYCLIC RIGS

1. QUARTZ LAMP BOX RIG (DELIVERY DATE - SEPTEMBER '83)
   FLAT PLATES WITH AND WITHOUT HOLES

2. QUARTZ LAMP ANNULAR RIG (DELIVERY DATE - APRIL '84)
   CYLINDRICAL SHELLS WITH AND WITHOUT HOLES
   SUBELEMENTS OF COMBUSTOR LINERS

FLAT PLATE SPECIMEN
CONFIGURATIONS TO BE ANALYZED AND TESTED

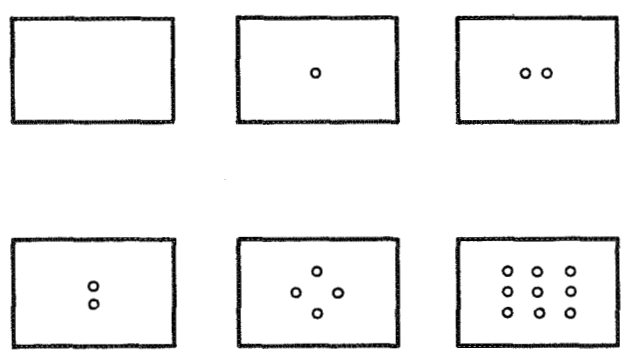

SCHEMATIC OF QUARTZ LAMP BOX RIG

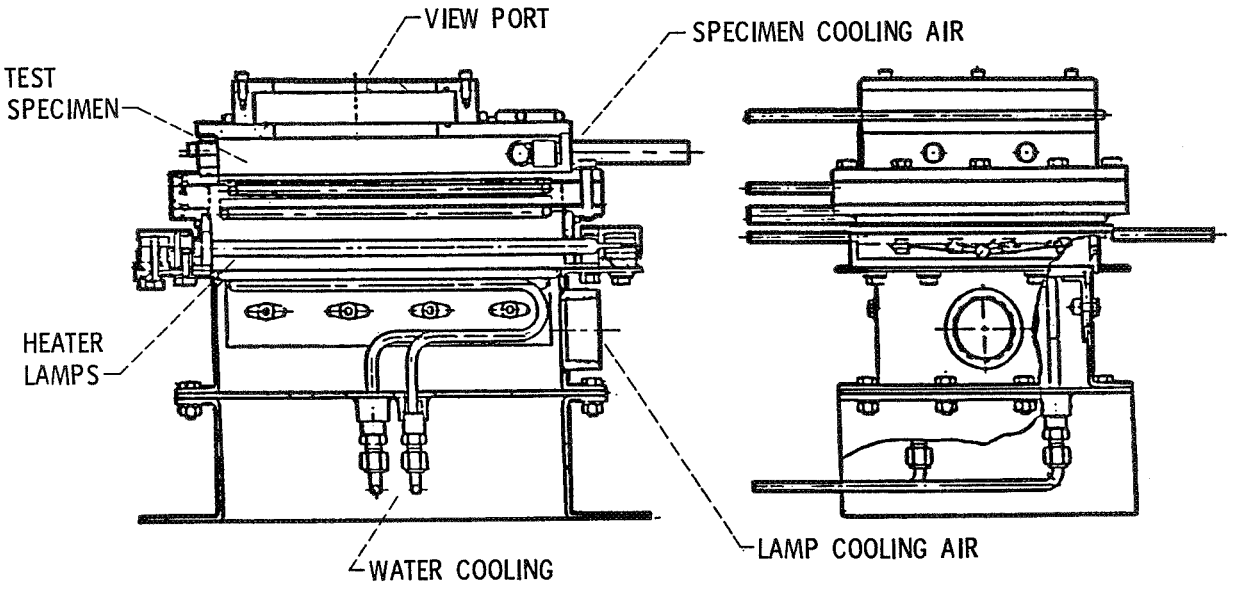

SCHEMATIC OF QUARTZ LAMP ANNULAR RIG

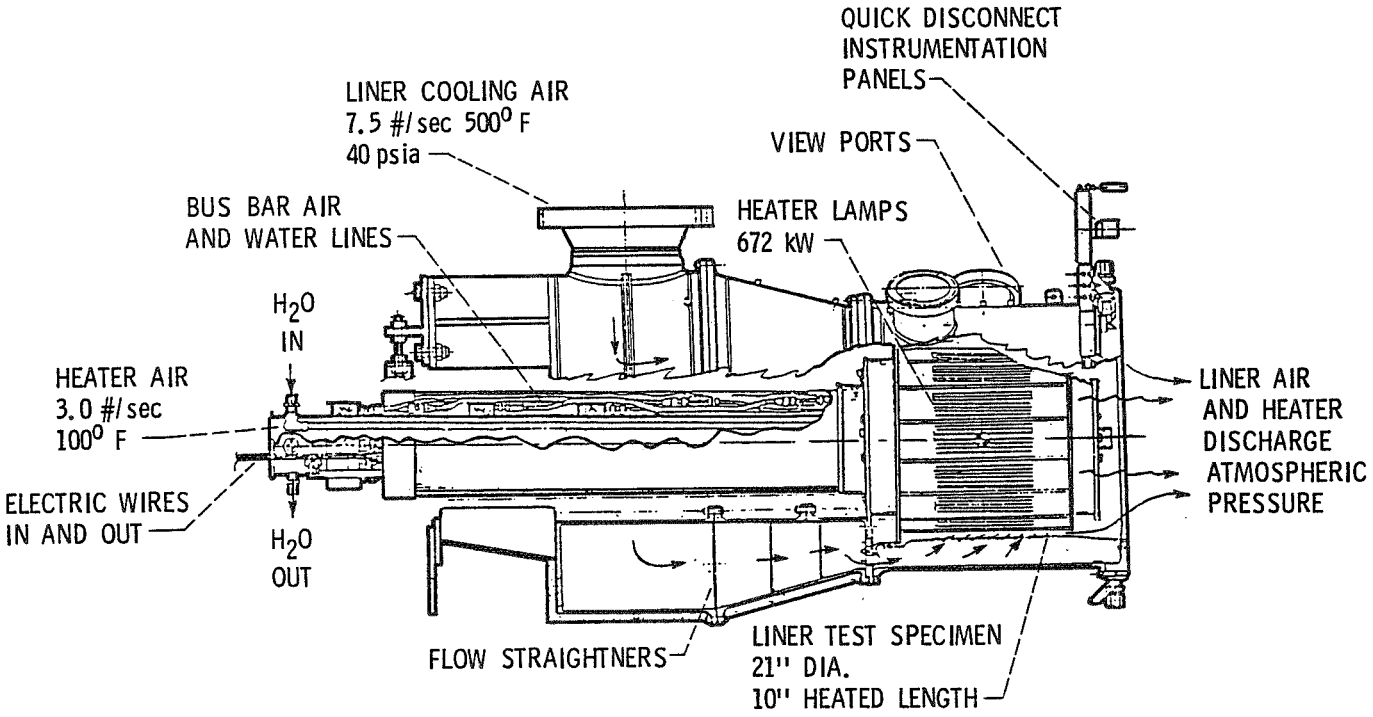
QUICK DISCONNECT INSTRUMENTATION PANELS
LINER COOLING AIR 7.5 #/sec 500° F 40 psia
VIEW PORTS
BUS BAR AIR AND WATER LINES
HEATER LAMPS 672 kW
H_2O IN
HEATER AIR 3.0 #/sec 100° F
LINER AIR AND HEATER DISCHARGE ATMOSPHERIC PRESSURE
ELECTRIC WIRES IN AND OUT
H_2O OUT
FLOW STRAIGHTNERS
LINER TEST SPECIMEN 21" DIA. 10" HEATED LENGTH

BOX RIG TEST SET UP

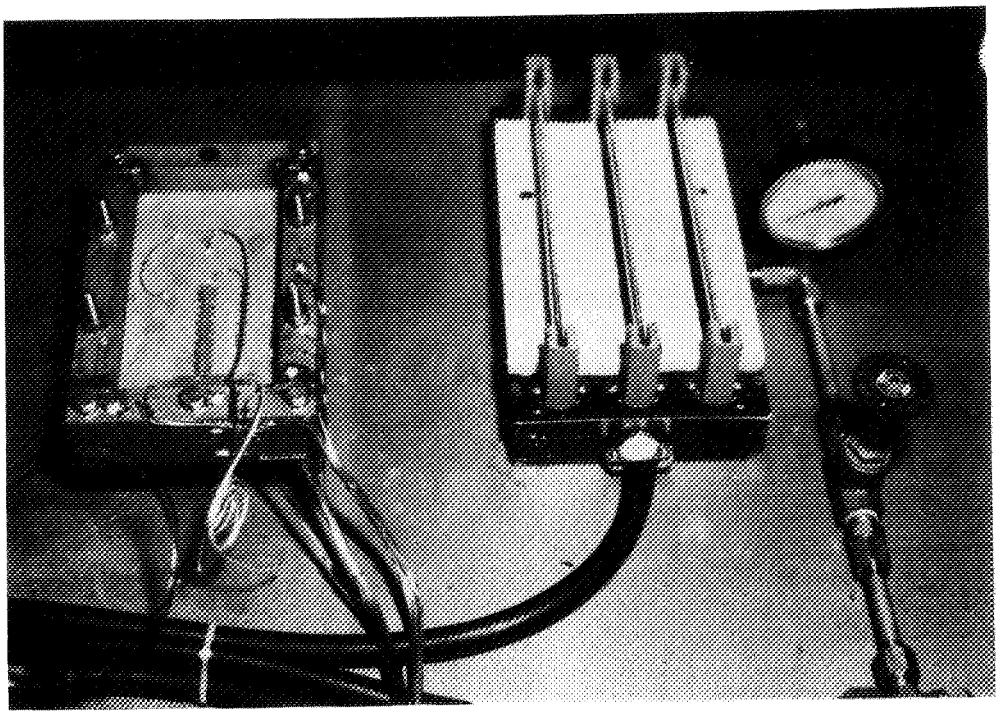

BOX RIG TEST SET UP

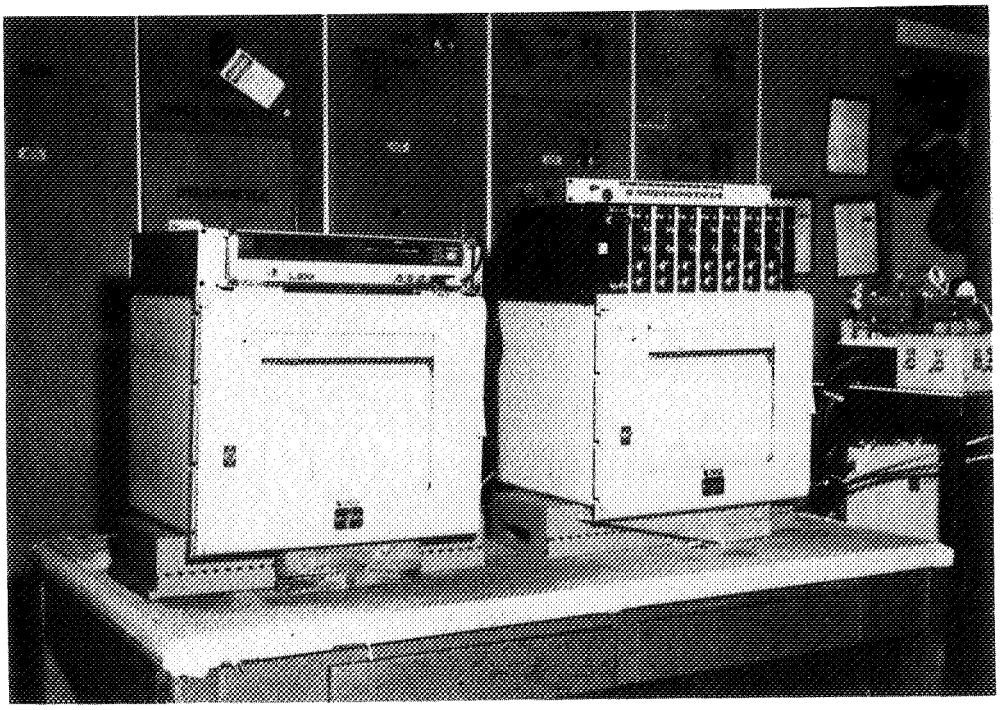

FRAME FOR HOLDING THE PLATE SPECIMENS

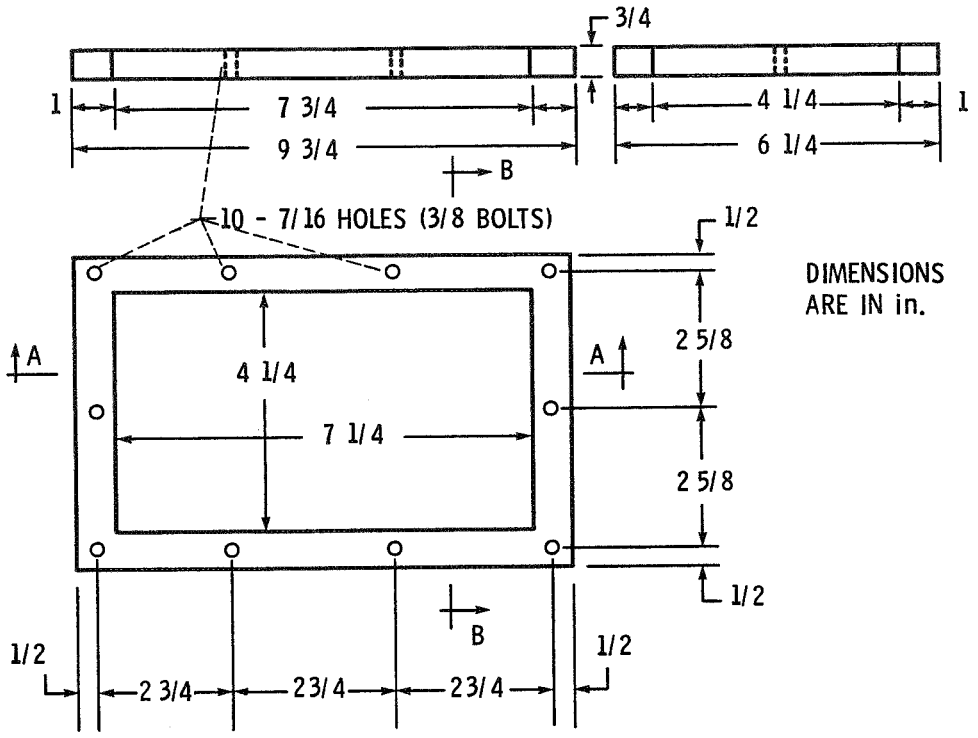

FRAME AND PLATE
THERMOCOUPLE AND STRAIN GAGE LOCATIONS

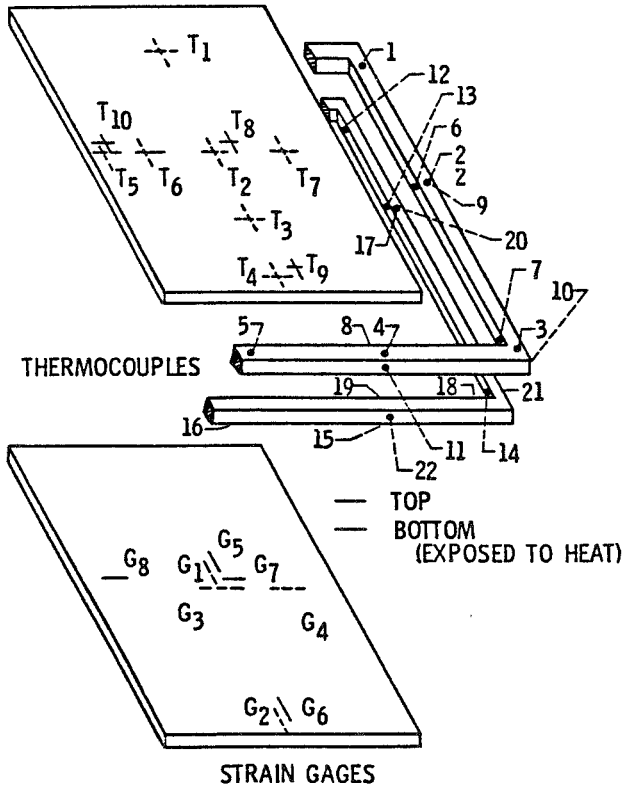

TEMPERATURE VARIATION OF
PLATE FOR A CHANGE IN POWER SETTING FROM 375 VOLTS TO 435 VOLTS

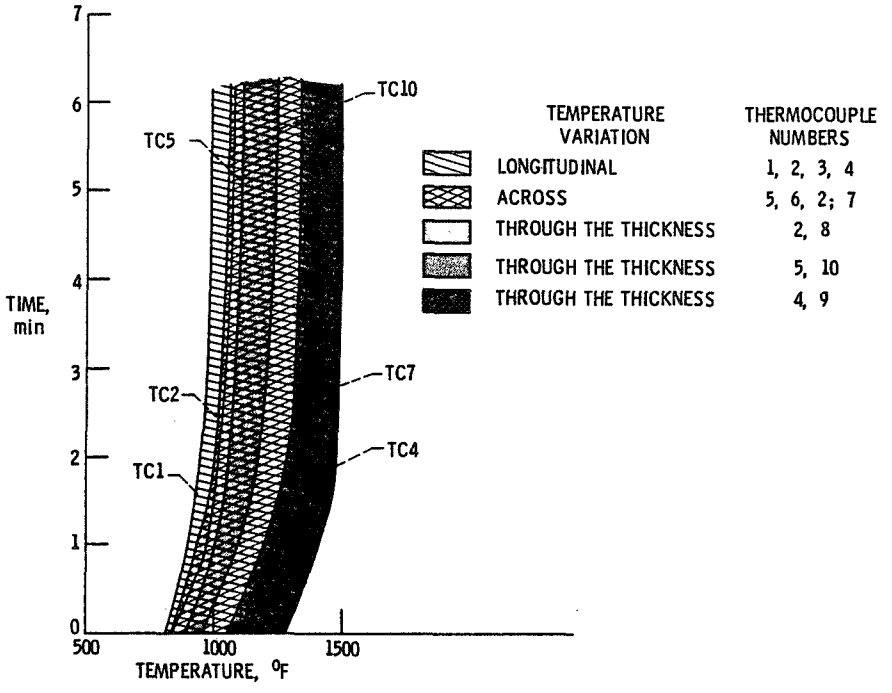

TEMPERATURE VARIATION OF
FRAME FOR A CHANGE IN POWER SETTING FROM 375 VOLTS TO 435 VOLTS

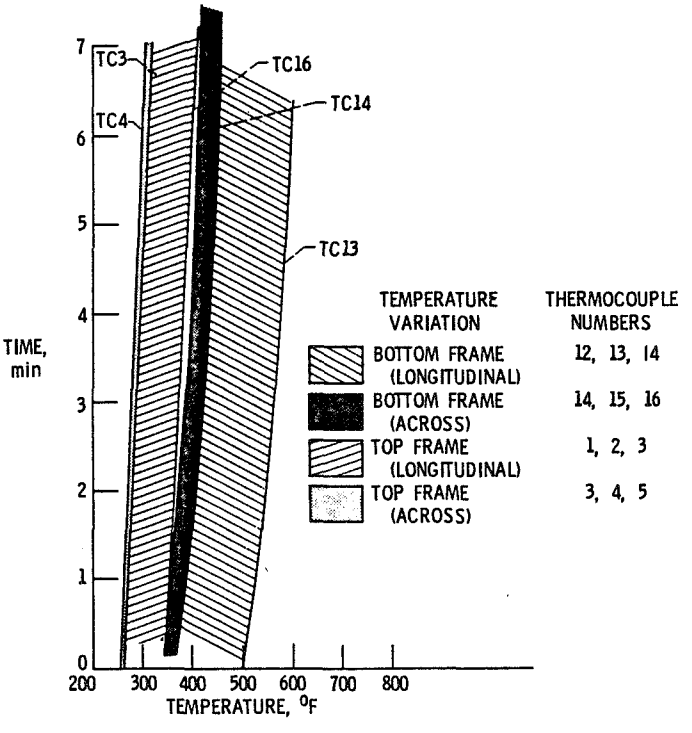

PLANE STRESS MESH FOR THE PLATE SPECIMENS

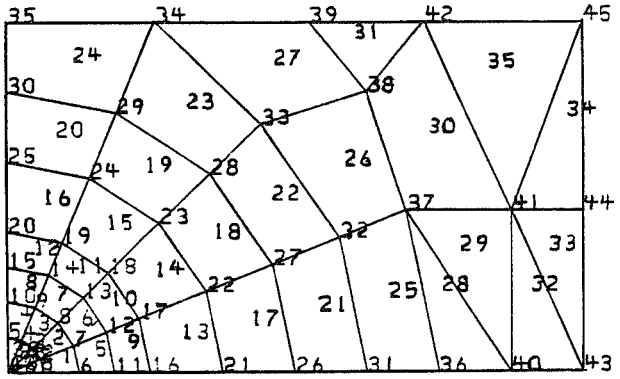

1/4 MESH - SOLID PLATE (NO HOLES)

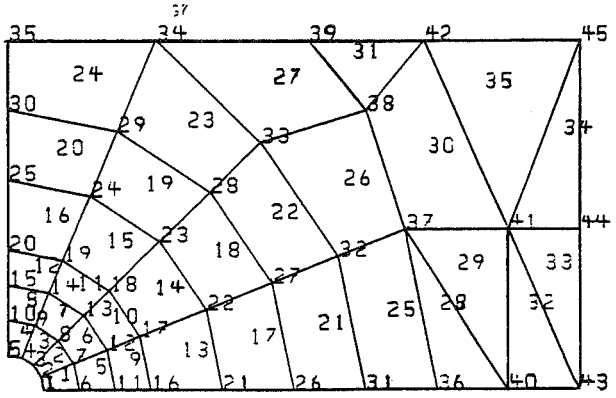

1/4 MESH - CENTER HOLE

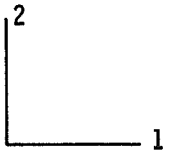

FINITE ELEMENT MODEL FOR THE FRAME AND PLATE

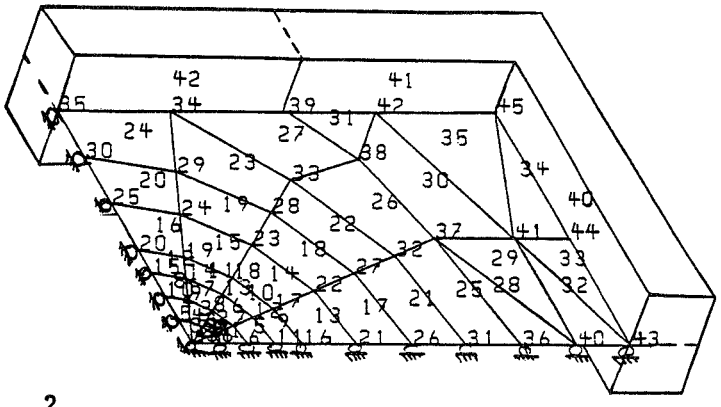

1/4 MESH

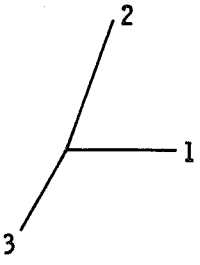

TIME VARIATION OF STRESS IN ELEMENT 18

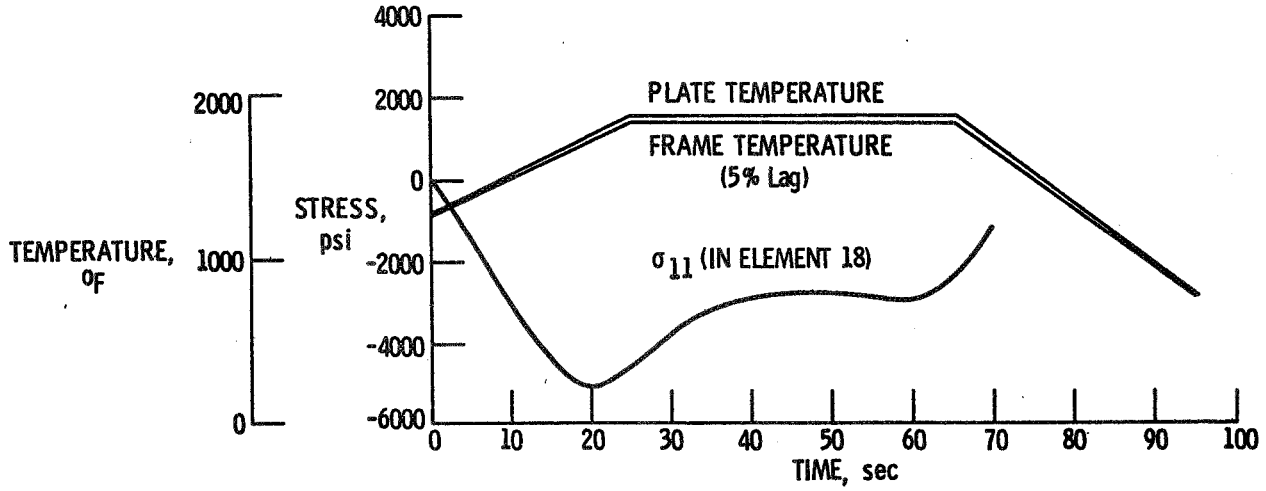

STRESS-STRAIN IN ELEMENT 18

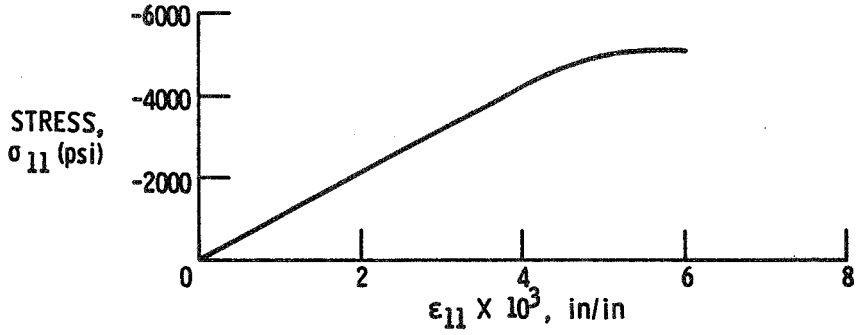

Page intentionally left blank

HOST LINER CYCLIC FACILITIES

FACILITY DESCRIPTION

Donald Schultz
National Aeronautics and Space Administration
Lewis Research Center
Cleveland, Ohio 44135

The HOST Liner Cyclic Program is utilizing two types of test apparatus, rectangular box rigs and a full annular rig. To date two quartz lamp cyclic box rigs have been tested and a third is to begin testing in late October 1983. The box rigs are used to evaluate 5x8 inch rectangular linear samples. A 21 inch diameter outer liner simulator is also being built up for testing beginning in April 1984. This annular test rig is being procured through a cooperative agreement with P&W-E, Hartford. Under this agreement they supply the test rig and two test liners while we supply the test facility. The data are shared by both. All rigs are atmospheric rigs.

The first box rig, a three 6-kVA lamp installation, was operated under adverse conditions to determine feasibility of using quartz lamps for cyclic testing. This work was done in December 1981 and looked promising.

The second box rig, again using three 6-kVA lamps, was operated to obtain instrumentation durability information and initial data input to a Finite Element Model. This limited test program was conducted in August 1983. Five test plates were run. Instrumentation consisted of strain gages, thermocouples and thermal paint. The strain gages were found to fail at 1200° F as expected though plates were heated to 1700° F.

The third box rig, containing four 6-kVA lamps, is in build-up for testing to beging in late October 1983. In addition to 33 percent greater power input, this rig has provision for 400° F backside line cooling air and a viewing port suitable for IR camera viewing. The casing is also water cooled for extended durability.

The 21 inch diameter outer liner simulator uses 112 6-kVA lamps to cyclicly heat the test liner. Power levels will be adjusted to simulate typical linear heat loadings. Air will be supplied to provide typical liner film and backside cooling. In addition to the test liners being supplied by P&W, which are production configurations, several simple liners will be tested to obtain confidence in the Finite Element Model.

This apparatus in addition to 672 kVA of 480 volt power, requires 7.5 lb/sec of 500° F air at 35 psia, 3.5 lb/sec of ambient temperature air at 5 psig, 1.5 lb/sec of ambient temperature air at 1 psig and 70 gal/min of cooling water. This apparatus is scheduled to go under testing in April 1984.

Special Test Instrumentation

Liner cold side temperatures will be measured using an IR-TV camera system with thermocouple measurements for varification. The IR-TV camera system will permit several hundred temperature measurements to be made in a relatively

small area. Linear hot side temperatures will be measured with thin film thermocouples. New technology high temperature strain gauges will be used to obtain local strain measurements.

Facility Preheater Test

The proposed natural gas fired vitiated preheater for the annular test rig was tested in February 1983. As part of this test, quartz tubing was placed in the preheater exhaust stream to determine if exhaust smoke would deposit on the quartz. The tubing remained soot free but an iron oxide deposit did appear. The rust is thought to have originated in the carbon steel laboratory air supply system. As a result a filter and stainless steel pipe will be used in the final rig installation. Additional preheater testing in the actual installation is scheduled for December 1983.

HOST LINER CYCLIC FACILITIES

I. QUARTZ LAMP BOX RIGS

- A. FIRST
- B. SECOND
- C. THIRD

II. QUARTZ LAMP ANNULAR RIG

FIRST QUARTZ LAMP BOX RIG

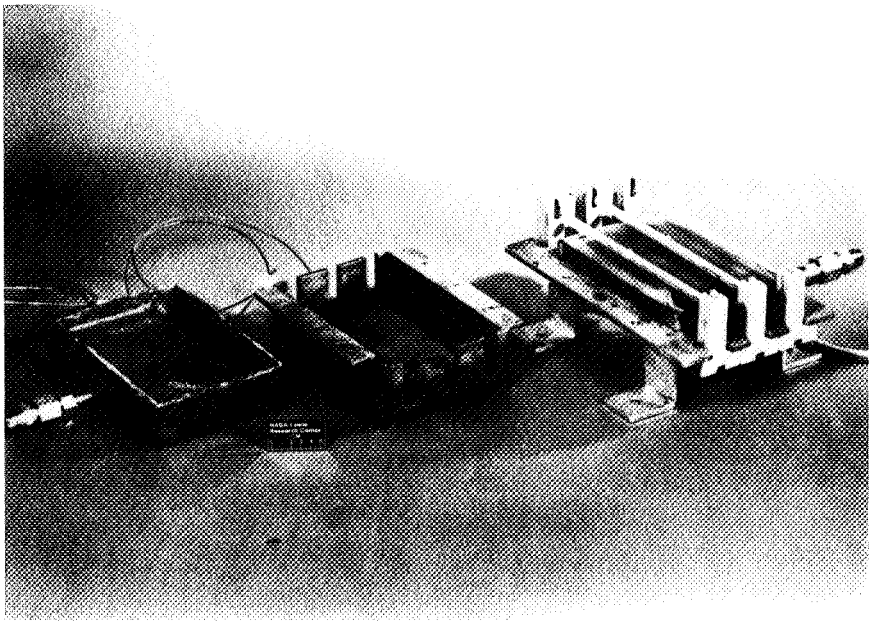

CS-82-2381

FIRST QUARTZ LAMP BOX RIG

- OBTAINED 2000° F TEST PLATE TEMPERATURE
- LIMITED LAMP LIFE

SECOND QUARTZ LAMP BOX RIG

OBJECTIVE:

- VERIFY PERFORMANCE AND DURABILITY OF INSTRUMENTATION
- PROVIDE INITIAL DATA IMPUT TO FINITE ELEMENT MODEL

TEST HARDWARE

- 5x8 in. FLAT HASTELLOY-X PLATES
  - TWO UNINSTRUMENTED
  - ONE INSTRUMENTED WITH THERMAL PAINT
  - ONE WITH THERMAL PAINT, NINE C/A-t/c's AND ONE STRAIN GAGE
  - ONE WITH THERMAL PAINT, NINE C/A-t/c's AND EIGHT STRAIN GAGES
- TEST PLATE SUPPORT FRAME WITH TWENTY-TWO C/A-t/c's

TEST RIG AND HARDWARE USED ON INITIAL FLAT PLATE TESTS

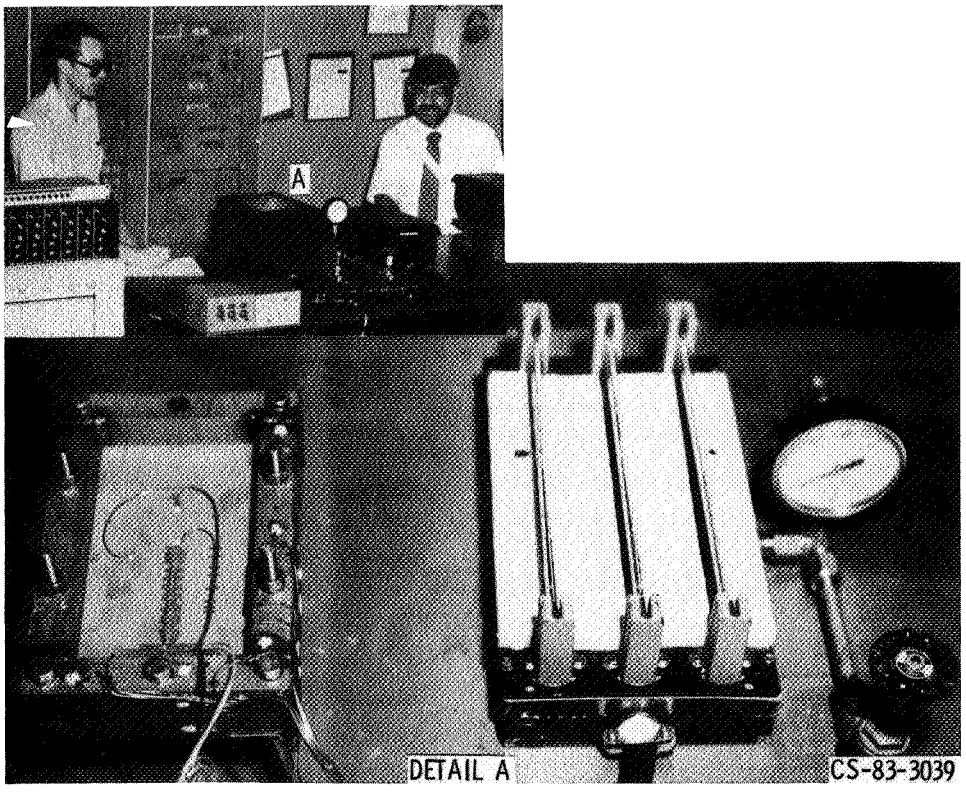

TEST RESULTS

- SUPPORT FRAME HEATED TO 1500° F
- SAMPLE PLATE TO 1700° F
- STRAIN GAGES FAILED AS EXPECTED AT 1200° F
- STRAINS WERE CONTROLLABLE BY VARYING LAMP POWER AND COOLING AIR FLOW RATE

QUARTZ LAMP BOX RIG

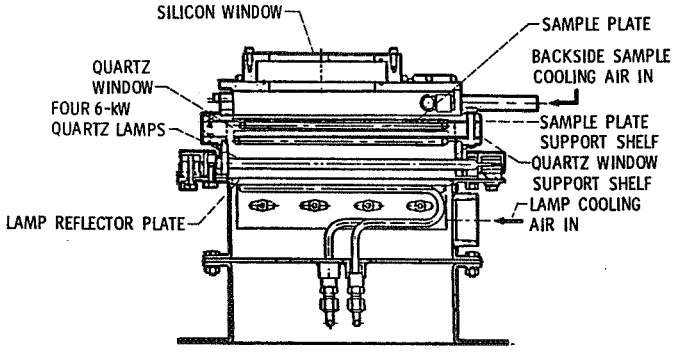

HOST QUARTZ LAMP ANNULAR RIG SCHEMATIC-ECRL-1

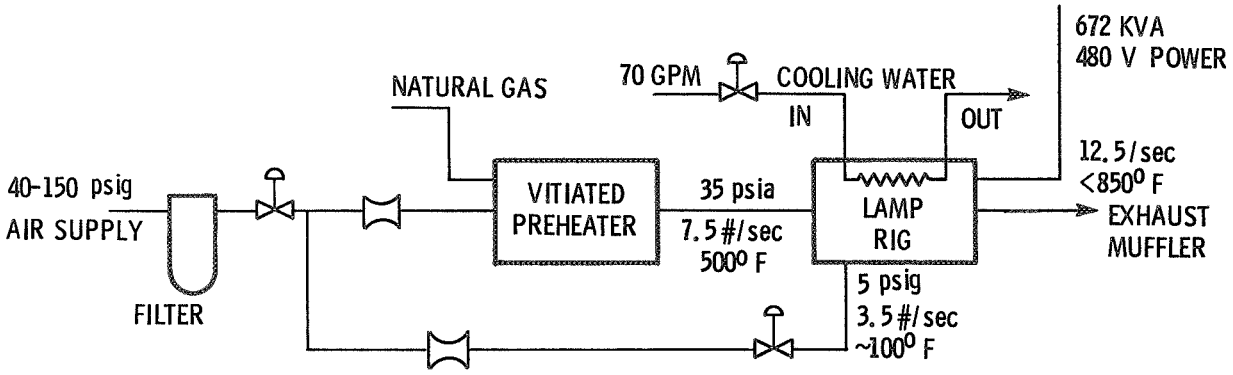

QUARTZ LAMP ANNULAR RIG HOUSING

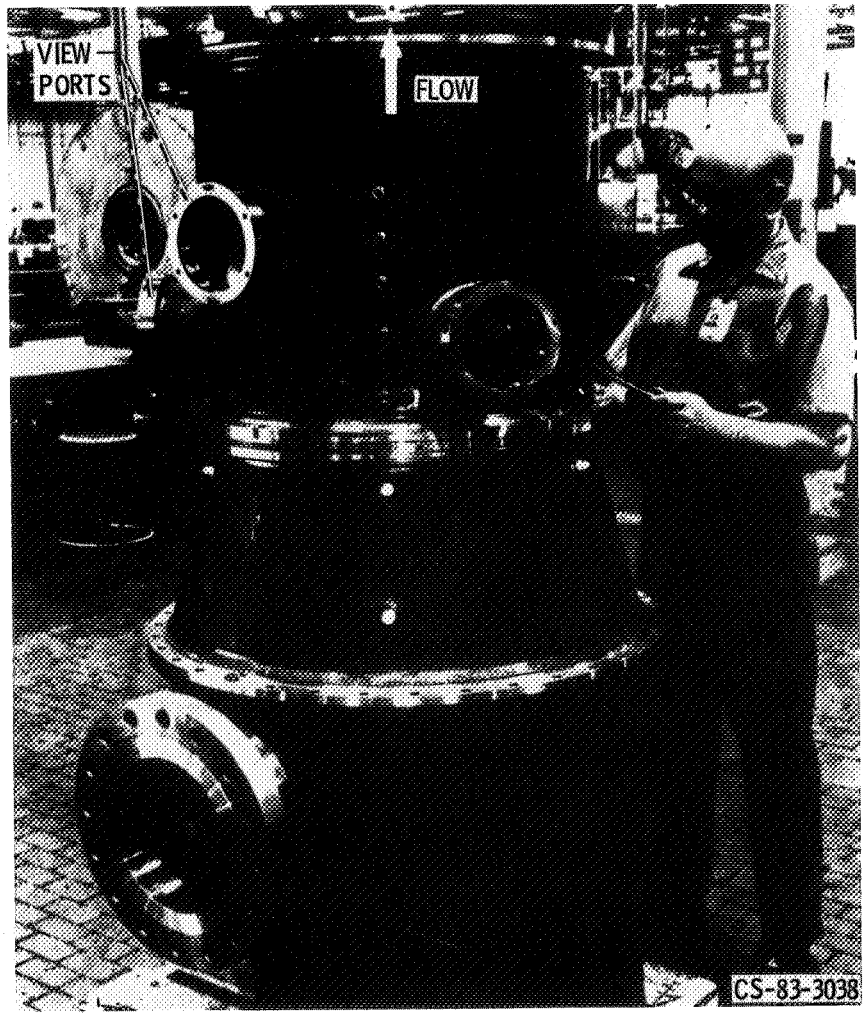

QUARTZ LAMP CYCLIC COMBUSTOR TEST RIG

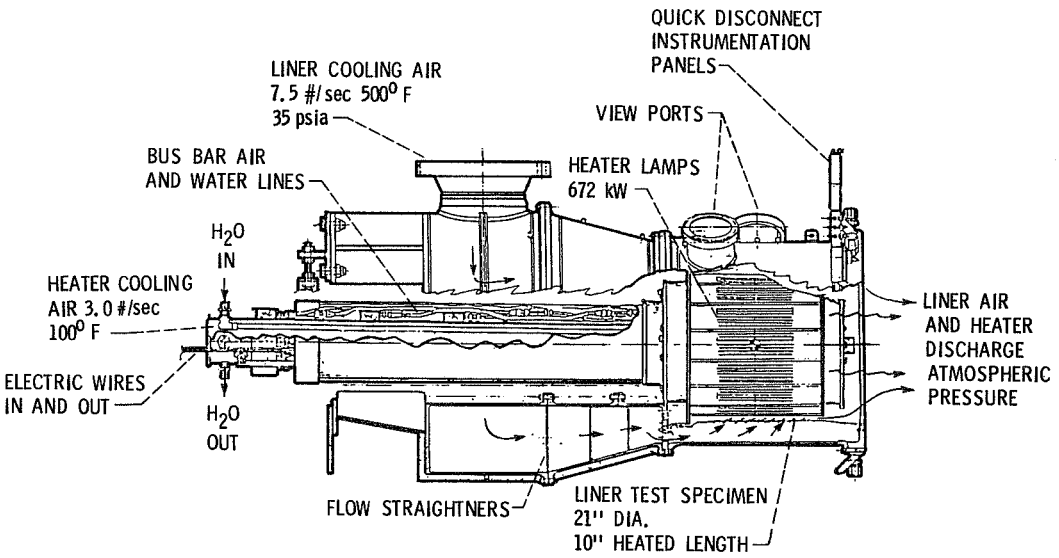
QUICK DISCONNECT INSTRUMENTATION PANELS
LINER COOLING AIR 7.5 #/sec 500° F 35 psia
VIEW PORTS
BUS BAR AIR AND WATER LINES
HEATER LAMPS 672 kW
H_2O IN
HEATER COOLING AIR 3.0 #/sec 100° F
LINER AIR AND HEATER DISCHARGE ATMOSPHERIC PRESSURE
ELECTRIC WIRES IN AND OUT
H_2O OUT
FLOW STRAIGHTNERS
LINER TEST SPECIMEN 21" DIA. 10" HEATED LENGTH

SPECIAL INSTRUMENTATION

I. IR - TV MONITORING OF LINER TEMPERATURES

II. THIN-FILM THERMOCOUPLES

III. LASER STRAIN GAUGE

IV. HIGH TEMPERATURE STRAIN GAUGES

FACILITY PREHEATER TEST

OBJECTIVE:

1. DETERMINE IF A NATURAL GAS FIRED VITIATED PREHEATER IS CLEAN ENOUGH FOR USE WITH THE ANNULAR LAMP RIG
2. EVALUATE PERFORMANCE OF LOW PRESSURE LINER CYCLIC CAN RIG VITIATED PREHEATER

TEST RESULTS

1. RUST FROM AIR SYSTEM PIPING DEPOSITED ON QUARTZ TUBES AT 500^{0} F
2. NO SMOKE
3. COMBUSTION EFFICIENCY OVER 95 PERCENT

DEPOSITS ON QUARTZ TUBING AFTER FACILITY PREHEATER TEST

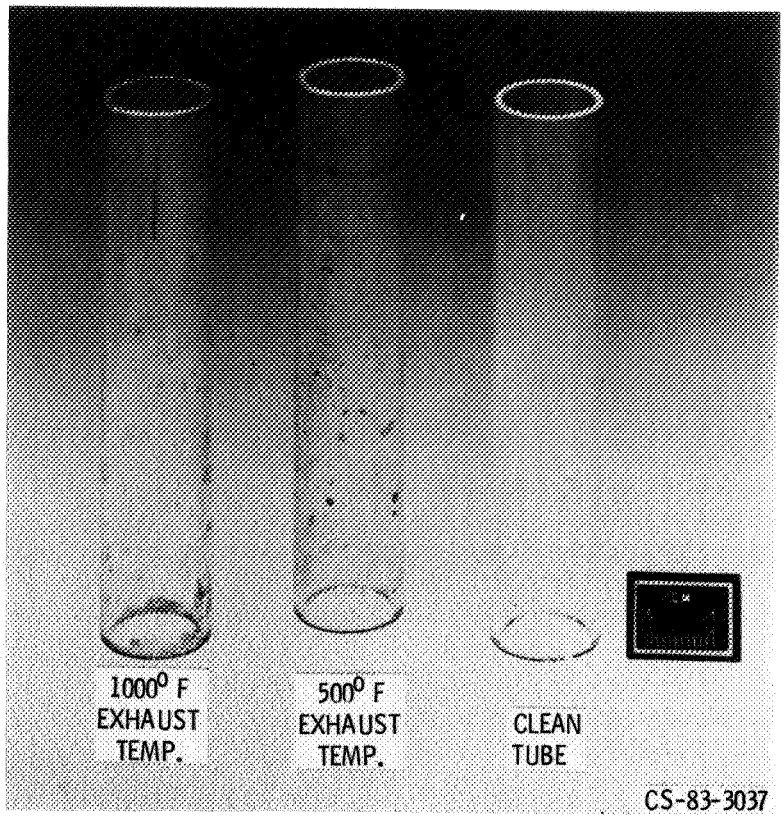

HOST CYCLIC LINER PROGRAM

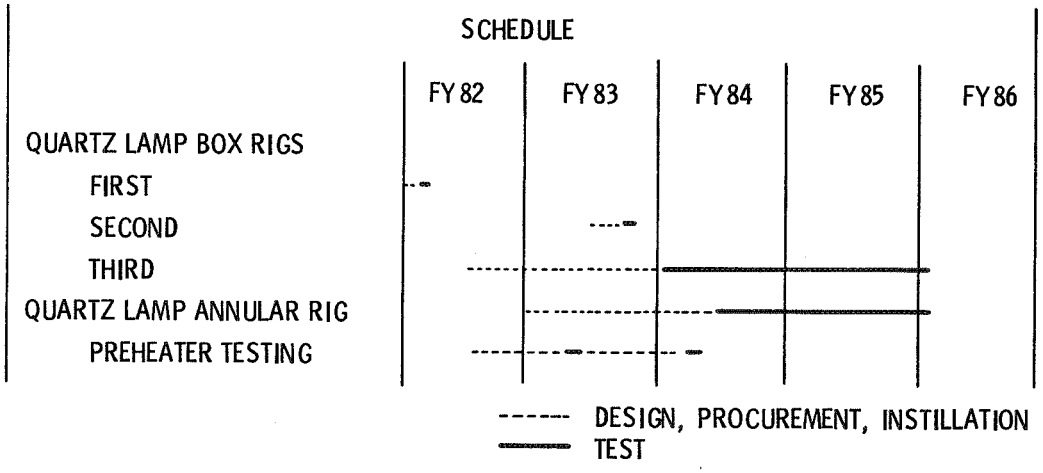

LIFE PREDICTION AND CONSTITUTIVE BEHAVIOR

G. R. Halford
National Aeronautics and Space Administration
Lewis Research Center
Cleveland, Ohio 44135

One of the primary drivers that prompted the initiation of the HOST Program was the recognized need for improved cyclic durability of costly hot section components. All too frequently, fatigue in one form or another was directly responsible for the less than desired durability, and prospects for the furture weren't going to improve unless a significant effort was mounted to increase our knowledge and understanding of the elements governing cyclic crack initiation and propagation lifetime. Certainly one of the important factors is the ability to perform accurate structural stress-strain analyses on a routine basis to determine the magnitudes of the localized stresses and strains since it is these localized conditions that govern the initiation and crack growth processes. Developing the ability to more accurately predict crack initiation lifetimes and cyclic crack growth rates for the complex loading conditions found in turbine engine hot sections is of course the ultimate goal of the life prediction research efforts.

It has been found convenient to divide the research efforts into those dealing with nominally isotropic and anisotropic alloys; the latter for application to directionally solidified and single crystal turbine blades.

I do want to emphasize the underlying thrust of these programs: The development and verification of WORKABLE engineering methods for the calculation, in advance of service, of the local cyclic stress-strain response at the critical life governing location in hot section components, and the resultant cyclic crack initiation and crack growth lifetimes.

In attacking the problems, we are utilizing the talents of industry, universities, and the government. Figures 1 to 4 display the specific programs that have been initiated and funded by the HOST Project Office. Those programs that have been on-going long enough to permit progress to be reported will be presented by the respective principal investigators. The remaining programs will be briefly touched upon either by the NASA Lewis Technical Program Manager or by myself.

CRACK INITIATION LIFE PREDICTION AND CONSTITUTIVE MODELING

(NOMIMALLY ISOTROPIC MATERIALS)

- CREEP-FATIGUE LIFE PREDICTION FOR ENGINE HOT SECTION MATERIALS (ISOTROPIC)
  - G. HALFORD, LERC TECHNICAL PROGRAM MANAGER
  - NAS 3-23288, PRATT & WHITNEY AIRCRAFT
  - V. MORENO, PRINCIPAL INVESTIGATOR
  - STARTED JUNE 1982
  - 2 YEAR BASE PROGRAM/3 YEAR OPTIONAL PROGRAM

- CONSTITUTIVE MODELING FOR ISOTROPIC MATERIALS
  - A. KAUFMAN, LERC TECHNICAL PROGRAM MANAGER
  - DUAL AWARDED PROGRAM
  - NAS 3-23927, GENERAL ELECTRIC COMPANY
  - J. LAFLEN, PRINCIPAL INVESTIGATOR
  - STARTED MAY 1983
  - 2 YEAR BASE PROGRAM/3 YEAR OPTIONAL PROGRAM

  - NAS 3-23925, SOUTHWEST RESEARCH INSTITUTE
  - U. LINDHOLM, PRINCIPAL INVESTIGATOR
  - STARTED MAY 1983
  - 2 YEAR BASE PROGRAM/3 YEAR OPTIONAL PROGRAM

IN-HOUSE HOST PROGRAMS

- FATIGUE LABORATORY UPGRADING PROGRAM
  - M. MCGAW, LERC PROGRAM MANAGER
  - MULTIYEAR EFFORT
  - - REMODELING OF LABORATORY
  - - MASTER/SLAVE COMPUTER SYSTEM
  - - BIAXIAL FATIGUE FACILITY
  - - LCF/HCF FACILITY

- SINGLE CRYSTAL DURABILITY PROGRAM
  - G. HALFORD, LERC PROGRAM MANAGER
  - MULTIYEAR EFFORT
  - JOINT EFFORT WITH MATERIALS DIVISION

CRACK PROPAGATION LIFE PREDICTION MODELING

- HIGH TEMPERATURE CRACK PROPAGATION

  T. ORANGE, LERC TECHNICAL PROGRAM MANAGER

  2 YEAR BASE PROGRAM/2 YEAR OPTIONAL PROGRAM

- CRACK GROWTH MECHANISMS

  J. SHANNON, LERC TECHNICAL PROGRAM MANAGER

  NAG 3-348, SYRACUSE UNIVERSITY

  PROF. H. LIU, PRINCIPAL INVESTIGATOR

  STARTED OCTOBER 1982

  3 YEAR GRANT PROGRAM

CRACK INITIATION LIFE PREDICTION AND CONSTITUTIVE MODELING

(ANISOTROPIC MATERIALS)

- LIFE PREDICTION AND MATERIAL CONSTITUTIVE BEHAVIOR FOR ANISOTROPIC MATERIALS

  R. BILL, LERC TECHNICAL PROGRAM MANAGER

  5 YEAR BASE PROGRAM/2 OPTIONAL PROGRAMS PARALLEL WITH BASE

- THEORETICAL CONSTITUTIVE MODELING OF ANISOTROPIC MATERIALS

  R. THOMPSON, LERC TECHNICAL PROGRAM MANAGER

  DUAL AWARDED PROGRAM

  NAG 3-XXX, UNIVERSITY OF CINCINNATI

  PROF. D. STOUFFER, PRINCIPAL INVESTIGATOR

  STARTED AUGUST 1983

  3 YEAR GRANT PROGRAM

  NAG 3-XXX, UNIVERSITY OF CONNECTICUT

  PROF. E. JORDAN, PRINCIPAL INVESTIGATOR

  STARTED SEPTEMBER 1983

  3 YEAR GRANT PROGRAM

Page intentionally left blank

CREEP FATIGUE LIFE PREDICTION FOR ENGINE HOT SECTION MATERIALS (ISOTROPIC)*

Vito Moreno
Pratt & Whitney Engineering
United Technologies Corporation

The presentation will summarize the activities performed during the first year of the NASA HOST Program, "Creep Fatigue Life Prediction for Engine Hot Section Materials (Isotropic)", being conducted by Pratt & Whitney Aircraft. The program is a 5-year, two part effort aimed at improving the high temperature crack initiation prediction technology for gas turbine hot section components. The two-year base program comprises the following tasks:

Task I - Material/Coating/Component Selection and Acquisition
Task II - Screen Candidate Life Prediction Approaches
Task III - Evaluate Best Candidate Life Prediction Approach
Task IV - Reporting

Significant results of the program produced thus far are listed below.

Task I - Material/Coating/Component Selection and Acquisition

1. Cast B1900 + Hf and wrought IN 718 were selected as the base and alternate materials, respectively.

2. A single heat of B1900 + Hf was obtained and test specimens fabricated.

3. The material was characterized with respect to grain size, γ' size, carbide distribution, and dislocation density.

4. Monotonic tensile and creep testing has shown engineering properties within anticipated scatter for this material.
5. Examination of the tensile tests has shown a transition from inhomogeneous "planar" slip within the grains at lower temperatures to more homogeneous matrix deformation.

6. Examination of the creep tests has shown a transgranular failure mode at 1400°F and an intergranular failure mode at 1600°F and 1800°F.

* NASA Contract NAS3-23288

Task II - Screen Candidate Life Prediction Approaches

1. A study was conducted to investigate the effects of test specimen geometry and fabrication process on fatigue life. As a result, axial strain controlled specimens were designed with a smooth (no extensometer ridges) gage section and fabricated using centerless grinding followed by light electropolishing.

2. A fatigue test matrix was established to provide baseline data to define crack initiation life as a function of major variables and for life prediction model evaluation. A total of 43 fully reversed strain controlled fatigue tests have been completed. Major variables investigated were temperature [871°C(1600°F) vs 538°C(1000°F)], strain range and strain rate.

3. Examination of specimens during testing indicated that measurable 76mm((.030 in.) surface cracks appear early in the specimen life i.e., 15% of total life at 871°C(1600°F) and 50% of life at 538°C(1000°F). This has been used as the definition of crack initiation for the initial model evaluation work.

4. Observed crack initiation sites are all surface initiated and associated with either grain boundary carbides or local porosity. The initiation life is not significantly affected by the character of the site.

5. Transgrannular cracking is observed at the initiation site for all conditions tested.

6. Grain dislocation structure is significantly less than that observed in monotonic tensile or creep tests.

7. A ranking procedure for evaluation of the prediction models has been established. The procedure assigns a numerical score based on the amount of data required, the predictive capability and the adaptability to engine relevant loading conditions for each model considered.

Task III - Evaluate Best Candidate Life Prediction Approach

1. Life prediction models representative of macroscopic (Coffin-Manson) and microscopic (Damage-Rate) approaches were selected for preliminary evaluation using the model ranking procedure developed in Task II.

2. Using limited data obtained at 871°C(1600°F)-(2 strain rates) and 538°C(1000°F)-(1 strain rate), the macroscopic approach obtained a higher overall score on the basis of data requirements and predictive capability.

CONSTITUTIVE MODELING FOR ISOTROPIC MATERIALS

A. Kaufman
National Aeronautics and Space Administration
Lewis Research Center
Cleveland, Ohio

Under HOST Contract NAS3-23288, crack initiation life prediction methods will be developed for hot section components fabricated from isotropic materials. To apply these methods it is first necessary to determine the component structural response, specifically the stress-strain history at the critical cracking location. The structural analysis method must be capable of accounting for cyclic thermomechanical loading, plastic flow during thermal transients, creep and stress relaxation during steady-state operation and inelastic strain ratchetting and reversal due to repeated flight cycles.

In recent years, nonlinear finite element computer codes such as ANSYS and MARC have become available for cyclic analysis of components involving inelastic strains. These codes are based on classical plasticity theory and use separate creep constitutive models. The classical methods utilize simplifying assumptions for computational convenience. Among these assumptions are the definition of a specific yield surface with associated flow rules and hardening models and the uncoupling of time-independent (plastic) and time-dependent (creep) inelastic strain effects. That these classical methods and their assumptions do not realistically represent superalloy material behavior under cyclic loading have been demonstrated in two pre-HOST programs (the turbine blade durability study reported in NASA CR-165268 and the combustor liner durability study reported in NASA CR-165250).

The objective of this program is to develop a unified constitutive model for finite-element structural analysis of turbine engine hot section components. This effort constitutes a different approach for nonlinear finite-element computer codes which have heretofore been based on classical inelastic methods. A unified constitutive theory will avoid the simplifying assumptions of classical theory and should more accurately represent the behavior of superalloy materials under cyclic loading conditions and high temperature environments. Model development will be directed toward isotropic, cast nickel-base alloys used for aircooled turbine blades and vanes. The Contractor will select a Base Material for model development and an Alternate Material for verification purposes from a list of three alloys specified by NASA. The candidate alloys represent a cross-section of turbine blade and vane materials of interest to both large and small size engine manufacturers. Material stock for the Base and Alternate Materials will be supplied to the Contractor by the Government.

The contractual effort will be conducted in two phases, a Basic Program of two years duration and an optical follow-on program also of two years duration. In the Basic Program, a unified constitutive model will be developed for the prediction of the structural response of isotropic materials for the temperatures and strain ranges characteristic of cooled turbine vanes in advanced gas turbine engines. The constitutive model will be implemented in an existing finite-element computer code or a new code specifically developed for unified models. An evaluation will be made of the capability of the analytical method to predict structural response for multiaxial stress states and nonisothermal conditions by conducting thermomechanical loading and benchmark

notch verification experiments and analyses. As a final evaluation of the analytical methods, a structural analysis will be performed for a hot section component fabricated of the Base Material for simulated engine operating conditions. In the Optical Program further development will be undertaken to consider thermal history effects and to correct any deficiencies indicated in the constitutive model or in the computational algorithms in the code. In addition, the constitutive model development will be verified for an alternate material.

This program will be conducted under a dual effort by the General Electric Company and Southwest Research Institute. The principal investigators are Dr. J. H. Laflen for General Electric and Dr. U. S. Lindholm for Southwest Research Institute. Successful completion of this program will result in a significant advance in structural analysis capabilities for gas turbine engine hot section components. These improvements in the structural analysis tools should result in better life prediction capability and greater hot section durability for the next generation of gas turbine engines.

CONSTITUTIVE MODEL REQUIREMENTS

- AVOID SIMPLIFICATIONS OF CLASSICAL THEORY (YIELD SURFACE, UNCOUPLED CREEP-PLASTIC STRAINS)
- APPLICABLE TO STRAIN-TEMPERATURE RANGES AT CRITICAL LOCATIONS OF TURBINE BLADES AND VANES
- CAPABLE OF REPRESENTING INELASTIC RESPONSE DURING TRANSIENT AND STEADY-STATE ENGINE OPERATION
- REASONABLE MATERIAL TESTING REQUIREMENTS
- PRACTICAL FOR IMPLEMENTATION IN NONLINEAR STRUCTURAL, FINITE-ELEMENT COMPUTER CODES

CONSTITUTIVE MODELING FOR ISOTROPIC MATERIALS

OBJECTIVE:

TO DEVELOP A UNIFIED CONSTITUTIVE MODEL FOR REPRESENTING CYCLIC INELASTIC BEHAVIOR OF ISOTROPIC CAST NICKEL-BASE ALLOYS USED FOR AIRCOOLED GAS TURBINE BLADES AND VANES

Page intentionally left blank

CONSTITUTIVE MODELING FOR ISOTROPIC MATERIALS

R.H. Van Stone
L.T. Dame
R.L. McKnight
J.H. Laflen
Aircraft Engine Business Group
General Electric Company

The inelastic finite element analytic model that is chosen for a particular type of numerical analysis of material behavior represents a compromise between (1) the requirements of physical versimilitude, (2) mathematical accuracy and stability, and (3) computational convenience and economy. In the past, the mathematical and computational problems have been so dominant that most analysts have been content to adopt simple uncoupled material models. Plasticity has been represented by an engineering stress-strain curve, monotonic or cyclic, and creep by a relatively uncomplicated power law equation.

It is well known that the simplest uncoupled material models ignored many of the more complex, well documented, types of high temperature material behavior: inelastic recovery, cyclic creep, strain rate effects, and thermomechanical (simultaneous temperature and load variation) effects on material response. Recent work has evolved constitutive theories which contain representations for various combinations of these effects. Frequently these models do not make the classical assumption which separates the analytical treatment of time dependent and time independent inelastic strains. These methods are generally referred to as unified theories. It will be the purpose of this program to thoroughly evaluate such methods for application to typical isotropic cast nickel base superalloys used for air-cooled turbine blades and vanes.

This objective will be accomplished through a two year combined analytical and experimental program. During this nine-task program, a nonlinear finite element program will be developed which contains at least two selected constitutive theories. These models will be evaluated using smooth thin-walled uniaxial Rene' 80 specimens. These experiments will be selected for both determining material constants and for verification purposes. Further experimental work on more complicated specimen geometries will be used to select the most promising constitutive model and to develop efficient numerical algorithims for the nonlinear finite element code. These additional experiments will involve multiaxial states of stress and a notch specimen geometry subjected to a variety of loading conditions. The finite element computer program will be additionally demonstrated by modeling an actual hot path component such a turbine blade or vane.

Work on this program commenced in May of 1983, and as such most of the efforts have gone toward defining the experimental plan. This includes the selection of the base (Rene' 80) and alternate (Mar-M-247) materials; development of the test matrix for all of the base program tasks; and selection of the specimen geometries for the uniaxial, multiaxial, and notched specimen experiments. Various unified constitutive theories which were identified through a literature search are currently under review. A series of criteria have been developed for selecting the preferred theories which will be further investigated during later tasks.

Page intentionally left blank

CONSTITUTIVE MODELING FOR ISOTROPIC MATERIALS*

Ulric S. Lindholm
Southwest Research Institute
San Antonio, TX 78284

The objective of this program is to develop a unified constitutive model for finite-element structural analysis of turbine engine hot section components. This effort constitutes a different approach for nonlinear finite-element computer codes which have heretofore been based on classical inelastic methods. A unified constitutive theory will avoid the simplifying assumptions of classical theory and should more accurately represent the behavior of superalloy materials under cyclic loading conditions and high temperature environments. Model development will be directed toward isotropic, cast nickel-base alloys used for air-cooled turbine blades and vanes. Recent studies have shown that this approach to the modeling of material behavior is particularly suited for determining the cyclic behavior of superalloy type blade and vane materials and is entirely compatible with three dimensional inelastic finite element formulations. More efficient and accurate inelastic analysis of hot section components - turbine blades, turbine vanes, combustor liners and seals - fabricated from "age hardenable" isotropic superalloy materials will be realized as the result of this activity. The final constitutive model, programmed in a stand-alone module suitable for incorporation in a general purpose structural analysis program, will be provided by Southwest Research Institute (SwRI) with the assistance of Pratt and Whitney Aircraft (PWA) as a principal subcontractor.

The program will be conducted in two phases. A basic program (Tasks A through I) and an optional follow-on program (Tasks J through M). In the Basic Program of twenty six months' duration a unified constitutive model will be developed for the prediction of the structural response of isotropic materials for temperatures and strain range characteristics of cooled turbine vanes in advanced gas turbine engines (Task A). A data base of uniaxial and multiaxial material properties required for the constitutive model development will be obtained for the base material (Tasks C and E). The constitutive model will then be incorporated into a finite-element computer code (Task D). An evaluation will be made of the capability of the analytical method to predict the structural response for multiaxial stress states (Task E) and nonisothermal conditions by conducting thermomechanical loading and benchmark notch verification experiments and analysis (Task F). As a final evaluation of the analytical model, a structural analysis will be performed for a hot section component fabricated from the base material for simulated engine operating conditions (Task G). In the optional program material property test procedures will be further developed to minimize the amount of testing

*Contract NAS3-23925.

required, and to study the possibility for estimating the material model constants from conventional property data (Task J). Further development of the model will be undertaken to consider thermal history effects and to correct any deficiencies indicated in the model or the computational algorithms in the code (Task K). In addition the constitutive model development will be verified for an alternate material (Task L).

Technical progress to date has concentrated on a review and screening of candidate constitutive models (Task A) and the fabrication of test specimens (Task B). The discussion below will concentrate on the formulation of unified constitutive theories. Test specimen fabrication is underway with the two alloys selected for study; PWA Alloy B1900+Hf and MAR M-247.

The unified theories considered will be based on two primary premises: First, that the total strain or strain rate may be partitioned into two components,

$$\dot{\varepsilon}_{ij} = \dot{\varepsilon}_{ij}^{e} + \dot{\varepsilon}_{ij}^{p} \tag{1}$$

where all inelastic deformation is included in $\dot{\varepsilon}_{ij}^{p}$ which is additive with the elastic strain rate. There is no further partitioning, e.g., between plasticity and creep. A second important premise is that both components of strain rate are continuous, non-zero functions of stress; i.e., there is no partitioning of stress space between purely elastic and elastic-plastic or elastic-viscoplastic regions as is typical of classical theories in plasticity. The latter premise results in computational efficiency since a single set of continuous equations can be integrated throughout loading, unloading, reverse loading and all other complex histories including strain rate and temperature variations. The classical yield criteria (plastic potential) and associated flow rule are replaced by evolutionary equations for a finite set of internal variables describing the progression of work hardening and recovery processes.

Most theories utilize one of four variations on the basic Prandtl-Reuss flow law. These are

$$\dot{\varepsilon}_{ij}^{p} = \lambda_1 \frac{\partial f}{\partial s_{ij}} \tag{2}$$

$$\dot{\varepsilon}_{ij}^{p} = \lambda_2 (s_{ij} - \Omega_{ij}) \tag{3}$$

$$\dot{\varepsilon}_{ij}^{p} = \lambda_3 s_{ij} \tag{4}$$

and

$$\dot{\varepsilon}_{ij}^{p} = \lambda_{ijkl} s_{kl} \tag{5}$$

Eq. 2 is in the form utilizing a flow potential $f = f(s_{ij}, \Omega_{ij}, K, T)$ with a limiting surface, f = constant, bounding elastic behavior. Eqs. 3-5 are unified theories without a yield surface. In Eqs. 3 and 4, λ is a scalar variable encorporating both isotropic and anisotropic variables. Most theories also employ the kinematic hardening tensor Ω_{ij}, often referred to as a "back" stress or "equilibrium" stress. An alternate approach to describe anisotropic hardening is the generalization of the isotropic flow law, Eq. 4, to the anisotropic case, Eq. 5. This latter form is relatively undeveloped.

A second basic feature of most constitutive models is the functional form selected for the kinematic relationship between plastic strain rate and stress or their invarients, $D_2^P = \dot{\varepsilon}_{ij}^P \dot{\varepsilon}_{ij}^P$, and $J_2 = (s_{ij}-\Omega_{ij})(s_{ij}-\Omega_{ij})$. Three typical examples found in the literature are given below and plotted in Figure 1.

$$D_2^P = A\,(J_2/K^2)^n \tag{6}$$

$$D_2^P = D_o^2 \exp\left[-\left(\frac{K^2}{J_2}\right)^n\right] \tag{7}$$

$$D_2^P = B\left[\sinh\,(J_2/K^2)^m\right]^n \tag{8}$$

where K is a hardening variable and A, B, D_o, m and n are material constants (possibly temperature dependent). The values of m and n are the dominant variables governing strain rate sensitivity.

An additional general concern is the choice of a tracking parameter to follow hardening and recovery processes. This parameter must include history dependence. The two most commonly used are $\int \dot{\varepsilon}^P dt$ and $\int \dot{W}_p dt$, integrals over the plastic strain rate or the plastic work rate history. Differences lie in whether hardening occurs in the direction of the strain increment or the stress increment.

Comparison and evaluation of existing models is now underway with the objective of clarifying limitations and recommending improvements. Some examples of computations using unified theory for cyclic uniaxial and biaxial strain histories are given in Figures 2 and 3. Biaxial, nonproportional strain paths are particularly critical to the development of the evolutionary equations for hardening and recovery.

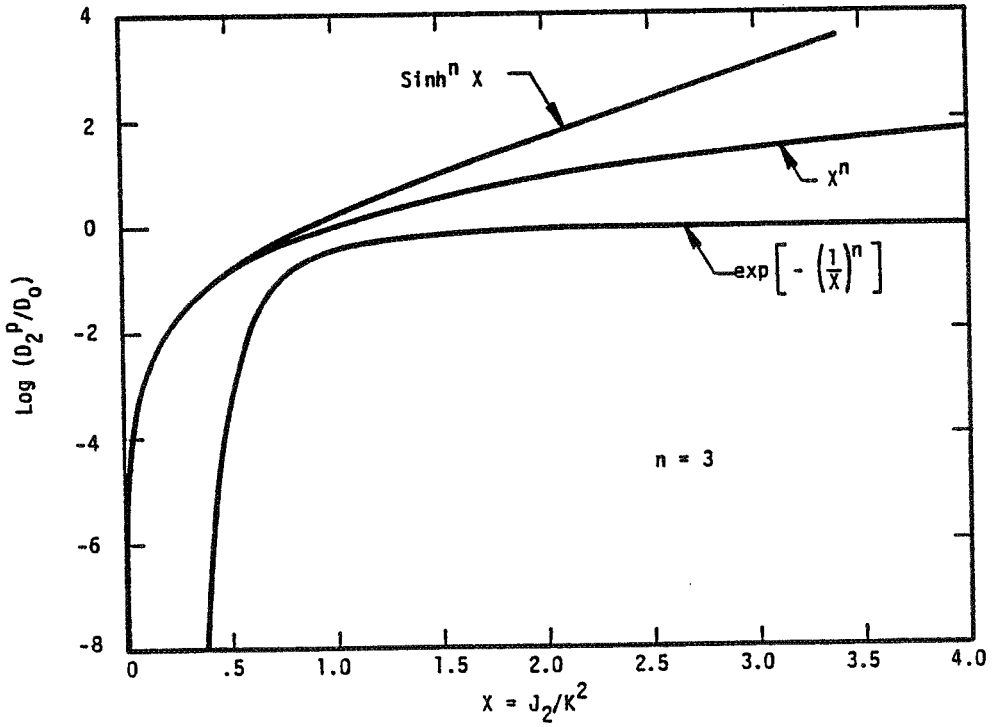

FIGURE 1. A COMPARISON OF THREE BASIC FORMS OF THE KINETIC EQUATION.

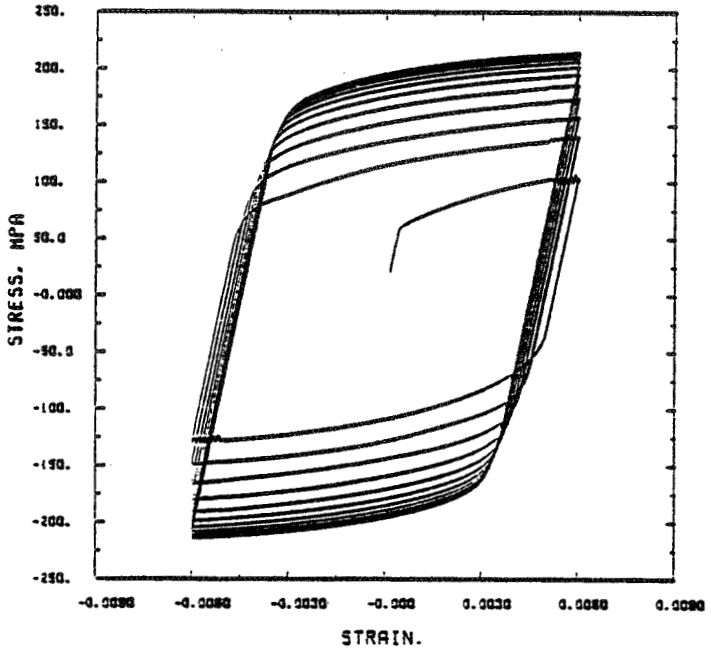

FIGURE 2. CYCLIC HARDENING RESPONSE FOR HASTELLOY X AT 1600F COMPUTED WITH UNIFIED THEORY.

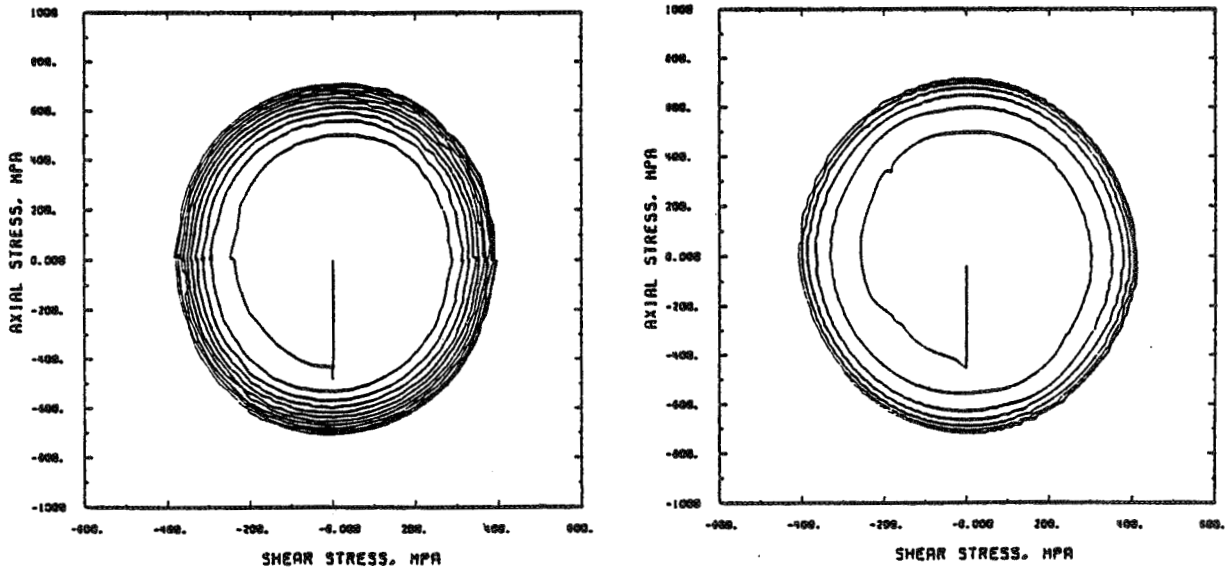

FIGURE 3. BIAXIAL HARDENING OF HASTELLOY X AT ROOM TEMPERATURE UNDER 90° OUT-OF-PHASE TENSION-TORSION STRAIN CYCLING, EXPERIMENT (LEFT) AND UNIFIED THEORY (RIGHT).

LIFE PREDICTION AND CONSTITUTIVE MODELS FOR ANISOTROPIC MATERIALS

Robert C. Bill
Propulsion Laboratory
AVRADCOM Research and Technology Laboratories
Lewis Research Center
Cleveland, Ohio

The trend toward improved engine efficiency and durability is placing increased demands on gas turbine materials, especially in the hot section. New materials and coatings are being developed to meet these demands. Turbine airfoil components present a particular challenge because they must survive in an especially hostile thermal, mechanical, and chemical environment. Here single crystal (SC) and directionally solidified or recrystallized (DSR) polycrystalline materials are finding application because of their inherently superior resistance to high temperature deformation and failure, compared to conventionally cast materials. Difficulties impeding the full implementation of SC or DSR materials include the limited knowledge and understanding of failure (crack initiation) mechanisms and constitutive behavior.

The objective of this program is to develop practical life prediction and constitutive behavior models for anisotropic SC and DSR materials employed in turbine airfoils. Though emphasis will be placed on the development of widely applicable models (not material specific), experimental work will focus primarily on SC and DSR materials that are likely candidates for service in the near future.

The program is divided into a base program and two options. The base program is concerned with single crystal materials under conditions pertinent to first stage turbine airfoil applications. Coating effects on airfoil durability and constitutive response are an important part of the base program. Option one will address the problem of single crystal blade root attachment, including the effects of attachment geometric features,

temperatures in the blade root area, and the type of loading encountered. The second option includes airfoil and blade root attachment considerations for DSR materials.

Upon completion of the program, generally applicable analytical models describing the time dependent cyclic stress-strain response, and models needed for life prediction and durability assessment of anisotropic materials will be available to the gas turbine design community. These models will be incorporated into a sophisticated structural analysis code available to the public.

CAST TURBINE BLADE MATERIALS

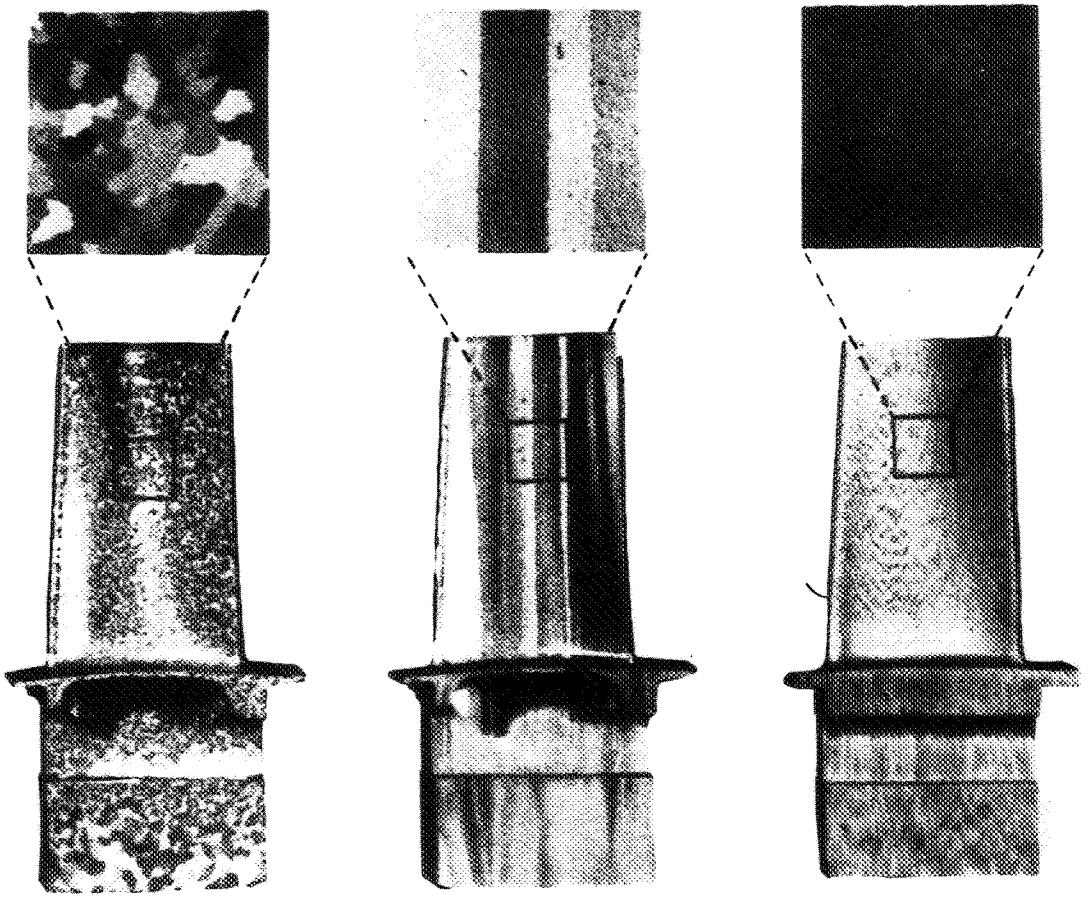

CONVENTIONALLY CAST

DIRECTIONALLY SOLIDIFIED

SINGLE CRYSTAL

CONTRACT:

CYCLIC CONSTITUTIVE MODELING AND LIFE PREDICTION METHODS FOR ANISOTROPIC MATERIALS

OBJECTIVE:

DEVELOP AND VERIFY CYCLIC MATERIALS CONSTITUTIVE MODELS AND LIFE PREDICTION METHODS FOR COMPONENT SPECIFIC ANISOTROPIC MATERIALS FOR USE IN STRUCTURAL ANALYSIS COMPUTER PROGRAMS

DURATION:

5 YEAR, 35 MAN-YEAR EFFORT

PROGRAM STRUCTURE: THREE PHASE PROGRAM

- BASE PROGRAM - COATED SC AIRFOILS
- OPTION 1 - UNCOATED SC BLADE ROOTS
- OPTION 2 - DSR MATERIALS

APPROACH:

- SELECT MATERIALS AND COATINGS
- SCREEN ADVANCED CONSTITUTIVE AND LIFE PREDICTION MODELS; SELECT BEST
- INTEGRATE MODELS WITH STRUCTURAL ANALYSIS PROGRAMS
- VERIFY IN SIMULATED COMPONENT TEST

PROGRAM WILL ADDRESS:

- CREEP-FATIGUE
- THERMOMECHANICAL FATIGUE
- ORIENTATION EFFECTS
- COATING/SUBSTRATE INTERACTIONS
- BIAXIAL LOADING
- ATTACHMENT STRESS CONCENTRATIONS

BASE PROGRAM

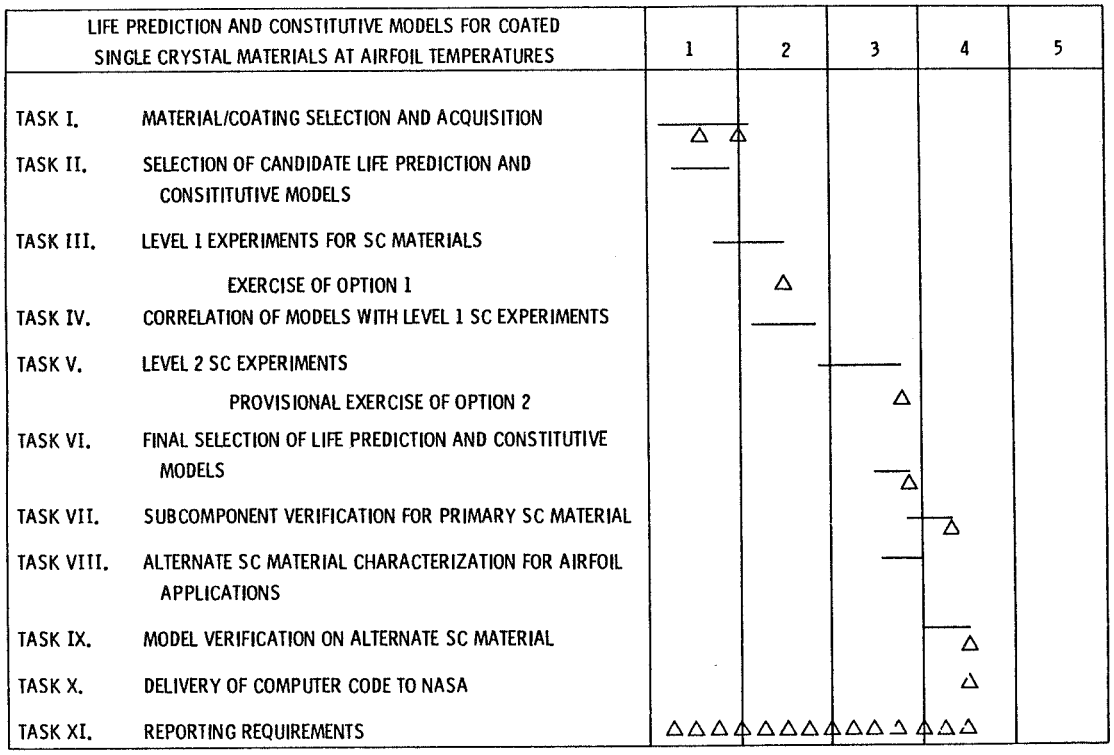
LIFE PREDICTION AND CONSTITUTIVE MODELS FOR COATED SINGLE CRYSTAL MATERIALS AT AIRFOIL TEMPERATURES
1
2
3
4
5
TASK I. MATERIAL/COATING SELECTION AND ACQUISITION
TASK II. SELECTION OF CANDIDATE LIFE PREDICTION AND CONSITITUTIVE MODELS
TASK III. LEVEL 1 EXPERIMENTS FOR SC MATERIALS
EXERCISE OF OPTION 1
TASK IV. CORRELATION OF MODELS WITH LEVEL 1 SC EXPERIMENTS
TASK V. LEVEL 2 SC EXPERIMENTS
PROVISIONAL EXERCISE OF OPTION 2
TASK VI. FINAL SELECTION OF LIFE PREDICTION AND CONSTITUTIVE MODELS
TASK VII. SUBCOMPONENT VERIFICATION FOR PRIMARY SC MATERIAL
TASK VIII. ALTERNATE SC MATERIAL CHARACTERIZATION FOR AIRFOIL APPLICATIONS
TASK IX. MODEL VERIFICATION ON ALTERNATE SC MATERIAL
TASK X. DELIVERY OF COMPUTER CODE TO NASA
TASK XI. REPORTING REQUIREMENTS

OPTION 1

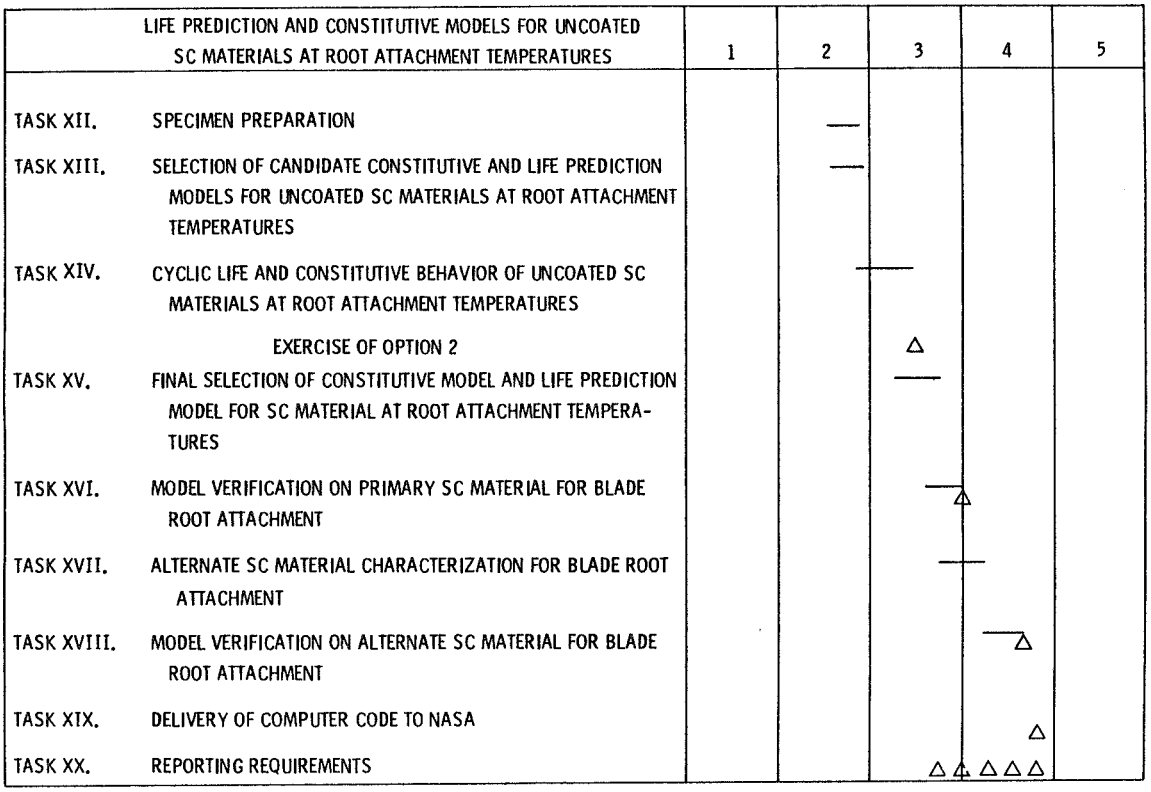
LIFE PREDICTION AND CONSTITUTIVE MODELS FOR UNCOATED SC MATERIALS AT ROOT ATTACHMENT TEMPERATURES
1
2
3
4
5
TASK XII. SPECIMEN PREPARATION
TASK XIII. SELECTION OF CANDIDATE CONSTITUTIVE AND LIFE PREDICTION MODELS FOR UNCOATED SC MATERIALS AT ROOT ATTACHMENT TEMPERATURES
TASK XIV. CYCLIC LIFE AND CONSTITUTIVE BEHAVIOR OF UNCOATED SC MATERIALS AT ROOT ATTACHMENT TEMPERATURES
EXERCISE OF OPTION 2
TASK XV. FINAL SELECTION OF CONSTITUTIVE MODEL AND LIFE PREDICTION MODEL FOR SC MATERIAL AT ROOT ATTACHMENT TEMPERATURES
TASK XVI. MODEL VERIFICATION ON PRIMARY SC MATERIAL FOR BLADE ROOT ATTACHMENT
TASK XVII. ALTERNATE SC MATERIAL CHARACTERIZATION FOR BLADE ROOT ATTACHMENT
TASK XVIII. MODEL VERIFICATION ON ALTERNATE SC MATERIAL FOR BLADE ROOT ATTACHMENT
TASK XIX. DELIVERY OF COMPUTER CODE TO NASA
TASK XX. REPORTING REQUIREMENTS

OPTION 2

LIFE PREDICTION AND CONSTITUTIVE MODELS FOR DSR MATERIALS		1	2	3	4	5
TASK XXI.	DSR SPECIMEN PREPARATION AND MATERIAL CHARACTERIZATION			△		
TASK XXII.	SELECTION OF CANDIDATE LIFE PREDICTION AND CONSTITUTIVE MODELS FOR DSR MATERIALS					
TASK XXIII.	CREEP-FATIGUE EXPERIMENTS FOR COATED DSR MATERIAL AT AIRFOIL TEMPERATURES					
TASK XXIV.	STRESS-STRAIN EXPERIMENTS FOR UNCOATED DSR MATERIALS AT ROOT ATTACHMENT TEMPERATURES					
TASK XXV.	FINAL SELECTION OF LIFE PREDICTION AND CONSTITUTIVE MODELS FOR DSR MATERIALS					△
TASK XXVI.	MODEL VERIFICATION FOR DSR MATERIALS AT AIRFOIL TEMPERATURES					
TASK XXVII.	MODEL VERIFICATION FOR UNCOATED DSR MATERIALS AT ROOT ATTACHMENT TEMPERATURES					
TASK XXVIII.	DELIVERY OF DSR MATERIAL COMPUTER CODES TO NASA					△
TASK XXIX.	REPORTING REQUIREMENTS			△△	△△△	△△△△

BASE PROGRAM - COATED SC MATERIALS

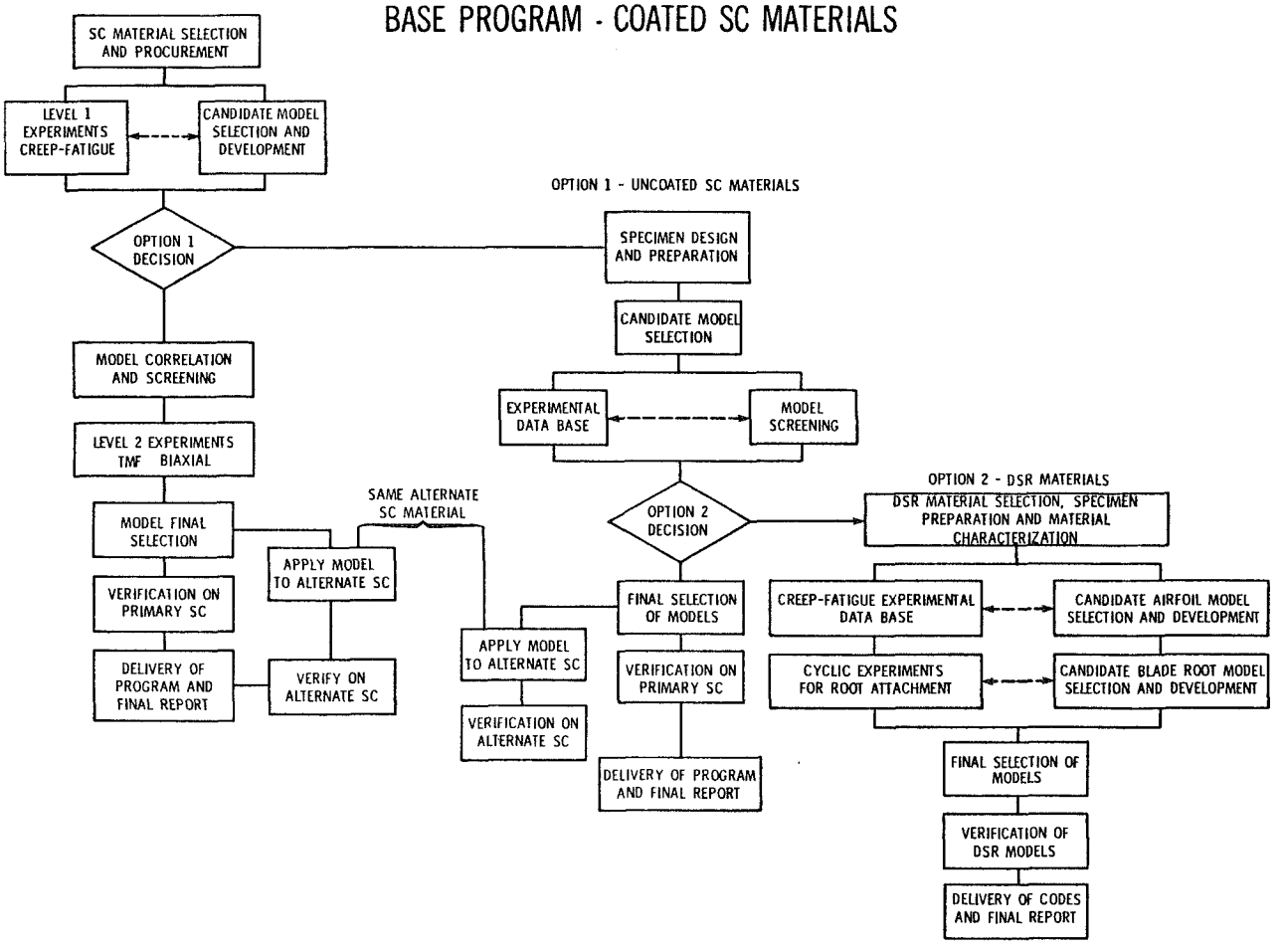
SC MATERIAL SELECTION AND PROCUREMENT
LEVEL 1 EXPERIMENTS CREEP-FATIGUE
CANDIDATE MODEL SELECTION AND DEVELOPMENT
OPTION 1 DECISION
OPTION 1 - UNCOATED SC MATERIALS
SPECIMEN DESIGN AND PREPARATION
CANDIDATE MODEL SELECTION
EXPERIMENTAL DATA BASE
MODEL SCREENING
MODEL CORRELATION AND SCREENING
LEVEL 2 EXPERIMENTS TMF BIAXIAL
MODEL FINAL SELECTION
SAME ALTERNATE SC MATERIAL
APPLY MODEL TO ALTERNATE SC
VERIFICATION ON PRIMARY SC
DELIVERY OF PROGRAM AND FINAL REPORT
VERIFY ON ALTERNATE SC
APPLY MODEL TO ALTERNATE SC
VERIFICATION ON ALTERNATE SC
OPTION 2 DECISION
OPTION 2 - DSR MATERIALS
DSR MATERIAL SELECTION, SPECIMEN PREPARATION AND MATERIAL CHARACTERIZATION
FINAL SELECTION OF MODELS
VERIFICATION ON PRIMARY SC
DELIVERY OF PROGRAM AND FINAL REPORT
CREEP-FATIGUE EXPERIMENTAL DATA BASE
CANDIDATE AIRFOIL MODEL SELECTION AND DEVELOPMENT
CYCLIC EXPERIMENTS FOR ROOT ATTACHMENT
CANDIDATE BLADE ROOT MODEL SELECTION AND DEVELOPMENT
FINAL SELECTION OF MODELS
VERIFICATION OF DSR MODELS
DELIVERY OF CODES AND FINAL REPORT

Surface Protection Overview

Stanley R. Levine
National Aeronautics and Space Administration
Lewis Research Center

Among the factors that must be considered in the design of turbine engine hot section components is the ability of the materials to withstand the environment at the design conditions of life, temperature and loads. In some instances the design envelope is governed by the environmental resistance of available alloys and coatings. The environmental attack processes of concern, oxidation and hot corrosion are illustrated schematically in Figure 1. The progress of these processes can by accelerated by particulate erosion. In the oxidation process, the less noble alloy constituents react to form oxides. These oxide scales may then spall as a result of thermal cycling. To combat the process, slow growing, adherent, non-volatile oxide scales such as alumina, Al_2O_3, are most desirable. In the hot corrosion process condensed salts formed from air or fuel impurities cause accelerated attack by penetration of the oxide scale via defects or by fluxing the oxide scale. Again, the best defense is the formation of a slow-growing, adherent scale that is not reactive with the condensed salt. As illustrated in Figure 2, the hot corrosion process can by more destructive than the oxidation process in spite of the fact that hot corrosion generally occurs below temperatures at which oxidation is a concern. The environmental attack processes can by quite destructive as illustrated in Figure 3. Here, the first stage vanes of a turboprop aircraft have been severely hot corrosion attacked. At earlier stages of this attack aerodynamic efficiency was no doubt impaired. Environmental attack can also disrupt the effectiveness of airfoil cooling designs by changing the dimensions or plugging passages via deposition or scale formation. In gas turbines where the gas temperature can exceed the alloy melting point, the consequences of cooling system breakdown can be severe.

Environmental attack can also be insidious, but equally destructive. For example, oxidation or hot corrosion can play a significant role in crack initiation and growth. Finally, the design envelope expanding metallic or ceramic coatings display mechanical properties that are very different from the structural alloys they protect. Thus, the mechanical behavior of these coatings, particularly with regard to creep and crack initiation and growth, must be considered by the designer.

To summarize, to adequately predict the consequences of environmental attack we must be able to predict salt deposition, the kinetics of oxidation and hot corrosion attack, the depletion of coatings via reaction with substrates and the effects of environmental attack and coatings on system mechanical response.

The objective of the HOST surface protection effort is to develop a first-cut integrated environmental attack life prediction methodology for hot section components. The program elements and the expected results are described in Figure 4. Environmental/mechanical property interaction is a joint effort involving the Fatigue and Fracture, Surface Protection, and Metallic Materials Branches. The airfoil deposition model effort resides in the High-Temperature Chemistry Section while the coating life prediction effort is primarily concentrated in the Surface Protection Section, both part of the Materials Durability Branch.

Further details of the surface protection effort are given in Figure 5. Those efforts which have been active through most of the previous year are reported by the principal investigators in this workshop. The primary new efforts for the coming year are the initiation of thermal barrier coating life prediction and dual cycle attack and procurement initiation for metallic coating life prediction verification.

SCHEMATIC OF MODES HIGH-TEMPERATURE ATTACK

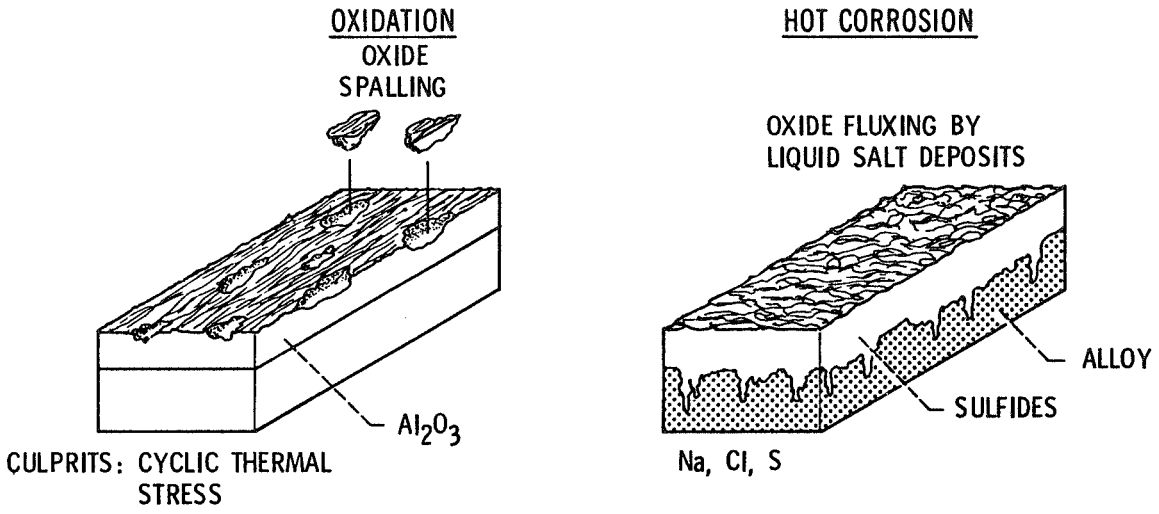

SCHEMATIC OF HOT SECTION COMPONENT LIFE CONTROLLING FACTORS

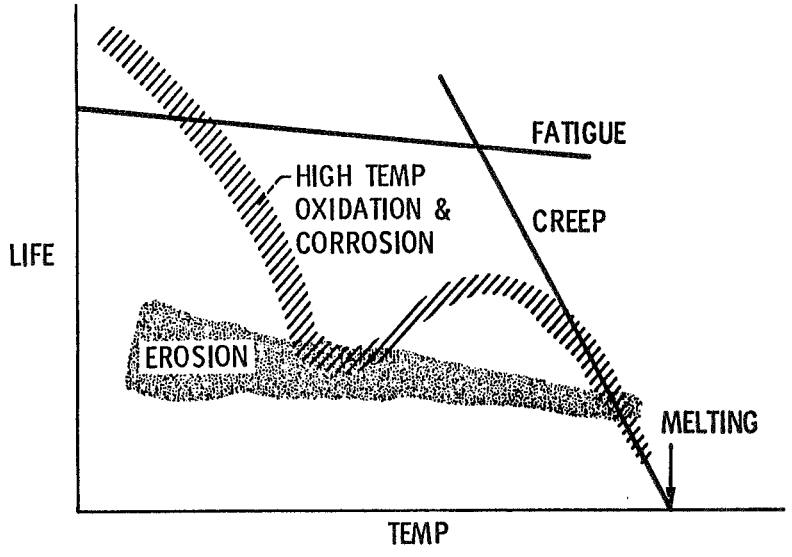

HIGH TEMPERATURE ENVIRONMENTAL ATTACK

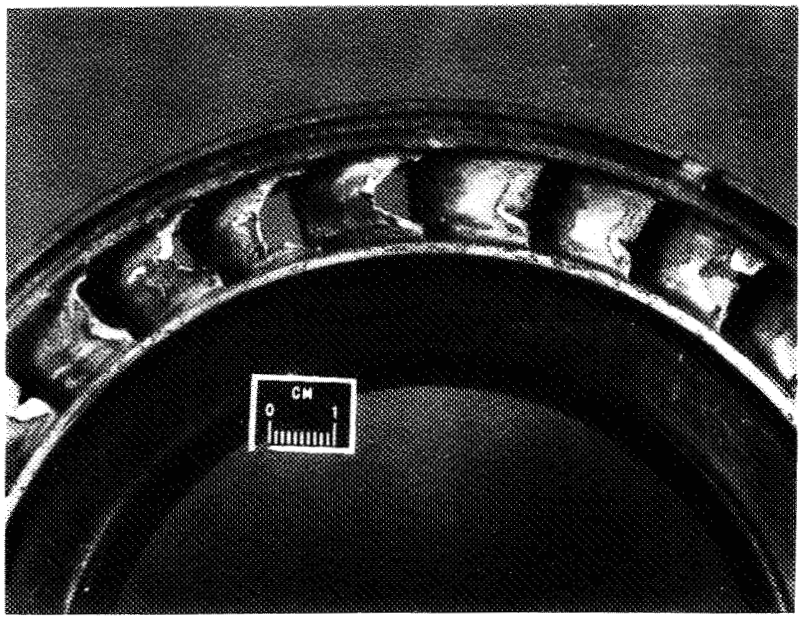

- REDUCES EFFICIENCY
- LIMITS LIFE
- COSTS $

SURFACE PROTECTION

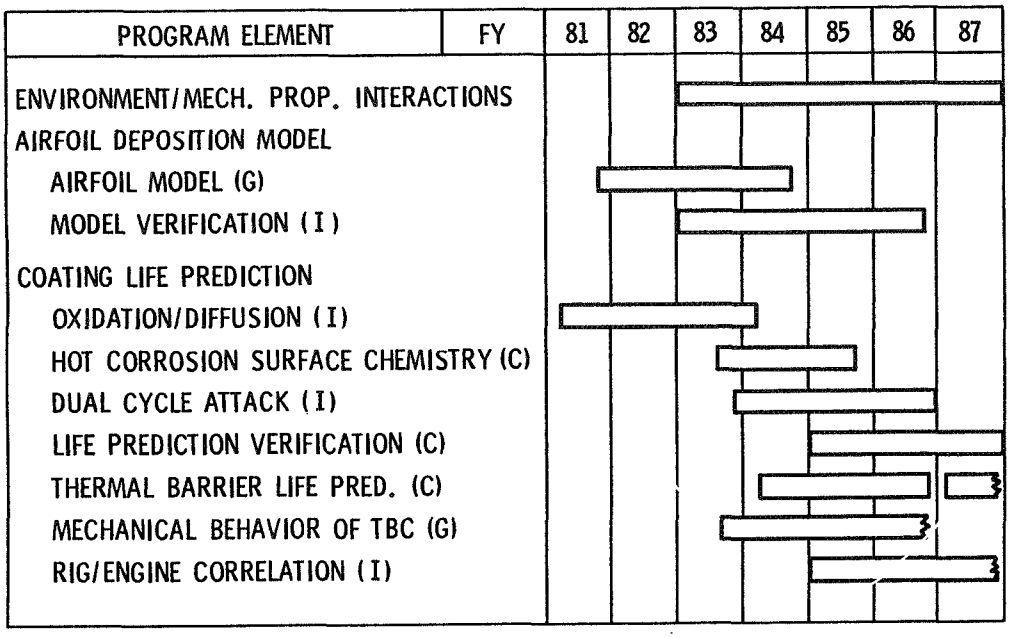

SURFACE PROTECTION

PROGRAM ELEMENT	FY81	82	83	84	85	86	87	EXPECTED RESULTS
ENVIRONMENT/MECHANICAL PROPERTY INTERACTIONS (TASKS OF C/F CONTRACTS)								MODEL FOR EFFECTS OF ENVIR. ATTACK& COATINGS ON CRACK INITIATION
AIRFOIL DEPOSITION MODEL								MODEL TO PREDICT THE LOCATION & POTENTIAL SEVERITY OF CORROSION/ ATTACK OF TURBINE AIRFOILS
COATING LIFE PREDICTION								CAPABILITY TO PREDICT COATING DEGRADATION ON BLADES, VANES, COMBUSTORS

Page intentionally left blank

TURBINE AIRFOIL DEPOSITION MODELS*

Daniel E. Rosner
Yale University
Department of Chemical Engineering

1. INTRODUCTION, OUTLINE

Gas turbine failures associated with sea-salt ingestion and sulfur-containing fuel impurities have directed attention to alkali sulfate deposition and the associated "hot corrosion" of gas turbine (GT) blades under some GT operating conditions. These salts deposit and form thin molten films which can undermine the protective metal oxide coating normally found on GT blades. This research project (fig. 1) deals with the prediction of molten salt deposition, flow and oxide dissolution, and their effects on the lifetime of critical turbine blades. Our goals include rationalizing and predicting corrosion patterns on operational GT rotors and stators, and, ultimately providing some of the "tools" required to design laboratory simulators and future corrosion-resistant high-performance engines.

2. DEPOSITION RATE THEORY

A necessary step in the complex sequence of events leading to hot corrosion failures is the deposition of the alkali salts from the combustion products onto turbine stator and rotor blades. A comprehensive but tractable method for predicting the rates of chemical vapor deposition (CVD) of, say, alkali sulfates from multicomponent salt-laden combustion products has accordingly been developed, illustrated, and tested (refs. 4,5,8). The theory predicts important effects of multicomponent diffusion, and thermal (Soret) diffusion (ref. 6) on dew points, CVD-rates and deposit compositions (ref. 7). For our present purposes, an important feature of the deposition rate is its dependence on surface temperature, shown in figure 2 for the case of K_2SO_4 vapor deposition (ref. 1). Note the existence of a "dew point" temperature (above which a macroscopic surface condensate is not stable) and a temperature-insensitive "plateau" deposition rate at temperatures sufficiently far below the dew point --i.e., features included in the abovementioned CVD-rate theory (see, e.g., refs. 4,5,7,8). While in its most general form allowance is made for the transport of each chemical species (i = 1,2, ...) containing the elements of interest (Na, S, ...) across the diffusion boundary layer (BL) (fig. 3), in order to study the dynamics of the resulting molten salt condensate layer (sections 3,4, below) we have exploited the single-component limiting form of the CVD theory to economically provide the spatial distribution of condensate "arrival" (see fig. 8, below). However, our approach also applies to the deposition rate of fine particles (refs. 9,10) — i.e., mist droplets small enough to behave like "heavy molecules" in the prevailing carrier gas flow field.

3. CONDENSATE LAYER DYNAMICS

An important process in the molten salt attack of GT blades is evidently the dissolution ("fluxing") of the normally protective metal oxide, and this, in turn, implies dynamic processes which allow dissolution/reaction to occur without "saturating" the molten salt "solvent." For these reasons, we have initiated studies of the dynamics of thin condensate liquid layers (ref. 11), allowing for the interplay of arrival rate (Section 2) and "run-off" induced by aerodynamic shear stress, τ_w (fig. 4) and blade rotation rate, Ω (fig. 5). These

*NAG3-201 :"Theory of Mass Transfer from Combustion Gases"

studies should ultimately prove useful in the interpretation of observed hot corrosion "maps" on blades removed from operational engines (Section 4). They have already guided the development and interpretation of laboratory "simulator" experiments (e.g., refs. 3,4,8) in which molten salt deposition and runoff necessarily occur.

In reference 11 the necessary liquid layer theory was developed and used to predict steady-state laminar condensate layers on smooth non-rotating, isothermal targets, with emphasis on the circular cylinder in high Reynolds number cross-flow. In our current studies, this approach has been extended to include the treatment of condensate layer flow along smooth non-isothermal rotor blades (fig. 5). Illustrative calculations are being made for a test turbine using the aerodynamic design data provided by Haas and Kofskey in NASA TP 1018 (1977). From the inviscid stream velocity data (fig. 6) we compute, using efficient integral methods, the corresponding distributions of gas-side momentum, heat- and mass-transfer coefficients, and the distribution of blade "recovery" temperature (used to estimate this root-cooled blade temperature distribution (shown in fig. 7 for the suction surface)). The corresponding condensate arrival rate distribution (fig. 8) and liquid viscosity distributions are then inserted into the partial differential equation (PDE) governing the liquid layer thickness δ_ℓ (x,z) (fig. 5). This nonlinear first order PDE is then numerically solved (by the method-of-characteristics) to provide the condensate layer streamline pattern (fig. 9), as well as the corresponding normalized liquid layer thickness $\delta_\ell(x,z)/\delta_\ell(0,0^+)$ (fig. 10). The absolute value of the root-nose liquid layer thickness, $\delta_\ell(0,0^+)$, is, of course, environment-(e.g., alkali-level) dependent, and is given by a simple explicit formula (derived in ref. 11) involving $-\dot{m}''(0,0^+)$ and $(\partial\tau_w/\partial x)_{x=0}$. Note that two byproducts of these calculations are a) the solvent "inventory" on the blade, and b) relative tip- and trailing edge salt runoff rates. The writer is indebted to his students, R. Nagarajan and S. Burke, for their assistance in generating these preliminary numerical results (figs. 6-10).

4. METAL OXIDE "DISSOLUTION" RATE DISTRIBUTIONS

Nonstoichiometric molten sodium sulfate is known to be a solvent for Al_2O_3 (s) or Cr_2O_3(s) --the oxides ordinarily relied upon for corrosion protection of the underlying blade alloys. Accordingly, the next step in this research program is prediction of the dissolution rate distributions associated with "solvent" flow patterns of the type described in Section 3. Indeed, it should be instructive to compare such predictions with hot corrosion rate patterns observed on blades removed from operational GT engines. Toward this end, estimates are first being made of the oxide diffusion coefficient in the solvent, equilibrium solubility, and maximum (kinetic) rate of dissolution. This information is then used to predict the solute diffusion-limited dissolution rate along each streamline (cf. fig. 9), using a generalization of Leveque-Levich BL-theory. Preliminary dissolution rate maps, now being obtained, will be checked, generalized, and discussed in terms of their parametric dependences, and agreement with operational experience.

5. IMPLICATIONS, FUTURE WORK

While much of the required input information remains to be tightened up, the present formalism is reaching the point where very instructive parametric studies can now be economically performed for both GT stator and rotor blades over a wide variety of environmental conditions (salt level, turbine inlet temperature, stagnation pressure level, blade contour and cooling, tip speed , etc.). Moreover, many aspects of the theory can now be generalized, including possibly mixed alkali deposits (ref. 7), partially "dry" and/or rough surfaces, condensate arrival by other (than vapor diffusion) mechanisms (refs. 9,10), and transient condensate flows. It may also be useful to examine the effects on localized dissolution rates of secondary flows, produced in part by surface tension gradients. Feedback and guidance from the participants of this interdisciplinary HOST Workshop will be especially welcome.

6. REFERENCES[†]

1. Rosner, D. E. and Atkins, R. M., "Experimental Studies of Salt/Ash Deposition Rates from Combustion Products Using Optical Techniques," Proc. Engrg. Foundation Int. Conf. Experimental Research Into Fouling and Slagging Due to Impurities in Combustion Gases (R. Bryers, ed.) Engineering Foundation (New York) 1983, 469-492.

2. Rosner, D. E. and Seshadri, K., "Experimental and Theoretical Studies of the Laws Governing Condensate Deposition from Combustion Gases," Eighteenth Int. Symposium on Combustion, The Combustion Inst. (Pittsburgh) 1981, 1385-1394.

3. Seshadri, K. and Rosner, D. E., "Optical Methods of Dew Point and Deposition Rate Measurement in Salt/Ash-Containing Combustion Gases —1. $B_2O_2(\ell)$ Deposition Rates by the Interference Method and Comparison with Theory," Amer. Inst. Chem. Engrs. (AIChE) J. (in press, 1983).

4. Kohl, F. J., Santoro, G. J., Stearns, C. A., Fryburg, G. C., and Rosner, D. E., "Theoretical and Experimental Studies of the Deposition of Na_2SO_4 from Seeded Combustion Gases," J. Electrochem. Soc., 126, 1054-1061 (1979).

5. Rosner, D. E., Chen, B. K., Fryburg, G. C., and Kohl, F. J., "Chemically Frozen Multicomponent Boundary Layer Theory of Salt and/or Ash Deposition Rates from Combustion Gases," Combustion Sci. and Technol., 20, 87-106 (1979).

6. Rosner, D. E., "Thermal (Soret) Diffusion Effects on Interfacial Mass Transport Rates," J. PhysicoChem. Hydrodynamics (Pergamon Press) 1, 159-185 (1980).

7. Rosner, D. E. and Nagarajan, R., "Transport-Induced Shifts in Condensate Dew Point and Composition in High Temperature Multicomponent Systems with Chemical Reaction," Chemical Engrg. Sci. (submitted, 1983).

8. Santoro, G. J., Kohl, F. J., Stearns, C. A., Rosner, D. E., and Gökoğlu, S., "Comparison of Experimental and Theoretical Deposition Rates from the Salt-Seeded Combustion Gases of a Mach 0.3 Burner Rig," NASA-TP 2225 (in press, 1983)

9. Gökoğlu, S. A. and Rosner, D. E., "Correlation of Thermophoretically-Modified Small Particle Deposition Rates in Forced Convection Systems with Variable Properties, Transpiration Cooling and/or Viscous Dissipation," Int. J. Heat and Mass Transfer Pergamon Press (in press, 1983).

10. Rosner, D. E., Gökoğlu, S. A., and Israel, R., "Rational Engineering Correlations of Diffusional and Inertial Particle Deposition Behavior in Non-isothermal Forced Convection Environments," Proc. Engrg. Foundation Int. Conf. on the Fouling of Heat Exchanger Surfaces (R. Bryers, ed.) (in press, 1983).

11. Rosner, D. E., Günes, D., and Anous, N., "Aerodynamically-Driven Condensate Layer Thickness Distributions on Isothermal Cylindrical Surfaces," Chem. Engin. Commun., 1347-1357 (1983).

[†]Preprints of references 3, 7, 9, 10, 11 are available via D. E. Rosner.

AIRFOIL DEPOSITION MODEL

GRANT NAG 3-201: "THEORY OF MASS TRANSFER FROM COMBUSTION GASES," WITH PROFESSOR D.E. ROSNER, ChE DEPARTMENT, YALE UNIVERSITY

EMPHASIS: TRACE SALT VAPOR DEPOSITION AND CORRESPONDING SHEAR-DRIVEN CONDENSATE LAYER FLOW

OBJECTIVE:

- OVERALL - DEVELOP MODEL TO PREDICT CORRODANT DEPOSITION ON TURBINE AIRFOILS
- 1ST YEAR - MODEL DEPOSITION RATE FOR SEVERAL SIMPLE GEOMETRIES
- 2ND YEAR - PREDICT AND DISPLAY LIQUID LAYER EVOLUTION ON TURBINE VANES AS A RESULT OF VAPOR DEPOSITION AND LIQUID LAYER FLOW

Figure 1

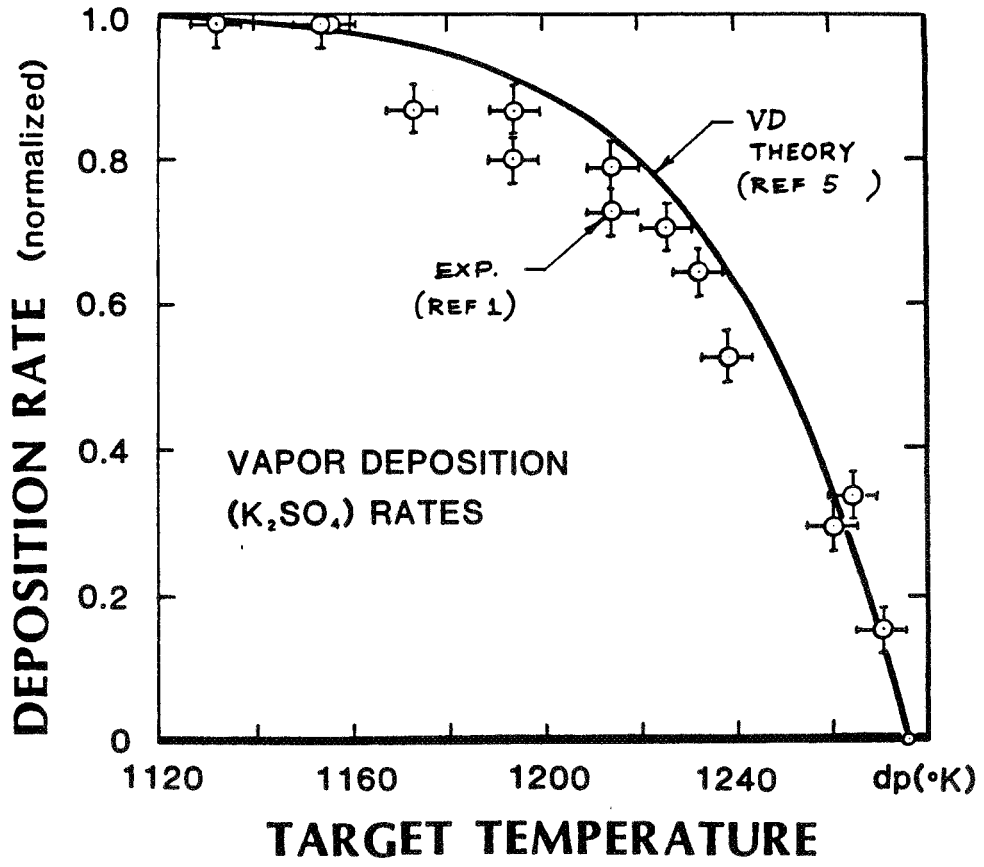

Figure 2

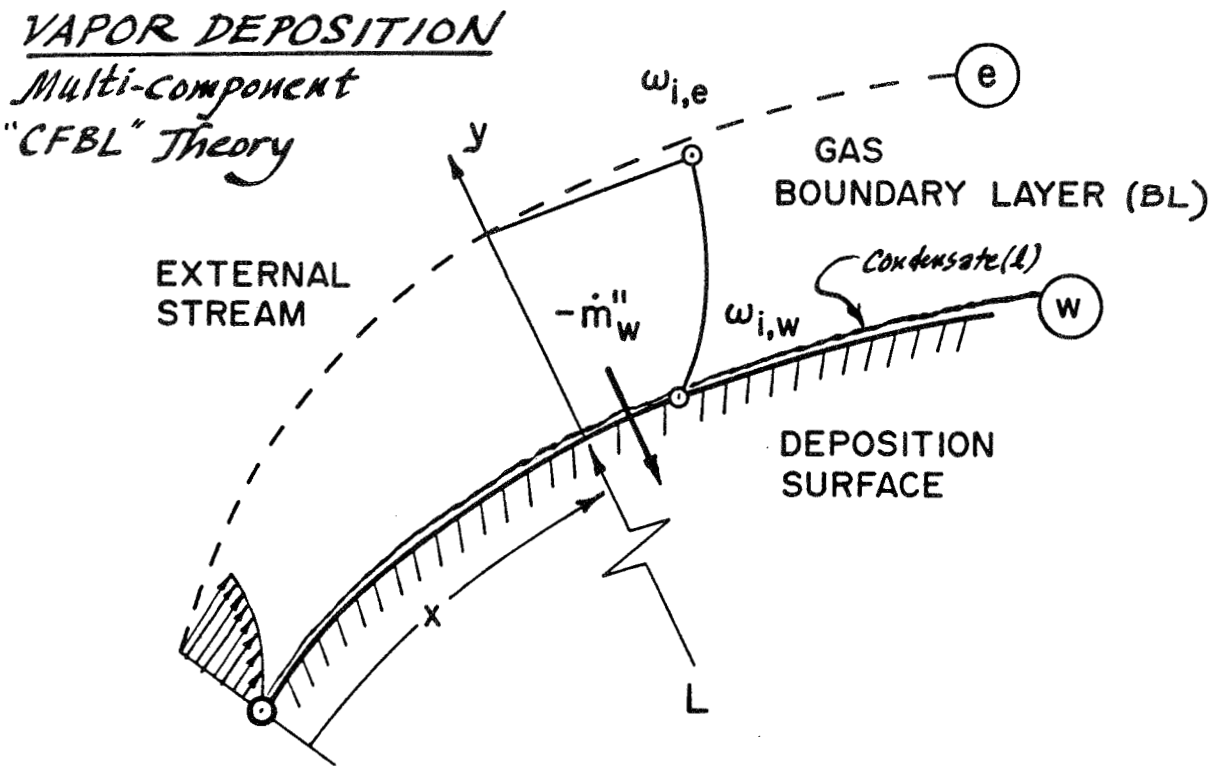

Figure 3

AERODYNAMICALLY-DRIVEN THIN CONDENSATE LAYER FLOW (REF 11)

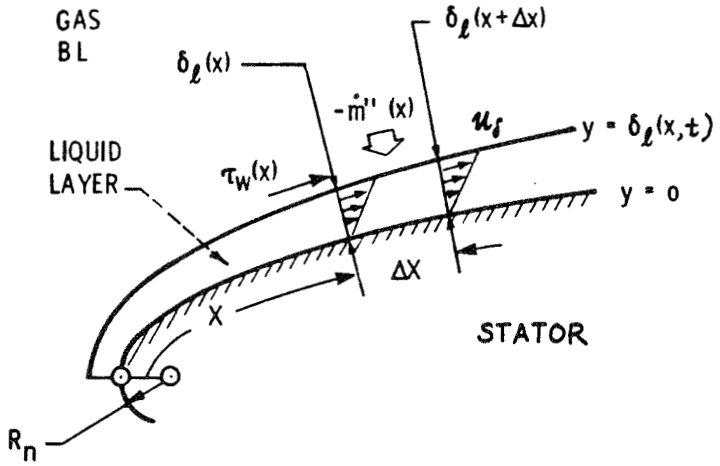

LIQUID LAYER THICKNESS, $\delta_\ell(x,t)$ IS GOVERNED BY

$$\frac{\partial \delta_\ell}{\partial t} + \frac{\partial}{\partial x}\left(\frac{\tau_w(x)}{2\mu_\ell}\cdot\delta_\ell^2\right) = -\frac{\dot{m}''(x)}{\rho_\ell}$$

Figure 4

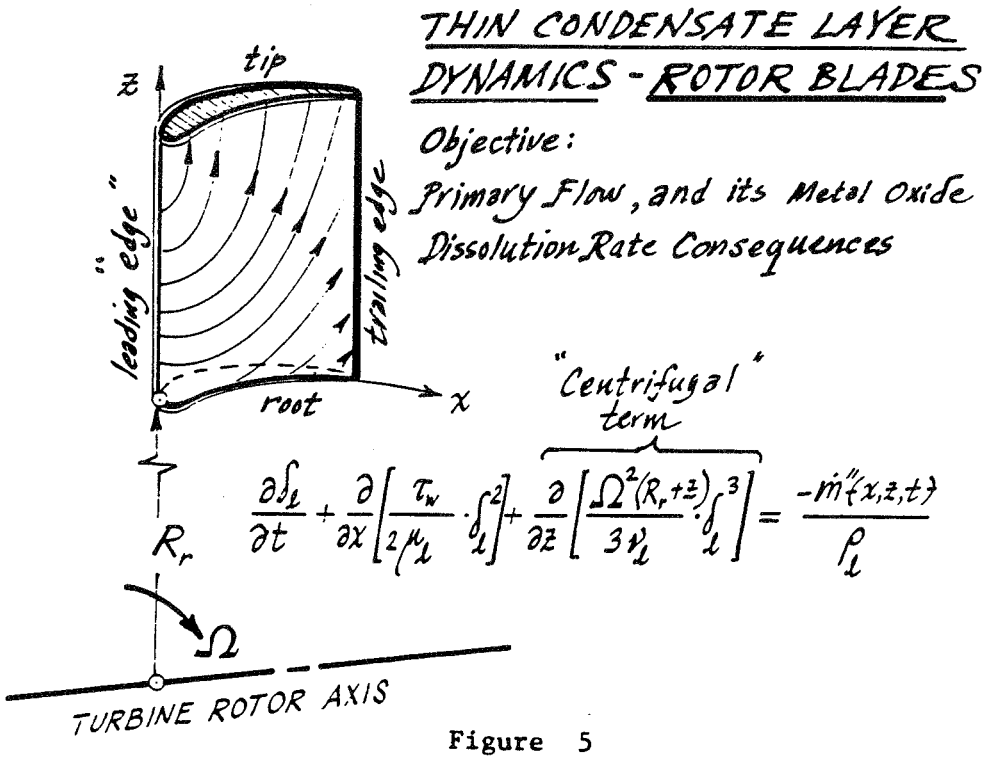

Figure 5

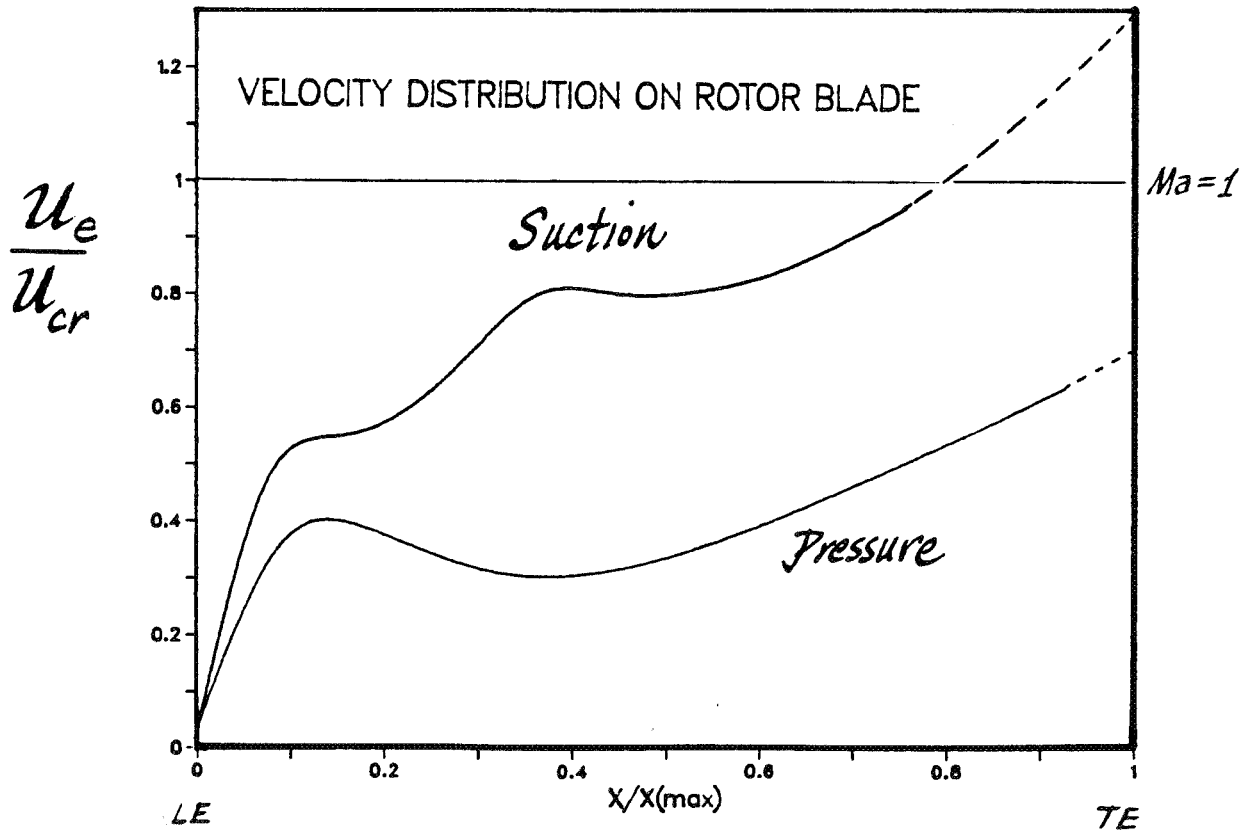

Figure 6

TEMPERATURE PROFILE ON SUCTION SURFACE

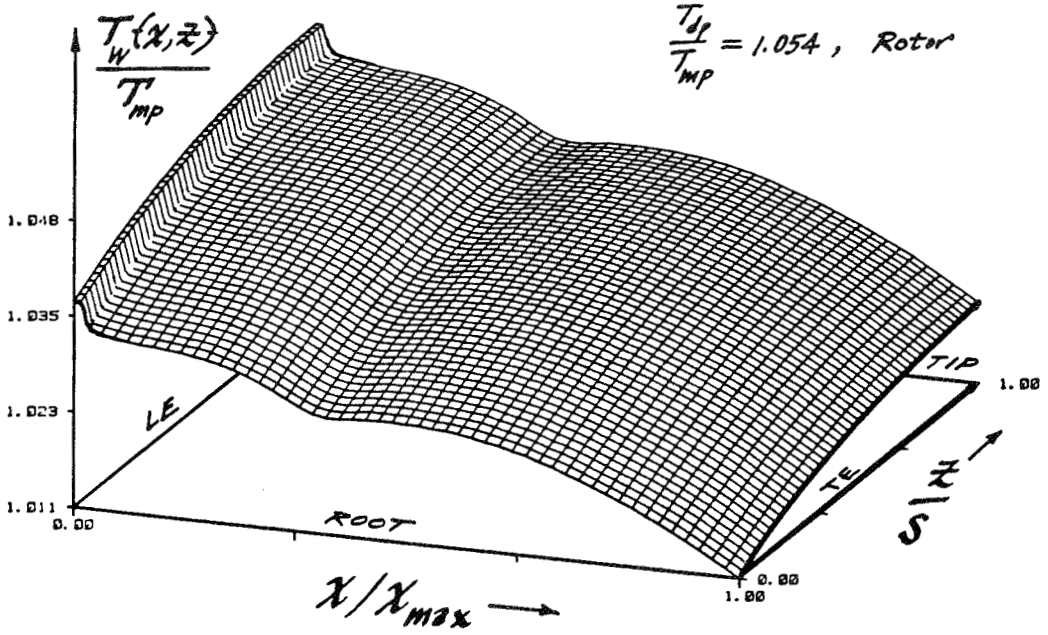

Figure 7

SALT DEPOSITION RATE PROFILE ON SUCTION SURFACE (Rotor)

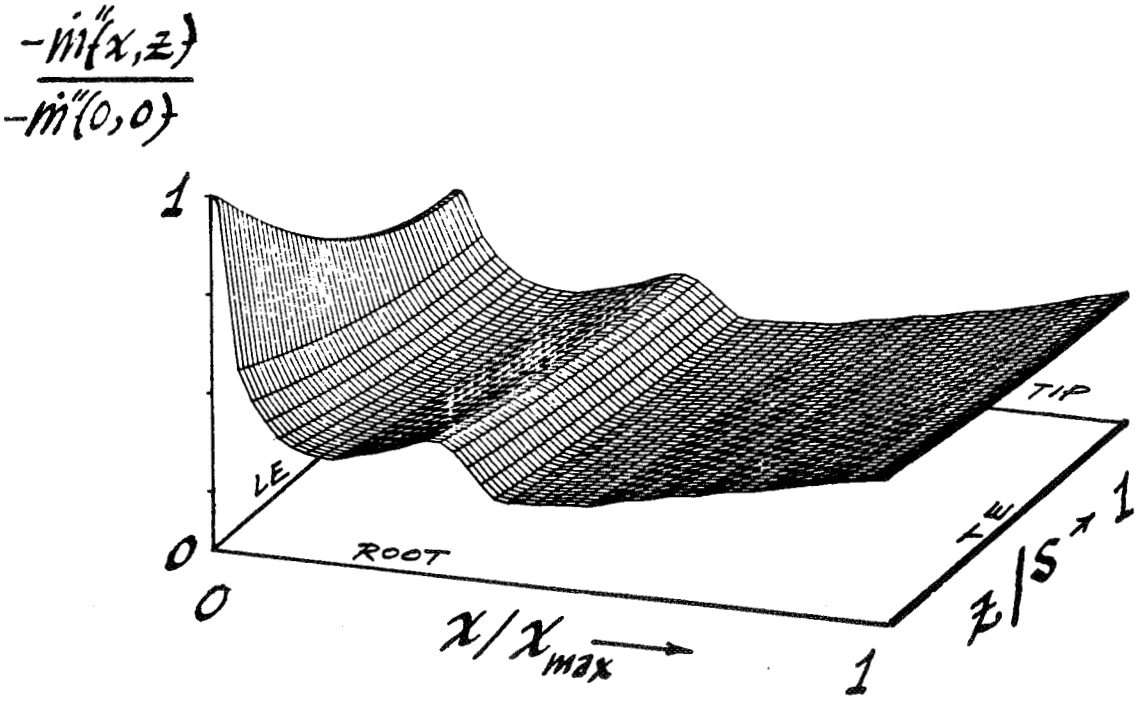

Figure 8

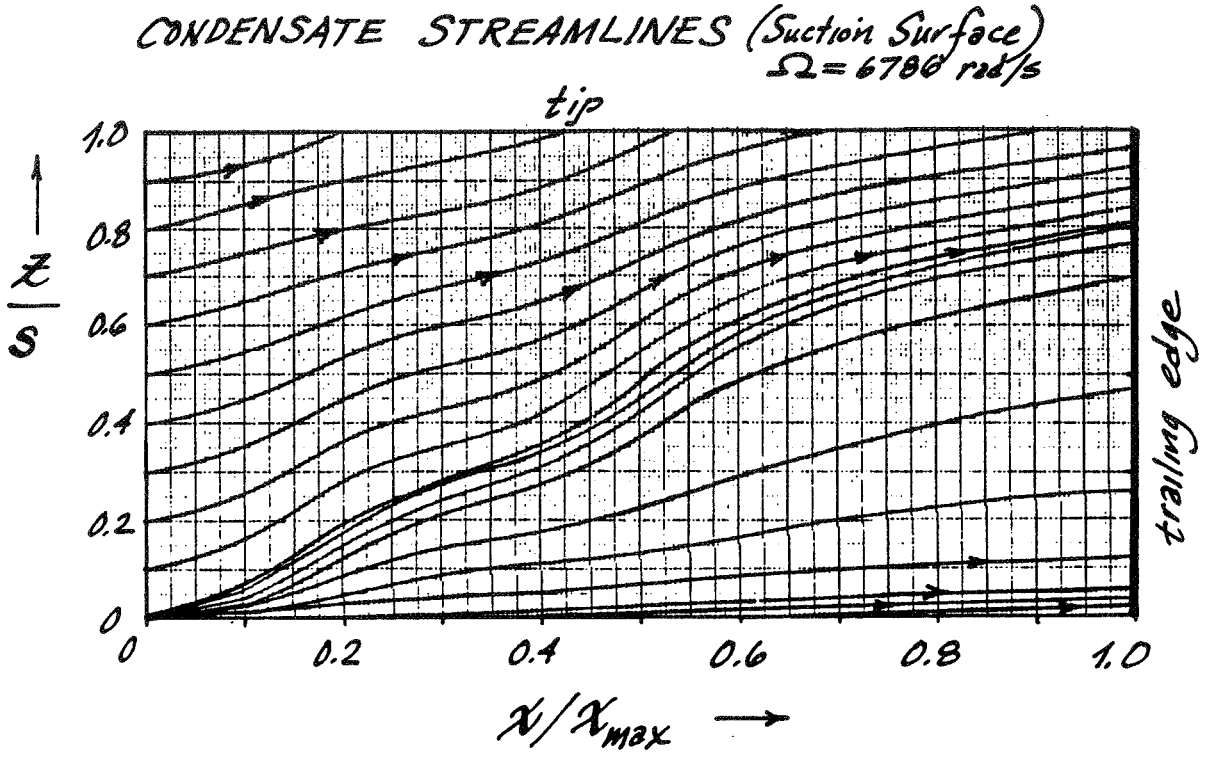

Figure 9

LIQUID LAYER THICKNESS PROFILE ON SUCTION SURFACE

(Ω = 6786 rad/sec)

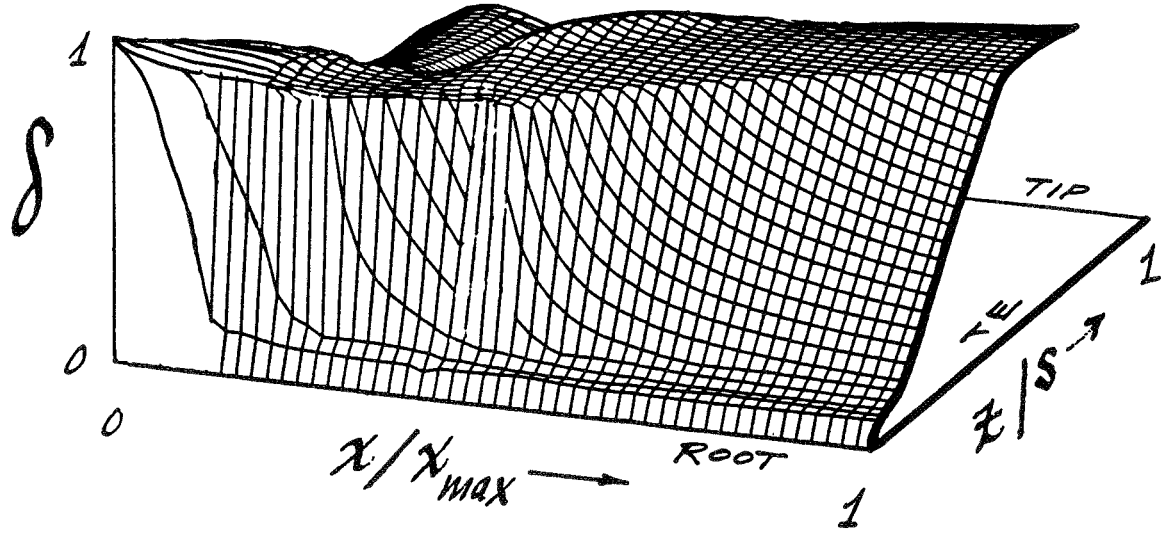

Figure 10

DEPOSITION MODEL VERIFICATION[1]

Suleyman A. Gokoglu
Analex Corporation
Cleveland, Ohio

This research is motivated by gas turbine failures associated with deposition, erosion, and accelerated "hot" corrosion. A comprehensive yet tractable theoretical framework of deposition from combustion gases has recently been developed covering the spectrum of various mass delivery mechanisms including vapor (refs. 1 and 2), thermophoretically-enhanced small particle (ref. 3), and inertially impacting large particle (ref. 4) deposition. Rational yet simple correlations have been provided to facilitate engineering surface arrival rate predictions (refs. 5 and 6). The goal of the program at NASA Lewis Research Center is to experimentally verify the deposition theory. Toward this end, a Mach 0.3 burner rig has been designed to measure deposition rates from salt-seeded combustion gases on an internally-cooled cylindrical collector (ref. 7).

Although very good agreement is obtained between the NaCl-seeded experiments and the chemically-frozen boundary layer (CFBL) vapor deposition theory, consistently higher values have been measured for sea-salt, $NaNO_3$, and Na_2SO_4-seeded experiments. Vaporization time calculations of the sprayed salt solution droplets during their residence time inside the combustor have shown the possibility of the presence of particles capable of inertially impacting the collector. In fact, deposition rate calculations based on the mean droplet size have agreed well with the experimental observations. The disagreement between the theory and the experiments above the melting point of the deposit is attributed to the shear-driven molten deposit layer flow and run-off from the smooth collector surface (ref. 8).

Future experiments will focus on the determination of parameters that will assure deposition by vapor diffusion only. Under these conditions, the deposition rate predictions of the CFBL theory will be verified using different salts (e.g., K_2SO_4, Na_2SO_4, NaCl, etc.). Above the melting point of the deposit, the theoretical molten layer thickness distribution prediction will be experimentally confirmed on a stationary cylindrical collector in crossflow. The experimental verification of the Mach number and the pressure dependence of the CFBL vapor deposition theory is also planned for the future.

REFERENCES

1. Rosner, D. E., Chen, B. K., Fryburg, G. C., and Kohl, F. J.: Chemically-Frozen Multicomponent Boundary Layer Theory of Salt and/or Ash Deposition Rates from Combustion Gases, Combustion Science and Technology, 20, 87-106, (1979).

2. Gokoglu, S. A., Chen, B. K., and Rosner, D. E.: Computer Program for the Calculation of Multicomponent Convective Diffusion Deposition Rates from Chemically-Frozen Boundary Layer Theory, NASA TP_____, (submitted 1983).

[1]Work done under NASA contract NAS3-23293 at the Lewis Research Center.

3. Gokoglu, S. A.: Thermophoretically-Enhanced Deposition of Particulate Matter Across Nonisothermal Boundary Layers, Ph.D. Thesis, Chem. Engrg. Dept., Yale University (1982).

4. Fernandez de la Mora, J. and Rosner, D. E.: Inertial Deposition of Particles Revisited and Extended: Eulerian Approach to a Traditionally Lagrangian Problem, J. PhysicoChem. Hydrodynamics (Pergamon), 2, 1-21 (1981).

5. Gokoglu, S. A. and Rosner, D. E.: Correlation of Thermophoretically-Modified Small Particle Deposition Rates in Forced Convection Systems with Variable Properties, Transpiration Cooling and/or Viscous Dissipation, Int. J. Heat and Mass Transfer (Pergamon) (in press, 1983).

6. Israel, R. and Rosner, D. E.: Use of Generalized Stokes Number to Correlate the Aerodynamic Capture Efficiency of Non-Stokesian Particles from a Compressible Gas Flow to Collectors of Different Geometry, J. Aerosol Sci. and Technol., 2, 45-51 (1983).

7. Santoro, G. J., Kohl, F. J., Stearns, C. A., Gokoglu, S. A., and Rosner, D. E.: Experimental and Theoretical Deposition Rates from Salt-Seeded Combustion Gases of a Mach 0.3 Burner Rig, NASA TP 2225 (in press, 1983).

8. Rosner, D. E., Gunes, D., and Anous, N.: Aerodynamically-Driven Condensate Layer Thickness Distributions on Isothermal Cylindrical Surfaces, Chem. Engrg. Commun. (in press, 1983).

BURNER RIG AND COLLECTOR CONFIGURATION

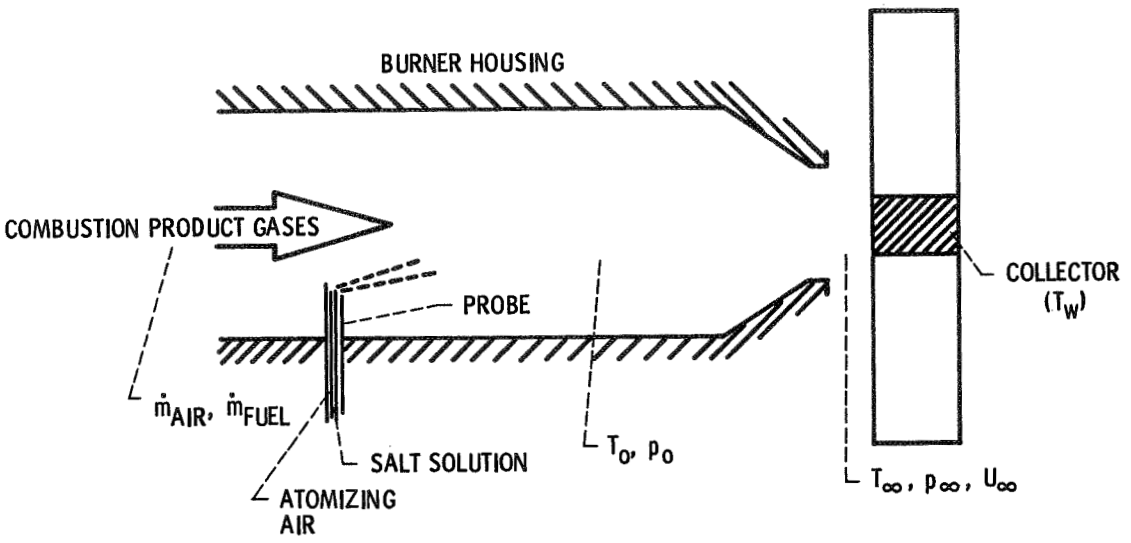

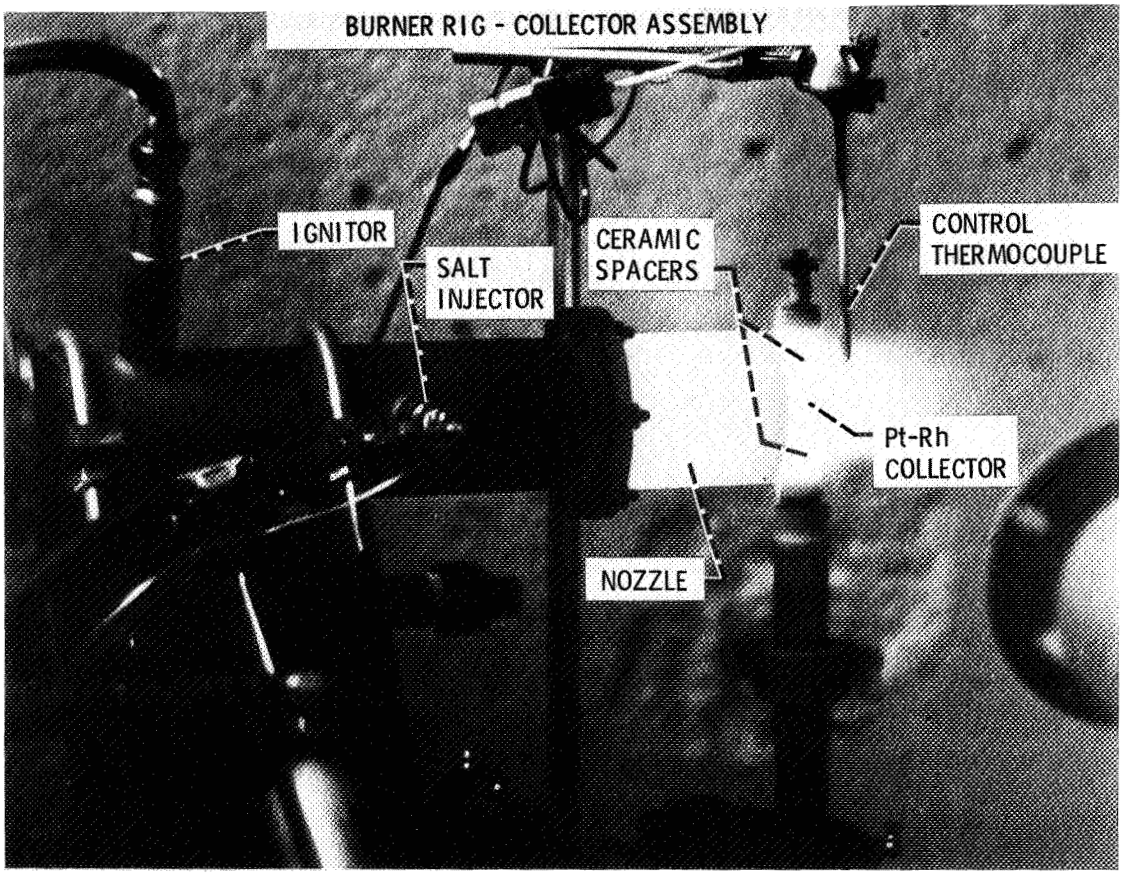

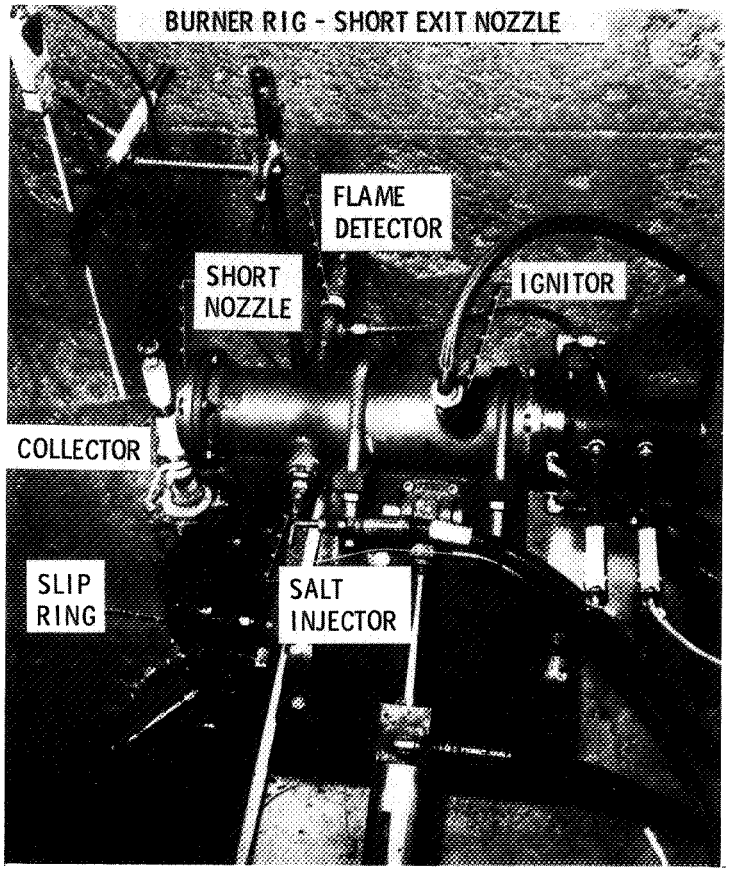
BURNER RIG - SHORT EXIT NOZZLE
FLAME DETECTOR
SHORT NOZZLE
IGNITOR
COLLECTOR
SLIP RING
SALT INJECTOR

NaCl SEEDED

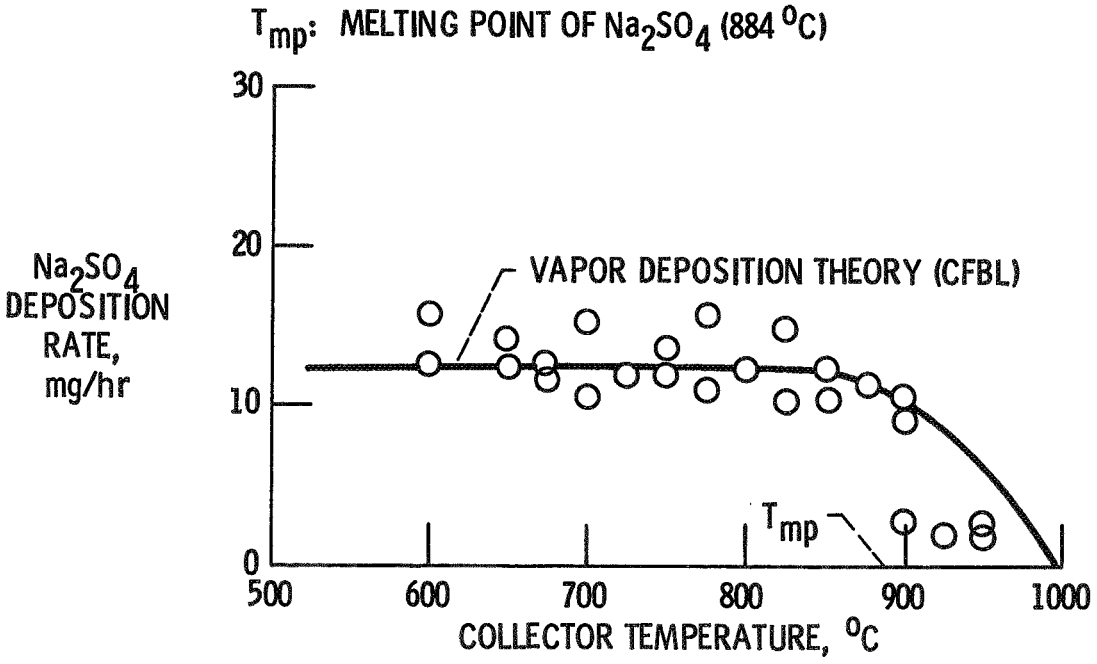
T_{mp}: MELTING POINT OF Na_2SO_4 (884 °C)
Na_2SO_4 DEPOSITION RATE, mg/hr
30
20
10
0
VAPOR DEPOSITION THEORY (CFBL)
T_{mp}
500
600
700
800
900
1000
COLLECTOR TEMPERATURE, °C

SYNTHETIC SEA SALT

T_{mp}: MELTING POINT OF Na_2SO_4 (884 °C)

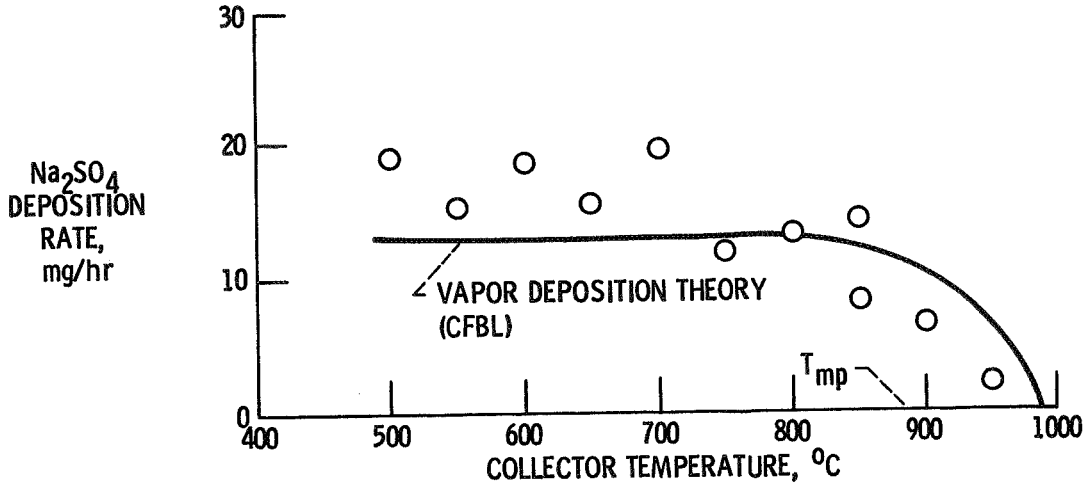

$NaNO_3$ SEEDED

T_{mp}: MELTING POINT OF Na_2SO_4 (884 °C)

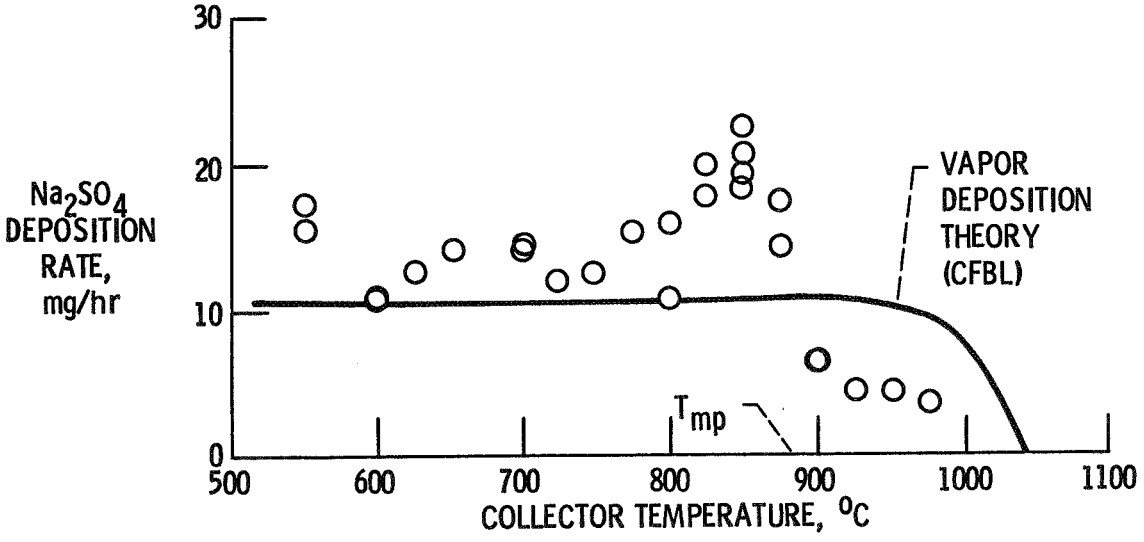

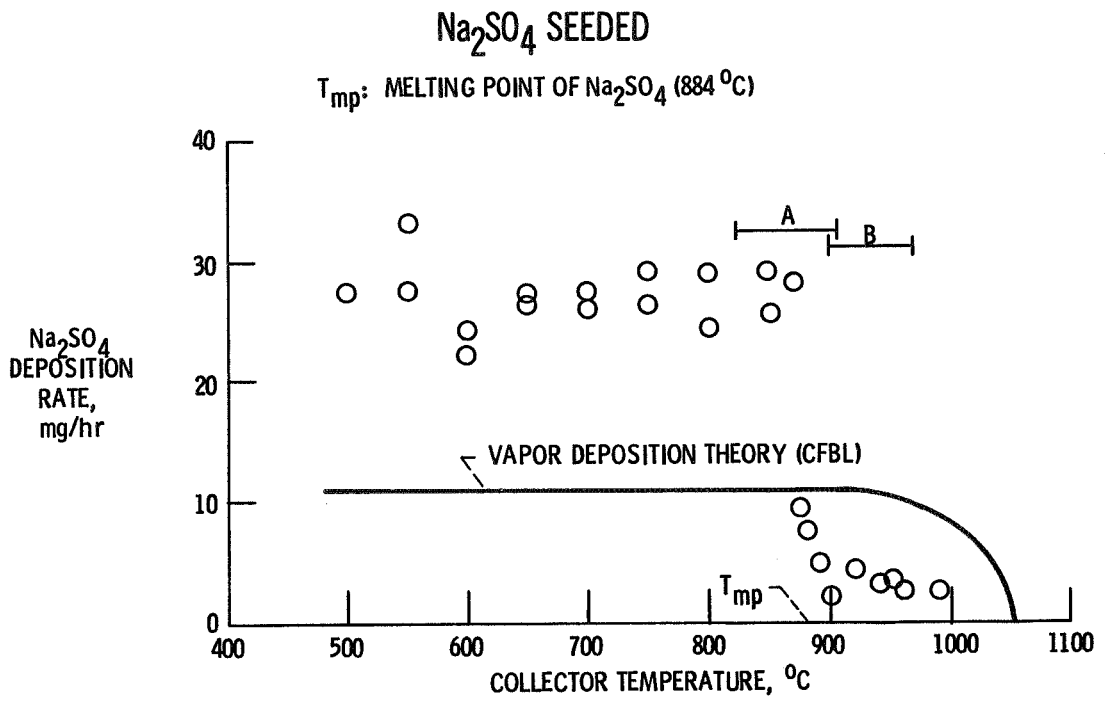
Na_2SO_4 SEEDED
T_{mp}: MELTING POINT OF Na_2SO_4 (884 °C)
Na_2SO_4 DEPOSITION RATE, mg/hr
40
30
20
10
0
A
B
VAPOR DEPOSITION THEORY (CFBL)
T_{mp}
400
500
600
700
800
900
1000
1100
COLLECTOR TEMPERATURE, °C

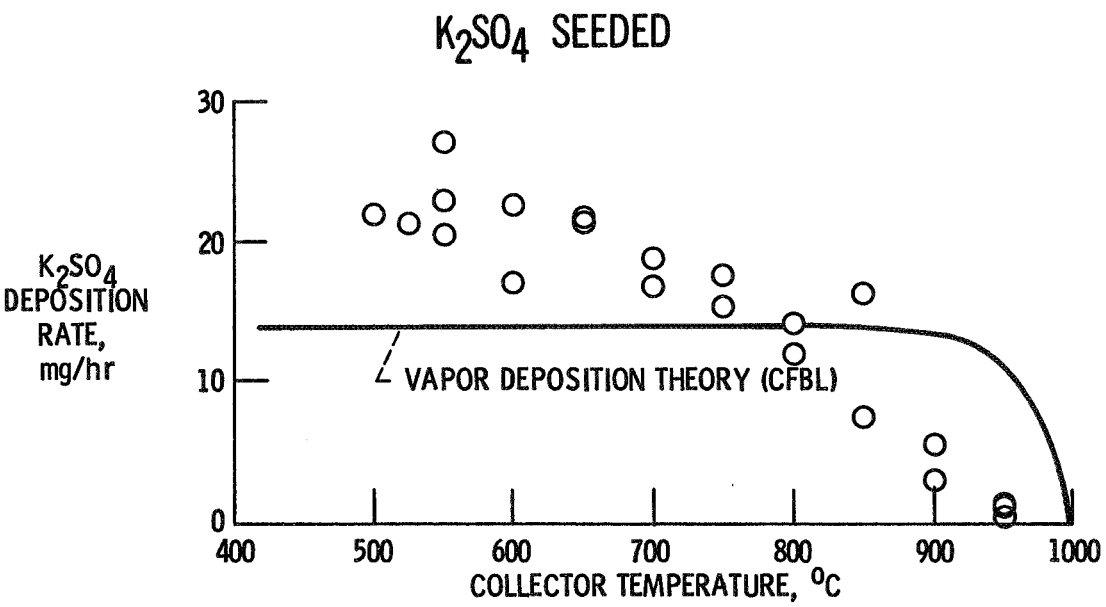
K_2SO_4 SEEDED
K_2SO_4 DEPOSITION RATE, mg/hr
30
20
10
0
VAPOR DEPOSITION THEORY (CFBL)
400
500
600
700
800
900
1000
COLLECTOR TEMPERATURE, °C

PREDICTED DEPENDENCE OF SODIUM SULFATE DEPOSITION RATE ON PARTICLE SIZE

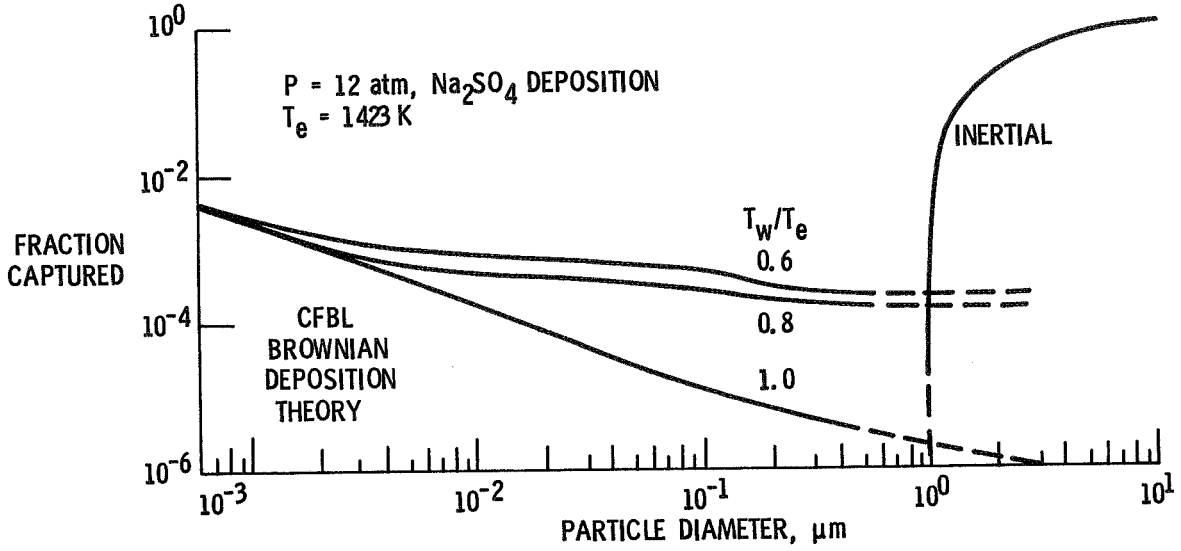

DROPLET SIZE DISTRIBUTION

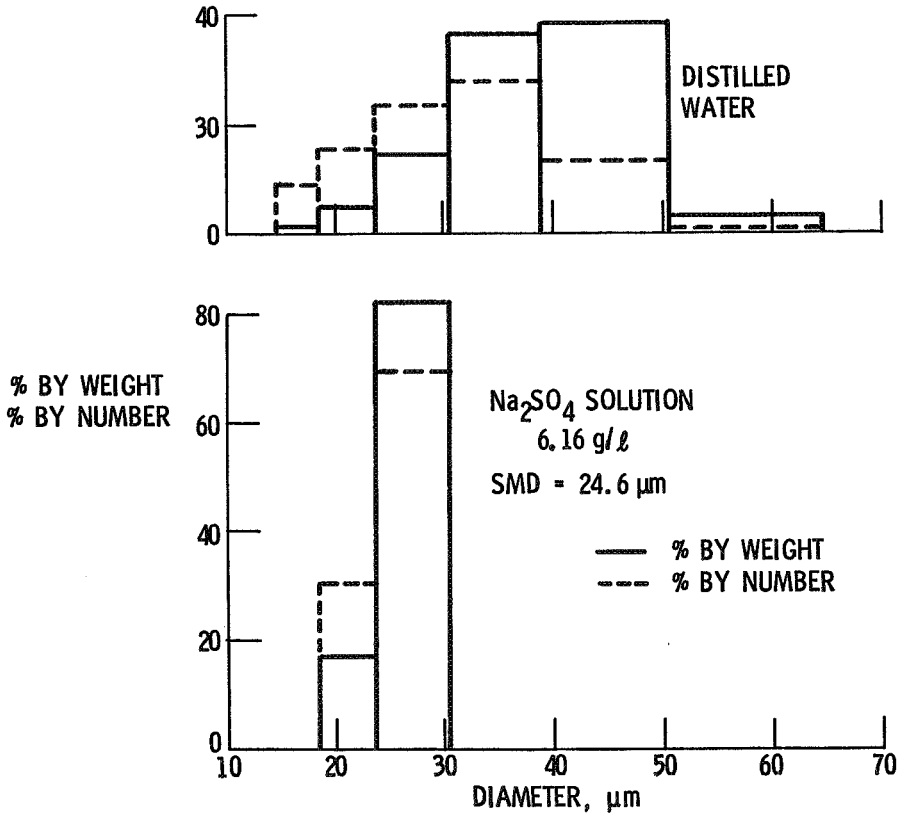

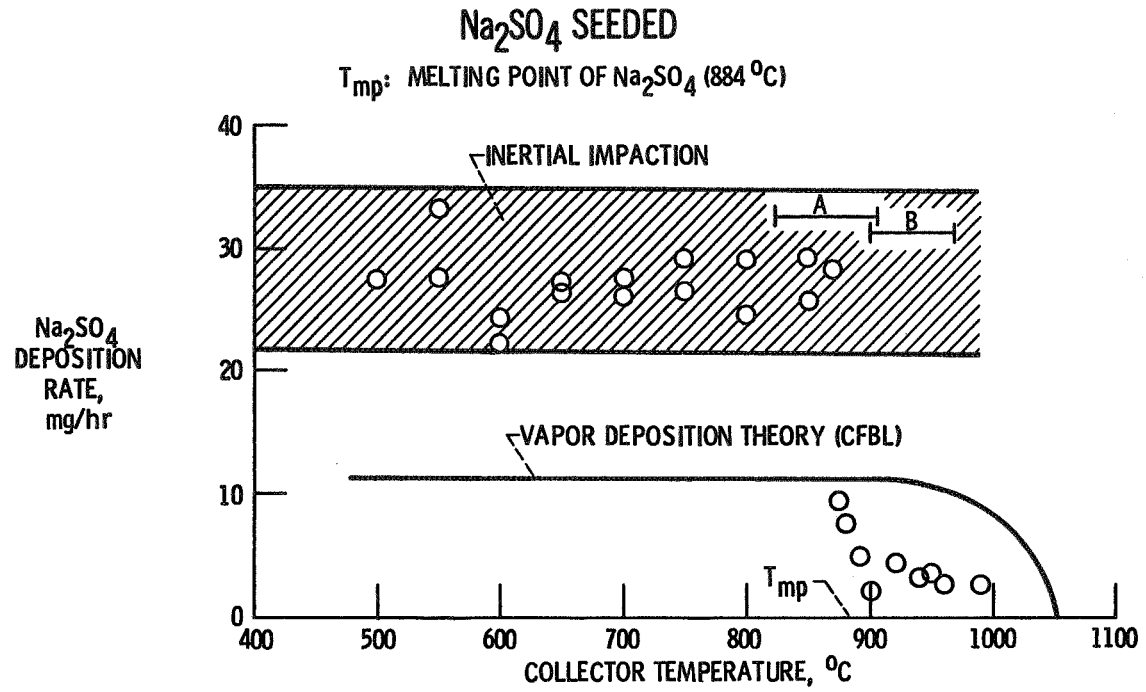
Na_2SO_4 SEEDED
T_{mp}: MELTING POINT OF Na_2SO_4 (884 °C)
INERTIAL IMPACTION
A
B
VAPOR DEPOSITION THEORY (CFBL)
T_{mp}
Na_2SO_4 DEPOSITION RATE, mg/hr
0
10
20
30
40
400
500
600
700
800
900
1000
1100
COLLECTOR TEMPERATURE, °C

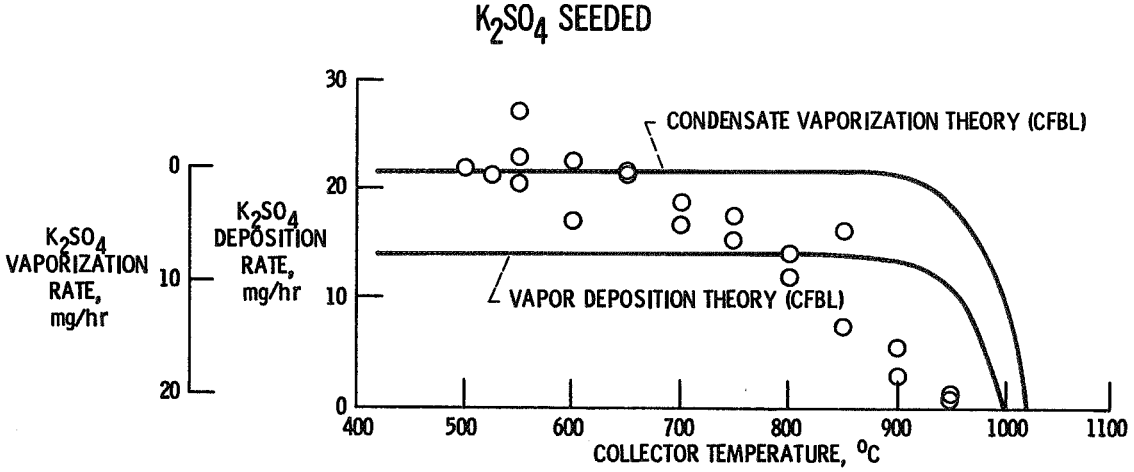
K_2SO_4 SEEDED
CONDENSATE VAPORIZATION THEORY (CFBL)
VAPOR DEPOSITION THEORY (CFBL)
K_2SO_4 VAPORIZATION RATE, mg/hr
K_2SO_4 DEPOSITION RATE, mg/hr
0
10
20
30
400
500
600
700
800
900
1000
1100
COLLECTOR TEMPERATURE, °C

PERTINENT TEST PARAMETERS

- SALT INJECTION SYSTEM:
  - SALT COMPOSITION
  - SALT CONCENTRATION
  - SALT SOLUTION PUMP SPEED
  - ATOMIZING AIR PRESSURE (FLOWRATE)
  - RESIDENCE TIME IN THE COMBUSTOR
  - SALT VAPOR PRESSURE
- BURNER:
  - MASS FLOW RATE
  - AIR TEMPERATURE INTO THE COMBUSTOR
  - COMBUSTION GAS TEMPERATURE
  - FUEL-TO-AIR RATIO
  - SULFUR CONCENTRATION
  - COMBUSTION GAS PRESSURE
  - COMBUSTOR LINER DESIGN
  - EXIT NOZZLE DESIGN
- COLLECTOR:
  - GEOMETRY
  - TEMPERATURE AND TEMPERATURE GRADIENTS
  - ΔT BETWEEN THE COLLECTOR AND GAS STREAM
  - SURFACE ROUGHNESS
  - ROTATING - NOT ROTATING

FUTURE WORK

- DETERMINATION OF DROPLET SIZE DISTRIBUTION AS A FUNCTION OF:
  - (a) SALT SOLUTION CONCENTRATION
  - (b) SALT SOLUTION FLOWRATE
  - (c) ATOMIZING AIR PRESSURE (FLOWRATE)
  - (d) MACH NUMBER

  AT CONSTANT Na (OR K) ELEMENT CONCENTRATIONS IN BURNER FOR DIFFERENT SALTS (Na_2SO_4, NaCl, K_2SO_4, ETC.)
- DETERMINATION OF PARAMETERS THAT ASSURE DEPOSITION BY VAPOR DIFFUSION ONLY
- DETERMINATION OF DISCHARGE COEFFICIENTS OF DIFFERENT NOZZLES USED IN DEPOSITION EXPERIMENTS
- VERIFICATION OF ENTIRE DEPOSITION RATE CURVE (VIA CFBL THEORY) USING K_2SO_4 SEEDED EXPERIMENTS
- VERIFICATION OF CFBL PREDICTED PLATEAU DEPOSITION RATES USING VARIOUS Na-SALT-SEEDED EXPERIMENTS
- VERIFICATION OF MOLTEN Na_2SO_4 DEPOSIT THICKNESS DISTRIBUTION AROUND STATIONARY CYLINDER IN CROSSFLOW
- VERIFICATION OF PRESSURE AND MACH NUMBER DEPENDENCE OF DEPOSITION THEORY

EFFECTS OF SURFACE CHEMISTRY ON HOT CORROSION LIFE*

R. E. Fryxell
General Electric Company

This new program has as its primary objective the development of hot corrosion life prediction methodology based on a combination of laboratory test data and evaluation of field service turbine components which show evidence of hot corrosion. This program is divided into five tasks. All burner rig testing will be performed by TRW. The discussion will describe the overall program with a brief summary of activity to date.

Task I involves the evaluation of six hot corroded components, having known operating history, to establish the degradation mechanisms in the corroded areas. Correlation of the corrosion with operating conditions will be made to the extent possible. Evaluation will include chemical and X-ray diffraction analyses of surface scales/deposits as well as metallography, scanning electron microscopy, and electron microprobe examination. Both uncoated and coated hardware will be evaluated and emphasis will be placed on the cause and effect parameters which are associated with hot corrosion. Task I will be completed by the end of this year.

Task II will establish a hot corrosion baseline for the program alloys and coatings in the as-processed condition and will involve up to 1000 hours exposure of duplicate specimens in a Mach 0.3 burner rig using Jet A fuel (0.045-0.065% sulfur) and in which 0.5 ppm sodium by weight, as NaCl, is added to the combustion air. The test cycle will be one hour at 900C followed by at least six minutes of forced air cooling to ambient temperature. Tests are scheduled to begin in December 1983.

At approximately 20 cycle intervals, specimens will be visually examined, photographed, and inductance readings taken. Specimens will be removed when evidence of hot corrosion is noted in three successive test intervals. Unexposed specimens will then be inserted, as space is available, for time periods of 100, 300, and 500 hours if these time periods do not exceed 2/3 the time the original specimen of the same material was exposed.

Specimens to be tested in this task include U700 and Rene' 80, both uncoated and with the following coatings:

pack aluminide RT21 (Chromalloy) and Codep (General Electric)
low pressure plasma NiCoCrAlY (Ni-23Co-18Cr-12Al-0.3Y)

Evaluation of tested specimens will be as in Task I.

In Task III, triplicate specimens of the above coated alloys will be aged at 1100C under a variety of conditions to determine effects of coating-alloy interdiffusion and/or oxidation on hot corrosion behavior.

*Contract NAS3-23926

These aging treatments will be isothermal inert atmosphere for 100 hours, isothermal air furnace oxidation for 100, 300, 600 hours, one hour air furnace cycles for 100 hours and cyclic burner rig oxidation for 100, 300 and 600 hours.

Weight changes will be determined on a regular basis (every 20 hours for cyclic exposures and at the end of exposure intervals for other cases). Also, specimen inductance shall be determined on the same basis.

One specimen representing each of the above conditions will be evaluated using the methods outlined in Task I; the remaining duplicate specimens representing each condition shall be used in Task IV which is a hot corrosion burner rig test identical with Task II.

At the conclusion of the Task IV test, all the data generated in Tasks I through IV will be evaluated and an empirical hot corrosion life prediction model based on these data will be proposed. Also, recommendations will be made for other test parameters to be evaluated, and evaluation methodology necessary to permit prediction of hot corrosion life.

Task V will be a hot corrosion high velocity cyclic burner rig test designed to check the validity of the proposed life prediction model. Duplicate specimens of a maximum of four alloys and five coatings will be tested up to a maximum of 1000 hours and evaluated as in Tasks II and IV. The alloys and coatings will be those from this program plus additional alloy-coating systems selected by the NASA Project Manager.

The Task V experiment will be designed to test two aspects of the life prediction model developed in Task IV. The ability of the model to predict hot corrosion life under different rig test conditions than those previously used in Task II and IV will be tested in one portion of the experiment. The second portion of the experiment will test the ability of the model to predict hot corrosion life of new alloys and coatings.

The ability of the model to predict hot corrosion life under different rig test conditions will be evaluated using alloys and coatings previously tested in Task II and Task IV. The hot corrosion tests for this portion of the program will use one or more variations of the test parameters used in Task II, III and IV. Test parameter variations that will be considered include the following:

- o A different salt level
- o A different test temperature
- o Intermittent salt injection
- o A different sulfur level in the fuel
- o Additional or modified aging cycles

The specific testing parameters will be derived from the results of Task II and Task IV, previous experience in evaluating field service hardware and previous experience in conducting hot corrosion testing under a variety of test conditions.

The ability of the model to predict hot corrosion resistance of new coatings and alloys will be evaluated using alloys and coatings that have not been evaluated previously in Task II and Task IV. Rig test conditions will be identical to those used in Task II and Task IV. The aging cycle will be chosen from the results of Task IV.

Life prediction for both portions of the Task V experiment will be based on the model developed in Task IV as well as extensive experience gained from evaluating

field service components and conducting hot corrosion tests. Knowledge of the effect of variations in both engine operating conditions and rig testing conditions will be used in predicting hot corrosion life under different rig test conditions in the first portion of the experiment with the same alloys and coatings tested in Task II and Task IV. Typical variations in the relative performance of four Ni base superalloys as a function of salt flux in a one atmosphere burner rig are shown in Figure 1. With respect to testing of additional alloys and coatings, use will be made of extensive empirical correlations of composition and hot corrosion performance in predicting hot corrosion life.

Current activity on this program is primarily in Task I. Six components have been selected, and include the following:

4 stage one high pressure turbine blades from CF6-50 engines, representing four different carriers. Codep coated Rene' 80.

1 stage one low pressure turbine nozzle from a CF6-50 engine. Uncoated Rene' 77.

1 stage one high pressure turbine blade from a J79 engine.

Evaluation is in progress and preliminary results will be described.

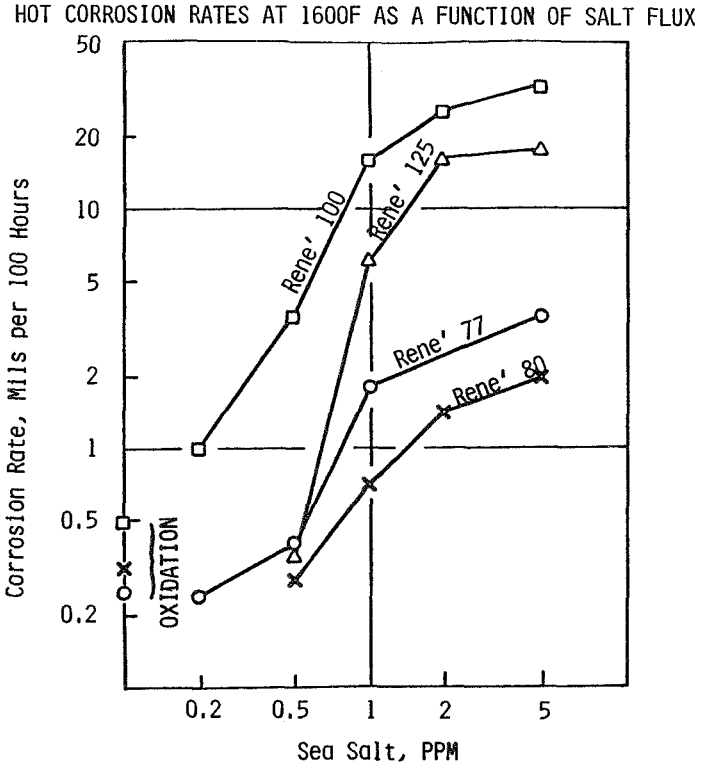

FIGURE 1

Page intentionally left blank

Coating Life Prediction

Michael A. Gedwill
National Aeronautics and Space Administration
Lewis Research Center

At elevated temperatures, high strength turbine alloys are life limited because of severe oxidation attack. To improve life, the hot section components of gas turbine engines are coated to take advantage of the oxidation resistance of metallic coatings. The oxidation resistance of these coatings is derived from the formation of a protective oxide (generally Al_2O_3) scale and reformation of the scale if it spalls during temperature excursions. During thermal cycling, reformation of the scale is very important since all scales eventually experience spallation; some significantly more than others. There are some scales (for example Cr_2O_3) that volitalize rapidly in a dynamic (high gas velocity) environment at elevated temperatures. Thus, the coating serves as a reservoir for the formation/reformation of the protective scale. Interactions of coating and substrate, however, reduce the tendency for reformation of the protective scale. Although vast improvements in life have been made and will be made in the future by coating turbine components, it should be obvious that coated components in themselves are life limited at high temperatures and during thermal cycling.

The engine designer/manufacturer needs reliable, accurate and precise information to properly design turbine engines to coating life limits. Such engines would be cost effective because they would be capable of operating either for longer times or at higher temperatures. The end-user would also benefit from less costly engine inspections and component replacements which now are many times made on a conservative basis. A methodology for predicting life of coated turbine airfoils would, therefore, benefit all.

The study to be discussed herein is a first-cut at an approach directed toward developing the life prediction methodology for metallic coatings on turbine alloys in cyclic oxidation. A cyclic oxidation/spalling computer model was developed at LeRC which predicts cyclic furnace oxidation behavior of bulk cast/wrought alloys over a range of cycling frequencies. The input data for the model are obtained from short-time isothermal oxidation tests. The required data are measurements of the oxide growth rate(s) and a spall constant, Q_0. The model predicts specific weight changes, specific metal consumption, oxide growth rate(s), oxide spall fractions, and an effective time. The agreement between the observed and predicted cyclic oxidation behavior of bulk alloys has been shown to be within ±10%. In the present study, the computer model is being applied to an aluminide coating on U-700, a low pressure plasma sprayed (LPPS) NiCoCrAlY coating on U-700, and a bulk LPPS NiCoCrAlY. To predict coating life in cyclic furnace oxidation, an empirical diffusion model to account for coating degradation (oxidation and coating/substrate interdiffusion) will be integrated with the oxidation/spalling model. The integrated model will then be verified/adjusted to predict cyclic burner oxidation. Further verification/adjustment will lead to life prediction model for coated turbine airfoils. Results of isothermal and cyclic furnace oxidation of aluminide coated U-700, in particular, will be

presented and discussed. The results will also include morphological changes observed during furnace oxidation.

COATING LIFE PREDICTION

OBJECTIVE:

DEVELOP IMPROVED METHODOLOGY FOR PREDICTING CYCLIC OXIDATION LIFE OF METALLIC COATINGS ON GAS TURBINE AIRFOILS

V-1721

ENVIROMENTAL AND SUBSTRATE REACTIONS DEGRADE COATINGS

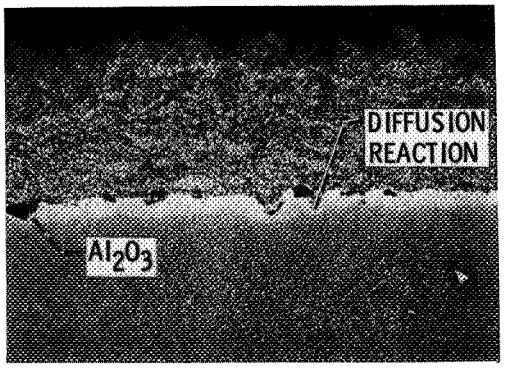

LPPS NiCoCrAlY COATED
U-700 ANNEALED
1080° C/4 hr/Ar

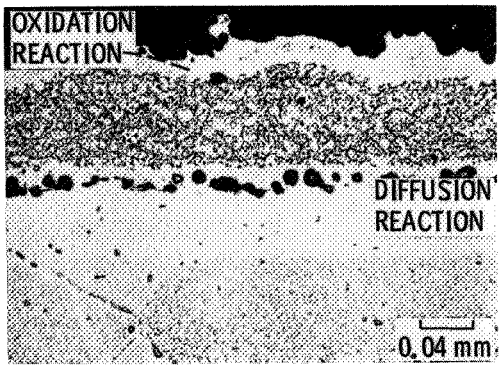

AFTER 100-1 hr CYCLES
AT 1100° C

V-1728

ISOTHERMAL VS CYCLIC OXIDATION

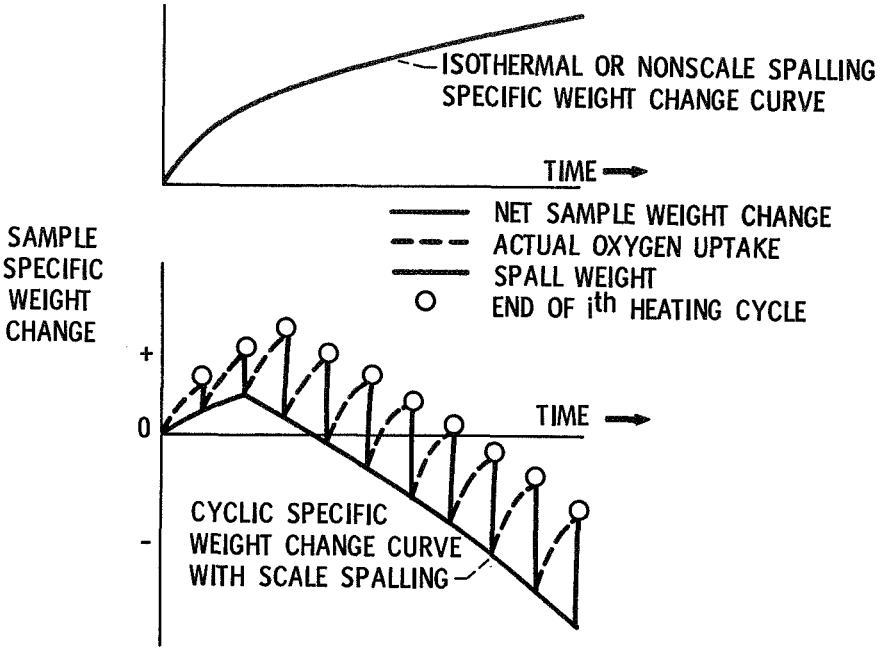

V-1723

BASIC SPALL EQUATION

$$W_s = Q_0 \left(W_r'\right)^{\alpha + 1}$$

WHERE:

W_s = SPECIFIC WEIGHT OF SPALL ON COOLING FROM i^{th} CYCLE

Q_0 = SPECIFIC SPALL CONSTANT

W_r' = SPECIFIC WEIGHT OF OXIDE PRIOR TO COOLING FROM i^{th} CYCLE

α = CONSTANT

V-1719

CYCLIC FURNACE OXIDATION OF ALUMINIDE COATED U-700

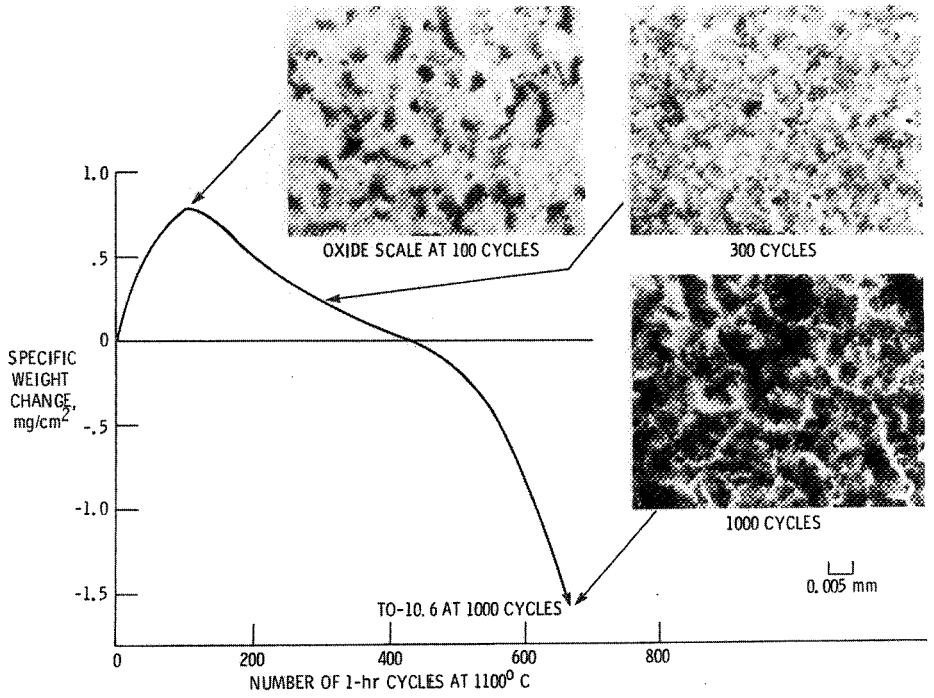

CYCLIC FURNACE OXIDATION OF ALUMINIDE COATED U-700

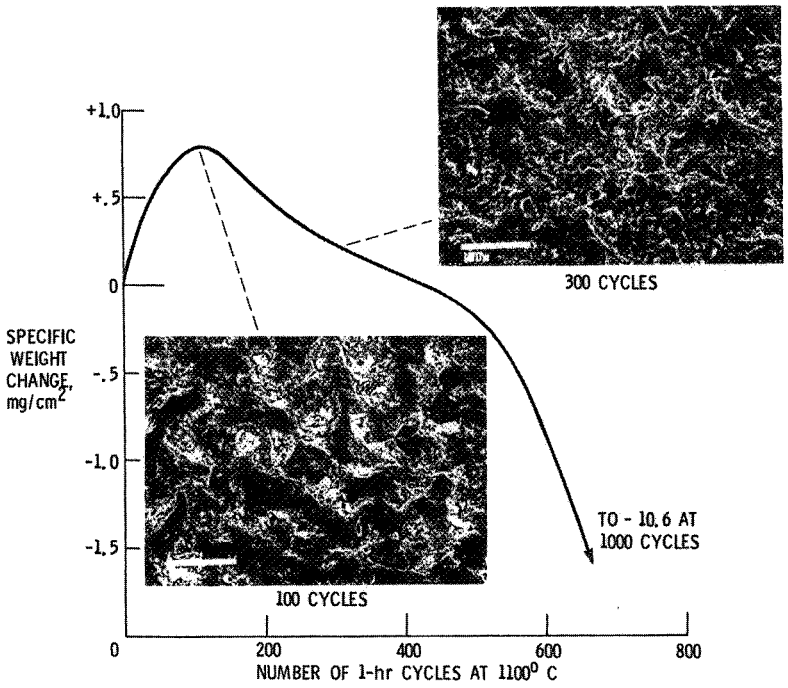

PHOTOMICROGRAPHS AS COATED U-700

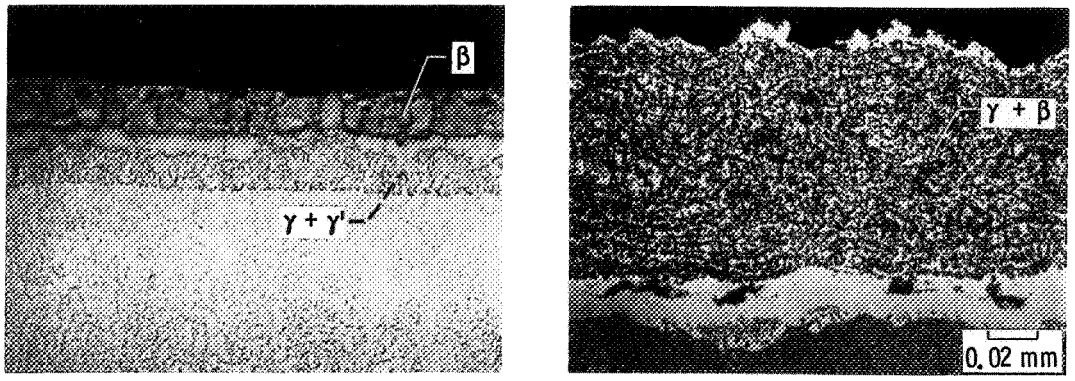

COATING: ALUMINIDE (TWO STEP)

LPPS NiCoCrAlY (ANNEALED 4 hr/1080° C/Ar)

V-1729

OXIDATION OF ALUMINIDE COATED U-700

1150° C

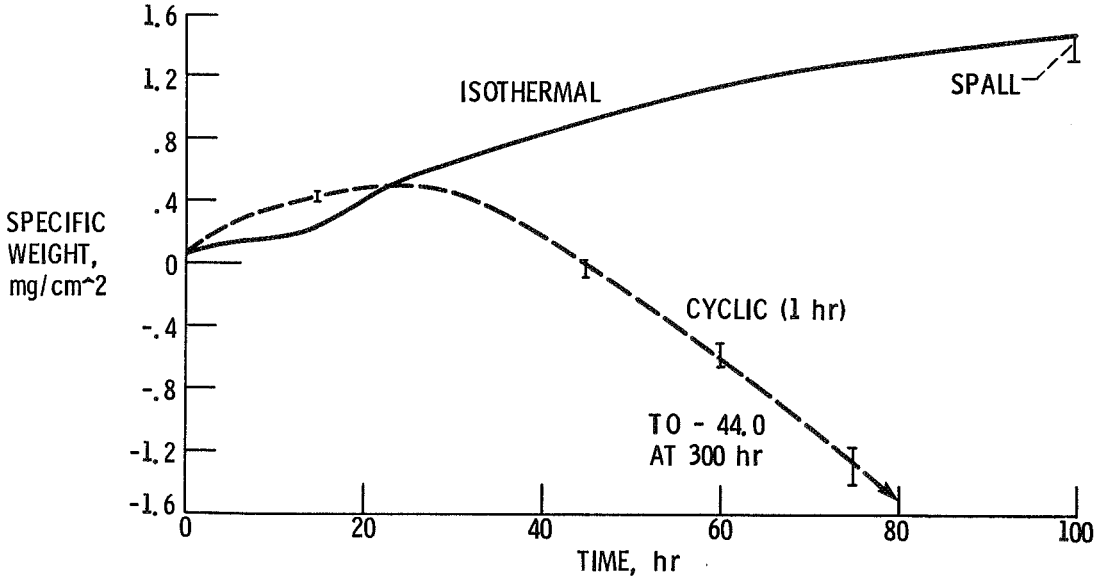

V-1722

APPROACH

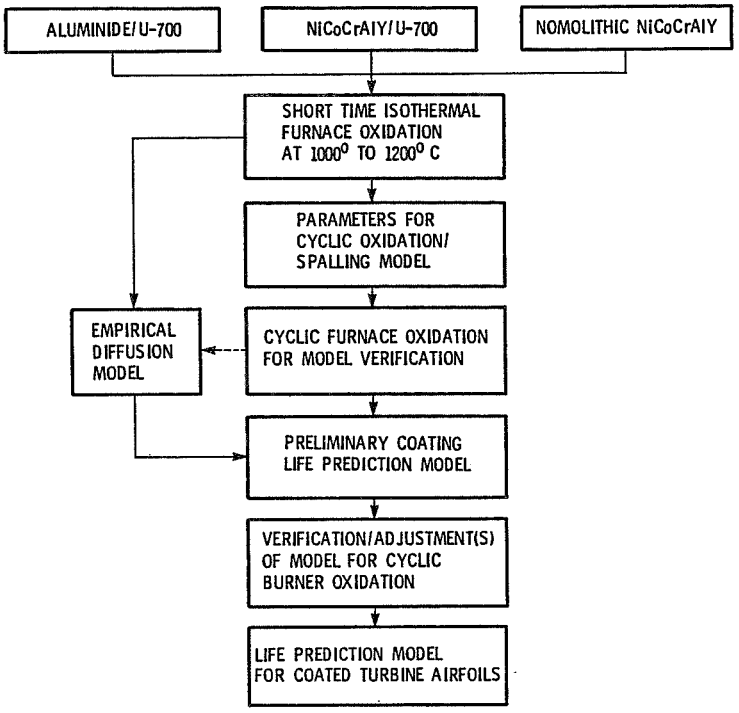
ALUMINIDE/U-700
NiCoCrAlY/U-700
NOMOLITHIC NiCoCrAlY
SHORT TIME ISOTHERMAL FURNACE OXIDATION AT 1000° TO 1200° C
PARAMETERS FOR CYCLIC OXIDATION/ SPALLING MODEL
EMPIRICAL DIFFUSION MODEL
CYCLIC FURNACE OXIDATION FOR MODEL VERIFICATION
PRELIMINARY COATING LIFE PREDICTION MODEL
VERIFICATION/ADJUSTMENT(S) OF MODEL FOR CYCLIC BURNER OXIDATION
LIFE PREDICTION MODEL FOR COATED TURBINE AIRFOILS

CS-82-2626 V-1827

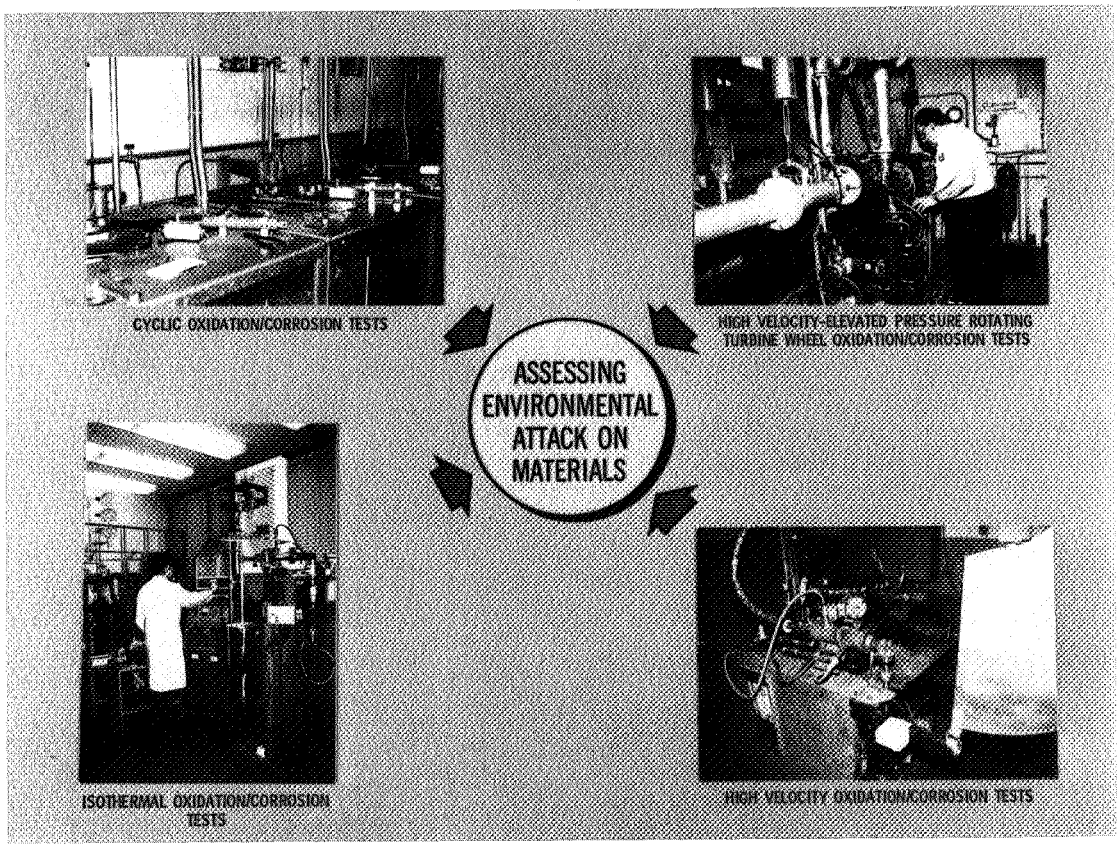
CYCLIC OXIDATION/CORROSION TESTS
HIGH VELOCITY-ELEVATED PRESSURE ROTATING TURBINE WHEEL OXIDATION/CORROSION TESTS
ASSESSING ENVIRONMENTAL ATTACK ON MATERIALS
ISOTHERMAL OXIDATION/CORROSION TESTS
HIGH VELOCITY OXIDATION/CORROSION TESTS

CYCLIC FURNACE OXIDATION OF ALUMINIDE COATED U-700

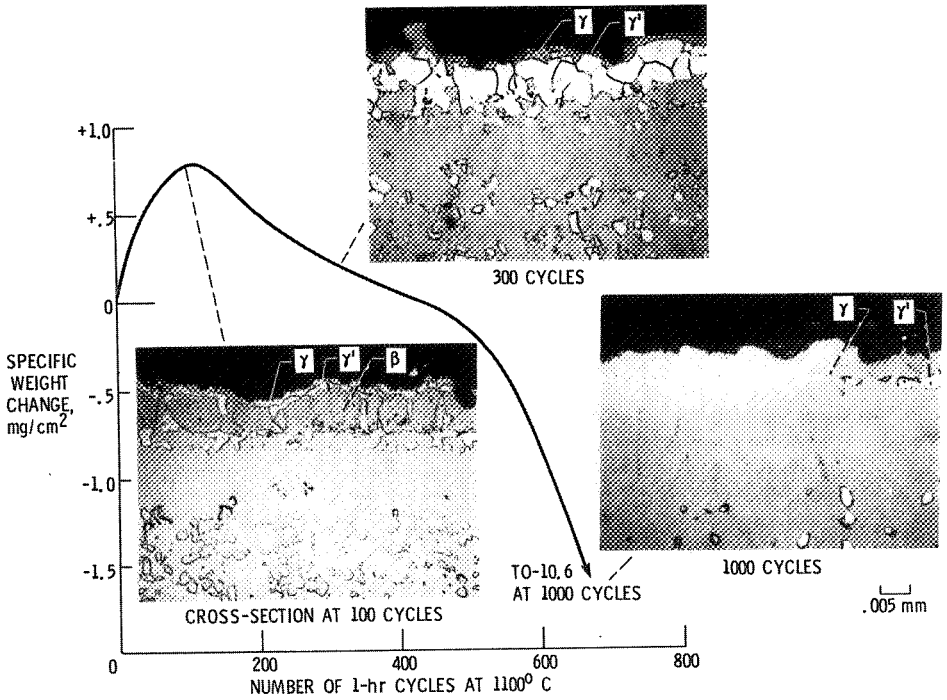

V-1726

OXIDATION OF ALUMINIDE COATED U-700

1100° C

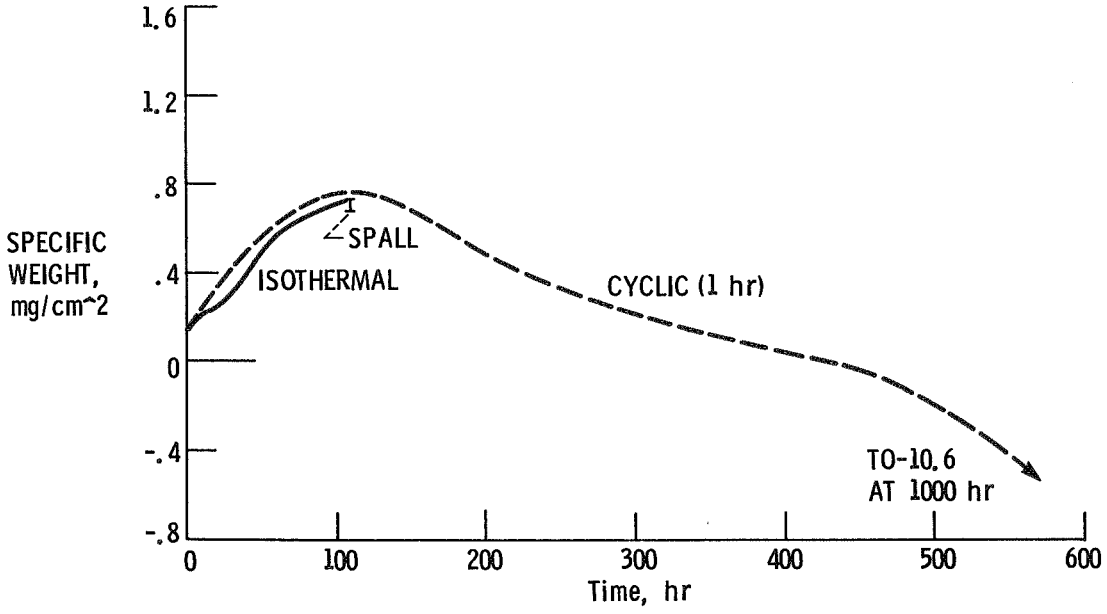

CALCULATED SPALL CONSTANT (Q_0) VALUES FROM ISOTHERMAL OXIDATION DATA

1150° C	TIME, hr	Q_0 VALUES cm^2/mg
ALUMINIDE	100[a]	0.017
COATED U-700	100	.019
	100	.045
	100	.042
NiCoCrAlY	100	.036
COATED U-700	100[b]	.104
NiCoCrAlY	20	.134
BULK ALLOY	100	.329
	100	.387
1100° C		
ALUMINIDE COATED U-700	110	.020
NiCoCrAlY BULK ALLOY	300	.463

a. POWER FAILURE DURING RUN

b. SEVERE COATING FAILURE ON ENDS

V-1720

Page intentionally left blank

CONCLUDING REMARKS: HOST 2nd ANNUAL WORKSHOP

Daniel E. Sokolowski

National Aeronautics and Space Administration
Lewis Research Center
Cleveland, OH 44035

As reported at this workshop, the HOST Project activities are well underway and are starting to produce results. Contractor annual and final reports are starting to become available and their number should increase in the future. Workshops such as this will continue on an annual basis; the HOST 3rd Annual Workshop is tentatively scheduled for October 23-24 of next year.

Figure 1 shows the objectives from the Aeronautics Long Range Plan of NASA. A review of the HOST activities, how they are being conducted, and their impact indicates that the HOST Project meets all five objectives of the plan. In addition, the HOST Project is now being recognized for the value of focused and interdependent research when compared with generic, independent base R&T activities. The nature of the problem being addressed, durability in this case, has much influence in advocating and successfully implementing such a project, however.

To date, $11.5 million has been invested in HOST. In FY '84 another $6.1 million will be spent. The present plan for FY '85-'86 is for $9.0 to 11.1 million per year. Such funding will support the future directions listed in Figure 2.

Finally, I want to say "Thank You" to the HOST Project Team for a job well done in conducting this workshop. In particular, I want to thank the contractor speakers, the Subproject Managers for being session chairmen, and my Assistant Manager, Bob Ensign and Administrative Assistant, Joanne Flowers for helping organize and coordinate the multitude of efforts required.

AERONAUTICS LONG RANGE PLAN OBJECTIVES

1. ESTABLISH RECOGNITION OF IMPORTANCE OF NASA AERONAUTICS TO BOTH CIVIL AND MILITARY AVIATION
2. PROVIDE U.S. R&T CAPABILITY BY MAINTAINING RESEARCH CENTERS IN POSITIONS OF UNDISPUTED EXCELLENCE IN FACILITIES, COMPUTATIONAL CAPABILITY AND TECHNICAL STAFF
3. RESTORE A BALANCED AERONAUTICS PROGRAM CONSISTING OF DISCIPLINE RESEARCH, SYSTEMS RESEARCH AND SELECTED PROOF OF CONCEPT ACTIVITIES WITH EMPHASIS ON COMMON APPLICABILITY TO BOTH CIVIL AND MILITARY AVIATION
4. STRENGTHEN NASA UNIVERSITY PARTNERSHIP IN AERONAUTICS R&T
5. STRENGTHEN USER INTERFACES TO PROMOTE TECHNOLOGY TRANSFER

FUTURE DIRECTIONS

- CONTINUING HOT SECTION DURABILITY RESEARCH
- SELECTED INTERDISCIPLINARY GRANTS
- STRONG NASA LEWIS IN-HOUSE RESEARCH EFFORTS
- COMPATIBILITY WITH DOD

1. Report No.	2. Government Accession No.	3. Recipient's Catalog No.
NASA CP-2289		

4. Title and Subtitle	5. Report Date
Turbine Engine Hot Section Technology (HOST)	October 1983
	6. Performing Organization Code 533-04-1A
7. Author(s)	8. Performing Organization Report No. E-1816
	10. Work Unit No.
9. Performing Organization Name and Address National Aeronautics and Space Administration Lewis Research Center Cleveland, Ohio 44135	11. Contract or Grant No.
	13. Type of Report and Period Covered Conference Publication
12. Sponsoring Agency Name and Address National Aeronautics and Space Administration Washington, D.C. 20546	14. Sponsoring Agency Code

15. Supplementary Notes

16. Abstract

A two-day workshop on the research and plans for turbine engine hot section durability problems was held on October 25 and 26, 1983, at the NASA Lewis Research Center. Presentations were made during six sessions, including structural analysis, fatigue and fracture, surface protective coatings, combustion, turbine heat transfer, and instrumentation, that dealt with the thermal and fluid environment around liners, blades, and vanes, and with material coatings, constitutive behavior, stress-strain response, and life prediction methods for the three components. The principal objective of each session was to disseminate the research results to date, along with future plans, in each of the six areas. Contract and government researchers presented results of their work. This publication contains extended abstracts and visual material presented during the workshop.

17. Key Words (Suggested by Author(s))	18. Distribution Statement
Turbine Engine Technology (HOST); Life prediction; Combustor liners; Turbine airfoils; Material behavior; Aircraft engines; Durability analysis methods	[redacted]

19. Security Classif. (of this report)	20. Security Classif. (of this page)	21. No. of pages	22. Price*
Unclassified	Unclassified	275	A12